ABC-ANZORS 2024 Annual Scientific Meeting

1-4 December 2024

Proceedings

Advanced Technologies Centre (ATC)

Swinburne University of Technology,

John Street, Hawthorn, Victoria, Australia

Table of Contents

President's Welcome

Dear Colleagues,

On behalf of the Australian and New Zealand Society of Biomechanics (ANZSB) and the Australian and New Zealand Orthopaedic Research Society (ANZORS), it is our pleasure to welcome you to the Combined ABC-ANZORS 2024 Scientific Meeting in Melbourne. This year's *Biomechanics meets Biology in Orthopaedics* meeting symbolises the inaugural gathering of our like-minded societies, the first of hopefully, many future meetings to come.

It's wonderful to bring the ANZSB and ANZORS communities together, to showcase and celebrate our latest achievements and advancements in biomechanics and musculoskeletal research. We warmly welcome old friends, new faces, and esteemed international guests.

Swinburne University of Technology kindly hosts this year's meeting. The Organising Committee, co-Chaired by A/Prof Oren Tirosh, Dr Elyse Passmore, Dr Martina Barzan and Prof David Ackland, has put together an exciting program of cutting-edge basic, translational and clinical science in biomechanics and orthopaedics, with broad appeal for all. We thank the Chairs and the wider Organising and Scientific Committee members for their hard work behind the scenes to bring you an innovative and thought-provoking program.

The scientific program features esteemed International Keynote Speakers A/Prof Anne Silverman (Colorado School of Mines, USA) and Prof Jess Snedeker (RTH Zurich & Uni Zurich), as well as several Keynote Speakers, A/Prof Laura Diamond (Griffith Uni.), Prof Richard Page (Uni. Melbourne), and Prof Kay Crossley (La Trobe Uni), Dr Bart Bolsterlee (UNSW), showcasing some of the very best biomechanic and orthopaedic research from across Australia.

As we come together to explore the theme *"Technology and Clinical Innovation in Biomechanics and Orthopaedics"*, we are reminded of the importance of connecting with colleagues and peers and encourage you to participate in the various social and networking events.

These include a Women's Networking Breakfast, an EMCR Social Event at Holey Moley and conference dinner at Abbotsford Convent. The Networking Event, also at the Convent, is also sure to be a highlight, and where we hope that you can establish new and long-lasting collaborations and friendships between ANZSB and ANZORS members.

A special thank you to our Sponsors: Qualisys, TRACKLAB, LOGEMAS, AIMEDICAL international, Biomechanix, Davies Collison Cave, h/p/cosmos, Marine Biomedical, Materialise, NORAXON and Zimmer Biomet. Without the generosity of our sponsors, these meetings would not be possible.

As well as enjoying four days of learning, networking and socialising, we encourage you to explore Melbourne, a cosmopolitan city renowned for its vibrant arts and coffee culture, iconic sports events, trendy laneways, and unpredictable weather, so we hope you packed your umbrella!

Thank you for being part of this exciting meeting. We encourage you to take full advantage of this event—participate in the sessions, engage in respectful discussions, and maximise networking opportunities with your fellow ANZSB and ANZORS attendees.

Dr Karen Mickle & A/Prof Nathan Pavlos
Presidents, ANZSB & ANZORS

Thanks to our sponsors:

ABC - ANZORS 2024
1-4 December 2024
abc14.com.au
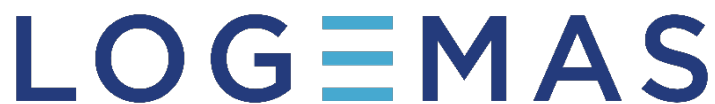
ANZSB Committee Members

President   University of New South Wales
Dr Karen Mickle

President-Elect   Macquarie University
A/Prof Tim Doyle

Past President   Queensland University of Technology
Prof Peter Pivonka

Secretary & Treasurer   University of Sydney
A/Prof Michelle Hall

Communications Officer   Murdoch Children's Research Institute
Dr Elyse Passmore

New Zealand Representative   University of Auckland
Dr Julie Choisne

Early Career Researcher Representative   University of Canberra
A/Prof Celeste Coltman

Student Representative   Macquarie University
Ayden McCarthy

Past Conference Liaison Officer   University of Queensland
Dr Patricio Pincheira Miranda

2024 Host Organisers

Dr Elyse Passmore   Murdoch Children's Research Institute

A/Prof Oren Tirosh   Royal Melbourne Institute of Technology

ANZORS Committee Members

President
A/Prof Nathan Pavlos

Associate Professor and Head, Bone Biology and Disease Laboratory, The University of Western Australia

Secretary
Dr Martina Barzan

Research Fellow, Australian Centre for Precision Health and Technology, Griffith University

Treasurer
Dr Dane Turner

Senior Lecturer, Faculty of Medicine, Health and Human Sciences, Macquarie University & Regional Research Manager ANZ, GE HealthCare

New Zealand Representative
Dr David Musson

Senior Lecturer, Department of Nutrition & Dietetics, School of Medical Sciences, The University of Auckland

Immediate Past President
A/Prof Egon Perilli

Associate Professor in Biomedical Engineering, The Medical Device Research Institute, College of Science & Engineering, Flinders University

Organising Committees

Conference Chairs

Dr Elyse Passmore, ANZSB
A/Prof Oren Tirosh, ANZSB
Dr Martina Barzan, ANZORS
Prof David Ackland, ANZORS

Local Conference Organising Committee

Dr Elyse Passmore	Murdoch Children's Research Institute
A/Prof Oren Tirosh	Royal Melbourne Institute of Technology
Dr Anna Murphy	Monash Health
Dr Elizabeth Bradshaw	Deakin University
Dr Fatemeh Malekipour	University of Melbourne
Prof Gavin Williams	University of Melbourne
Dr Kane Middleton	La Trobe University
Dr Kwong Ming TSE	Swinburne University
Dr Luis Eduardo Cofre Lizama	Swinburne University
Dr Luke Perraton	Monash University
Dr Scott Starkey	University of Melbourne
Dr Yi-Chung Lin	Australian Catholic University
Jinella Lopez	The Royal Children's Hospital Melbourne
Sarah Safavi	University of Melbourne
Dr Sarah Woodford	University of Melbourne

Program Organising Committee

Dr Elyse Passmore	Murdoch Children's Research Institute
Dr Martina Barzan	Griffith University
Dr Karen Mickle	University of New South Wales
A/Prof Nathan Pavlos	University of Western Australia

Scientific Committee
(alphabetical first name order)

Dr Aaron Fox	Deakin University
Dr Anna Murphy	Monash Health
Prof Ashvin Thambyah	University of Auckland
Ayden McCarthy	Macquarie University
Dr Bart Bolsterlee	NeuRA
Dr Benjamin Mentiplay	La Trobe University
Bradley Cornish	Griffith University
Britney Kerr	Royal Children's Hospital Melbourne
Dr Brook Galna	Murdoch University
Prof David Ackland	University of Melbourne
Prof David Findlay	University of Adelaide
Dr David Musson	University of Auckland
A/Prof Dominic Thewlis	University of Adelaide
Dr Elizabeth Bradshaw	Deakin University
Dr Elizabeth Wojciechowski	University of Sydney
Dr Elyse Passmore	Murdoch Children's Research Institute
Dr Fatemeh Malekipour	University of Melbourne
Dr Gavin Williams	University of Melbourne
Prof Jiake Xu	University of Western Australia
Jinella Lopez	Royal Children's Hospital Melbourne
Dr Jodie Wills	Macquarie University
Dr Joe Lynch	Australian National University
Dr John Arnold	University of South Australia
Dr Julie Choisne	University of Auckland
Dr Kane Middleton	La Trobe University
Dr Kwong Ming TSE	Swinburne University
Dr Luis Eduardo Cofre Lizama	Swinburne University
Dr Luke Perraton	Monash University
Dr Martina Barzan	Griffith University
A/Prof Michelle Hall	University of Sydney
A/Prof Nathan Pavlos	University of Western Australia
Dr Patricio Pincheira Miranda	University of Queensland
Dr Peter Smitham	University of Adelaide
Dr Ryan Quarrington	University of Adelaide
A/Prof Saulo Martelli	Queensland University of Technology
Dr Scott Starkey	University of Melbourne
Dr Stuart Callary	University of Adelaide
A/Prof Taylor Dick	University of Queensland
Prof Thor Besier	University of Auckland
A/Prof Tim Doyle	Macquarie University
Dr Yi-Chung Lin	Australian Catholic University

ANZORS Travel Grant Recipients

(alphabetical surname order)

ANZORS is proud to support its early career researchers. This year we have awarded 22 travel grants. This represents a significant reinvestment of our funds to support the dissemination of quality orthopaedic research.

Surname	First Name	Institution
Arjmandi	Reza	The University of Auckland
Beaumont	Patrick	The University of Queensland
Bennett	Kieran	Flinders University
Blaker	Carina	The University of Sydney
Chen	Xiaojun	The University of Western Australia
Cho	Chan Hee	The University of Adelaide
Dastgerdi	Ayda	Griffith University
Hammat	Aaron	The University of Adelaide
Herath	Salindi	Flinders University
Johansen	Harrison	The University of Sydney
Kim	Julie	The University of Auckland
Kim	Nancy	The University of Auckland
Kok	Jean	Indiana University School of Medicine
Labrune	Melody	Macquarie University
Lange	Tyra	Flinders University
Lees	Robert	The University of Queensland
Modiz	Corinna	Queensland University of Technology
Perera	Randika	The University of Auckland
Ranjan	Rahm	University of New South Wales
Thwaites	Simon	The University of Adelaide
Zhang	Longbin	Nanyang Technological University
Zhou	Yixiao	The University of Western Australia

ANZSB Travel Grant Recipients

(alphabetical surname order)

Surname	First name	Institution
Allevard	Enzo	University of Auckland
Cornish	Bradley	Griffith University
Hambly	Matthew	Griffith University
Jones	Nicole	University of Southern Queensland
Oprescu	Ioana	University of Queensland
Quarrington	Ryan	University of Adelaide
Sgarzi	Andrea	University of New South Wales
Starkey	Scott	University of Melbourne
Wojciechowski	Elizabeth	The Children's Hospital at Westmead
Zimmer	Manuela	University of Stuttgart

International Keynote Speakers

A/Prof Anne Silverman

Associate Professor, Mechanical Engineering; Core Faculty, Quantitative Biosciences and Engineering; Director, Functional Biomechanics Laboratory; Colorado School of Mines, USA

Dr. Silverman is an Associate Professor in Mechanical Engineering and Quantitative Biosciences and Engineering at the Colorado School of Mines in Golden, CO, USA. Her research program centers on understanding musculoskeletal biomechanics and movement coordination to develop effective training interventions, prevent injury, and improve mobility. As director of the Functional Biomechanics Laboratory, she uses experimental movement analysis and computational whole-body modeling techniques to evaluate muscle action, joint loading, and device function during movement. Recent projects have evaluated military service members, people with lower-limb amputations, and older adults. Her work has been funded by the U.S. National Institutes of Health, National Science Foundation, and the Department of Defense and has been published in the *Journal of Biomechanics, Journal of Biomechanical Engineering* and *Gait & Posture*. She serves on editorial boards for *Gait & Posture* and the *Journal of Applied Biomechanics.* She is a Fellow of the American Society of Mechanical Engineers.

Prof Jess Snedeker

Professor of Biomechanics, ETH Zurich (Switzerland), Department of Health Sciences & Technology; Vice Chair for Research, Departent. of Orthopaedics, University of Zurich (Medical Faculty); Chief Scientific Officer, Balgrist Campus.

Jess Snedeker is a Full Professor of Orthopedic Biomechanics, holding joint appointments at ETH Zurich (Department of Health Sciences and Technology) and the University of Zurich (Medical Faculty), where he also serves as Vice Chair for Research in the Department of Orthopedics. Since 2015, he has been the Chief Scientific Officer at Balgrist Campus, a nationally recognized center for musculoskeletal research funded by the Swiss federal government. The campus is a vibrant research community with over 20 independent groups and more than 220 researchers. Dr. Snedeker's own research is at the forefront of tendon mechanobiology and regenerative orthopedic surgery research. His group is committed to both basic scientific discovery and the clinical translation of innovative orthopedic devices, aiming to enhance patient outcomes and quality of life.

National Keynote Speakers

A/Prof Laura Diamond

Deputy Director, Australian Centre for Precision Health and Technology (PRECISE), Griffith University, Gold Coast, QLD

Dr Laura Diamond is an NHMRC Emerging Leadership Fellow, Associate Professor, and Research Lead at Griffith Centre of Biomedical and Rehabilitation Engineering, Griffith University. She is a trained biomedical engineer (Dalhousie U, Canada) with a PhD in biomechanics (U of Melbourne) leading a research program focused on development and application of novel technologies to understand and treat the biomechanical mechanisms of musculoskeletal and orthopaedic conditions. Laura has attracted >AU$14M in grant funding, invented 1 National Phase patent, and published >80 scientific papers/book chapters. She is incoming Deputy Director of the Australian Centre for Precision Health and Technology (PRECISE), has an extensive community engagement portfolio, and is an advocate for participation of schoolgirls/women in STEM.

Prof Richard Page

Director, Barwon Centre of Orthopaedic Research and Education; Chair of Orthopaedics, Deakin University (Melbourne, VIC)

Professor Richard Page is an orthopaedic shoulder and upper limb surgeon. He was appointed as Foundation St John of God and Barwon Health Chair of Orthopaedics at Deakin University in 2014. He is Director of Orthopaedic Research at Barwon Health, the Barwon Centre of Orthopaedic Research and Education (B-CORE) and Medical Director of the Barwon Health Bone Bank. His research interests include outcomes of shoulder and wrist surgery, upper limb osteoarthritis and joint replacement surgery, biomechanics and a range of trauma and fragility fracture outcome topics. He manages two lab-based research programmes, the first investigating biofilms and biomarkers in prosthetic joint infections in orthopaedics, the second focussed on the genetics and potential intervention biomarkers in painful musculoskeletal conditions in a human shoulder model.

Prof Kay Crossley

Director, La Trobe Sport and Exercise Medicine Research Centre, La Trobe University (Melbourne, VIC)

Professor Kay Crossley is the Director of the La Trobe Sport and Exercise Medicine Research Centre. Her main research focus is on preventing and managing knee and hip pain and injuries, and early-onset osteoarthritis after sports-related injuries. Kay maintains a strong research interest in enhancing treatments for knee conditions (injuries, pain and osteoarthritis). She also focuses on preventing osteoarthritis following sports-related injuries, with fields in patellofemoral osteoarthritis following patellofemoral pain, knee osteoarthritis following ACL reconstruction, and hip osteoarthritis following hip-related injuries. She is passionate about promoting the health of women and girls participating in sport and physical activity (including injury prevention) and the careers and opportunities for women working in sport and exercise physiotherapy/medicine.

Dr Bart Bolsterlee

Senior Research Fellow, Neuroscience Research Australia; Associate Lecturer in Biomedical Engineering, University of New South Wales (Sydney, NSW)

Dr Bart Bolsterlee is a mechanical (BSc) and biomedical engineer (MSc, PhD) who holds positions as a Senior Research Fellow at Neuroscience Research Australia (Sydney) and as Adjunct Senior Lecturer at UNSW. His research spans the fields of biomechanics and medical imaging, with applications in the study of muscle adaptation with neuromuscular disease. His specific expertise is in quantitative magnetic resonance imaging of skeletal muscle. Dr Bolsterlee developed diffusion tensor imaging methods to reconstruct and quantify the three-dimensional architecture of living human skeletal muscles. His recent work includes the use of artificial intelligence to automate the analysis of MRI scans, facilitating the use of detailed MRI-based measures in large-scale research. He currently leads the MUGgLE study – a large-scale, longitudinal imaging study into childhood muscle growth which includes 200 typically developing children and 80 children with cerebral palsy.

Venue

Advanced Technologies Centre (ATC)

Swinburne University of Technology,

John Street, Hawthorn, Victoria, Australia
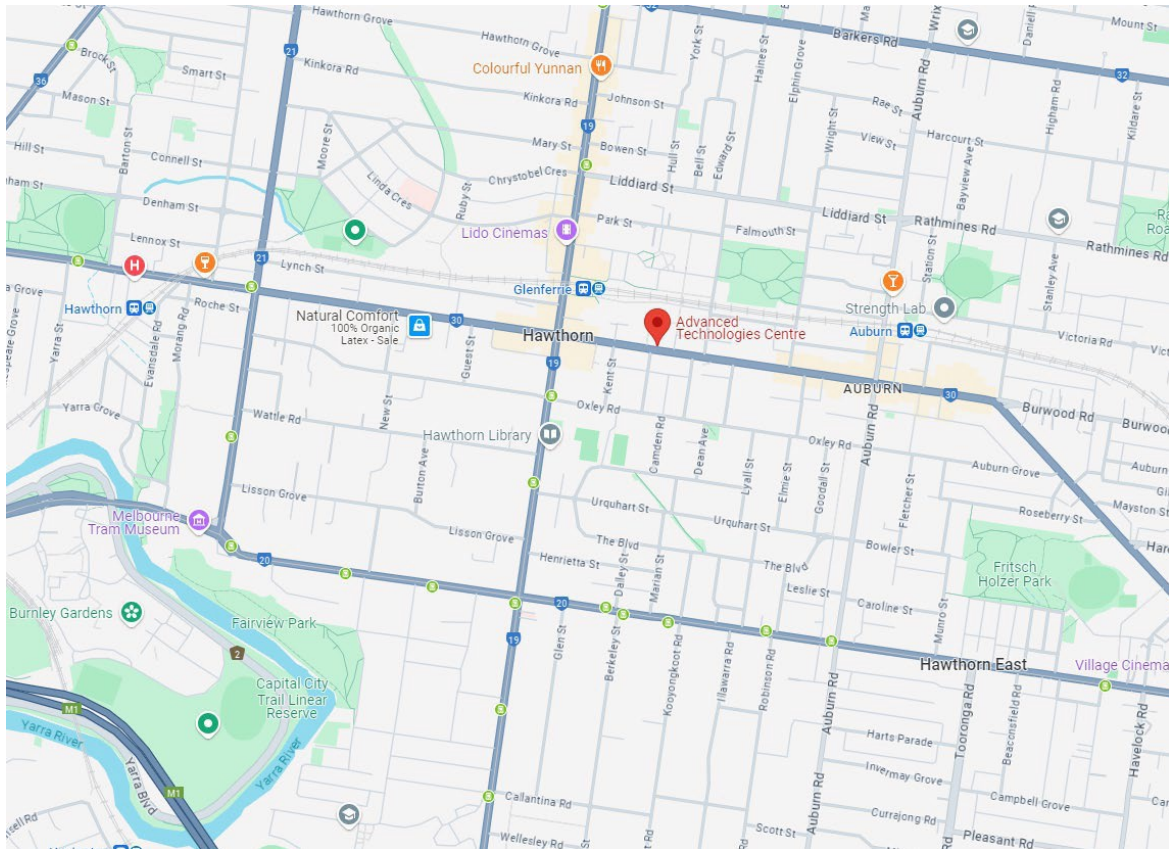
Google maps

Wi-Fi Access: Events@Swin
Password: swin3324

PROGRAM

Sunday, December 1

Time	Session	Location
8:00-8:30	Conference registration and coffee	Foyer, SPW Building
8:30-10:30	Materialise workshop	SPW Building room 111
10:15-11:00	Morning tea	Foyer, SPW Building
10:30-12:00	Tracklab workshop	SPW Building biomechanics lab room 011
12:00-13:00	Lunch	Foyer, SPW Building
12:00-14:00	Qualisys workshop	SPW Building biomechanics lab room 011
14:00-14:30	Afternoon tea	Foyer, SPW Building
14:00-16:30	Women in biomechanics Wikipedia workshop	SPW Building room 111
15:30-16:30	Conference registration	Foyer, ATC Building
16:30-17:00	**Opening Ceremony/Presidents' welcome:** **Dr Karen Mickle, A/Prof Nathan Pavlos**	ATC101 Lecture Theatre
17:00-18:00 **Session chair: Dr Karen Mickle**	**International Keynote: A/Prof Anne Silverman, Colorado School of Mines, Colorado, USA** **"Muscle Function and Coordination Linking to Whole Body Balance and Injury Risk"**	ATC101 Lecture Theatre
18:00-20:00	**Welcome Reception**	Swinburne University Foyer, ATC building Map: Google maps

Monday, December 2

07:30-08:20	**Women's Breakfast;** ATC101 Lecture Theatre		
08:00-08:30	Coffee and registration; Foyer, ATC Building		
08:30-09:00 ATC101 Lecture Theatre **Session chair: Dr Elyse Passmore**	**Keynote: A/Prof Laura Diamond, Griffith University, Gold Coast, Queensland** **"From mechanisms to management: Precision health technology for hip osteoarthritis"**		

09:00-10:00	**Name**	**Surname**	**Abstract title**
ABC Podium 1 – Locomotion & human movement *Parallel session* ATC101 Lecture Theatre Session chairs: A/Prof Laura Diamond, Dr Anna Murphy	Julie	Choisne	3D gait analysis in children using wearable sensors and machine learning
	Leanne	Dwan	Two-year 3D gait outcomes following in-situ pinning or modified Dunn procedure in children with slipped capital femoral epiphysis
	Julie	Choisne	Lumbar loads during walking with sagittal spinopelvic alignments
	Rahm	Ranjan	Towards improved clinical kinematic references for gait analysis using human pose estimation
	Kayne	Duncanson	Modelling individual variation in human walking gait across populations and walking conditions via gait recognition
	Zhou	Fang	A digital twin platform for joint motion measurement and task classification in the home

09:00-10:00	**Name**	**Surname**	**Abstract title**
ANZORS Podium 1 *Parallel session* Building EN, room EN313 Session chairs: A/Prof Elizabeth Clarke, A/Prof Laura Wilson	Maya	Braun	Investigating variations in elastin content across different human tendons and ligaments
	Xiaojun	Chen	Targeting Oxr1 to regulate osteoclast differentiation and function
	Carina	Blaker	Age-associated proteomic changes in a mouse model of knee osteoarthritis
	Yixiao	Zhou	The Rab7 guanine nucleotide exchange factor complex Mon1-Ccz1-Rmc1 differentially regulates osteoclast formation, bone resorption and endosome-to-lysosome maturation
	Dean	Mayfield	The history dependence of muscle contraction: insights from a muscle contracting against a spring
	Randika	Perera	An in vivo imaging study of fascia thickness and muscle volume in the lower limb of healthy adult humans

10:00-10:40 Morning coffee & tea; Foyer, ATC Building			

10:40-11:50	**Name**	**Surname**	**Abstract title**
ABC Podium 2 – Sports biomechanics *Parallel session* ATC101 Lecture Theatre Session chairs: Dr Luke Perraton, Dr Kane Middleton	Elizabeth	Bradshaw	Dangerous high tackles in rugby: measuring what happens to the opponents head
	Ryan	Quarrington	The effect of head-forward posture on risk of lower neck dislocation during head-first impacts: a preliminary computational and dynamic experimental investigation
	Tess	Rolley	Effect of concussion on side-stepping biomechanics in women's Australian football
	Karen	Mickle	Investigating a sports science approach to warm-up practices in dance: can we improve dance performance?
	Aaron	Fox	Barefoot ballet with a rigid foot: are common methodological choices limiting our understanding of foot and ankle biomechanics in ballet?
	Haydee	Ferguson	Can we accurately measure multi-segment foot kinematics in a ballet pointe shoe?
	Ceridwen	Radcliffe	The energetic behaviour of the human foot during landing

10:40-12:00	**Name**	**Surname**	**Abstract title**
ANZORS Podium 2 *Parallel session* Building EN, room EN313 Session chairs: Prof	Kate	Hoare	Structural and biomechanical properties of articular cartilage in different joints
	Phoebe	Del Rosario	Double screw fixation in the surgical repair of unstable scaphoid fractures
	Maxence	Lavaill	Spatial tracking of the shoulder bones using optical motion capture and 3D ultrasound: a simulation and cadaveric study

Peter Pivonka, Dr Natalia Castoldi	Melody	Labrune	Validation of a subject specific Opensim shoulder model using in-vitro experimental data
Peter Pivonka, Dr Natalia Castoldi	Melody	Labrune	Validation of a subject specific Opensim shoulder model using in-vitro experimental data

Roshni	Raghvani	Combined shape model of the torso and upper limb
Saulo	Martelli	Onlay-Grammont hybrid design increases humeral implant stiffness but not fracture load in reverse shoulder arthroplasty
Alec	McKenzie	The shoulder toolkit: enhancing end-user application
Wolbert	Van den Hoorn	Neural drive to the deltoid segments in healthy shoulders

12:00-13:15 Lunch & Sponsor exhibition; Foyer, ATC Building

13:15-13:45 ATC101 Lecture Theatre Session chair: Prof David Ackland	Keynote: Prof Richard Page, Deakin University, Melbourne, Victoria "Shoulder in reverse: a twenty-year journey"	

13:45-14:25	Name	Surname	Abstract title
ABC Podium 3 – Sports biomechanics *Parallel session* Building EN, room EN313 Session chairs: Dr Yi-Chung Lin, Dr Meghan Keast	Celeste	Coltman	The association between symptoms of pelvic floor dysfunction & running mechanics
	Stephen	Halle-Worrall	Distinct tibialis anterior electromyography profiles in strength and endurance athletes revealed by principal component analysis
	Sienna	Gosney	Profiling the sprint-paddling kinematics of female and male competitive surfers
	Alan	Abraham	Exploring the use of OpenCap in capturing cricket bowling kinematics

13:45-14:25	Name	Surname	Abstract title
ANZORS Minghao Zheng Orthopaedic Innovation Award Final *Parallel session* ATC101 Lecture Theatre Session chairs: Prof Richard Page, Dr Kieran Bennett	Alireza	Yahyaiee-Bavil	Effects of varied neck-shaft angle on interfragmentary strains following proximal femoral osteotomies
	Rachel	Li	Circulating microRNA in arthrofibrosis patients of post total knee arthroplasty
	Rui	Ruan	Development of bioactive bone substitute (PearlBone™) using Mother-of-Pearl sourced from Broome, Western Australia
	Peilin	Chen	The efficacy of a novel porcine-derived collagen membrane on guided bone regeneration: a comparative study in canine model

14:25-15:30 Afternoon coffee & tea and poster viewing; (poster viewing will take place between 15:00-15:30)
Foyer, ATC Building

15:30-16:50	Name	Surname	Abstract title
ANZORS Podium 4 *Parallel session* ATC101 Lecture Theatre Session chairs: Dr Carina Blaker, Dr Olga Panagiotopoulou	Fatemeh	Malekipour	Mechanical load distribution in equine metacarpal condyles: a computational model using standing CT images
	Jaqui	Couldrick	Knee joint moment changes following a structured education and exercise program (GLA:D®) for knee osteoarthritis and the relationship to radiological OA severity and body weight
	Egon	Perilli	Ovine vertebral bone strain analysis after overload by combining mechanical testing and micro-CT
	Mark	Taylor	Reduced micromotion of cementless tibial implants is related to increased interference fit: a micro-CT and DVC study
	Harrison	Johansen	Understanding cardiac co-morbidity with osteoarthritis in mice
	Natalia	Castoldi	Experimental-computational platform to study cortical bone remodelling
	Corinna	Modiz	Analysis of bone mineralisation using discrete and continuous models of bone remodelling
	Tyra	Lange	Acoustic and torsional factors as predictors of bone quality and screw purchase

15:30-17:00	Name	Surname	Abstract title
ANZ Clinical Motion Analysis Group *Parallel session*	Prof Chris Carty, Dr Elyse Passmore, Prof Thor Besier, Motion Connect "Introducing the ANZ clinical motion analysis database"		

Building EN, room EN313	Britney	Kerr	The effect of clusters and inverse kinematics on a cohort with idiopathic torsional deformities

Session chair: Dr Anna Murphy	Jinella	Lopez	Defining the knee joint axis for clinical gait analysis in a paediatric population
	Taylor	Dick	Predictive simulations reveal mechanistic links between altered muscle-tendon form and locomotor function in aging
	Panel discussion: Prof Chris Carty, Dr Elyse Passmore, Prof Thor Besier, Dr Taylor Dick		
18:00-20:40	**ANZSB Student and ECR Night/ANZORS Young Investigator Event** **Honours/Masters/PhD students and ECRs get free meal; must have indicated attendance during registration** at [Holey Moley] **Map: [Google maps]**		

Tuesday, December 3

08:00-08:15	Coffee & tea		
08:15-09:15 ATC101 Lecture Theatre **Session chair: A/Prof Nathan Pavlos**	**International Keynote: Prof Jess Snedeker, ETH Zurich and University of Zurich, Zurich, Switzerland** **"Multiscale Biomechanics and the Cell-Matrix Interactions behind Tendon Adaptation to Exercise"**		
09:15-10:35	**Name**	**Surname**	**Abstract title**
ABC & David Findlay ECR Award Final ATC101 Lecture Theatre Session chairs: A/Prof Anne Silverman, A/Prof Celeste Coltman	Julie	Kim	Robust workflow for diaphyseal cortical bone thickness calculation in long bones
	Jean	Kok	Targeting WNT inhibitors to improve bone mass after spinal cord injury
	Kieran	Bennett	Internal tibial bone displacements and strains due to implantation with cementless tibial trays
	Deepti	Sharma	Carboxylated osteocalcin- a potential biomarker of improved cortical and trabecular bone properties
	Elizabeth	Wojciechowski	Validation of wearable sensors against three-dimensional gait analysis
	Cristian	Riveros-Matthey	Optimising muscle mechanics and energetics in human cycling: a prescribed and EMG-assisted approach across saddle variations
	Meghan	Keast	The acute effects of gait and footwear interventions on tibial strain during running
	Danielle	Vickery-Howe	Biomechanics of load carriage walking at military-relevant speeds and loads: differences between males and females
10.35-11:15 Morning coffee & tea; Foyer, ATC Building			
11:15-12:55	**Name**	**Surname**	**Abstract title**
ABC Student & ANZORS PhD Award Final ATC101 Lecture Theatre Session chairs: Prof Jess Snedeker, Tyra Lange	Nicole	Jones	Quantifying the contralateral repeated bout effect of the triceps surae
	Matthew	Hambly	Rapid calibration of EMG-informed NMS models using differentiable physics
	Ioana	Oprescu	Using predictive musculoskeletal simulations to explore the effect of altered gravity on locomotor performance
	India	Lindemann	Exploring the neuromechanics of the ankle plantar- and dorsi-flexors during slip perturbations to human walking
	Brody	McCarthy	Lower limb joint work in runners with and without a history of knee surgery
	Zhengxu	Cheng	Reduced radiation dose enables multi-positional high resolution computed tomography wrist data for computational modelling without substantial geometric inaccuracy
	Patrick	Beaumont	Using sonography to assess the condition of the lumbar multifidus following restorative neurostimulation: a preliminary analysis
	Mohammad	Yavari	Artificial intelligence in the prediction of persistent foot drop in children with cerebral palsy after gastroc-soleus lengthening
	Ayda	Karimi Dastgerdi	Influence of anterior cruciate ligament reconstruction parameters on kinematics and cartilage stresses in pediatric knee
	Chan Hee	Cho	Optimising early acetabular implant migration thresholds
12.55-13:15	**Lunch to be taken into AGMs**		
13:15-14:15	**ABC & ANZORS AGMs** **All delegates welcome and encouraged to attend** **Lunch can be taken into AGMs**		

17:00-19:00	**Networking Event** **At [Abbotsford Convent](#) -Rosina Courtyard** **(bus transport provided)** **Pickup from 16:30, in front of conference venue** **Map: [Google maps](#)**

19:00-22:30	**Conference Dinner, including Awards Announcements** **At [Abbotsford Convent](#)** (bus transport back to conference venue/Melbourne CBD provided) Pickup from 22:30, in front of venue **Map:** [Google maps](#)

Wednesday, December 4

08:30-09:00	Coffee & tea; Foyer, ATC Building		
09:00-09:30 ATC101 Lecture Theatre **Session chair: A/Prof David Saxby**	**Keynote: Prof Kay Crossley, La Trobe University, Melbourne, Victoria "Biomechanics and early OA - is underloading the new black?"**		

09:30-10:30	Name	Surname	Abstract title
ABC Podium 5 – Locomotion & human movement *Parallel session* Building EN, room EN313 Session chairs: Dr Brook Galna, A/Prof Michelle Hall	Harry	Driscoll	Dynamic simulation of trunk muscle function during vertical jumping
	Ayden	McCarthy	Stride length significantly decreases in a fatigued state of a jerry can carry
	Shanyuanye	Guan	Patellofemoral joint contact area depends primarily upon the knee flexion angle during daily activities
	Jodie	Wills	Hose drag task demands of aviation firefighters
	Kylie	Tucker	Back in action: asymmetry in paraspinal muscle size, composition and activation in adolescent idiopathic scoliosis
	Robert	Lees	How does motor unit recruitment differ across knee extension tasks? A preliminary analysis

09:30-10:30	Name	Surname	Abstract title
ANZORS Podium 5 *Parallel session* ATC101 Lecture Theatre Session chairs: Dr Stuart Callary, Dr Luca Modenese	Aaron Scott	Hammat	Septic vs aseptic: a cost-analysis of revision THA at a tertiary referral centre
	Salindi	Herath	Knee joint reaction forces are positively correlated with changes in the bone of the proximal tibia following primary total knee replacement surgery
	Taisha	D'Apollonio	Does the number of previous revision surgeries influence the survivorship of implants used at revision hip arthroplasty?
	Emmanuel	Eghan-Acquah	Effect of blade plate implant size selection on biomechanical surgical outcomes following proximal femoral osteotomy
	Daniel	Hopkins	A fully automated pipeline for medical image reconstruction, surgical planning and simulation of post-operative joint function following revision hip arthroplasty involving acetabular defects
	Simon	Thwaites	Objective kneeling assessments may help discern differences in patient outcomes between tibial nailing approaches: interim results from a pilot RCT

10:30-11:10 Morning coffee & tea; Foyer, ATC Building			

11:10-12:00	Name	Surname	Abstract title
ANZORS Podium 6 *Parallel session* ATC101 Lecture Theatre Session chairs: Dr Fatemeh Malekipour, Dr Ben Ferguson	Natali	Uribe	A parametric finite-element model of the femur spanning the entire adulthood
	Fuyuan	Liu	Finite element analysis of a customized pelvic fracture implant to monitor fracture healing
	Julie	Choisne	Can statistical shape and density models predict femoral and tibial stress in a paediatric population?
	Reza	Arjmandi	Biomechanical advantages of a partial facetectomy in the surgical management of pars interarticularis fractures
	Enzo	Allevard	Tibia and fibula bones prediction from external shank skin shape in a paediatric population

11:10-12:00	Name	Surname	Abstract title
ABC Podium 6 – Clinical biomechanics *Parallel session* Building EN, room EN313 Session chairs: Prof Kay	Benjamin	Mentiplay	Leg stiffness during running in adults with traumatic brain injury
	Jack	Beard	Postural alignment during unsupported walking following acquired brain injury: application of a new measure
	Matthew	Savage	Are altered knee joint biomechanics associated with the onset and progression of post-traumatic osteoarthritis? A systematic review of longitudinal studies.

Crossley, Dr Leane Dwan	Jodie	McClelland	Altered trunk movements and lower limb moments during running after anterior cruciate ligament reconstruction

	Anna	Butcher	Biomechanical risk factors associated with anterior cruciate ligament injury and the link to pubertal maturation: a systematic review

12:00-13:15 Lunch & poster viewing (poster viewing will take place between 12:30-13:00) Foyer, ATC Building

13:15-13:45 Session chair: Dr Julie Choisne	**Keynote: Dr Bart Bolsterlee, University of New South Wales, Sydney, New South Wales** **"Quantitative magnetic resonance imaging to study skeletal muscle during childhood development"**

13:45-14:35	**Name**	**Surname**	**Abstract title**
ABC Podium 7 - *Emerging technology Parallel session* ATC101 Lecture Theatre Session chairs: Dr Eduardo Cofre, Dr Alexis Brierty	James	Williamson	The task dependent neuromuscular response of older adults to exoskeleton assistance during standing balance tasks
	Miyuki	Chamberlain	Predictive musculoskeletal simulations to explore the energetics of hopping with a joey in macropods
	Simon	Heinrich	Optimal control simulation of full hand flexion movements exploiting optical marker tracking
	Longbin	Zhang	Quantitative fall risk assessment via an enhanced timed up and go test with markerless motion capture and machine learning
	Grace	McConnochie	Lidar-based scaling of Opensim human models is a viable alternative to marker-based approaches

13:45-14:45	**Name**	**Surname**	**Abstract title**
ANZORS Podium 7 *Parallel session* Building EN, room EN313 Session chairs: Dr Bart Bolsterlee, Randika Perera	Bradley	Cornish	A physics-informed neural network for estimation of hip biomechanics
	Matheus	Pinto	Medial gastrocnemius muscle and fascicle dynamics in vivo during eccentric contractions
	Manuela	Zimmer	A comprehensive pipeline for in vivo determination of skeletal muscle and connective tissue anatomy using magnetic resonance imaging
	Alice	Hatt	The effect of intramuscular fat on the anisotropic viscoelastic properties of human skeletal muscle in vivo
	Andrea	Sgarzi	Assessment of two muscle models with coupled activation and contraction dynamics
	Ryan	Konno	A neuromechanical model for muscle energy use in vivo

14:45-15:15	**Presidents' closing address:** **Dr Karen Mickle, A/Prof Nathan Pavlos**

POSTERS presented on Monday, December 2
ATC Building, room 206

| 12:00-13:15 | Lunch break | | |
| 14:25-15:30 | Afternoon break | | |
Poster #	First name	Surname	Abstract title
1	Ayda	Karimi Dastgerdi	Insights into patellofemoral kinematics and cartilage stresses following pediatric anterior cruciate ligament reconstruction
2	Ben	Jones	Between-day reliability of gait variability measures calculated from an inertial measurement unit
3	Brooke	Hoolihan	The effect of biological sex on lower-limb coupling variability in military personnel
4	Cristian	Riveros-Matthey	Regional effects of rapid eccentric stretch on tibialis anterior muscle shear modulus and motor unit discharge frequency during moderate isometric contractions: preliminary results
5	Francois	Bruyer-Monteleone	Predicting humeral version angle for shoulder surgery using statistical pose models
6	Hossein	Mokhtarzadeh	Enhancing scientific reproducibility in biomechanical studies with Google colab
7	James	Williamson	The biomechanics of walking with mnd: a joint-level perspective on the lower-limb
8	John	Kerr	Lower limb prosthesis user gait symmetry across multiple walking speeds
9	Maxence	Lavaill	Automatic segmentation of shoulder anatomy from magnetic resonance imaging using NNU-net
10	Nicolaos	Darras	Movement efficiency can be measured using mixed reality
11	Oscar	Stelzer-Hiller	Assessing an intra-session tackle technique intervention in rugby league for altering head kinematics: a preliminary analysis
12	Ryan	Tiew	Influence of osseointegrated implant length on femoral fracture strength
13	Sami	Alahmari	Effects of arm-cycling exercise during triceps surae neuromuscular electrical stimulation on torque output and fatigue
14	Yareni	Guerrero	Test-retest reliability study of three-dimensional kinematic gait modeling parameters and antropometric measurements in overweight obese adults with knee osteoarthritis
15	Zhengxu	Cheng	Effect of altering ligament-bone attachment bushing stiffness on multibody dynamics simulation of wrist motion

Please see next page for posters presented on Wednesday.

POSTERS presented on Wednesday, December 4
ATC Building, room 206

Poster #	First name	Surname	Abstract title
10:30-11:00	Morning break		
12:00-13:15	Lunch break		
16	Alireza	Bavil	Computational toolbox for bone deformation modelling in finite element analysis of the femur to aid clinical diagnoses and surgical planning
17	Benjamin	Carling	How knee kinematics relate to function in adults with knee osteoarthritis
18	Brooke	Galna	Synchronisation of multiple unconnected inertial measurement units
19	Ben	Ferguson	Estimating bone modulus of sheep mandible using inverse methodology combining finite element updating method, ex vivo mechanical testing, and digital image correlation
20	Christopher	Bird	Non-invasive estimates of neuromuscular properties using ultra-wideband radar
21	Grace	McConnochie	Optimal control simulations tracking wearable sensor signals provide comparable running gait kinematics to marker-based motion capture
22	James	Davies	Pre-operative EQ-5D-5L is a strong predictor of meaningful improvement in quality of life following primary total knee arthroplasty
23	Yihe (Claire)	Li	Identification of novel small-molecule modulator of sorting nexin 10 to inhibit osteoclastic bone resorption
24	Laura	Wilson	Relevance of bilateral asymmetry for mirror reconstruction techniques in the management of distal tibial fractures
25	Mounir	Boudali	The design and validation of an apparatus for biomechanical testing of patellofemoral and knee joints using a robotic testing platform
26	Nisal	Jayaneththi	Cyclic loading of Achilles tendon using physiologically representative loads
27	Nikolaos	Darras	Evaluating the intellevent algorithm on an external normal dataset
28	Salindi	Herath	Patient related factors affect bone mineral density in the proximal tibia six months following total knee replacement surgery
29	Sarah	Safavi	A framework for the design of patient-specific porous femoral stems
30	Zhengliang	Xia	Predicting Achilles tendon force using 2D video data
31	Ziming	Chen	Impacts of anterior cruciate ligament rupture on the nuclei of ligament cells: a histology and single-cell gene expression-based study

<u>All</u> posters will be displayed for the whole duration of the conference and presented on either Monday or Wednesday by the author as indicated.

ABSTRACTS

Sunday, December 1

International Keynote 1 – A/Prof Anne Silverman

Muscle Function and Coordination Linking to Whole Body Balance and Injury Risk

Characterizing the link between whole-body movement and joint mechanics is critical to prevent injury, optimize assistive devices, and reduce medical costs. Musculoskeletal injury and joint health are at least partly driven from internal dynamic conditions during movement, which are challenging to measure directly. Balance control during dynamic tasks is driven by muscle coordination and musculoskeletal capacity. This presentation will share recent work using experimental and musculoskeletal modelling techniques to evaluate musculoskeletal biomechanics during dynamic whole-body movements. Specifically, military service members are routinely required to perform biomechanically demanding tasks, which can result in long-term overuse injuries. Younger and older adults have varying muscular capacities driving how they maintain balance during transitional movements. Insights from these studies can drive personalized models, develop training guidelines, and recommend movement strategies to preserve long-term mobility.

Monday, December 2

National Keynote 1 – A/Prof Laura Diamond

From mechanisms to management: Precision health technology for hip osteoarthritis

Non-surgical and non-drug interventions (e.g. exercise, weight loss) are recommended globally for clinical management of hip osteoarthritis (OA). However, patients often report only mild improvements in symptoms, and no existing treatment can alter structural disease progression. These poor outcomes are because mechanical targets for treatment of hip OA are not well defined, not personalised, and not measurable outside the laboratory. Using novel experimental methodology and validated computational models of the neuromusculoskeletal system, my team has proven that abnormal hip loading is a key biomarker of hip OA severity and pain levels, and that hip loading is patient-specific and modifiable through personalised movement retraining. Leveraging our laboratory-based discoveries, we are now co-designing and validating smart wearable technology to enable movement retraining in a natural environment (e.g., home, outdoors, gym, clinic) to maximise therapeutic benefit for people with hip OA. Our technology integrates a physics-informed neural network trained on a large dataset of our high-fidelity neuromusculoskeletal models and advanced wearable technology in a body-worn device designed to improve symptoms and promote cartilage health in people with hip OA. This talk will detail the key mechanistic discoveries and technology development pipeline which underpin our push towards delivering ultra-personalised movement retraining for people with hip OA in a natural environment.

Monday, December 2

ABC Podium 1
Locomotion & human movement

3D Gait Analysis in children using wearable sensors and machine learning

[1]Shima Moghadam, [1]Ted Yeung, [1]Pablo Ortega and [1]Julie Choisne

[1]Auckland Bioengineering Institute, The University of Auckland, Auckland, NZ
email: j.choisne@auckland.ac.nz

INTRODUCTION

Three-dimensional gait analysis (3DGA) is crucial for understanding and treating lower limb movement disorders in children, traditionally performed using Optical Motion Capture (OMC). Inertial Measurement Units (IMUs) offer a cost-effective alternative, although challenges persist. Machine learning (ML) models can mitigate these issues in adults [1], prompting an investigation into their applicability to a heterogeneous paediatric population. Therefore, the aim of this study was to assess the feasibility and accuracy of using IMUs combined with machine learning models for collecting 3DGA in school-aged children

METHODS

Seventeen Typically developing children (9 F, age: 10.5 ± 2.8 years old) underwent overground walking for 3DGA (n=15 trials) at self-selected speed. 37 marker trajectories from OMC (VICON), ground reaction forces (GRFs) from 3 force plates (Bertec) and 2 IMUs (IMeasureU) placed on the feet were recorded and synchronized with Nexus (VICON). The pelvis (3 DOF), hip (3DOF), knee flexion/extension and ankle inversion/eversion and dorsi/plantarflexion kinematics and kinetics were computed from the markers' trajectories and GRFs in OpenSim (gait2392). A combination of raw IMU data (acceleration and angular velocity) and a random forest machine learning model was used to predict pelvis, hip, knee and ankle joints' kinematics and kinetics. Intra-subject (training and testing on the same participant) and inter-subject (training and testing on different participant using a leave one out (LOO) analysis) examination were performed for each participant. We then compared the IMU-predicted kinematics and kinetics accuracy to the ones derived from the OMC using Root Mean Square Error (RMSE) and Normalized RMSE (NRMSE).

RESULTS AND DISCUSSION

The average intra-subject predicted IMU kinematics RMSE and kinetics NRMSE were lower than 5 degrees and 14% respectively for all joints and planes of motion throughout the gait cycle compared to the OMC kinematics. For the inter-subject examination (LOO analysis) the average kinematics and kinetics prediction errors were higher (table 1).

CONCLUSIONS

The current study showed that a pair of IMU combined with a random forest model exhibited comparable results for the intra-subject examination than optical motion capture systems for 3DGA within a typically developed paediatric population. The inter-subject model would need more participants to lower the prediction error as growing children have a bigger variety of gait than adults [1]. The presented workflow not only reduces processing time but could also streamline the integration of wearable sensors in clinical settings.

ACKNOWLEDGEMENTS

REFERENCES

1. Moghadam, S.M. Scientific Reports, 2023. 13(1): p. 5046.

Table 1: NMRSE ± SD for joint angle and joint moment prediction in intra and inter-subject examinations.

NRMSE (%) ± SD		Pelvis			Hip			Knee	Ankle	
		Tilt	Obl.	Rot	Flex/Ext	Add/Abd	Rot	Flex/Ext	Flex/Ext	Inv/Ev
Intra-subject	Kinematics	14.1 ±5.1	9.6 ±2.7	13.8 ±2.7	6.1 ±1.7	8.1 ±1.9	11.9 ±2.3	5.2 ±1.6	6.7 ±1.8	10.1 ±2.2
	Kinetics	13.7 ±1.9	13.2 ±2.1	12.8 ±3.4	11.8 ± 2.1	8.5 ± 2.1	9.6 ±2.9	8.5 ±1.9	6.4 ±1.3	12.5 ±2.3
Inter-subject	Kinematics	33.1 ±20.4	19.7 ±9.8	23.0 ±13.1	17.7 ±8.4	18.4 ±6.9	21.2 ±7.1	9.6 ±6.6	15.3 ±5.7	21.4 ±5.9
	Kinetics	13.9 ±3.6	16.8 ±5.2	13.4 ±3.8	26.4 ±14.5	15.1 ±8.8	10.9 ±3.3	10.3 ±2.6	11.7 ±9.6	18.5 ±7.3

TWO-YEAR 3D GAIT OUTCOMES FOLLOWING IN-SITU PINNING OR MODIFIED DUNN PROCEDURE IN CHILDREN WITH SLIPPED CAPITAL FEMORAL EPIPHYSIS

[1,2]Leanne Dwan, [3]David Little, [3]Oliver Birke, [1,2]Elizabeth Wojciechowski, [2]Anita Mudge, [1]Marnee McKay, [3]Justine St George, Joshua Burns[1,2,4]

[1]University of Sydney School of Health Sciences, Faculty of Medicine and Health, Sydney, NSW, Australia;
[2]Paediatric Gait Analysis Service of New South Wales, Sydney Children's Hospitals Network, Westmead, NSW, Australia
[3]Department of Orthopaedics, The Children's Hospital at Westmead, Sydney, NSW, Australia
[4]St. Jude Children's Research Hospital, Memphis, Tennessee, USA.
email: leanne.dwan@sydney.edu.au

INTRODUCTION

Slipped Capital Femoral Epiphysis (SCFE) is femoral head slippage off the femoral neck through the physis occurring in children aged 8-16 years. Surgical intervention is required and there is no universal agreement on choice of surgical procedure. The goal of treatment is to either stop progression of slippage or restore anatomical alignment of the head and neck of femur and reduce the risk of pain and reduction in function requiring secondary surgery [1]. This research investigated the two-year 3D gait outcomes in children with SCFE who have undergone in-situ pinning (PIN) or modified Dunn procedure (MDP) compared with normative reference values.

METHODS

17 children with SCFE who had undergone PIN (n=7, slip severity mild to moderate) or MDP (n=10, slip severity moderate to severe) surgical procedures prospectively underwent a 3D gait analysis post-surgery ($2 \cdot 0 \pm 0 \cdot 5$ years). Ten age-matched children were also recruited to provide normative reference values. The conventional gait model was modified to incorporate Hara hip equations [2] and Lerner pelvic tracking methods [3]. Gait Profile Scores, Gait Variable Scores, kinematics, kinetics and spatiotemporal data were calculated for each group.

RESULTS AND DISCUSSION

Overall gait pattern, determined by the Gait Profile Score [4], indicated that both SCFE groups differed from the normative reference group (PIN $6 \cdot 6 \pm 2 \cdot 5°$, MDP $6 \cdot 2 \pm 2 \cdot 0°$ vs. $4 \cdot 0 \pm 1 \cdot 3°$ norm, $p<0 \cdot 05$; Figure 1). MDP gait traces were less deviated

from the norms traces than the PIN group (Figure 1). Mean hip rotation over the gait cycle was external in the PIN group ($-4 \cdot 1°$) and was significantly different to both the MDP and normative reference groups (MDP $2 \cdot 5°$, norms $3 \cdot 6°$, p=0·01). Severe slippage is a risk factor for secondary osteoarthritis [1] and a restoration of anatomical alignment using a MDP in severe slips, particularly improving hip rotation during gait may avoid progression to osteoarthritis secondary to SCFE.

CONCLUSIONS

Gait patterns of children with SCFE treated with PIN was more markedly altered than that of children with SCFE treated with MDP, despite having lower SCFE severity. MDP improves hip rotation during gait in severe slips more than mild to moderate slips addressed with a PIN. Therefore the use of the corrective MDP in severe slips which normalises hip rotation may reduce the risk of secondary oteoarthritis.

ACKNOWLEDGEMENTS

REFERENCES

1. Caskey et al., *J Pediatr Orthop* **34**: 668–673, 2014.
2. Hara R, et al., *Scientific Reports* **6**:1-9, 2016.
3. Lerner ZF, et al., *Med Sci Sports Ex* **46**(6): 1261-7, 2014.
4. Baker R, et al., *Gait & Post* **30**(3): 265-9, 2009.
5. Poorter J, et al., *J Children Orthop,* **10**(5): 371-9, 2016.
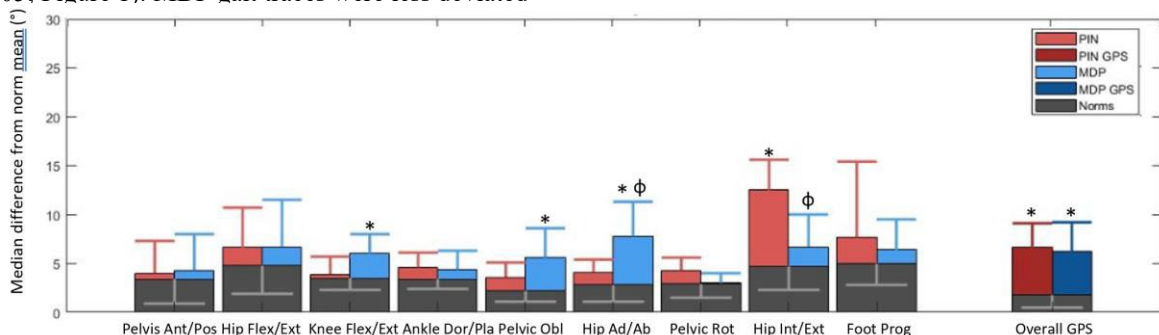
Figure 1: Gait Profile Score and Gait Variable Scores between PIN, MDP and norm groups.

*significantly different to normative reference group ($p < 0.05$). ϕsignificantly different to the PIN group ($p < 0.05$).

Lumbar Loads during Walking with Sagittal Spinopelvic Alignments

[1]Jie Chen, [1,2,3,4]Patria A. Hume, [5,2]Hannah Wyatt, [1]Ted Yeung, [1]Julie Choisne

[1] Auckland Bioengineering Institute, The University of Auckland, Auckland, New Zealand
[2] Sports Performance Research Institute New Zealand (SPRINZ), Faculty of Health and Environmental Science, Auckland University of Technology, New Zealand
[3] Traumatic Brain Injury Network (TBIN), Auckland University of Technology, Auckland, New Zealand
[4] Technology and Policy Lab - Law School, The University of Western Australia, Perth, Australia
[5] Sport, Health and Rehabilitation Research Cluster, Faculty of Health, The University of Canterbury, Christchurch, New Zealand
Email: jche973@aucklanduni.ac.nz

INTRODUCTION

Deviant sagittal spinopelvic alignment is commonly assumed as one of the factors to accelerate lumbar degenerative processes, which may lead to low back pain (LBP) [1]. This deviant alignment may result in abnormal lumbar loads or load distribution, exerting a pivotal mechanical influence on the etiology of LBP [2]. Nonetheless, association between spinopelvic alignment and LBP remains controversial, with studies yielding inconsistent findings [3]. This study aimed to investigate the effects of simulated sagittal spinopelvic alignment via altered lumbar lordosis (LL) on lumbar vertebral joint contact forces during walking.

METHODS

A full-body OpenSim model with custom lumbar joints was developed to calculate lumbar vertebral joint loads, including both compressive and sagittal shear forces acting on the vertebral bodies, and compressive loads at the facet joints, for walking gaits of 18 healthy participants. LL values were set to simulate hyperlordosis (85°, 75°, 65°), normal lordosis (55°, 45°, 35°), and hypolordosis (25°, 15°, and 5°) during walking. Relationships between sacral slope value and LL of each gait trial were outputted and compared with previous studies for the validation of modified gait simulations.

RESULTS AND DISCUSSION

From 5 to 45° of LL, both vertebral body compression and sagittal shear forces increase in the present walking simulation (Fig.1, A&B). From 45 to 85° of LL, excessive LL caused the lumbar sagittal shear force and facet compressive force of L3-L4 and L5-S1 to increase rapidly, but the compressive force and sagittal shear force at vertebral body of L1-L2 to decrease during walking (Fig.1, A&B&C).
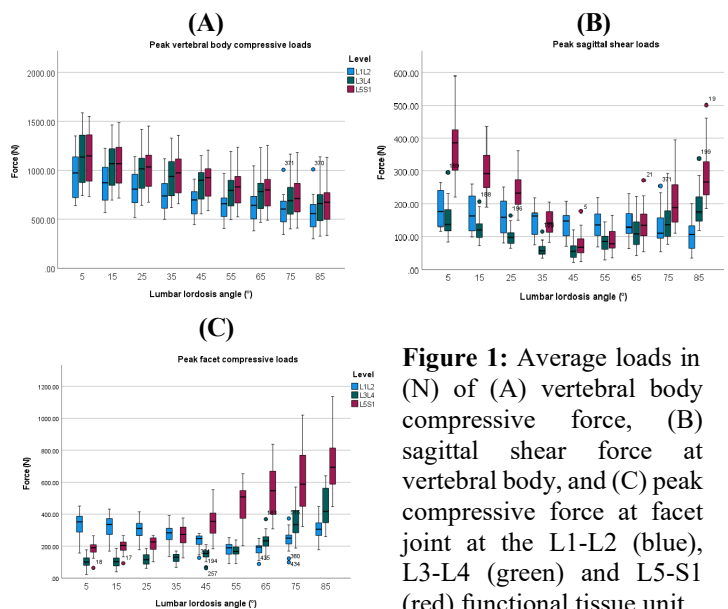
Figure 1: Average loads in (N) of (A) vertebral body compressive force, (B) sagittal shear force at vertebral body, and (C) peak compressive force at facet joint at the L1-L2 (blue), L3-L4 (green) and L5-S1 (red) functional tissue unit.

CONCLUSIONS

Limited LL during walking increased compressive and shear forces at vertebral bodies, which significantly impacts the intervertebral discs. The consequences of excessive lordosis included increased compression of the facet joint and shear force at vertebral body of caudal level (L3-L4, L5-S1), potentially progressing to different types of LBP. Future studies should investigate LL in patients with different specific types of LBP and try to draw more definitive associations between LL and specific LBP.

ACKNOWLEDGEMENTS

REFERENCES

[1] Nourbakhsh MR, et al. J Back Musculoskelet Rehabil. 19(4):119-28, 2006.
[2] Adams MA, et al. Orthopedics. 5(11):1461-5, 1982.
[3] Mirzashahi B, et al. Med J Islam Repub Iran, 2023

Towards improved clinical kinematic references for gait analysis using human pose estimation.

[1,2]Rahm Ranjan, [1]Juno Kim, [1]Branka Spehar,[2]David Ahmedt-Aristizabal, [2]Mohammad Ali Armin
[1]The University of New South Wales, Sydney, NSW
[2]Data 61 CSIRO, Canberra, ACT
email: rahm.ranjan@unsw.edu.au

INTRODUCTION
This study evaluates the clinical validity of using human pose estimation (HPE) for the measurement and establishment of kinematic parameters of normal gait. Characterising Defining normal parameters in gait kinematics is clinically important and required for the identification and classification of movement abnormality [1]. 3D motion capture (MoCap) systems are considered gold-standard for accuracy. However, clinical access and use of MoCap equipment and data is often limited by access, cost, set-up and calibration barriers. Instead, clinicians subjectively evaluate gait with methods such as video analysis that still utilises giant kinematic parameters. HPE is emerging as a promising tool in biomechanics research and in clinical settings due to its non-invasiveness and ease of use. However, its accuracy compared to traditional motion capture (MoCap) systems needs rigorous assessment so that researchers and clinicians can be confident in its use.

METHODS
80 gait cycles from 33 subjects were identified by a clinician and analysed from the GPJATK video dataset [2]. Vicon MoCap and BlazePose HPE [3] systems were used to extract limb position data to calculate the left knee joint angle. Statistical Parametric Mapping (SPM) analysis with a paired t-test on time series data allowed comparison of the knee joint angle measures from both methods across all gait cycles.

RESULTS AND DISCUSSION
Normalised measures of the left knee joint angle are shown in Figure 1 for both MoCap (in black) and HPE (in red) systems. Both trajectories show a similar measure of change over the entire gait cycle indicating that HPE is a promising tool for clinical use. However, using SPM analysis, we find that the differences between measures from MoCap and HPE are statistically significant (grey shade in bottom chart). The cluster-level analysis indicated statistical differences in measures throughout the whole gait cycle except for between 15 and 40 percent of the cycle. The differences are greatest between 70% and 80% of the gait cycle, which is when the most flexion is occurring during the mid-swing phase. Our findings reflect the system differences between gold standard MoCap,

which uses a 3D system, and the more cost-effective and clinically accessible HPE – a 2D system of measurement like that used by clinicians observing human movement in video.
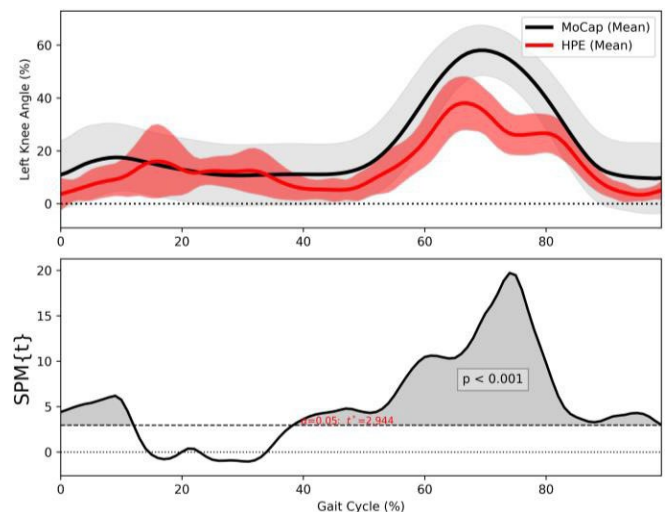
Figure 1: Comparison between MoCap and HPE for left knee joint angle measures normalised over gait cycle (%). The gait cycle starts and ends at left initial contact. Top figure shows mean (solid line) and ±1 standard deviation (shade) in black for MoCAP and red for HPE. The bottom row shows the statistical relationship (SPM{t}) between joint angle measures across the gait cycle.

CONCLUSIONS
Our findings show that HPE is a promising tool for measuring kinematic parameters in clinical settings. However, it requires more comprehensive validation, including comparison to human clinician observations to understand its effective utility in clinical settings. Future research should focus on the variance introduced by anatomical regions, camera perspectives, and HPE models to further establish its reliability and accuracy.

REFERENCES
1. Baker R. In: Beth A. Winkelstein, eds. Orthopaedic Biomechanics 2012:419-444.
2. Kwolek B, et al., Multimedia Tools and Applications. 2019;78:32437-32465.
3. Bazarevsky V, et al. CVPR Workshop on Computer Vision for AR/VR. IEEE; 2020.

Modelling individual variation in human walking gait across populations and walking conditions via gait recognition

[1]Kayne A. Duncanson, [2]Fabian Horst, [3]Ehsan Abbasnejad, [4]Gary Hanly, [5]William S.P. Robertson and [1]Dominic Thewlis

[1]Adelaide Medical School, The University of Adelaide, Adelaide, AUS
[2]Department of Training and Movement Science, Johannes Gutenberg-University, Mainz, GER
[3]Australian Institute for Machine Learning, The University of Adelaide, Adelaide, AUS
[4]Information Sciences Division, Defence Science and Technology Group, Edinburgh, AUS
[5]School of Electrical and Mechanical Engineering, The University of Adelaide, Adelaide, AUS
email: kayne.duncanson@adelaide.edu.au

INTRODUCTION

Detecting and explaining variation in bipedal walking gait enables efficient human characterisation in healthcare and security. Both domains would benefit from a deeper understanding of individual level variation in gait but they traditionally employ disparate methods. This study combined the strengths of research in healthcare (e.g., measurement standards) and security (e.g., multivariate modelling) to enable simultaneous characterisation of individual, group and dataset level variation in gait. The aim was to investigate if demographic attributes and walking conditions affect the distinguishing features of gait.

METHODS

This study used four large-scale walking ground reaction force (GRF) datasets from around the world: AIST, Gutenberg, GaitRec and ForceID-A [1-4]. Acquired in different countries for different purposes, these datasets collectively represent a diverse set of population demographics and walking conditions. Machine learning models (20 different neural network architectures) were developed and evaluated for gait-based person recognition using 72 different configurations of the datasets, namely: I) Same-dataset configurations, where models were trained, validated and tested on separate groups from a given dataset; II) Mixed-dataset configurations, where a given training set from Part I was updated to include at least one other dataset; and III) Cross-dataset configurations, where models were trained and validated on at least one dataset and then tested on a novel dataset. An input sample was defined as the filtered and normalised (time: linear interpolation, scale: z-score) GRF and center of pressure measures from a gait cycle. Datasets were balanced to contain 1850 samples (185 individuals × 10 samples). Performance was measured as mean recognition accuracy over five-fold cross-validation. Uniform Manifold Approximation and Projection (UMAP) and occlusion sensitivity analysis were used as Explainable AI (XAI) tools to gain insights into the performance of the models.

RESULTS AND DISCUSSION

Models developed on GaitRec and ForceID-A achieved high performance on all four datasets, whereas models developed on AIST and Gutenberg only achieved high performance on these datasets (e.g., Table 1 – rows). Models developed and evaluated on GaitRec or ForceID-A performed worse than models developed on either of these datasets and evaluated on AIST or Gutenberg. Performance trends and XAI analyses indicated that dataset level differences in footwear, walking speed, mass, sex and height altered relationships among individual gait patterns. For example, Figure 1 shows that barefoot, preferred speed samples (AIST and Gutenberg) were mapped separately to shod, multi-speed samples (GaitRec and ForceID-A).

Table 1: Accuracy of top five architectures based on the dataset used for development (rows) vs. evaluation (columns) in parts I and III. *Shod samples from healthy individuals.

	AIST	Gutenberg	GaitRec*	ForceID-A
AIST	100%	96-98%	64-77%	63-75%
ForceID-A	99%	96-98%	91-97%	89-96%
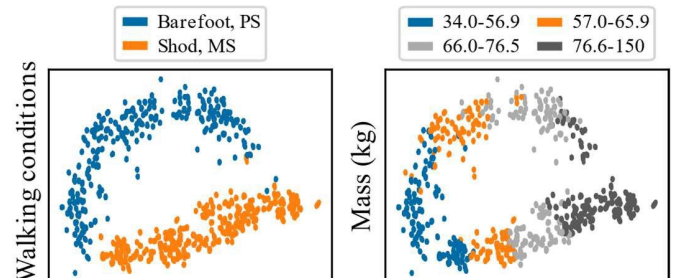
Figure 1: UMAP of features extracted from gait samples in a training set comprising all four datasets. PS = preferred speed, MS = multi-speed (either slow, preferred or fast).

CONCLUSIONS

The defining features of gait can be affected by multiple demographic attributes and walking conditions that vary across datasets. Machine learning gait recognition models developed on large and diverse GRF datasets are a promising means to personalise gait analysis in healthcare and security.

REFERENCES

1. Kobayashi Y, et al., AIST Gait Database. https://unit.aist.go.jp/harc/ExPART/GDB2019_e.html, 2019.
2. Horst F, et al., *Sci. Data*. **8**:232, 2021.
3. Horsak B, et al., *Sci. Data*. **7**:143, 2020.
4. Duncanson KA et al., *Sensors*. **23**:3392, 2023.

A Digital Twin Platform for Joint Motion Measurement and Task Classification in the Home

[1]Zhou Fang, [1]Mohammad Yavari, [1]Yiqun Chen, [1]Davood Shojaei, [1]Peter Lee, [1]Abbas Rajabifard, [1]David Ackland
[1]Faculty of Engineering and Information Technology, The University of Melbourne, Parkville, VIC
email: zhouf1@student.unimelbe.du.au

INTRODUCTION

Mobility conditions such as arthritis and age-related physical decline are significant global health concerns. Older adults with mobility conditions are particularly susceptible to injuries, especially within the home environment where most falls and accidents most commonly occur [1]. The ability to remotely monitor movement and assess mobility in the home setting has application in identifying sedentary behaviour, evaluating rehabilitation, fall prevention, and tele-medicine. However, this environment presents unique challenges in measuring movement over extended periods due to the variability and complexity of daily activities. Wearable technology has demonstrated capacity to quantify joint movement and classify tasks wirelessly and unobtrusively, but significant challenges remain in sensor data processing and interpretation for users without technical expertise. To address these challenges, a digital twin framework was developed, defined as a virtual replica of the home that supports measurement and visualisation of human movement in real-time [2]. The aim of this study was to employ this framework to assess accuracy of monitoring human movement and classification of movement patterns using wearable sensors and an indoor spatial tracking system.

METHODS

Ten healthy subjects (6 female and 4 male, age: 27.7±1.8 years) were recruited. Human movement experiments were conducted inside a fully furnished single-bedroom apartment containing five living areas: a kitchen, living room, study, bathroom and bedroom (Fig 1A). Participants were instructed by an operator to perform up to 19 upper and lower limb tasks of daily living in random order, such as tooth brushing, lifting, hair combing, sit to stand, lying on a bed, and walking over a duration of 2 hours. Twelve IMUs (Inertial Measurement Units) placed on body segments were used to calculate joint angles during tasks [3]. Four video cameras placed in the lab were used to capture each subject's movements and time-stamp each task. A UWB (Ultra-wideband) indoor GPS sampling at 5 Hz, and accurate to 5cm, was used to track real-time indoor spatial location. The UWB coordinate system was registered to a digital model of the home, which was created by 3D scanning the home interior using Matterport. A machine learning model was then developed to classify tasks from IMU data. The model was subsequently validated against the reference task labels from the video footage.

RESULTS AND DISCUSSION

On average, subjects spent 36.4±5.6, 11.1±5.6, 31.0±5.1, 25.5±5.6, and 22.5±5.1 minutes in the bedroom, kitchen, living room, study, and bathroom, respectively. The mean total distance walked by each participant over the 2 hours was 1,605±663 meters (Fig.1B). The averaged task classification accuracy for the 10 leave-one-subject-out tests was 82.3%, with the highest test accuracy of 89.3%. Tasks with distinctive and repetitive patterns, such as tooth brushing and food chopping, were recognised with the highest accuracy (>95%), and the quantitative mobility features derived from IMU joint angles such as the maximum shoulder elevation were predicted more accurately compared to transient tasks with higher variability, such as door opening and reaching (<90%) (Table 1). However, seated tasks, such as chair sitting, and working at desk, resulted in lower classification accuracy due to fewer distinct posture and movement features.
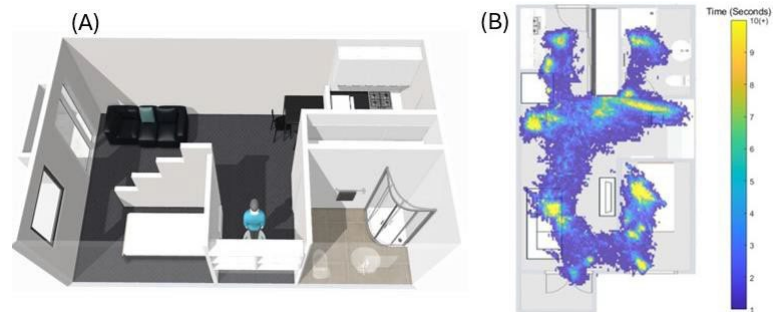
Figure. 1(A) A three-dimensional render of the digital twin lab, and (B) heatmap of the average time participants spent in each living lab.

CONCLUSIONS

This study developed a digital twin platform that can be used to visualize human activities of daily living in the home, calculate joint angles and analyse levels of mobility wirelessly. Task recognition in the home showed the highest accuracy for movements with distinctive features, and mobility metrics evaluated using IMUs closely matched reference values. This framework supports remote classification of continuous daily activities at home, such as grooming, meal preparation, and navigating in the living space. The performance of our platform may be further enhanced using advanced classifiers including deep learning algorithms. This framework will have application for mobility tracking and analysis in telemedicine and aged-care facilities.

REFERENCES

1. Sjögren H, et al., *Accid. Ana. Prev.* **21,** 3, 1989
2. Lattanzi L, et al., *Int. J. Comput.Integr.Manuf.* **34,** 6, 2021
3. Fang Z, et al., *Sensors.* **23,** 6535, 2023.

Table 1: Shoulder joint mobility metrics during selected tasks. Abbreviations include: Recog., Recognised; Ref., reference.

Task	Tooth brushing		Food chopping		Door opening		Picking up		Reaching		Working at desk	
Classification accuracy (%)	96.5		97.8		89		95		88.8		93.8	
Mobility metircs	Recog.	Ref.	Recog.	Ref.	Recog.	Ref.	Recog.	Ref.	Recog.	Ref.	Recog.	Ref.
Cumulative task duration (s)	169.0	170.3	241.8	240.5	165.1	171.6	163.8	156	174.2	158.6	367.9	348.4
Max. shoulder elevation (^{o})	78.3	78.5	38.9	39.0	45.7	52.4	73.7	83.7	57.9	59.8	73.2	79.0

Monday, December 2

ANZORS Podium 1

INVESTIGATING VARIATIONS IN ELASTIN CONTENT ACROSS DIFFERENT HUMAN TENDONS AND LIGAMENTS

[1,2]Maya Braun, [1,3]Carina Blaker, [1,2]Samantha Hefferan, [1,2]Dylan Ashton, [1,2]Christopher Little, [1,2]Elizabeth Clarke

[1]The Kolling Institute, University of Sydney and Northern Sydney Local Health District, [2]Sydney MSK Health, School of Medical Sciences, Faculty of Medicine and Health, University of Sydney, [3]Faculty of Science, University of Sydney, Sydney, NSW
email: mbra4709@uni.sydney.edu.au

INTRODUCTION

Tendons and ligaments are crucial for the musculoskeletal system in both humans and animals, transmitting forces from muscles to bones and stabilising joints during movement. However, these tissues are commonly affected by traumatic injury, accounting for ~50% of all musculoskeletal injuries in the US [1]and contributing to $416 million in annual healthcare costs in Australia [2]. Age-related degeneration, and chronic diseases, such as tendinopathy can also lead to discomfort, pain and increased susceptibility to wider degenerative joint disease [3].

Whilst the composition of tendons and ligaments, including collagen, glycosaminoglycans (GAGs), and proteoglycans, is well-documented, the quantification of elastin content in human tendons and ligaments remains largely unexplored. Elastin is a critical component of the extracellular matrix (ECM), assisting storage and recoil under load[4]. Previous studies have primarily focused on various animal tendons, ligaments, and skin, including bovine, porcine, and rodent tissue [4]. Determining the elastin content of human tendons and ligaments will allow a more comprehensive understanding of these tissues, so that we can develop grafts that mimic the natural composition and understand why certain tendon and ligament injuries are more common.

METHODS

The elastin content of tendons and ligaments from 8 fresh-frozen cadaveric donors aged 49-65 years (3 females, 5 males) with no known history of musculoskeletal injuries or conditions was measured using the Fastin^{TM} Elastin Assay, a colorimetric method that uses a synthetic porphyrin dye (TPPS) to bind elastin. A total of 400 samples have been analysed from 50 individual tissues including 15 lower limb and 31 upper limb tendons, and 4 knee ligaments.

Tissue samples weighed between 5-10 mg (dry weight). Elastin was extracted and solubilised into α-elastin by heating tissue samples in hot oxalic acid (95-100°C) for 1 hour (2-3 extractions per sample). A standardised sample volume of 50 µL was then used to measure the amount of elastin-bound dye at an absorbance peak of 513 nm. The elastin concentration was determined using a linear standard curve with known elastin concentrations ranging from 5 to 70 µg, corresponding to absorbance readings between 0.05 and 1.0 respectively.

The elastin content was normalised by dry tissue weight and analysed using mixed-effects linear regression (covariates: age, sex, height, and weight). Pairwise comparisons will determine differences between ligaments and tendons. The correlation between elastin content and tissue biomechanical properties (strength and elastic modulus) will be analysed.

RESULTS AND DISCUSSION

While previous literature posits a typical elastin content range of 1%-5% in bovine tendons, and 3% in equine tendons, our investigation unveiled a broader spectrum ranging from 1.8-13% across multiple different human tendons and ligaments. Thus far results have yielded an upper limb tendon range of 2.6-13%, a lower limb range of 1.8- 11%, and the knee ligaments range of 2.1- 9.5%. Previous findings of the human Achilles tendon found a 2.1% elastin content [5], whereas we found a range of 5.8-8.8%, which is almost triple what was previously identified. This indicates that previously reported values for elastin content in tendons and ligaments are not broadly applicable to all human tendons and ligaments.

CONCLUSIONS

This study addresses the gap in understanding of elastin content in human tendons and ligaments. Our results show a broader range of elastin content in human tendons and ligaments than previously reported in animal studies. This research enhances our knowledge of tissue composition and informs the development of better grafts and treatments for tendon and ligament injuries. Further analysis will clarify the relationship between elastin content and biomechanical properties, aiding clinical applications and injury prevention.

ACKNOWLEDGEMENTS

REFERENCES

1. Jung, H.J., et al., *Sports Med Arthrosc Rehabil Ther Technol,* **1**(1): p. 9, 2009.
2. AIHW. *Health Expenditure*. AIHW: Canberrra, 2023.
3. Hashemi, J., et al., *Clin Biomech*, **20**(6): p. 645-652, 2005.
4. Kannus, P. *Scand J Med Sci Sports*, **10**(6): p. 312-20, 2000.

Targeting Oxr1 to regulate osteoclast differentiation and function

[1,2]Xiaojun Chen, [1,3]Xiangyun Jin, [2]Killugudi Swaminatha Iyer, [1]Nathan J. Pavlos, [2,4]Haibo Jiang and [1,2]Kai Chen

[1]School of Biomedical Sciences, [2]School of Molecular Sciences, The University of Western Australia, Perth, WA
[3]Renji Hospital, School of Medicine, Shanghai Jiao Tong University, Shanghai, China
[4]Department of Chemistry, University of Hong Kong, Hong Kong, China
Email: xander.chen@research.uwa.edu.au

INTRODUCTION

Osteoclasts are unique bone-digesting cells that regulate skeletal homeostasis. Aberrant osteoclast formation and function contribute to detrimental bone disorders, such as osteoporosis and Paget's disease [1]. Here, we identified the novel role of oxidation resistance 1 (Oxr1) in osteoclast biology and revealed its previously unknown mechanisms driving autophagy during osteoclast formation.

METHODS

We integrated scRNA-seq with bulk RNA-seq analysis and identified Oxr1 as a signature regulator during osteoclast differentiation. Immunostaining was used to spatially define the Oxr1 expression in the bone microenvironment. This was followed by the verifications using qPCR and Western Blotting (WB) assays. Gene knock-down, using siRNA targeting Oxr1, was combined with bulk RNA-seq, bone resorption assay, and electron microscopy (EM) to investigate the effects of Oxr1 deficiency on osteoclast formation *in vitro*. Mechanistically, we used co-immunoprecipitation (CO-IP) and surface plasmon resonance (SPR) assays to identify the target that directly interacts with Oxr1. Furthermore, we used high-throughput *in silico* screening by docking drug molecules into the Oxr1 protein structure to repurpose clinical-stage therapeutics for osteoporosis treatment using preclinical animal models.

RESULTS AND DISCUSSION

Immunostaining of murine bone tissue revealed that Oxr1 is specifically expressed in osteoclasts (**Figure 1A**), as compared with other bone cell types, and the expression of Oxr1 significantly increased during osteoclastogenesis. Intriguingly, Oxr1 knockdown inhibited osteoclast differentiation and bone resorption (**Figure 1B**), for which EM revealed the disrupted mitochondria integrity (**Figure 1C**) and the bulk RNA-seq suggested the downregulated oxidative phosphorylation and autophagy. Given Oxr1's previously known antioxidant capability [2], we reasoned that Oxr1 is important for maintaining mitochondria redox homeostasis during osteoclast formation. CO-IP and SPR assays (**Figure 1D**) further revealed that Oxr1 directly binds to Keap1, which is known to essentially mediate the P62-independant autophagy (mitophagy) through mitochondrial ubiquitination [3]. This is consistent with our EM results which indicated the accumulations of autophagosomes following Oxr1 knockdown (**Figure 1C**), probably due to compromised degradation. Therefore, our results supported the notion that Oxr1 stabilises the P62-Keap1 interactions and promotes autophagy to facilitate osteoclast formation. Next, two FDA-approved drugs, Velpatasivr and Thiothixene, were

discovered as directly binding to Oxr1, inhibiting osteoclast differentiation, and preventing estrogen deficiency-induced bone loss.
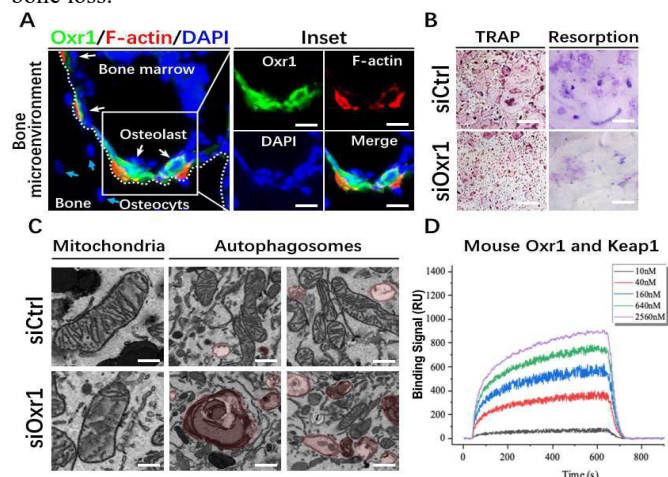
Figure 1. **A**. Oxr1 is highly and specifically expressed in osteoclasts. Scale bars, 10 μm. **B**. Oxr1 knockdown inhibits osteoclast formation and function *in vitro*. Scale bars, 50 μm.
C. Oxr1 deficiency leads to compromised mitochondria integrity and autophagy. Autophagosomes are coloured in red. Scale bars, 500 nm. **D**. SPR assay indicates the direct interactions between Oxr1 and Keap1. Keap1 were diluted into five concentrations and primed through the chip surface that printed with Oxr1 protein.

CONCLUSIONS

Oxr1 is required for osteoclast differentiation and could serve as a promising therapeutic target for osteoclast-related bone disorders.

REFERENCES

1. Veis DJ, et al., *Annu Rev Pathol*. **18:**257-281, 2023.
2. Lin X, et al., *Genome Biol. 24(1):216*, 2023.
3. Yamada T, et al., *Cell Metab.,* **28(4):**588-604, 2018.

AGE-ASSOCIATED PROTEOMIC CHANGES IN A MOUSE MODEL OF KNEE OSTEOARTHRITIS

[1,2,3]Carina Blaker, [2]Raymond Andriono, [2]Matthew McKay, [2]Linze Li, [1,2,3]Sanaa Zaki, [2]Mark Molloy and [2,3]Christopher Little

[1]Sydney School of Veterinary Science, Faculty of Science, University of Sydney, Sydney, NSW
[2]Kolling Institute, Faculty of Medicine & Health, University of Sydney and Northern Sydney Local Health District, Sydney, NSW
[3]Sydney Musculoskeletal Health, University of Sydney, Sydney, NSW
email: carina.blaker@sydney.edu.au

INTRODUCTION

Osteoarthritis (OA) affects over 2 million Australians and accounts for an estimated $4.3 billion in annual healthcare costs [1]. OA becomes increasingly common with age and is the leading cause of disability in adults [2]. In the absence of a cure, global cases of this chronic and progressive disease are expected to increase by up to 75% over the next 25 years [2]. The development of new therapeutics requires an improved understanding of the complex pathophysiology of OA alongside changes associated with natural ageing. This study aimed to investigate underlying age and OA-associated molecular changes in a preclinical mouse model of knee OA.

METHODS

Formalin-fixed, paraffin embedded knee joints from young (6 months) and aged (18 months) male C57BL/6 mice (n=4/group) were evaluated for structural OA histopathology and proteome changes. Sections were collected from all three knee compartments: medial and lateral tibiofemoral joints (MTF, LTF), and the patellofemoral (PF) joint. Cartilage, subchondral bone and synovial pathology were scored by 2 blinded scorers (CB/CL) at standardised levels within each compartment. The remaining sections were pooled within each compartment and proteins extracted using a mechanical, trypsin digestion. The digested proteins were analysed using a data-independent acquisition mass spectrometry workflow and peptides with > 1% false discovery rate were removed. Histological results were analysed using non-parametric Mann-Whitney U tests while differentially expressed proteins were evaluated using two-sided t-tests.

RESULTS AND DISCUSSION

Cartilage significantly worsened with age in both MTF and LTF compartments (Fig 1A; $p < 0.05$) while the PF joint was unaffected. Subchondral bone scored worse in MTF but did not significantly change with age in any compartment (Fig 1B). Synovial tissues similarly had no age-/OA-associated changes (Fig 1C). Over 2000 proteins were identified in each age-group and compartment. Between 75-80% of these proteins were shared across compartments within each age-group. The most notable differences observed occurred between age groups (Fig 2), and included extracellular matrix proteins (e.g. collagens 1, 6 and 9); glycoproteins (e.g. lubricin); and cytokines (e.g. IL-17, TGFB1). While the proteins identified aligned with the expected composition of joint tissues and the proteomic profiles changed substantially with age, there were few compartment-specific changes that aligned with histological indicators of structural OA.
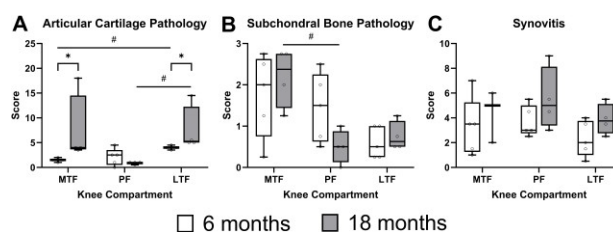
Figure 1: Age-associated OA histopathology: A) cartilage; B) subchondral bone; C) synovitis. Box plots (min to max) across the medial and lateral tibiofemoral compartments, and the patellofemoral joint (MTF, LTF, PF). # $P < 0.05$ between compartments. * $P < 0.05$ between 6 and 18 months.
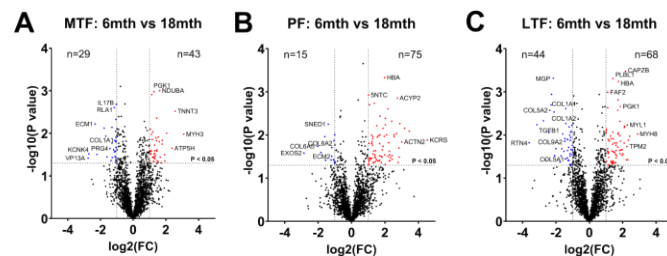
Figure 2: Differentially expressed proteins between 6- and 18-month old mice within knee compartments: A) medial tibiofemoral; B) patellofemoral; C) lateral tibiofemoral. Proteins that were less abundant (blue dots) and more abundant (red dots) with age were identified as having a P-value < 0.05 (-log10P > 1.3) and >2-fold change (log2FC >1).

CONCLUSIONS

The molecular profiles of knee compartments differed with age but were not always reflected in the structural pathology of individual joint tissues. However, disease-independent changes occurring within the joint as individuals age may still affect the progression of disease and response to treatment. Future research will investigate the functional pathways affected and how these differ between OA phenotypes to better understand OA pathophysiology across patient cohorts.

REFERENCES

1. AIHW, *Chronic musculoskeletal conditions.* 2024

2. GBD Collaborators, *Lancet Rheumatol* **5:** e508-522, 2023

The Rab7 Guanine Nucleotide Exchange Factor Complex Mon1-Ccz1-Rmc1 Differentially Regulates Osteoclast Formation, Bone Resorption and Endosome-To-Lysosome Maturation

[1]Yixiao Zhou, [1]Jamie Tan, [1]Nathan J. Pavlos

[1]Bone Biology & Disease Laboratory, School of Biomedical Sciences, The University of Western Australia, Nedlands, W.A. 6009
email: yixiao.zhou@research.uwa.edu.au

INTRODUCTION
Osteoclasts are giant multinucleated cells responsible for bone resorption, a process essential to the repair and maintenance of the skeleton. Imbalances in osteoclast activity or numbers lead to bone-wasting diseases such as osteoporosis and rare high bone mass conditions like osteopetrosis[1]. Osteoclasts resorb bone through the ruffled border membrane, a specialized endo-lysosomal organelle derived from the fusion of secretory lysosomes[2] with the bone-lining plasma membrane. Secretory lysosomes originate from the convergence of endosomes and lysosomes, a process regulated by the late-endosomal Rab7 GTPase[3]. Rab7 activation is mediated by its guanine nucleotide exchange factor (GEF) complex Mon1-Ccz1-Rmc1, which facilitates the transition from early endosomes (Rab5) to late endosomes (Rab7) along the endolysosomal pathway[4]. Despite the established function of Rab7 in osteoclast-mediated bone resorption, the contributions of the Mon1-Ccz1-Rmc1 complex to osteoclast formation, function and endo-lysosomal homeostasis remain unclear.

METHODS
Osteoclasts were differentiated *in vitro* from primary mouse bone marrow monocytes (BMMs) stimulated with cytokines (M-CSF and RANKL). Rab7/Mon1/Ccz1 and Rmc1 mRNA levels were specifically depleted in osteoclasts using small-interfering RNA (siRNA) directed against each target gene. Gene silencing efficacy and cell viability was assessed by qPCR, Western blotting (WB) and MTT proliferation assays, respectively. TRAP staining and WB analyses of osteoclast markers were used to monitor the effects of siRNAs on osteoclast morphology and differentiation. Bone resorption activity was assessed using toluidine blue staining and reflective optical microscopy. Cell morphology and endo-lysosomal phenotypes was quantified using immunofluorescence confocal microscopy. Transferrin recycling assays were used to visualise cargo endocytosis and recycling.

RESULTS AND DISCUSSION
Reduction of Rab7, Mon1(a/b), Ccz1, and Rmc1 expression in primary BMMs differentially altered their ability to form multinucleated TRAP-positive osteoclasts and diminished their capacity to resorb bone. This disruption corresponded with morphologically disturbances in the osteoclast endo-lysosomal system including the appearance of enlarged early endosomes as well as defects in endocytic cargo progression, indicating impaired endosome-to-lysosome maturation.

CONCLUSIONS
Our results demonstrate that components of the Rab7 GEF Mon1-Ccz1-Rmc1 complex play distinct yet overlapping roles in osteoclast formation, function, and endosome-lysosome maturation. This implies accessory roles for this GEF complex in osteoclasts that extend beyond Rab7 activation. Together these data provide new insights into osteoclast biology and lend support to the notion that targeting components of the osteoclast endo-lysosomal system may be an alternative therapeutic avenue for bone-wasting diseases like osteoporosis[5].

ACKNOWLEDGEMENTS

REFERENCES
1. Boyle WJ, Simonet WS, Lacey DL, *Osteoclast differentiation and activation*., Nature, **423:**337-342, 2003.
2. Cappariello A, Maurizi A, Veeriah V, Teti A, *The Great Beauty of the osteoclast*., Arch Biochem Biophys, **558:**70-78, 2014.
3. Borchers AC, Langemeyer L, Ungermann C, *Who's in control? Principles of Rab GTPase activation in endolysosomal membrane trafficking and beyond*., J Cell Biol, **220:**e202105120, 2021..
4. Kümmel D, Herrmann E, Langemeyer L, Ungermann C, *Molecular insights into endolysosomal microcompartment formation and maintenance*., Biol Chem, **404:**441-454, 2022.
5. Ng PY, Brigitte Patricia Ribet A, Pavlos NJ. *Membrane trafficking in osteoclasts and implications for osteoporosis*. Biochem Soc Trans. **47:**639-650, 2019. doi: 10.1042/BST20180445. Epub 2019 Mar 5.

THE HISTORY DEPENDENCE OF MUSCLE CONTRACTION: INSIGHTS FROM A MUSCLE CONTRACTING AGAINST A SPRING

[1]Dean L Mayfield and [1]Natalie C Holt

[1]Evolution, Ecology, & Organismal Biology, University of California, Riverside, Riverside, California, USA
email: dean.mayfield@uqconnect.edu.au

INTRODUCTION
The mechanical output of skeletal muscle is influenced by contraction history. Stretch-induced force enhancement and shortening-induced force depression are long-lasting phenomena that underscore the history dependence of muscle contraction. Residual force enhancement (RFE) and force depression (FD) are typically studied by imposing lengthening or shortening upon the muscle, respectively. We recently demonstrated with an isolated muscle preparation attached in-series to a spring that substantial FD can occur even during an isometric contraction because active shortening occurs against the stretch of series elasticity. Whilst we predicted this outcome, we did not anticipate that recoil of the attached spring during muscle relaxation would result in active stretch and passive force enhancement (PFE), the passive component of residual force enhancement. Given the source of the stretch, the unconventional timing of stretch, and the preceding force depression, we observed PFE under unique conditions that may not only reveal valuable insight into the underlying mechanism but reveal a broader functional relevance for the history dependence of muscle contraction.

METHODS
We constructed active and passive force-length relationships from fixed-end contractions with and without added compliance for the semitendinosus muscle of 17 bullfrogs. PFE with added compliance was defined as elevated passive force after contraction compared to the passive force at a matched length prior to contraction (Figure 1A) and after contraction without added compliance.

RESULTS AND DISCUSSION
We observed significant PFE. For several muscles, PFE exceeded 10% of maximum tetanic force (P_0). PFE exhibited a strong dependence on fascicle length (Figure 1A); PFE was largely absent at lengths on the ascending limb (<0.90 L_0 [optimum length]) and most pronounced at the longest lengths studied (~1.50 L_0). Accordingly, PFE could not be predicted from active force and stretch amplitude alone. When effective spring compliance and stretch amplitude were accounted for, PFE increased in an almost linear fashion with increasing length but also exhibited a strong dependence on spring compliance (Figure 1B). Stretch-normalised PFE increased as a function of decreasing spring compliance at any given length. It is generally accepted that PFE is consistent with a passive structural element being engaged upon activation and producing elevated force

upon stretch. Our finding that stretch-normalised PFE decreased with increasing spring compliance could indicate that active shortening slackens this passive element. Alternatively, greater FD with increasing spring compliance may indicate that active shortening during activation interferes with the engagement of a passive element. Faster rates of spring recoil with increasing compliance may also be responsible since fast stretches can partly inhibit or abolish PFE.
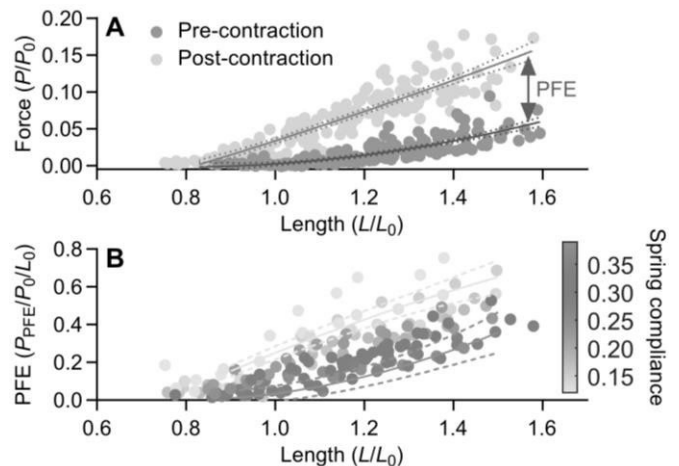
Figure 1: (A) Passive force before and 2 s after the end of stimulation (n =17). (B) PFE normalized to stretch amplitude (n = 17). L_0, optimum length; P_0, maximum tetanic force.

CONCLUSIONS
Our findings demonstrate the impact of stretch imposed upon relaxing muscle, highlighting the importance of considering the delay between electrical 'inactivity' and deactivation under dynamic conditions. Using a more conventional shorten-stretch cycle, shortening attenuates or abolishes PFE, indicating that shortening slackens the spring-like element engaged during isometric force development. We provide further evidence that shortening preceding stretch limits PFE. However, since shortening occurred during force development, and appreciable PFE arose when shortening and stretching were of equal magnitudes, shortening during force development may have a unique effect on PFE.

ACKNOWLEDGEMENTS

An in vivo Imaging Study of Fascia Thickness and Muscle Volume in the Lower Limb of Healthy Adult Humans

[1]M. Randika Perera, [2,3]Paul Condron, and [1]Geoffrey Handsfield

[1]Musculoskeletal Modeling Group, Auckland Bioengineering Institute, University of Auckland, New Zealand
[2]Matai Medical Research Institute, Gisborne, New Zealand.
[3]Faculty of Medical and Health Sciences Centre for Brain Research, The University of Auckland, Auckland, New Zealand
email: mper162@aucklanduni.ac.nz

INTRODUCTION

Connective tissue structures play a crucial role in human and animal movement mechanics. Skeletal muscle, central to force generation, works with connective tissues to transmit force [1]. Muscle volume, an essential metric derived from imaging, helps assess muscle functional capacity and quality[2]. Recent developments in medical imaging have made direct in vivo investigation of connective tissues possible via MRI, e.g. imaging of fascia. Recent studies[3] have inspired interest in whether in vivo fascia thickness may correlate with body size and muscle size in humans. Current literature has limited studies on muscle and fascia together, and none have addressed fascia thickness alongside muscle volumes in vivo. Here, we use advanced MRI to image the fascia in vivo in lower limbs of 30 healthy adults, aiming to assess muscles, fascia, and bones. We determine the relative volumes and lengths of muscles and bones, measure fascia thickness in the thigh and shank, and explore how these scale with deep fascia, mass, sex, and age.

METHODS

We imaged the thigh and calf region of thirty adult participants on a 3T MRI scanner using a dual-echo ultrashort echo time (UTE) non-Cartesian sequence with unique vendor versions [4]. In plane spatial resolution was 0.7 x 0.7 mm^2, slice thickness was 4mm. Post-processing methods were used to increase contrast. Following image acquisition, segmentation was performed for deep fascia, bones and lower limb muscles using ITK Snap software on axial images. We developed a custom algorithm to compute thickness spatially throughout the lower limb and we explored possible relationships between muscles, bones, fascia and variables of mass, age and sex.

RESULTS AND DISCUSSION

Fascia thickness of the thigh and calf regions were 1.0564±0.208 mm and 0.9632±0.089 mm, respectively, which is consistent with literature. We observed a statistically significant positive relationship between thigh fascia thickness & thigh muscle volume as well as a significant negative relationship between age and thigh fascia thickness. In contrast, both calf muscle volume and tibia volume showed a negative correlation with fascia thickness in the calf. Similar to the thigh region, age showed a significant negative correlation with calf fascia thickness. Body mass did not significantly influence calf fascia measurements, although we found a non-significant positive trend with thigh fascia thickness. It should be noted that these relationships were all relatively statistically weak. Further exploration is needed to add power to the present findings and determine additional relationships between body measurements and fascia thickness.

CONCLUSIONS

Using advanced MRI, this study assessed fascia thickness, muscle volumes, and bone volumes in the lower limbs of 30 healthy subjects. The findings revealed significant variation in fascia thickness among individuals, with notable correlations between fascia thickness and age, muscle volumes, and body weight in the thigh area. In the calf, muscle volume, tibia volume, and age all negatively correlated with fascia thickness. These relationships, though statistically weak, highlight the need for further research to better understand the connections between body measurements and fascia thickness.

ACKNOWLEDGEMENTS

REFERENCES

1. Mukund & Subramaniam., (2020), S Sys. Bio. & Med.12:1-46
2. Handsfield, G., (2014), Journal of Biomechanics, 47(3), 631–638.
3. Schleip, R., (2019), Frontiers in Physiology, 65(2), 273–277.
4. Qian et al., (2008), Magn Reson Med.60:135-145
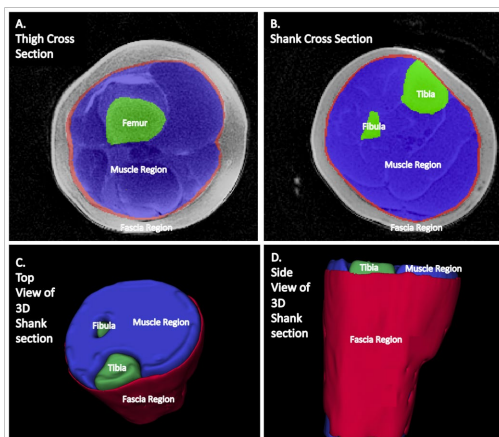
Figure 1-Visual representation of the segmentation and reconstruction of tibia, femur, muscle sections, and the encasing fascia. Muscles, bones, and fascia were segmented in axial MR Images (A and B) and reconstructed in 3-D (C and D) to obtain volumes.

Monday, December 2

ABC Podium 2
Sports biomechanics

ANZSB
anzsb.asn.au

DANGEROUS HIGH TACKLES IN RUGBY: MEASURING WHAT HAPPENS TO THE OPPONENTS HEAD

[1,2]Elizabeth Bradshaw, [3]Alex Conte-Biggar, [4]Brad Morris, [1]Eric Drinkwater, [4]Patria Hume, and [4]Doug King

[1]Centre for Sport Research, Institute of Physical Activity and Nutrition, Deakin University, Melbourne, VIC, Australia.
[2]Sports Performance Research Institute New Zealand (SPRINZ), Auckland University of Technology, Auckland, New Zealand.
[3]Department of Physiotherapy, Division of Allied Health, Austin Hospital, Melbourne, VIC, Australia.
[4]School of Science and Technology, University of New England, Armidale, NSW, Australia.
Email: liz.bradshaw@deakin.edu.aui

INTRODUCTION

Rugby poses a risk of injury due to the high contact nature of play, and high forces that are imparted onto the athletes' bodies. Concussion in rugby (league, union) [1] accounts for 9% of all injuries within legal play, increasing to 29% of all injuries that involve illegal gameplay [2]. The high shoulder tackle to the opponent's (receivers) head is an example of an illegal tackle that is frequently observed in match-play and contributes to these injury statistics [3]. Aside from specific match rules and infringement penalties, various strategies have been employed to lower the risk of head injury during rugby match-play including protective headgear. The purpose of this study was to develop a novel, contextually valid protocol for laboratory measurement of dummy head biomechanics, with and without headgear, during a high tackle by rugby players.

METHODS

A dummy was instrumented with an inertial measurement unit (IMU; 1200 Hz). Eleven rugby players with a shoulder placed IMU executed right shoulder high tackles to the left side of the dummy's head at a closing velocity of 5.83-6.39 m/s monitored by infra-red timing gates. Three randomised conditions were tested; no headgear, club-level and professional-level headgear. IMU peak resultant linear acceleration and rotational velocities for the player's shoulder and dummy's shoulder-head impact (impact 1) and head-ground impact (impact 2) were calculated. A classification system was used for adult football players, indicating a 50% likelihood of concussion at over 65.1 g/1747 rad/s² and a 75% likelihood at over 88.5 g/2296 rad/s². [4].

RESULTS AND DISCUSSION

A summary of the impact acceleration results is shown in Table 1. Testing identified that the shoulder-head collision (impact 1) had linear accelerations higher than 85 g, indicative of a 50% or greater likelihood of concussion injury. Rotational accelerations of the player's shoulder were very high (~5000 rad/s²). As a result, both shoulder-head & head-ground impact events were well above the 75% threshold for likelihood of concussion injury.

CONCLUSION

This study introduced a protocol measuring linear and rotational accelerations of a dummy's head during a high-speed rugby tackle where the player's shoulder hit the dummy's head and the dummy's head hit the floor. Trialling the protocol showed high impact accelerations experienced when receiving a tackle did not reduce with headgear. The experimental method developed provides the basis for more contextually valid and complete testing of head biomechanics in tackles.

REFERENCES

1. King D, et al., *Journal of Neurological Science.* **399**: 61-68, 2019.
2. Gardner A, et al., *British Journal of Sports Medicine*. **49**: 495-498, 2015.
3. McLellan TL, *International Sports Medicine Journal.* **15**, 328-332, 2014.
4. McIntosh AS, *BMJ Open*. **4**, e005078, 2014.

Table 1: Peak linear accelerations (g) and peak rotational accelerations (rad/s²) for the player's shoulder and dummy's head for three conditions (two with headgear) reported as MDN = median; IQR = inter-quartile range; and LOC = Likelihood of concussion rating.

Headgear Condition	Player's Should r MDN; IQR	LOC	Shoulder-Head Coll sion MDN; IQR	LOC	Head-Ground Collision MDN; IQR	LOC
Linear Accelerations (g)						
None	13.19; 4.26	1	87.77; 15.23	2	49.16; 9.84	1
Club-level	12.23; 4.58	1	101.76; 53.67	3	61.95; 44.46	1
Professional-level	11.44; 4.83	1	104.11; 12.62	3	51.61; 49.57	1
Rotational Accelerations (rad/s²)						
None	4935.30; 8315.23	3	6948.36; 1510.75	3	7122.72; 2276.49	3
Club-level	4825.33; 9880.25	3	6673.42; 1867.89	3	8433.95; 4012.75	3
Professional-level	5178.45; 4056.30	3	6592.21; 3222.03	3	5852.51; 4772.31	3

THE EFFECT OF HEAD-FORWARD POSTURE ON RISK OF LOWER NECK DISLOCATION DURING HEAD-FIRST IMPACTS: A PRELIMINARY COMPUTATIONAL AND DYNAMIC EXPERIMENTAL INVESTIGATION

[1]Mario Mongiardini, [2]Aaron Stevenson, [3]Claire Jones, [4]Ryan Quarrington

[1]Centre for Automotive and Safety Research, The University of Adelaide, Adelaide, SA [2]Spinal Surgery Unit, Royal Adelaide Hospital, Adelaide, SA [3]School of Electrical and Mechanical Engineering, The University of Adelaide, Adelaide, SA [4]Centre for Orthopaedic and Trauma Research, The University of Adelaide, Adelaide, SA

email: ryan.quarrington@adelaide.edu.au

INTRODUCTION

Subaxial cervical facet dislocation (CFD) is a severe neck injury that most often results from head-first impacts (HFI) [1]. Replicating CFD in computational and experimental HFIs has proven challenging, hindering the advancement of effective injury prevention strategies. Prior investigations have indicated that an eccentric head-forward posture and horizontal Frankfort plane (FP) at impact might elevate the risk of CFD [2]. Therefore, the aim of this study was to use computer simulations and dynamic *ex-vivo* experiments to investigate the effect of pre-HFI head eccentricity on head-neck kinematics, kinetics, and CFD risk.

METHODS

Simulations: HFI was simulated using a detailed head-neck model (GHBMC M50-HN v6.0; cephalus-T1; Fig 1A). T1 was rigidly connected to a geometrical representation of a 16 kg drop carriage [3] constrained to vertical translation only. After initial model reposturing to obtain a horizontal FP and the desired eccentricity (0 to 50 mm), a 2 m/s HFI was simulated. Impact and intervertebral loads, and kinematics, were extracted.

Experiments: Four fresh-frozen human cadaver head-necks (cephalus-T1) underwent inverted HFI drop tower experiments (2 m/s impact velocity). Horizontal FP and head eccentricity were controlled via a specimen-specific mount that attached the skull to an adjustable auxiliary parallel drop rail (Fig 1B). Head constraints were removed immediately prior to impact. Six-axis impact loads and drop carriage position were measured at 50 kHz. Kinematics were measured by tracking three-marker clusters embedded at each spinal level, and in the cephalus, using stereo-calibrated high-speed cameras (10 kHz). Injuries were identified via post-test inspection and CT scan. Qualitative kinematic analyses of the simulation and experimental data were performed; loads at key timepoints were extracted.

RESULTS AND DISCUSSION

HFI simulations have been completed for three head-neck postures with horizontal FP: 0 mm (neutral [E_N]); 30 mm [E_S]; and, 50 mm [E_L] eccentricity. In all simulations, the torso started compressing the neck ~1 ms after head impact, forcing the upper head-neck into extension and C7/T1 into flexion ("buckled" neck pose [1]) without concomitant head translation. Additional torso compression caused failure of C7/T1 supra- and interspinous ligaments. Subsequent head extension rotation and forward motion caused C7/T1 anterior shear translation (Fig 1C). Peak T1 compression forces were similar for all simulations (2.25-2.32 kN) but peak C7/T1
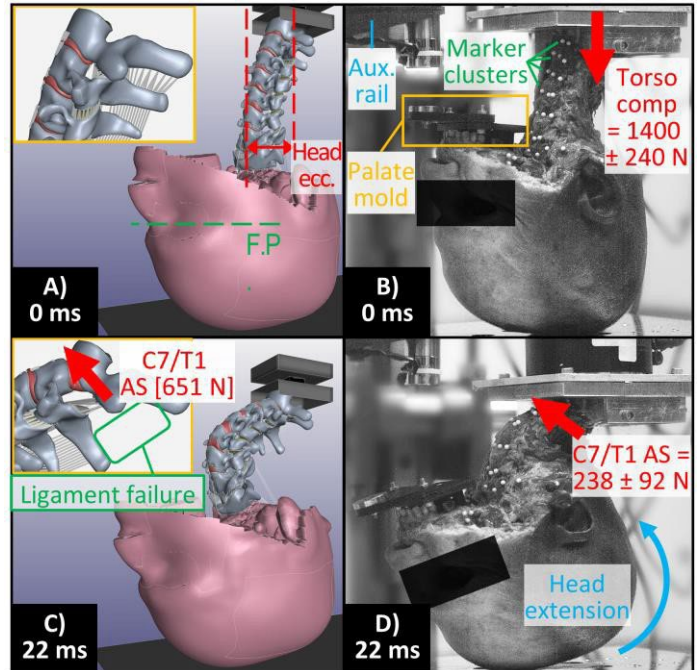
Fig 1. *Exemplar HFI simulations [left column] and experiments [right]. A-B) onset of loading. C-D) C7/T1 anterior shear (AS) causing CFD.*

anterior shear force (the primary contributor to CFD [1]) was largest for E_S (650.7 N; 315.0% and 29.6% ↑ than E_N and E_L, respectively). Therefore, the E_S posture was investigated experimentally. C7/T1 bilateral CFD was produced in 3 of 4 specimens; the other failed via T1 vertebral body fracture. Kinematics and kinetics preceding CFD closely followed the E_S simulation (Fig 1 C vs D), but limitations of tissue failure criteria prevented CFD occurring in the simulation. Despite these limitations, the GHBMC model appropriately simulated the pre-CFD head-neck response to HFI.

CONCLUSIONS

The results of this preliminary study indicate that CFD risk is highly sensitive to pre-HFI head eccentricity when the FP is horizontal, and that this posture produces neck trauma at lower impact velocities (2 m/s) than previously reported [3]. These findings will inform improved neck injury prevention devices.

REFERENCES

[1] Nightingale et al., *Clin Biomech* **64**:90-97, 2019. [2] Bauze et al., *JBJS* **60-B**: 239-45, 1978. [3] Nightingale et al., *J Biomech* **29**(3):307-18, 1996

EFFECT OF CONCUSSION ON SIDE-STEPPING BIOMECHANICS IN WOMEN'S AUSTRALIAN FOOTBALL

[1]Tess Rolley, [1]Natalie Saunders, [1]Ashlee Hendy, [2]Brendan Major, [3]Alicia Goodwill, [2]Sandy Shultz, [1]Aaron Fox

[1]Institute for Physical Activity and Nutrition (IPAN), Deakin University, Melbourne, Australia
[2]Monash University, National Trauma Research Institute, Melbourne, Australia
[3]Physical Education and Sport Science Academic Group, Nanyang Technological University, Singapore
email: tlrolley@deakin.edu.au

INTRODUCTION

Anterior cruciate ligaments (ACL) injuries and concussions are common in the women's Australian football league (AFLW)[1]. AFLW ACL injuries frequently occur when performing a reactive side-step cutting manoeuvre[2]. In this scenario, cognitive function plays a critical role in processing an opponent's movement cues to coordinate a movement response[3]. Concussion is known to negatively impact cognitive function[4] and is associated with increased lower limb injury risk, including ACL injuries[5]. We therefore sought to understand potential differences in cognitive performance and knee loading during side-stepping in recently concussed versus non-concussed women's Australian football players.

METHODS

Thirty-one women's Australian football players free from any current lower limb injury and any musculoskeletal disorders that affected the lower limb participated. Twenty participants (age = 24.32 ± 5.16 y; mass = 67.28 ± 8.04 kg, height = 1.69 ± 0.06 m) were allocated to a non-concussed (i.e. had not suffered a concussion in the last six-months), and eleven participants (age = 22.73 ± 3.84 y, mass = 69.8 ± 7.17 kg, height = 1.73 ± 0.06 m) to a concussed group (i.e. suffered a concussion in the last three-months). Cognitive performance was determined through a neurocognitive testing battery. Correct response reaction time and the percentage of accurate responses were assessed across various tests. Biomechanical analyses involved unanticipated performance of three sport-specific movements (45° side-step, 180° change of direction, straight line run) where a life-sized video stimulus dictated the task performed. Cognitive performance (independent t-tests) and three-dimensional knee joint moments (SPM1D independent t-tests)

from the 45º side-step were compared between the non-concussed and concussed groups.

RESULTS AND DISCUSSION

Concussed participants recorded a lower response accuracy (%) on the one-card learning test compared to non-concussed participants ($t = 2.48$, $p = 0.02$). All other cognitive test results were similar between groups ($p > 0.05$). The most challenging cognitive tasks (i.e. 3-Back, OCL), however, produced the lowest scores for response accuracy in the concussed group (Table 1) – suggesting that cognitive deficits may remain in more challenging scenarios. No statistically significant differences ($p > 0.05$) were identified for knee joint moments between groups. These findings conflict with the notion that concussion elevates ACL injury risk. However, the cognitive demand of the laboratory-based testing may fall short of that in a sport-specific environment – and this elevated cognitive demand may be a factor in increasing knee injury risk.

CONCLUSIONS

Cognitive performance and knee loading during a side-step were similar between non-concussed and concussed women's Australian football players. Further work is required to determine the underlying mechanism surrounding elevated lower limb and knee injury risk post-concussion.

REFERENCES

1. 2022 AFLW Injury Report – Season 7, AFL Doctors Association.
2. Rolley T, et al., *Sci Med Football.* 2023;7(2):106-23.
3. Swanik C et al., *Am J Spoets Med.* 2007;35(6):943-8
4. Voormolen D et al., *Injury.* 2019;50(5):1068-74
5. McPherson A et al., *Sports Med.* 2020;50(6)1203-10

Table 1: Cognitive performance results between the non-concussed and concussed groups.

	S-RT	4-RT	1-Back	2-Back	3-Back	OCL*	Sport-RT
Reaction Time (ms)							
Non-Concussed	276.0 ± 26.4	441.0 ± 55.3	890.7 ± 316.5	1374.6 ± 546.9	1998.5 ± 1034.6	1334.0 ± 368.7	-58.4 ± 82.4
Concussed	276.2 ± 15.9	444.5 ± 36.7	911.1 ± 345.4	1530.4 ± 440.7	1694.3 ± 452.1	1243.9 ± 372.5	-67.4 ± 68.5
Response Accuracy (%)							
Non-Concussed	100.0 ± 0.0	94.3 ± 9.2	98.0 ± 3.7	86.9 ± 9.3	84.6 ± 6.2	83.0 ± 5.2	97.1 ± 2.1
Concussed	100.0 ± 0.0	84.3 ± 25.1	99.6 ± 0.8	88.2 ± 7.8	79.5 ± 12.8	78.5 ± 4.5	96.7 ± 3.0

S-RT – simple reaction time; 4-RT – 4-choice reaction time; 1/2/3-Back – one/two/three-back learning; OCL – one-card learning; Sport-RT – sport-specific reaction time test; * - statistically significant difference in response accuracy between groups

Investigating a Sports Science Approach to Warm-Up Practices in Dance: Can We Improve Dance Performance?

Michelle Briggs[1,2], Annie Jeffries[2,3,4], Karen J Mickle[1,2]

[1]Applied Sport Science and Exercise Testing Laboratory, University of Newcastle, Ourimbah, Australia.
[2]School of Biomedical Science & Pharmacy, College of Health, Medicine and Wellbeing, University of Newcastle, Australia.
[3]Active Living Program, Hunter Medical Research Institute, Australia.
[4]Faculty of Health, School of Sport, Exercise and Rehabilitation, University of Technology Sydney, Australia.
Email: michelle.briggs@uon.edu.au

INTRODUCTION

Dancers require a distinctive skill set, through the combination of both artistry and athleticism in their performance. Unlike many sports, dance movements requires both strength and flexibility [1]. Traditionally, a dancer warms-up by extensively holding static stretches, to support the range of motion (ROM) required to aesthetically execute movements [1, 2].

Static stretching in warm-ups has raised concerns in other sports, due to possibly temporarily reducing muscle strength and power [3]. Therefore, research conducted on other athletic populations suggests that dynamic stretching may produce superior performance qualities, compared to static stretching [4]. However, dance research is limited regarding the effects of different warm-up methods on performance. Due to this, there is a need for further research investigating the effects of warm-ups, to provide dancers with evidence-based training methods to ultimately enhance performance.

METHODS

Ten high-level dancers (9 female, 1 male), aged 13.7 ± 2.5 years, were assessed on three occasions, using a double-blinded study design. Each session started with a cardiovascular warm-up, followed by one of three randomly selected stretch conditions, either static stretching, dynamic stretching, or no stretching (control). Immediately following this, the participants performed a single-leg balance, countermovement jump (CMJ), hop and ROM tests (active straight leg raise test, hip abduction, Thomas test, ankle dorsiflexion). A repeated-measures ANOVA was used to determine whether warm-up type influenced each performance measure ($P<0.05$).

RESULTS AND DISCUSSION

Post-hoc analysis revealed that dynamic stretching significantly increased left hop vertical jump height (Figure 1 – A) and take-off velocity, compared to the control and static stretching ($p < 0.05$). There was no main effect of warm-up on the CMJ ($p > 0.05$), although there was a 6% improvement in jump height, compared to the control and static stretching conditions (Figure 1 – B). There was no main effect found for the balance and ROM tests ($p > 0.05$).

This is the first study to examine the acute effects of warm-up protocols on single-leg movements in dance. In this study, we found that dynamic stretching significantly increased left hop jump height and take-off velocity when compared to the control and static stretching warm-ups. This finding suggests that

incorporating dynamic stretching into a warm-up may offer distinct advantages for enhancing skills requiring single-leg movements in dance.

Figure 1: Means and Standard Deviations for left hop (A) and CMJ (B) vertical jump height (cm), following each warm-up.

CONCLUSIONS
Dynamic stretching in a warm-up can increase a dancer's jump height, particularly for a single-leg take-off. Furthermore, balance and ROM were not significantly impacted by the warm-up protocols. Therefore, it is proposed that dynamic stretching will offer greater advantages in comparison to static stretching and should be adopted in dance practices. This study underlines the need for the dance community to prioritise evidence-based practices to achieve peak performance.

REFERENCES
1. Morrin, N. and E. Redding, *Acute Effects of Warm-up Stretch Protocols on Balance, Vertical Jump Height, and Range of Motion in Dancers.* Journal of Dance Medicine & Science, 2013. **17**(1): p. 34-40.
2. Zaggelidou, E., et al., *The effect of different types of warm- up protocols on the range of motion and on motor abilities of rhythmic gymnastics athletes and ballet dancers.* Central European Journal of Sport Sciences and Medicine, 2023. **42**: p. 31-44.
3. Cramer, J.T., et al., *Acute effects of static stretching on characteristics of the isokinetic angle–torque relationship, surface electromyography, and mechanomyography.* Journal of sports sciences, 2007. **25**(6): p. 687-698.
4. Behm, D.G. and A. Chaouachi, *A review of the acute effects of static and dynamic stretching on performance.* European journal of applied physiology, 2011. **111**: p. 2633-2651.
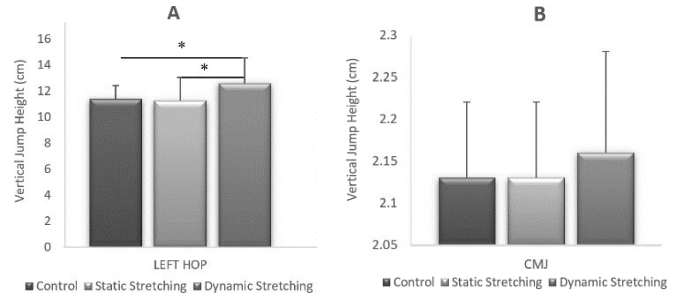
BAREFOOT BALLET WITH A RIGID FOOT: ARE COMMON METHODOLOGICAL CHOICES LIMITING OUR UNDERSTANDING OF FOOT AND ANKLE BIOMECHANICS IN BALLET?

[1]Aaron S. Fox, [1]Jason Bonacci, [1]Dominique Condo, [1]Rhiannon Snipe and [1]Haydee Ferguson

[1]Centre for Sport Research, Institute for Physical Activity and Nutrition, Deakin University, Geelong, VIC
email: aaron.f@deakin.edu.au

INTRODUCTION

Classical ballet uses distinct biomechanics that are unseen in other sports, including the requirement of dancers to weight-bear in extreme ankle positions while wearing pointe shoes [1]. Most biomechanical studies in ballet use rigid single-segment foot models and/or investigate movements in barefoot or soft ballet shoes [2]. These approaches potentially limit our understanding of how the foot functions in ballet, particularly in pointe shoes. We sought to: (i) understand if joint kinematics are altered when performing ballet movements barefoot vs. in a pointe shoe; and (ii) explore joint mechanics in a pointe shoe when modelling with a multi-segment vs. rigid foot.

METHODS

Twelve female ballet dancers (18.5 ± 3.5 years of age) with a minimum of two years dancing *en pointe* participated. Participants completed ballet movements in barefoot (plié, tendu, temps levé) and pointe shoe (plié, tendu, temps levé, relevé, rise) conditions. Three-dimensional kinematics and kinetics were tracked using a motion capture system and two force plates. Markers were attached to consistent locations on the skin across conditions by placing holes in the pointe shoe. A generic OpenSim model with multi-segment feet [3] was scaled to each participant. A corresponding 'rigid foot' model was created by locking all joints in the foot, and non-sagittal ankle and subtalar rotations. Joint kinematics, kinetics and energetics were estimated across both conditions using filtered (8 Hz) marker and ground reaction force data via inverse kinematics and dynamics. Kinematics between barefoot and pointe shoe conditions were compared via root mean squared differences (RMSD). Range of motion was quantified in the pointe shoe condition with the multi-segment foot model. Joint contributions to lower limb work in pointe shoes were compared between the multi-segment and rigid foot models.

Table 1: Mean (± SD) RMSD for barefoot vs. pointe shoe conditions across foot and ankle kinematics (º).

	Plié	Tendu	Temps Levé
Ankle Flex.	3.44 ± 1.37	5.84 ± 2.00	6.08 ± 3.34
Ankle Inv./Eve.	1.74 ± 0.97	1.80 ± 0.69	2.08 ± 1.14
Ankle Rot.	0.51 ± 0.75	1.87 ± 0.64	1.22 ± 0.68
Midtarsal Angle	5.14 ± 3.12	3.78 ± 1.21	6.54 ± 2.14
TMT Angle	8.30 ± 4.39	7.27 ± 1.83	11.11 ± 4.77
MTP Angle	5.47 ± 2.77	7.04 ± 2.19	9.29 ± 4.99

TMT – tarsometatarsal; MTP - metatarsophalangeal

RESULTS AND DISCUSSION

Ankle and foot kinematics varied between the barefoot and pointe shoe conditions, with the largest differences for joints in the foot (midtarsal, tarsometatarsal, metatarsophalangeal) (Table 1). The prominence of barefoot studies in ballet [2] likely means we have limited accurate knowledge around how the foot functions in pointe shoes. Range of motion (º) in the foot averaged across all tasks in the pointe shoe were relatively large (i.e. midtarsal = 13.09 ± 7.31; tarsometatarsal = 13.48 ± 6.38; metatarsophalangeal = 12.22 ± 6.58) and were greatest in movements transitioning from a flat foot to pointe. The use of a rigid vs. multi-segment foot model tended to overestimate the contribution of the ankle to total lower limb joint work, whereby unmodelled subtalar and foot joint contributions are likely reallocated to the ankle (Figure 1).
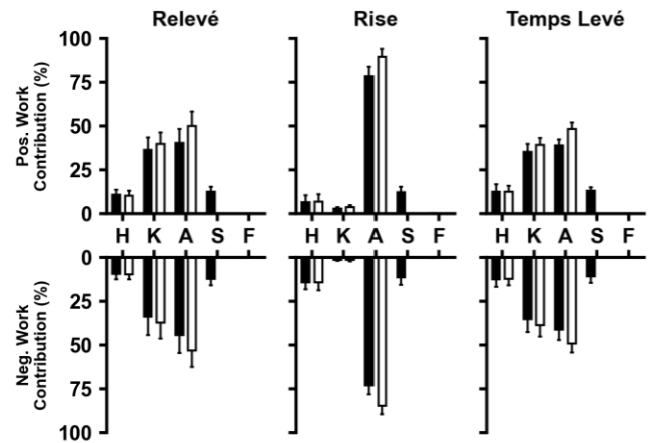
Figure 1: Hip (H), knee (K), ankle (A), subtalar (S) and foot (F) joint contributions to lower limb work when using a multi-segment (black) vs. rigid foot (white) model.

CONCLUSIONS

The significant internal foot motion suggests that rigid foot models do not accurately quantify ballet pointe movements. Future work investigating the biomechanics of dancers in pointe shoes should strongly consider the use of a multi-segment foot model.

REFERENCES

1. Russel JA, et al., *J Dance Med Sci.* **12**:75-82, 2008.
2. Veirs KP, et al., *J Dance Med Sci*, **26**:69-86, 2022.
3. Maharaj JN, et al., *Comput Methods Biomech Biomed Eng*, **25**:554-565, 2022.

CAN WE ACCURATELY MEASURE MULTI-SEGMENT FOOT KINEMATICS IN A BALLET POINTE SHOE?

Haydee Ferguson, Jason Bonacci, Rhiannon Snipe, Dominique Condo and Aaron Fox
Centre for Sport Research, Institute for Physical Activity and Nutrition, Deakin University, Geelong, Australia
Email: hrferguson@deakin.edu.au

INTRODUCTION
Pointe shoes are unique to classical ballet allowing dancers to stand and move on the tips of their toes, known as *en pointe*. Ballet dancers are at a high risk of injury, with the majority of injuries occurring in the foot and ankle [1,2]. Female ballet dancers spend most of their professional career wearing pointe shoes, therefore, it is imperative to study the detailed biomechanics of an *en pointe* position to identify any cause-effect relationships pointe shoe may have to injury. Previous studies have looked at the biomechanics of ballet movements in barefoot or soft shoe conditions [3], likely due to the validity of current foot models requiring skin contact for the markers. However, the unique position of the foot and ankle in a pointe shoe cannot be replicated in barefoot conditions. Due to the expense and customisation requirements of a pointe shoe, developing a method for assessing the biomechanics of the dancer's foot *en pointe* without damaging the shoe is warranted. The aim of this study was to assess the measurement error of a validated multi-segment foot model [4] in using markers placed on the skin vs. the shoe during *en pointe* movements.

METHODS
Twelve female ballet dancers aged 18.5 ± 3.5 years participated in this study. All dancers had a minimum of two years of experience dancing *en pointe* and were currently participating in two or more hours of pointe work per week.

Participants were provided with two pairs of pointe shoes in their preferred style and size with two weeks provided to prepare them. To measure the kinematics of the foot and ankle, a total of 62 retro reflective markers were attached to anatomical landmarks of the participants body at the lower limb, foot and torso in accordance with an established model [4]. For the validation condition, one pair of the provided pointe shoes had a series of holes cut into the shoe's box in line allowing markers to stay attached to the skin while remaining visible to the motion capture system. Participants were asked to perform a series of ballet movements (*plié, tendu, rise, relevé, hop, temps levé and posé)* across two force plates with a *barre* for support. Participants then changed to the second, intact pair of pointe

shoes and the reflective markers previously covered by the shoe were transposed onto the external surface of the intact pointe shoe. Participants then repeated the ballet movements for the experimental condition.

A generic OpenSim (v 4.5) lower limb and multi-segment foot skeletal model [4, 5] was linearly scaled to each participant. Joint angles were estimated across both conditions using low-pass filtered (8 Hz) marker data via inverse kinematics. Joint angles were averaged across movement repetitions and root mean square error (RMSE) used to compare values between the validation and experimental conditions.

RESULTS AND DISCUSSION
The largest errors between the validation and experimental conditions were observed in the midtarsal, tarsometatarsal and metatarsophalangeal joints (Table 1). These findings are not surprising, as these regions of the foot were primarily covered by the shoe and hence where marker placement was altered in the experimental condition. Despite this, measurement errors were small (typically < 3-5°) and consistent across movements.

CONCLUSIONS
Our findings suggest that a validated multi-segment foot model with reflective markers placed on the external surface of a pointe shoe can assist researchers in measuring the biomechanics of the dancer's foot *en pointe*. Future researchers should consider the potential small errors relative to when markers are placed on the skin. While our findings demonstrate measurement consistency, the accuracy of motion capture in pointe shoes still requires validation against a criterion measure (e.g. biplanar fluoroscopy).

REFERENCES
1. Smith PJ, et al. *Phys Ther Sport.***3(7)**:2015
2. Smith TO, et al. *Phys Ther Sport.***1(19)**: 50-56,2016
3. Veirs KP, et al. *J Dance Med Sci.* **26(2)**:69-86, 2022.
4. Maharaj JN, et al. *CMBBE.* **25(5)**:554-65, 2022.
5. Rajagopal A, et al. *IEEE. Trans. Biomed. Eng.* **63(10)**: 2068-79, 2016

Table 1: Mean (± SD) root mean square error for ankle and foot kinematics (°) between validation and experimental conditions

	Plie	Tendu	Rise	Relevé (B)	Relevé (U)	Hop	Temps Levé	Posé
Ankle Flex	2.15 ± 1.20	3.98 ± 1.58	3.04 ± 1.44	4.42 ± 2.82	4.80 ± 2.59	3.50 ± 1.39	4.41 ± 1.46	4.80 ± 3.56
Ankle Inv/Ev	1.27 ± 0.58	2.03 ± 1.27	1.95 ± 1.00	1.64 ± 0.73	1.78 ± 0.81	1.45 ± 0.66	1.91 ± 0.76	2.34 ± 1.87
Ankle Rot	0.38 ± 0.22	1.50 ± 0.77	1.23 ± 0.62	1.26 ± 0.33	1.37 ± 0.54	1.07 ± 0.49	0.88 ± 0.38	2.32 ± 0.85
MT Angle	3.83 ± 1.85	3.32 ± 1.39	4.13 ± 1.31	4.70 ± 1.87	4.82 ± 1.88	3.99 ± 1.09	4.98 ± 1.71	6.77 ± 5.68
TMT Angle	4.74 ± 1.90	5.82 ± 3.12	7.59 ± 3.39	7.20 ± 2.82	7.00 ± 2.78	6.88 ± 3.53	6.02 ± 2.25	7.98 ± 4.00
MTP Angle	4.69 ± 3.02	5.59 ± 3.48	5.57 ± 3.13	5.69 ± 3.30	5.92 ± 2.73	5.44 ± 3.57	5.84 ± 2.22	5.62 ± 3.73

B: bilateral, U: unilateral, MT: metatarsal, TMT: tarsometatarsal, MTP: metatarsophalangeal

THE ENERGETIC BEHAVIOUR OF THE HUMAN FOOT DURING LANDING

[1]Ceridwen R. Radcliffe, [1]Jerushah J. Bull, [1,2]Nicholas A.T Brown, [1]Phil Newman, and [1]Wayne A. Spratford

[1]University of Canberra Research Institute for Sport and Exercise, Canberra, ACT
[2]School of Clinical Sciences, Queensland University of Technology, Brisbane, QLD
email: ceridwen.radcliffe@canberra.edu.au

INTRODUCTION

The human foot contributes to absorbing and returning energy during human movement via the foot spring mechanism [1]. Researchers have quantified the energetic behaviour of the foot during running, finding that the foot contributed 8% -17% of energy recycling [2], and in single leg drop jump tasks, finding the foot contributes 8% to 18% of COM negative work [3]. The foot's energetic capacity increases as drop height and running speed increase, maintaining a constant contribution to decelerating and propelling the COM [2,3]. However, it remains unclear how the energetic behaviour of the foot changes as the characteristics of the landing task change.

In sport, landing tasks vary, and include single and double leg landings, as well as landings that need to be 'stuck', and landings that require a subsequent jump. Therefore, this study aimed to quantify the energetic behaviour of the human foot during single and double leg drop landing and drop jump tasks.

METHODS

61 participants attended a single testing session where they completed 36 landing tasks from a height of 30cm. Landing tasks included single and double leg drop jump and drop landing tasks. Reflective markers were affixed to the skin of participants feet according to the Istituti Ortopedico Rizzoli multisegmented foot marker set [4]. Data were labelled in Vicon Nexus software. Data were filtered using a fourth-order zero-lag Butterworth filter with a cut-off frequency of 14Hz for trajectory data and 30Hz for analogue data. Instantaneous power of the foot segment was calculated using a modified Unified Deformable model, as in Kelly et al. [2], and negative and positive work were calculated by integrating foot power and time.

Linear mixed effects models were estimated using the 'lme4' package [5] in R statistical software (v.4.2.1) [6]. Pairwise comparisons between the landing tasks were conducted using the 'emmeans' package [7].

RESULTS AND DISCUSSION

Results are presented in Figure 1. Negative work done by the foot in the single leg landings was significantly greater than the double leg landings (p<0.001; -0.88 and -0.40 J/kg, respectively). Negative foot work was significantly greater in double-leg drop jumps compared to double leg drop landings (p=0<0.001; -0.84 and -0.40 J/kg). Negative (p<0.001; -1.10 and -0.84 J/kg) and positive (p<0.001; 1.05 and 0.75 J/kg,)

work done during the single leg jumps was significantly greater than double leg jumps. The findings suggest that drop jump tasks demand the foot to absorb and return more energy, with up to five times more work done by the foot during the single leg drop jump task (p<0.001; -1.10J.kg and +1.05J/kg) compared to the drop landing task (-0.88J/kg and +0.21J/kg) .
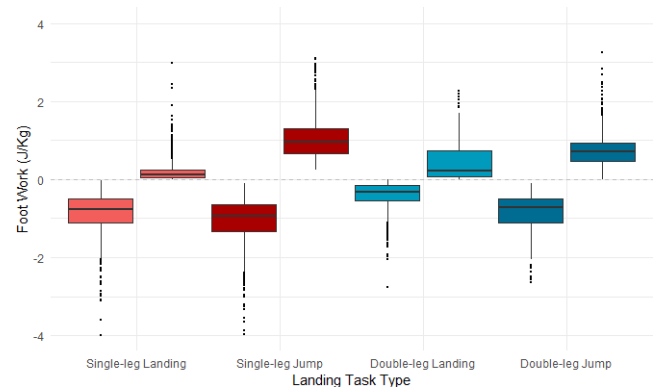
Figure 1: Positive and negative work of a single foot during single and double leg drop landing and drop jumps (J/kg).

CONCLUSIONS

Energetic behaviour of the foot differs between landing tasks, with drop jump tasks absorbing and returning more energy than drop landing tasks. The results are consistent with literature suggesting the foot functions as a damper when energy needs to be attenuated, such as during the drop-landing tasks, and functions as a spring when energy needs to be both attenuated and generated, such as during the drop-jump tasks [8]. The findings highlight the complex and dynamic function of the foot during human movement, and have practical implications for human performance, injury prevention and rehabilitation.

REFERENCES

1. Ker *Nature*. **325**:147-149, 1987.
2. Kelly et al. *Scientific Reports*. **8**:1-6, 2018
3. Smith et al. *Journal of Experimental Biology*. **224**:242-263, 2021
4. Leardini et al. *Gait & Posture*. **25**:453-462, 2007
5. Bates et al. *Journal of Statistical Software*. **67**:1-48,2015
6. R: Foundation for statistical computing, 2022.
7. Lenth et al. R Package 'Emmeans', **v1.10.3-0900003**, 2024.
8. Behling et al. *Biological Reviews*. **98**:2136-2151, 2023

Monday, December 2

ANZORS Podium 2

STRUCTURAL AND BIOMECHANICAL PROPERTIES OF ARTICULAR CARTILAGE IN DIFFERENT JOINTS
ABSTRACT SUBMISSION 2024 ABC-ANZORS MEETING

[1,2]Kate Hoare, [1,3]Carina Blaker, [1]Emma Cunningham, [1,2]Sam Hefferan, [1,2]Christopher Little and [1,2]Elizabeth Clarke

[1]The Kolling Institute, University of Sydney and Northern Sydney Local Health District, [2]Sydney MSK Health, School of Medical Sciences, Faculty of Medicine and Health, University of Sydney, [3]Faculty of Science, University of Sydney, Sydney, NSW
email: elizabeth.clarke@sydney.edu.au

INTRODUCTION
Our foundational understanding of articular cartilage primarily stems from studies on animal tissue, or human tissue from a limited range of joints[1,2]. Examining various human joints can reveal why some are more prone to osteoarthritis (OA) than others. Analysing how different joints structurally respond to load may deepen our understanding and aid researchers in developing improved techniques for cartilage engineering based on these structural responses.

METHODS
This study investigates the histological structural characteristics of human cartilage samples from various joints, including the hip, knee, ankle, shoulder, elbow, interphalangeal, and carpometacarpal joints. Cartilage samples (n=146 total) were subjected to indentation creep testing (1hr) then formalin-fixed under load and processed for histological structural analysis of indented and un-indented regions. Key parameters assessed include shear modulus, elastic modulus, total cartilage thickness, zonal layer thickness, cell density, cell morphology, and the region affected by the indenter (based on angle and length of the deformed surface from the indenter) with n=19 analysed so far. Preliminary correlation analysis between creep modulus, elastic and structural characteristics were performed.

RESULTS AND DISCUSSION
Zonal layer thicknesses in different joints varied from previous studies on human knee and ankle tissue, which reported 16% for the superficial zone (SZ), 31% for the middle zone (MZ), and 53% for the deep zone (DZ)[3].
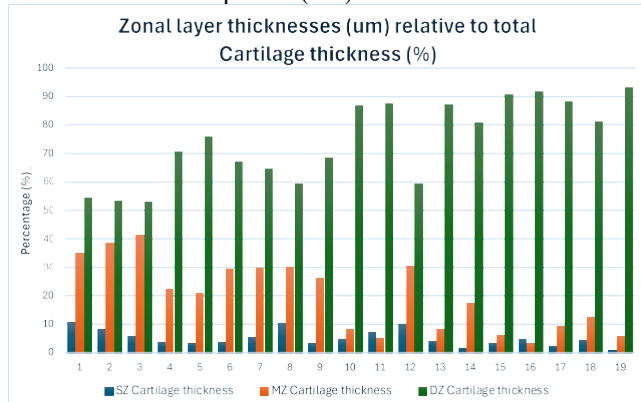
Figure 1: Illustrates the variation in human cartilage zonal layer thicknesses amongst 19 different samples across all joints.

Our data shows an average of 5% for SZ, 20% for MZ, and 75% for DZ, with a wide variety across different joints (Figure 1). Our preliminary data for 19 specimens analysed so far reveal no significant correlations between shear modulus or elastic modulus with any structural characteristics measured. For example, figure 2 shows no significance correlation between shear modulus and SZ thickness. This contrasts with previous studies that have shown strong correlation between shear modulus and SZ thickness in the knee and shoulder of canine cartilage[2]. This may be because of the limited number of joints that study possessed, or this could be a species difference. Our final analysis will confirm whether biomechanical properties and zonal architecture are related only the knee and shoulder of dogs[3], or weather this extends to a wider range of joints in humans.
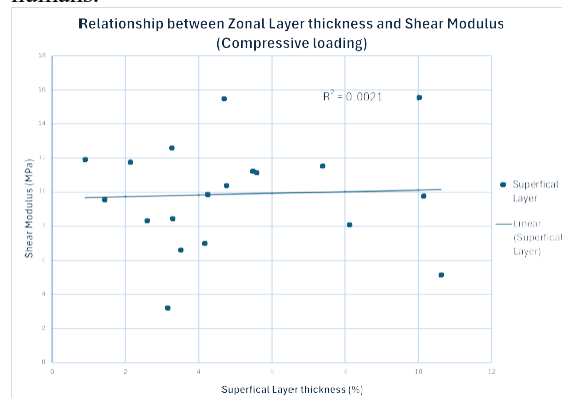
Figure 2: Illustrates the poor correlation between Shear modulus and thickness of the superficial layer.

CONCLUSIONS
Our results raise questions about the generalisability of cartilage biomechanical and structural characteristics which have been previously reported in a limited range of joints, implying that tissue engineered cartilage may require joint-specific customisation. Further research is needed to confirm our discovery of poor correlation between cartilage biomechanical and structural characteristics.

REFERENCES
1. Antons, J., et al. (2018). *Journal of Materials Science: Materials in Medicine*, *29*, 1-8.
2. Korhonen, R. K., et.al. (2002). Medical engineering & physics, 24(2), 99-108.
3. Modl, J. M., et.al. (1991). *Radiology*, *181*(3), 853-855.

ANZSB
anzsb.asn.au

DOUBLE SCREW FIXATION IN THE SURGICAL REPAIR OF UNSTABLE SCAPHOID FRACTURES

[1]Phoebe del Rosario, [2,3]Carsten Surke, [1,2]Lachlan Huntington, [2,4]Eugene Ek, [2,5]Stephen Tham, [1]David Ackland
[1]Department of Biomedical Engineering, The University of Melbourne, VIC, Australia; [2]Hand and Wrist Biomechanics Laboratory, O'Brien Institute, VIC, Australia; [3]University Hospital, Bern, Switzerland; [4]Melbourne Orthopaedic Group, VIC, Australia; [5]Department of Surgery, Monash University, VIC, Australia;
email: dackland@ unimelb.edu.au

INTRODUCTION

The scaphoid is the most commonly fractured carpal bone, representing around 60% of all carpal fractures, and 2% of all fractures in the body [1]. Single headless compression screw fixation is the gold standard fixation technique for the treatment of the displaced fractured scaphoid; however, lack of rotational stability associated with this technique is known to contribute to development of non-unions in up to 7% of cases [2]. Although technically more demanding than single screw fixation, the double screw fixation may improve rotational strength and reduce the overall stress at the screw bone interface, thus improving construct resistance to higher loads; however, at present, the biomechanical strength and integrity of double-screw techniques for the treatment of scaphoid fractures remains poorly understood. The objective of the present study was to compare the torsional and cantilever strength in single screw with a strut graft, single screw with a wedge graft, and double screw fixation techniques for the treatment of unstable caphoid fractures.

METHODS

Forty-eight embalmed human scaphoids were harvested from 12 male and 18 female cadavers (mean age: 83.5 years). Computed Tomography (CT) scans of each specimen were taken, and custom 3D printed cutting guides developed to create a standardised unstable fracture via a 3mm volar open wedge shaped osseos defect at the scaphoid waist. Specimens were randomised into three scaphoid fracture treatment groups of 16 specimens, which included (i) single screw and strut graft repair (ii) single screw and wedge graft repair (iii) double screw repair. Each surgery was undertaken using custom 3D printed cutting and drilling guides, and wedge grafts were harvested from embalmed metacarpal bones. For cantilever bending testing, eight specimens in each test group were potted in a metal fixture with their long axis a 45° angle. These specimens were then mounted to an Instron Materials Test system and the scaphoid displaced downward at a rate of 10mm/min. The load at 2.0mm displacement was recorded. Cyclic torsion testing was then undertaken in the remaining specimens by rotating constructs by 1° in each

direction, increasing rotation by 1° until 10° of rotation was achieved. Analysis of variance was used to compare bending and torsional strength and stiffness between groups.

RESULTS AND DISCUSSION

The double screw fixation technique resulted in a significantly higher load to 2mm displacement compared to the single screw and wedge technique (mean difference: 78.3N, p<0.05). The double screw group had a significantly higher maximum torque in the screw tightening (clockwise) direction compared to both, the single screw and strut group (mean difference: 65.6 Nmm, $P < 0.001$), and the single screw and wedge group (mean difference: 60.6 Nmm, $P < 0.001$). It also had a significantly higher maximum stiffness in the screw tightening direction compared to the single screw and strut group (mean difference: 4.8, $P < 0.050$), and the single screw and wedge group (mean difference: 9.3, $P < 0.001$).
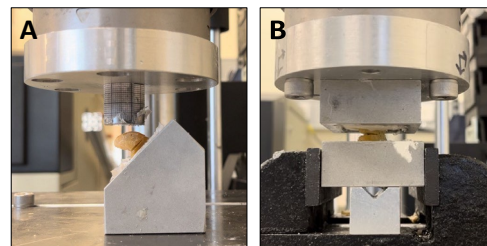
Figure 1: Scaphoid repair constructs were mounted to an Instron Materials Test System to support loading in cantilever bending (A) and torsion (B)

CONCLUSIONS

Double screw fixation of unstable, mid-waist scaphoid fractures yields greater rotational stability than that of single screw with a strut or wedge techniques, and greater overall bending resistance than that of the single screw and wedge technique. These findings suggests double screw fixation may better prevent persistent non-union for scaphoid waist fractures with volar bone loss. The results of this study will help in the surgical management of scaphoid fractures.

REFERENCES

1. Hove, L.M. *J Plastic Recon Surg*. 33(4), 423-426, 1999
2. Matson, A.P. et al. *Hand*. 12(4): 362-368, 2017

Spatial tracking of the shoulder bones using optical motion capture and 3D ultrasound: a simulation and cadaveric study

[1,*]Maxence Lavaill, [2]Ahmed Sewify, [1]Dermot O'Rourke, [2]Jacqueline Roots, [2]Davide Fontanarosa and [1]Saulo Martelli

[1]School of Mechanical, Medical and Process Engineering, Queensland University of Technology, Brisbane, QLD
[2]School of Clinical Sciences, Queensland University of Technology, Brisbane, QLD
[*]e-mail: maxence.lavaill@qut.edu.au

INTRODUCTION

Accurate measurement of skeletal motion is of paramount importance for most biomechanically related applications. Current bone tracking methods like skin-based motion capture, bi-fluoroscopy and intra-cortical bone pins have limitations, including invasiveness, radiation, high cost and skin artifacts. Moreover, the complex anatomy and soft tissues of the shoulder make it a challenging region to track. Ultrasound (US) imaging provides non-invasive, non-ionising, cheap and real-time means of assessing internal anatomical structures [1]. The combination of stereophotogrammetry and 3D US technologies holds great promise for bypassing skin-motion artifacts at the shoulder. Our proposed method involves registering acquired full bone shapes to spatially dispersed small bony surface patches segmented from 3D US. The accuracy and feasibility of such a method are yet to be investigated. This work aimed 1) to determine, *in-silico*, the level of accuracy allowed by the proposed US bone tracking methodology and 2) to prove, *ex-vivo*, its applicability.

METHODS

First, a simulation study was undertaken by utilising CT-based segmentations of an individual's humerus and scapula. 40x40 mm patches at accessible bony landmarks (7 for humerus, 6 for scapula [2]) were virtually duplicated and isolated from the bony surfaces using *3Matic* (Materialise, Belgium). Using *Matlab*, the full bony surfaces were randomly posed in space (± 5 cm, ± 15°) and registered back to the ideal US patches using either an Iterative-Closest-Point (ICP) or a Coherent Point Drift (CPD) algorithm. 1000 iterations were undertaken to quantify the accuracy of the registration algorithms (i.e., root mean square error – RMSE, between pre- and post-registration full bone point clouds) and their dependence on initial positions.

Second, a cadaveric study was undertaken under QUT human ethics, on a female donor (73 yo, 62 kg, 168 cm). Bone pins with 4 reflective markers were inserted into the right humerus and scapula. Anatomical reconstructions of the bones with pins were segmented from previously acquired CT scans (*Mimics*, Materialise). The donor was sat with their right upper arm clamped at low, middle and high shoulder elevation angles. At each of these angles, an experienced sonographer acquired 3D US volumes of 6 scapular and 7 humeral landmarks (Philips VL13-5 probe with reflective marker cluster with EPIQ7 US system), while a 3-camera motion capture system (VICON, UK) tracked the US probe and the pinned bones in. All CT and US images were expressed in the lab space. The full humerus and scapula shapes were subsequently registered to segmentations of the 3D US bone surfaces. Point cloud RMSE between reference (bone pins) and registered bones (US) informed the experimental accuracy of the proposed method.

RESULTS

In the simulation, CPD consistently found perfect solutions despite randomised initial positions for both bones (RMSE < 1e-4 mm), as opposed to ICP (RMSE ranged [2.3; 99.9] mm depending on the initial positions). In the cadaveric experiment, humerus and scapula were spatially registered using CPD with humeral RMSE of 2.0/7.2/14.1 mm and with scapular RMSE of 15.1/16.8/27.5 mm, at low/medium/high shoulder elevations, respectively.

Figure 1: Humerus (left) and scapula (right) bone registration to patches segmented from ultrasound volumes (Green) at mid elevation angle. Red point cloud is the target bone (bone pins) and blue point cloud is the registered bone.

CONCLUSIONS

We demonstrated the feasibility and accuracy of using 3D US and motion capture to track shoulder bones in a simulation and reported the current accuracy of a pilot cadaveric experiment. The simulation showed that the proposed method can, under ideal conditions, track shoulder bones with extreme accuracy using CPD. Furthermore, the cadaveric pilot study proved the feasibility of the proposed US bone tracking method applied to shoulders despite errors higher than expected (>1 cm). A list of potential sources of error and improvements will be investigated in the future.

REFERENCES
[1] Niu et al., *PLoS ONE*, **13(6)**, 2018;

[2] Wu et al., *J Biomech*, **38(5)**: 981-992, 2005.

VALIDATION OF A SUBJECT SPECIFIC OPENSIM SHOULDER MODEL USING *IN-VITRO* EXPERIMENTAL DATA

[1]Mélody C. Labrune, [2]Seyyed Hamed Hosseini Nasab, [1,3]David T. Axford, [1]Robert Potra, [1]Joseph Cadman,
[1]Danè Dabirrahmani, [2]William R. Taylor, [1,3]Louis M. Ferreira, [1]Sumit Raniga and [1]Richard Appleyard

[1]Faculty of Medicine, Health and Human Sciences, Macquarie University, Sydney, Australia.
[2]ETH, Institute for Biomechanics, Zürich, Switzerland.
[3]Dept of Mechanical and Materials Engineering, Western University, London, Canada.
Email: melody.labrune@hdr.mq.edu.au

INTRODUCTION

The human shoulder joint is at high risk of soft tissue injury because it is highly unconstrained. Soft tissue injuries in the shoulder commonly involve tears of the rotator cuff (RC) muscles and have been classified according to tear pattern [1]. The impact of RC tears on shoulder biomechanics can be studied non-invasively using *in-silico* and *in-vitro* approaches. The goal of this study was to validate a musculoskeletal model under different RC tear patterns against *in-vitro* data from an advanced cadaveric shoulder simulator [2].

METHODS

Subject-specific musculoskeletal models were developed using OpenSim [3]. Patient specific bone geometries were generated from CT scans and each model was comprised of a six degree of freedom glenohumeral joint actuated by eight muscles including the three deltoid heads and the five RC muscles. Muscle forces were predicted using Concurrent Optimization of Muscles Activation and Kinematics (COMAK) algorithm [4] for two motions {Scapular Plane Elevation (SPE) and Forward Flexion (FF)} under seven conditions {intact (I), supraspinatus tear (S), Collin's classification types (A through E) [1]}. Muscle tears were simulated using a zero maximum isometric force thereby ensuring no force was applied to those muscles. Subject-specific kinematics from the cadaveric simulator were used as inputs into each model. Pearson's correlation coefficient was used to compare the resulting *in-silico* muscle forces to those measured by the cadaveric simulator.

RESULTS AND DISCUSSION

The subject-specific musculoskeletal model muscles presented a high Pearson's correlation coefficients ($r > 0.5$) when compared to the *in-vitro* data (Figure 1) for all major muscles (anterior deltoid, lateral deltoid, supraspinatus, infraspinatus and subscapularis superior), except for the infraspinatus (intact) for SPE and infraspinatus (type B) for SPE and FF, and for subscapularis superior (type E) for SPE and FF. This might be explained by their small muscular forces.

The posterior deltoid, subscapularis inferior and teres minor mostly presented a low Pearson's correlation coefficient ($r < 0.5$) with the simulator. This is because the musculoskeletal models predicted these muscles to be antagonists (muscle length

increased/muscle relaxation with arm activation) and therefore these muscles experienced little or no load.
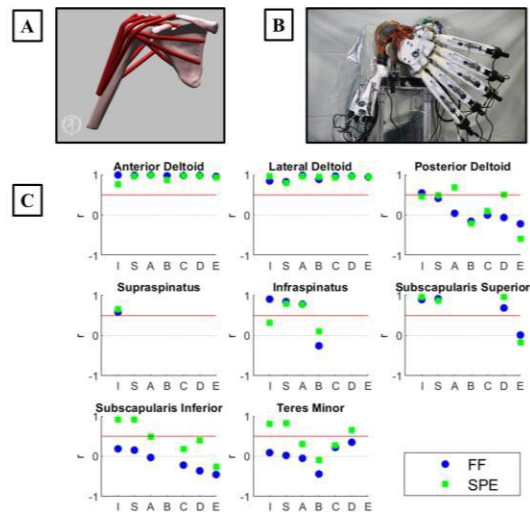
Figure 1: (A) *In-silico* model; (B) *In-vitro* model [2]; (C) Pearson's correlation coefficient (r) between muscle forces estimated by the *in-silico* model and the corresponding *in-vitro* data during FF and SPE {Red line : $r = 0.5$}.

CONCLUSIONS

This study compared results from *in-silico* and *in-vitro* studies. The *in-silico* subject-specific models showed good agreement with the *in-vitro* data for the FF and SPE agonist muscles. Our validated *in-silico* approach provides a non-invasive tool to further assess shoulder soft tissue injuries.

ACKNOWLEDGEMENTS

REFERENCES

1. Collin P., et al., *J Shoulder Elbow Surg* (2014)**23**,1195-1202.
2. Axford D.T., et al., *J. Clin. Med*, 2023, **12**(14), 4596.
3. Delp S.L., et al*., IEEE Trans Biomed Eng*. 2007; **54**(11): 1940-50.

4. Smith C. R., et al., *J Biomech*, **82**, 124-133.

COMBINED SHAPE MODEL OF THE TORSO AND UPPER LIMB

[1]Roshni Raghvani, [1]Eric Shen, [1]Harnoor Saini, [1]Julie Choisne, [1]Ted Yeung, [2]Marc Hirner, and [1]Thor Besier
[1]Auckland Bioengineering Institute, University of Auckland, Auckland, New Zealand
[2]Department of Orthopaedic Surgery, Whangarei Hospital, Whangarei, New Zealand
email: rrag962@aucklanduni.ac.nz

INTRODUCTION

The human upper limb displays a large range of motion thanks to the kinematic coupling of the shoulder girdle (clavicle, scapula and humerus). This functional interdependence is likely to be present in the morphological form of the upper limb bones. Prior studies have used statistical shape modelling to investigate bone morphology of the scapula and humerus [1,2], but coupling across other upper limb bones has not been investigated. Here we present a combined statistical shape model of the upper limb bones and torso to understand morphological coupling between bones and establish variance in bone size and shape across a population.

METHODS

A shape modelling pipeline (GIAS3, [3]) was used to create a combined shape model of the torso, clavicle, scapula, humerus, radius and ulna from 94 de-identified CT scans (Figure 1). Principal Component Analysis was performed to capture the morphological variation across the population. Correlation analyses were performed to analyse the relationship between the torso, scapula and clavicle, along with the upper limb long bones.
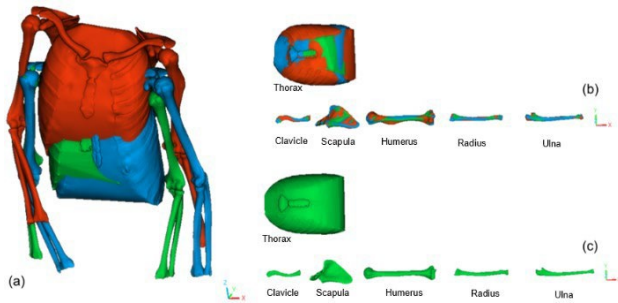
Figure 1: (a) Torso and upper limb segmentation examples, (b) Mesh fitting and alignment, (c) Mean shape template of the torso and upper limb bones.

RESULTS AND DISCUSSION

The first 13 principal components accounted for 90% of the variation in the population (Table 1). Anthropometric data of torso width and scapula width demonstrate a linear correlation (Figure 2). Along with the linear trend, the shape model also captures the non-linear relationship that exists in the bone morphological variation.
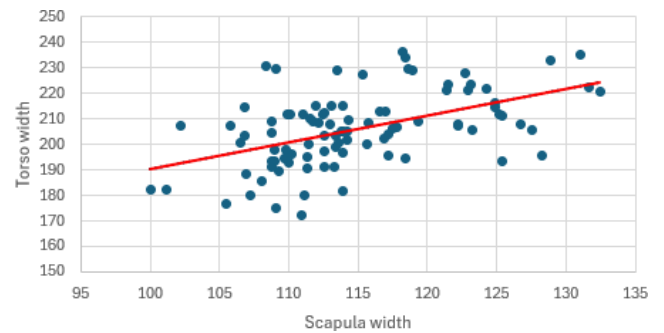
Figure 2: Correlation of scapula width to torso width

CONCLUSIONS

We have developed a shape model that accounts for the coupled morphology that exists within the bones of the upper limb. This model has application to predict bone morphology for surgical planning, ergonomics, prosthetics and forensic science.

ACKNOWLEDGEMENTS

REFERENCES

1. Soltanmohammadi, P., et al.., *J Biomech Eng.* **142**:249-259, 2020.
2. Yang, Y.M., et al., *Computer Methods in Biomech and Biomed Eng.* **11**:19-30, 2008.
3. Zhang, J., et al., *Computer Methods in Biomech and Biomed Eng.* **21**:498-502, 2018.

Table 1: Percentage and cumulative variance of the first 13 principal components.

PC	1	2	3	4	5	6	7	8	9	10	11	12	13
Variance	58.1	10.2	4.0	3.4	3.0	2.4	1.9	1.6	1.4	1.3	1.2	1.0	0.9
Total Variance	58.1	68.3	72.2	75.6	78.6	80.9	82.8	84.4	85.8	87.0	88.2	89.2	90

ONLAY-GRAMMONT HYBRID DESIGN INCREASES HUMERAL IMPLANT STIFFNESS BUT NOT FRACTURE LOAD IN REVERSE SHOULDER ARTHROPLASTY

Dermot O'Rourke[1], Xiaolong Fan[1,2] Ashish Gupta[1,2,4], Kenneth Cutbush[1,2,4], Saulo Martelli[1,2]

[1] School of Mech., Medical & Process Eng, Queensland University of Technology, Brisbane, QLD; [2] Queensland Unit for Advanced Shoulder Research, Brisbane, QLD; [3] School of Exercise and Nutrition Sciences, QUT, QLD; [4] Orthopaedic Surgery, Sports Injury, Orthopaedics, Greenslopes Private Hospital, Brisbane, QLD, [5] Zimmer Biomet, Warsaw, IN
email: saulo.martelli@qut.edu.au

INTRODUCTION

Onlay humeral stem designs in reverse shoulder arthroplasty preserve a greater amount of proximal bone than inlay designs aiming at increasing the stiffness and stability of the bone-implant construct [1]. However, there is limited information comparing the stability under load of inlay and onlay implants. A time-elapsed micro-CT protocol enabled measuring the displacement of the entire implant under controlled loading up to causing failure of the implant [2]. This study compared the stability in a Grammont-style inlay and a hybrid onlay-Grammont design under a high-risk physiological load.

METHODS

The left and right humerus specimens were obtained from a male donor aged 75 years (large bone size) and a female donor aged 72 years (small bone size). Ethics clearance was obtained institutional HREC (# 2021000088). The Aequalis reversed II stem (Stryker Inc.) was implanted. Each pair was implanted using a standardized Grammont-style inlay technique (left) and hybrid onlay-Grammont technique (right). Concomitant mechanical testing and micro-CT scanning were performed using a protocol for causing failure to the implant under a physiological load expected to maximize the risk of implant distal migration [2]. The implant was imaged using a nominal 150N pre-load, 650 N and immediately after failure by controlling the compressive displacement. Failure was defined as a sudden drop of the reaction force and/or displacement reaching 12 mm. The axial slices were reconstructed using CTPro3D software (Nikon Metrology) and saved as 8-bit unsigned integer volumes each 3956 × 2558 × 2502 pixels in size. The displacement of the implant and the deformation of the bone were analyzed in the images co-registered to the pre-load test. The reaction force, the implant displacement, and the failure behavior were compared across surgical techniques and specimen sizes.

RESULTS AND DISCUSSION

The onlay was stiffer (123 N/mm and 288 N/mm) than the inlay design (112 N/mm and 226 N/mm) under physiological loading in both the large and small specimens. Failure of the implant displayed a longitudinal opening of the cortex associated with a sudden drop of the compressive force. However, the small inlay implant showed no cortical opening and the highest distal implant migration (12 mm). This implant displayed limited trabecular support of the implant before loading, and during loading the implant migrated finding a distal cortical support (Figure 1). The large hybrid onlay-Grammont had a greater failure load than the inlay design (2800 N v 2000 N) whereas the small onlay implant displayed a fracture load equal to 1050 N while the inlay design displayed a reaction force equal to 1800 N at 12mm displacement when loading was stopped.
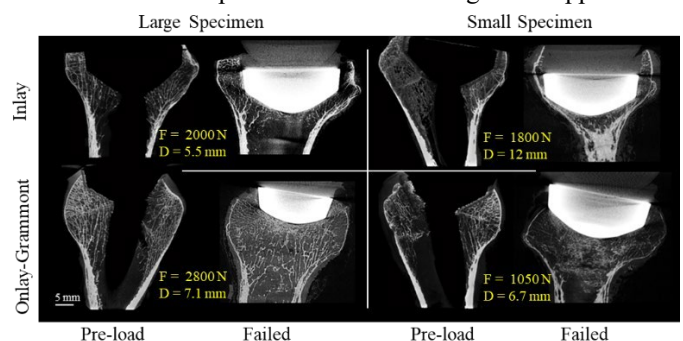
Figure 1: The inlay (to row) and the onlay (bottom row) for the large (left column) and the small (right column) implant. Each panel displays a cross-section of the bone microstructure under the pre-load (left) and the failed implant (right). The peak force and the displacement to fracture are also annotated.

CONCLUSIONS

The present study showed two different failure mechanisms of the humeral component in reverse shoulder arthroplasty, which may help explain the increase of complications in small patients. Bone preservation and humeral grafting was found to result in less implant movement and affective loading of the proximal cortex. A reduced amount of bone supporting the implant may become the weakest implant link, allowing excessive distal migration of the implant. Further research is necessary to elucidate the load transfer mechanism within the implant.

ACKNOWLEDGEMENTS

REFERENCES

[1] Jackson et al., Shoulder Elbow 15(1), 4–13, 2023.
[2] Martelli et al., J Orthop Surg Res, 19(1), 2024.

THE SHOULDER TOOLKIT: ENHANCING END-USER APPLICATION

Steven Duhig[1], Alec McKenzie [1], Daneh Turner[2]

1 School of Health Sciences and Social Work, Griffith University, Gold Coast, Queensland, Australia

2 General Electric Healthcare, Sydney, Australia

email: s.duhig@griffith.edu.au

INTRODUCTION

The development of accessible and cost-effective methods for assessing and monitoring musculoskeletal (MSK) structures represents a transformative advancement in healthcare. Currently, MSK ultrasonography requires significant expertise, limiting its widespread application. However, technological advancements are poised to extend its usability to novices. Magnetic resonance imaging, despite accessibility and budget barriers, is commonly utilised to evaluate the risk of MSK injuries. Ultrasound machines, being more accessible and affordable, mitigate the need for radiology clinic visits. Nonetheless, acquiring accurate and reliable ultrasound images demands a considerable level of expertise.

This study examined the performance of a new Shoulder Toolkit (STK) application (designed to improved confidence, satisfaction and workflow) for point-of-care MSK ultrasound with traditional methods, analysing outcomes between novice and expert users. The aims were (i) evaluate user confidence and satisfaction, (ii) assess perceived workload, usability, and proficiency, and (iii) examine differences in image quality.

METHODS

A total of 33 participants (novice = 17, expert = 16) completed a pre-test survey to assess baseline confidence levels. Following training on the STK (Venue Go, General Electric Healthcare) and traditional methods (novices-only), participants used both techniques to examine six shoulder structures. Subsequent assessments of confidence, satisfaction, usability, net promoter score, perceived workload were conducted through specific questions, System Usability Scale (SUS), Net Promoter Score (NPS), User Experience Quality (UXQ), NASA-TLX workload questionnaires. Image quality was assessed on a 5-point scale.

RESULTS AND DISCUSSION

For novices, significant differences in confidence levels were observed across three conditions (χ^2 = 16.2, p < 0.001), with no significant changes among experts (p > 0.05). Between-group analysis showed significant differences in the PRE (p = 0.003) and TRAD (p < 0.001) conditions, but not in STK (p = 0.088). Pairwise comparisons for novices indicated significant improvements in confidence from both PRE to STK (p = 0.003) and TRAD to STK (p = 0.002). Experts showed no significant differences in any comparisons, including STK (Figure 1).
SUS revealed experts rated the traditional condition's usability significantly higher than novices (U = 65.5, Z = -2.547, p = 0.010). Similarly, the NPS showed experts preferred the traditional setup over novices (U = 71.5, Z = -2.361, p = 0.019).

UXQ findings showed experts favoured the traditional condition in terms of satisfaction scores compared to novices (U = 73.0, p = 0.023). NASA-TLX results showed, under traditional conditions, experts experienced significantly lower frustration and demonstrated better performance than novices (frustration: U = 69.0, p = 0.015; performance: U = 35.0, p < 0.001), and reported lower mental workload than novices in the STK condition (U = 78.5, p = 0.037). Image quality assessment (novices = 340; experts =320) indicated a significant difference in the distribution of scores between the two groups (Mann- Whitney U = 28,438; Wilcoxon W = 86,408; Z = -11.243; p <

.001). Experts demonstrated higher image quality scores with a mean rank of 411.63 compared to 254.14 for novices.
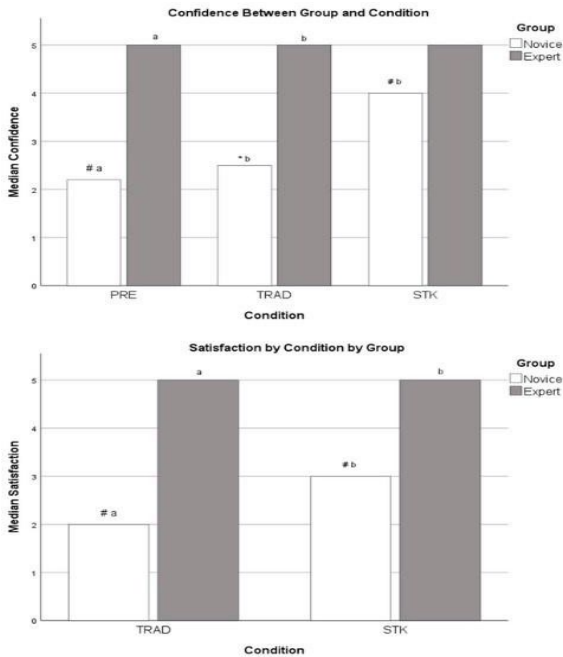
Figure 1: Confidence (top) and satisfaction (bottom) levels for novice (white bar) and experts (shaded bar) for before using ultrasound (PRE – novices only), after traditional (TRAD), and Shoulder Toolkit (STK) methods.

CONCLUSIONS
This study highlights the potential of the STK application to democratize musculoskeletal ultrasonography, significantly enhancing novice confidence and satisfaction.

ACKNOWLEDGEMENTS

Neural drive to the deltoid segments in healthy shoulders

[1,2,3]W van den Hoorn, [4]F Hug, [1,2]E Hill, [2]F Dupuis, [3]A Gupta, [3]K Cutbush, [1,3]G Kerr, [4]K Tucker

[1]Queensland University of Technology, School of Nutrition and Exercise Sciences, ARCITTC joint Biomechanics, Brisbane, QLD
[2]The University of Queensland, School of Biomedical Sciences, Brisbane, QLD
[3]Queensland Unit for Advanced Shoulder Research, Queensland University of Technology, Brisbane, QLD
[4] Universite Cŏte D'azur, Laboratory of Human Motor Skills, Expertise, Sports and Health, France
email: w.vandenhoorn@qut.edu.au

INTRODUCTION
Functional outcomes following total reverse shoulder replacement surgery vary. Poor recovery is associated with inefficient shoulder control including co-activation of deltoid portions (i.e., the anterior, middle, and posterior portions) during tasks which do not typically require this control strategy [1]. However: i) the interpretation using classical surface electromyography (EMG) are limited to the *muscle-level, i.e., is the muscle region active or not*; ii) there is evidence that complex movements are controlled at the level of individual or grouped motor units (an alpha motoneuron and all the muscle innervated muscle fibres) not at the muscle-level [2]; and (iii) the level of common drive to motor units varies between muscles, between activities and between people [3]. Based on this knowledge, it is reasonable to hypothesise that the level of common drive to motor units across the deltoid may differ between muscle-heads, between activities and between people. The overall goal of our extended work is to understand how the central nervous system controls shoulder muscles in health and disease, and whether this control impacts recovery from surgery. The specific aim of this study was to determine the organisation of neural drive to the deltoid muscle at the single motor unit level in individuals with healthy shoulder function.

METHODS
Three high-density EMG grids were used to record activity of the three deltoid portions during force-matched abduction tasks with different mechanical constraints. Participants with healthy shoulder function [n=11, 1 female; age: 29 (10) yrs; height: 1.78 (0.09) m; weight: 74 (14) kg] were seated, with their shoulder positioned in 45-degrees abduction. In separate trials within the same session, participants produced isometric force in the direction of abduction (A), abduction combined with flexion (AF), and abduction combined with extension (AE). In each direction, participants matched a trapezoidal force target with 4 repetitions of 5s ramp up, 20s hold, 5s ramp down. EMG signals were decomposed into motor unit spike trains using blind source separation, and manually edited. Common drive within and between deltoid heads was determined using coherence spectral analysis in the 0-5Hz band. Coherence values were Z-transformed; values >1.65 were considered significant. Linear mixed models tested if common drive was affected by force direction, deltoid portion (within muscle), or pairs of deltoid portions (between muscles) and their interactions.

RESULTS
Within deltoid portions: significant common drive was observed within deltoid portions in the 3 force directions. A significant muscle x force direction (p=0.01) was observed; common drive within the middle deltoid was higher in A than AF (p=0.05) and was lower in the posterior than middle deltoid during A (p=0.03). Between deltoid portions: Differences in common drive were dependent on pairing of deltoid portions (p<0.001) but were not force direction dependent (p=0.45). Most participants exhibited significant common drive between lateral-posterior, and lateral-anterior deltoid portions, whereas most participants exhibited low, insignificant common drive between the posterior-anterior deltoid portions.

DISCUSSION AND CONCLUSIONS
The common drive within the middle deltoid depended on force direction, suggesting task-dependent flexible control. Because the moment arm of posterior deltoid is small or even negative at 45-degree shoulder abduction, lower common drive to the posterior than middle deltoid portion could be interpreted as being efficient. High common drive between lateral-posterior, and lateral-anterior portions suggests a neuromechanical functional unit enabling force production in the AE and AF directions. However, this common drive was independent of force direction, suggesting a relatively fixed common drive to these deltoid portions. Strong common drive within deltoids portions and low common drive between posterior and anterior deltoid portions would allow for flexible control between these portions. These findings offer crucial insights into the neural control of healthy deltoid muscles.

REFERENCES
1. Smith RA, et al., *J Orthop,* **22**, 165-169, 2020.
2. Hug F, et al., *J Physiol* **601**, 11-20, 2023.
3. Avrillon S, et al., *J Appl Physiol (1985)* **130**, 269-281

2021.

Monday, December 2

National Keynote 2 – Prof Richard Page

Reverse Total Shoulder Replacement – State of the Art

The first ever recorded joint replacement was a linked total shoulder replacement in Paris by Dr. Jules-Émile Péan in 1893 for tuberculosis in a French waiter. Since the evolution of contemporary reverse total shoulder replacements (rTSR) by Grammont, usage for the spectrum of shoulder arthritis has risen dramatically over the last decade. The Australian Orthopaedic Association National Joint Replacement Registry in 2023 recorded a 285% increase in shoulder replacements since it commenced collection of full national data from November 2007. There were 10,436 replacement surgeries last year, with over 85% being rTSR.

The introduction of rTSR was primarily to deal with cuff tear arthropathy (Grammont and Baulot 1993) resulting in a painful, pseudoparetic shoulder in elderly patients. The altered biomechanics of rotator cuff insufficiency results in superior migration of the humeral head, eccentric joint loading and cartilage shear resulting causing a specific pattern of arthritis.

The rTSR was designed to compensate for a superior migrated shoulder and originally incorporated:

- Medialised Centre of Rotation to the glenoid
- Deltoid lengthening
    - Improved pre-load
    - More efficient muscle lever / action
- 155 deg initial design – optimising stability
- Inlay design to limit humeral length effect

Lengthening of the deltoid improves recruitment of the segments of the muscle, according to Kapandji, with an increase in deltoid Wrap around the humerus.

Contemporary use of rTSR has expanded to include

- Osteoarthritis
- Proximal humerus fractures - displaced 4 part
- Rheumatoid / inflammatory arthritis
- Revision surgery

This talk will cover the history, evolution of rTSR and improvements in design that have had a positive impact on clinical outcomes.

Monday, December 2

<u>ABC Podium 3</u>
Sports biomechanics

THE ASSOCIATION BETWEEN SYMPTOMS OF PELVIC FLOOR DYSFUNCTION & RUNNING MECHANICS

[1]Celeste E. Coltman, [2]Gráinne M. Donnelly, [2]Hans von Lieres Und Wilkau and [2]Isabel S. Moore

[1] Research Institute for Sport and Exercise (RISE), University of Canberra, Canberra, Australia
[2] Cardiff School of Sport and Health Sciences, Cardiff Metropolitan University, Cardiff, United Kingdom
email: Celeste.Coltman@Canberra.edu.au

INTRODUCTION

Pelvic floor dysfunction refers to any compromise to the muscles and tissues of the pelvic floor and their associated role in continence, excretion, pelvic organ support and sexual function [1]. Pelvic floor dysfunction is prevalent during the perinatal period and can be a barrier to women returning to running postpartum [1]. It is currently unknown whether running biomechanics are related to the severity of pelvic floor dysfunction. The study aimed to explore the association between pelvic floor dysfunction and running mechanics in a cohort of women with symptoms of pelvic floor dysfunction.

METHODS

The Australian Pelvic Floor Questionnaire [2] quantified pelvic floor dysfunction symptom severity (weighted score out of 40) in 25 postpartum women (mean ± SD age: 38 ± 4 years; mean ± SD body mass: 64.5 ± 8.9 kg; median (range) number of births: 2 (1 – 4); mode of delivery: 86% vaginal, 14% caesarean). Pelvic floor muscle strength and endurance (Modified Oxford Manual Muscle Testing Scale [3]) were assessed in a crook position via digital palpation. Participants completed a 7-minute treadmill run at 10 km·h^{-1} with retro-reflective markers and inertial measurement units (Blue Trident, 225Hz) affixed. Coordinate and analogue data were synchronously captured using a 14-camera 3D motion analysis system (Vero/Vantage, Vicon, 250 Hz) and two force plates (Kistler Instruments AG, 1000 Hz) positioned underneath a treadmill (Sprintex, Mar Systems Ltd.).

Coordinate and analogue data were analysed in Visual 3D. Acceleration data were processed using a customised Matlab script. The mean of 20 steps were analysed for the left and right. Generalised linear regression models determined whether there was a relationship between pelvic floor weighted symptom score and ground reaction force (GRF) and acceleration outcome variables ($p < 0.05$).

RESULTS AND DISCUSSION

Pelvic floor dysfunction symptom severity weighted scores are shown in Figure 1 (mean ± SD score: 6 ± 4 out of 40, score range: 1 – 14). Pelvic floor muscle strength and endurance data are shown in Table 1. We found no significant association between pelvic floor dysfunction symptom severity and ground reaction force ($p = 0.209 – 0.410$) or pelvic acceleration ($p = 0.081 – 0.947$) outcome measures.
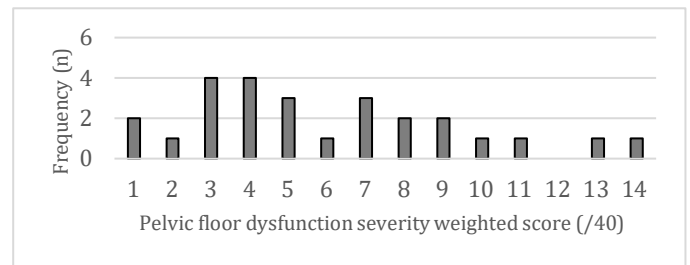
Figure 1: The frequency of participant's total pelvic floor dysfunction symptom severity weighted scores is shown.

CONCLUSIONS

We found no significant association between pelvic floor dysfunction symptom severity and GRF or acceleration outcome measures, suggesting that among the participant population recruited, symptoms of pelvic floor dysfunction are not associated with running mechanics.

ACKNOWLEDGEMENTS

REFERENCES

1. Donnelly & Moore, *Curr Sports Med Rep* **22**:82-90, 2023.
2. Baessler et al., *Int Urogynecol J,* **21**:163-172, 2010.
3. Laycock & Jerwood, *Physiotherapy,* **87**:631-642, 2001.

Table 1: Mean, standard deviation and 95% confidence interval data for participant's pelvic floor muscle strength and endurance.

Pelvic Floor Muscle Strength and Endurance Measure	Mean ± SD	95% CI Lower	95% CII Upper
Crook Pelvic Muscle Strength (MVC) (score /5 Oxford Scale)	3 ± 1	2	3
Crook Pelvic Muscle Endurance (0-10 second interval)	9 ± 2	8	10
Crook Pelvic Muscle Repetitions (no of sustained MVC reps)	4 ± 2	3	5

| Crook Pelvic Muscle Rapid Repetitions (no of quick MVC reps) | 9 ± 2 | 9 | 10 |

DISTINCT TIBIALIS ANTERIOR ELECTROMYOGRAPHY PROFILES IN STRENGTH AND ENDURANCE ATHLETES REVEALED BY PRINCIPAL COMPONENT ANALYSIS

[1]Hale-Worrall, S., [1]Mann, K.J., & [1]Chang, M.

[1]School of Allied Health, Exercise and Sports Sciences, Charles Sturt University,
Panorama Avenue, Bathurst, NSW 2795, Australia.
email: shaleworrall@gmail.com

INTRODUCTION

Recent data science advances have provided powerful methods to utilise biomechanical data sets through machine learning (ML) techniques. This includes classification of various populations from discriminating kinematic, kinetic, and electromyography (EMG) measures, particularly using support vector machines (SVM) [1]. Despite this, there is limited SVM literature on athletic characteristics. Since muscle fibre type is linked to exercise-specific adaptations [2], SVM classification of athlete types may provide insight into these adaptations. Our previous work used a forward selection approach in SVM models to distinguish between strength- and endurance-trained athletes, identifying the tibialis anterior (TA) as the most discriminatory muscle with 82.83% accuracy in the best-performing model using only TA EMG features [3]. Building upon and extending these previous findings, this study used Principal Component Analysis (PCA) to examine differences in TA EMG stance phase patterns between these same strength- and endurance-trained athletes.

METHODS

Fourteen healthy adult recreational athletes (5 endurance, 9 strength), actively training, without a gait-affecting injury participated in the study. Written informed consent was obtained, and the study was approved by Charles Sturt University's Human Research Ethics Committee (H22058).

Participants completed 50 walking gait trials at their preferred speed. Surface EMG from TA was recorded (2500Hz) using wireless electrodes (Trigno, Delsys Inc., Boston). Data were synchronised with ground reaction force events, initial contact and toe off, defining the stance phase, using force plates (2500Hz; Kistler Corp., Winterthur, Switzerland).

EMG signals were rectified, smoothed with a 4th order zero lag Butterworth filter (100 Hz cutoff), and time-normalised to 101 points (0-100% of the stance phase). Conducted on a 700×101 matrix (50 trials per participant) using MATLAB r2022a (The MathWorks Inc., Natick, Massachusetts), PCA was used to test differences in participants' TA EMG waveforms between strength- and endurance-trained athletes. PCA transforms the data into independent PC scores that reveal maximal variance, suitable for statistical analysis [4]. Linear Mixed Models were analysed using SPSS version 29 (IBM Corp., Armonk, New York), accounting for participant and repeated measures with a diagonal covariance structure.

RESULTS AND DISCUSSION

Based on examination of the Scree plot, PCA on TA EMG waveforms retained the first three principal components, accounting for 73.52% of the total variance. Linear Mixed Models analysed the effect of Athlete Type (strength and endurance) on PC1–3. Significant differences were found in PC1, PC2, and PC3 scores ($F(1, 420.583) = 106.176$, $F(1, 603.778) = 121.649$, $F(1, 533.635) = 28.126$, respectively; $p < .001$) between endurance (M = -3.331, 1.760, -0.758, respectively) and strength athletes (M = 0.849, -1.123, 0.164, respectively).
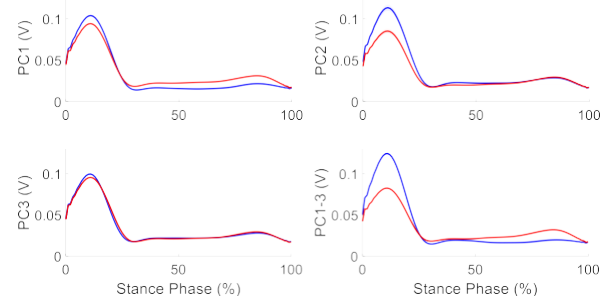
Figure 1: Reconstructed EMG signals for tibialis anterior (TA) during the gait stance phase, showing the first three principal components (PC1, PC2, and PC3). Graphs compare mean signals (solid lines) and 95% confidence intervals (shaded) between endurance (blue) and strength-trained athletes (red).

CONCLUSIONS

During the gait stance phase, reconstructed EMG signals of TA (Figure 1) indicate greater early activation in endurance compared to strength-trained athletes. Conversely, strength-trained athletes exhibit greater activation of TA in the latter two-thirds of the stance phase. These patterns likely reflect skill-based adaptations associated with respective dominant activities.

REFERENCES

1. Halilaj, E., et al., *Journal of Biomechanics* **81**:1-11, 2018.
2. Plotkin, D. L., et al., *Sports.* **9**:127-137, 2021.
3. Hale-Worrall, S., et al., *Classification of athletic gait patterns using electromyography and a machine learning approach.* Manuscript in preparation.
4. Robertson, D., et al., *Research Methods in Biomechanics* 2nd ed., Human Kinetics, Boston, USA, 2013.

PROFILING THE SPRINT-PADDLING KINEMATICS OF FEMALE AND MALE COMPETITIVE SURFERS

[1,2,3]Sienna Gosney, [1,2]Luke MacDonald, [1,2]Joanna Parsonage, [1]Matthew Worsey, [4]Justin Keogh, [1,2,3]April Denny, [1,5]Clare Minahan

[1]Griffith Sports Science, Griffith University, Gold Coast, QLD
[2]Surfing Australia, High Performance Centre, Casuarina, NSW
[3]Sport Performance Innovation and Knowledge Excellence (SPIKE) Unit, Queensland Academy of Sport, Nathan, QLD
[4]Faculty of Health Sciences and Medicine, Bond University, Gold Coast, QLD
[5]Female Performance and Health Initiative, Australian Institute of Sport, Canberra, ACT
Email: sienna.gosney@griffithuni.edu.au

INTRODUCTION

Sprint-paddling efforts are critical in surfing as they determine a surfer's positioning, optimal wave entry, and the ability to avoid being swept shoreward [1,2]. Sprint-paddling may contribute to surfing performance by increasing the number of waves surfed, time spent riding waves, and enhancing the ease and control at which the surfer can drop in, generate speed, and execute manoeuvres effectively [2,3].

Evidence from front-crawl swimming research indicates that technical execution of the arm stroke is responsible for 90% of the speed achieved [4]. The ability to elicit effective force and velocity simultaneously is vital, and monitoring kinematics can decipher how arm and hand movements influence this efficacy [4,5,6]. Spatiotemporal variables have not been explored in sprint-paddling and include stroke distance within distinct phases of a stroke cycle (glide, pull, push, recovery), where 'pull' and 'push' are propulsive phases. Considering the similar movement patterns of sprint-paddling and front-crawl swimming, a detailed analysis of paddling kinematics could highlight specific movement variables important for maximal surfboard speed.

METHODS

31 surfers (female: n = 15, 20±6 yr, 59.6±4.7 kg, 163.6±5.8 cm; male: n = 16; 22±7 yr, 72.8±14.9 kg, 174.8±7.5 cm) who competed in the World Surf League participated in the current study. The testing protocol included a pool-based testing session comprising three 15-m sprint-paddle trials with four min of rest between each. A horizontal position transducer (I-Rex, Southport) was mounted on pool deck atop a standardised frame. 5-, 10-, and 15-m split times were recorded via RX Capture software. For kinematic review and analysis, an above water top view, and an underwater side view camera (GoPro Inc., USA) recorded the surfer during each trial. A MATLAB (The MathWorks Inc., MA) code segmented each trial into acceleration (ACC) and speed maintenance (SM) periods, then AMR RX Motion Player Software (Swordfish, Southport) was used to assess the distances covered within each stroke phase (glide, pull, push, recovery) in these periods. All analysis was performed on the surfer's best trial as determined by their fastest 15-m split time. R Studio statistical software (Posit, MA) was used to employ a LASSO regression to identify the spatiotemporal variables most influential on each performance variable and any sex interaction effects.

RESULTS AND DISCUSSION

Regression analysis determined multiple spatiotemporal variables significantly associated with all split times, including a sex interaction (r^2=0.749, 0.791, and 0.794 respectively). For all surfers, push distance in ACC and pull distance in SM were indicative of faster split times. For male surfers, pull distance in ACC and SM was indicative of a faster 5-m time and pull distance in SM alone was indicative of faster 10-m and 15-m times. No variables were indicative of faster times for female surfers only. Implementing strategies targeted at increasing propulsive distances are thus likely to enhance sprint-paddling and positively impact surfing performance. Future investigations should seek to develop a more comprehensive sprint-paddling profile, particularly for female surfers, ultimately fostering their continued success alongside their male counterparts.

CONCLUSIONS

The results indicated that the development of a technique which promotes greater propulsive distances, and an additional investigation of the female surfer should be encouraged to further afford optimal sprint-paddling success in both sexes.

ACKNOWLEDGEMENTS

REFERENCES

1. Farley O, PhD Thesis, Edith Cowan University, 2016.
2. Volschenk W, et al., *International Journal of Aquatic Research and Education.* **13**(2). 2021.
3. Sheppard J, et al., *International Journal of Sports Science and Coaching.* **8**(1):45-52, 2013.
4. Lee J, et al., *Procedia Engineering.* **13**:148-153, 2011.
5. Cappaert J, *Biomechanics and Medicine in Swimming,* **8**:141-145, 1999.
6. Cortesi M, et al., *Journal of Sports Science and Medicine.* **18**:438-447, 2019.

EXPLORING THE USE OF OPENCAP IN CAPTURING CRICKET BOWLING KINEMATICS

[1]Alan Abraham, [1]Simon Feros, and [1]Aaron Fox
[1] Centre for Sport Research, Institute for Physical Activity and Nutrition (IPAN), Deakin University, Geelong, Australia

INTRODUCTION

OpenCap combines pose estimation algorithms with video-based IOS devices (e.g. iPad, iPhone) as a means to deliver a convenient, low-cost field-based motion capture solution [1]. Currently, OpenCap has been assessed for accuracy in movements such as squats, walking, sit-to-stands, and jump-landing tasks [1,2]. The accuracy of joint kinematic estimates from OpenCap has yet to be tested in sport-specific upper-limb dominant tasks. This study assessed the accuracy of OpenCap for cricket bowling against marker-based motion capture.

METHODS

One male right-arm off spin bowler (20 y, 180.1 cm, 74.85 kg) participated. The participant completed a 48-ball (i.e. 8-overs) spell guided by Feros et al. [3]. Data were simultaneously collected from OpenCap and marker-based motion capture. OpenCap data were captured using 3-ios devices and recommended practices [1]. Motion capture data were captured using markers placed according to the UWA model [4]. OpenCap joint kinematics were estimated automatically using the detailed shoulder model. An identical musculoskeletal model was scaled to the motion capture data from a static trial, and motion capture joint kinematics estimated using marker data and inverse kinematics via OpenSim 4.5. Shoulder (elevation plane and elevation), elbow (flexion) and knee (flexion) joint kinematics were extracted at ball release for each ball bowled, with ball-to-ball root mean squared error (RMSE) between OpenCap and motion capture calculated.

RESULTS AND DISCUSSION

Of the 48 balls bowled, 16 balls were deemed ineligible. Errors in OpenCap data (i.e. inaccuracies in body kinematics) accounted for 13 ineligible trials, while motion capture system errors accounted for the other three. The remaining 32 balls were compared for shoulder, elbow and knee joint kinematics (Table 1). The largest average RMSEs (~10-25º) at ball release were found for the shoulder joint angles. These findings likely stem from the large range of motion and complex positions at the shoulder inherent to cricket bowling, alongside potential issues limiting the pose estimation algorithms ability to track the arm (e.g. obscured from camera by body). Knee and elbow angles recorded smaller average RMSEs, likely reflecting the greater ability of OpenCap to track sagittal kinematics in agreement with existing work [2]. Despite the relatively large errors, overall body position at ball release was relatively well captured by OpenCap compared to motion capture (Figure 1).

Figure 1: Sample trial comparison of OpenCap (red) versus motion capture (black) data at ball release.

CONCLUSIONS

OpenCap demonstrated promise in capturing overall body position at ball release in cricket bowling. The relatively large and moderate errors versus motion capture for shoulder and elbow kinematics, respectively, may limit its use in areas where high accuracy is required (e.g. bowling action legality testing).

REFERENCES

1. Uhlrich SD, et al., *PLoS Comput Biol*, 19: e1011462, 2023.
2. Turner JA, et al., *J Biomech*, 171: 112200, 2024.
3. Feros SA, et al., *Int J Sports Physiol Perf*, 13:151-155, 2018.
4. Lloyd DG, et al., *Journal Sports Sci*, 18: 975-982, 2000.

Table 1: Mean (± SD) shoulder, elbow and knee joint angle estimates (º) at ball release estimated by OpenCap and motion capture systems. Ball-to-ball root mean square error (RMSE; mean ± SD) for the different joint functions at the point of ball release during the bowling action.

	OpenCap	Motion Capture	RMSE
Shoulder Elevation Plane	20.18 ± 9.54	9.01 ± 22.01	19.25 ± 11.54
Shoulder Elevation Angle	135.07 ± 2.04	122.44 ± 5.99	12.63 ± 5.76
Shoulder Axial Rotation	-18.61 ± 3.71	-27.95 ± 26.41	24.77 ± 11.76
Elbow Flexion	16.62 ± 5.60	18.12 ± 5.15	6.17 ± 3.98

| Knee Flexion | 74.06 ± 4.97 | 72.02 ± 9.30 | 5.96 ± 4.29 |

Monday, December 2

ANZORS Minghao Zheng Orthopaedic Innovation Award Final

EFFECTS OF VARIED NECK-SHAFT ANGLE ON INTERFRAGMENTARY STRAINS FOLLOWING PROXIMAL FEMORAL OSTEOTOMIES

[1]Alireza Y. Bavil, [1]Emmanuel Eghan-Acquah, [1]Laura Diamond, [1]Rod Barrett, [1]Christopher Carty, [1]David Saxby, [2]Stefanie Feih
[1]Griffith Center of Biomedical and Rehabilitation Engineering (GCORE), Griffith University, Australia
[2]School of Engineering and Build Environment, Griffith University, Australia
email: alireza.yahyaieebavil@griffithuni.edu.au

INTRODUCTION

Proximal femoral osteotomy (PFO) is a surgical intervention correcting femoral deformities in paediatric/adolescent patients. Despite the efficacy of PFO in treatment of femoral deformities, the surgery carries risks such as delayed healing in the femur. Strain at the cut (interfragmentary) region of the femur following PFO, can affect the callus formation rate [1]. Likewise, post-op neck-shaft angle (NSA) may also influence interfragmentary (IF) strain. This study examined how surgical variations in NSA affect IF strains during walking gait. This work was carried using a sequentially-linked and personalized neuromusculoskeletal (NMSK)-informed finite element analysis (FEA) to simulate PFO and post-operative IF strain.

METHODS

Three paediatric patients with femoral deformities underwent a thorough pre-operative biomechanical analysis involving acquisition of detailed motion capture data and computed tomography (CT) images of the lower limbs. Virtual corrective surgeries systematically incorporated three femoral NSAs (128°, 135°, and 143°) for each patient custom computer assisted design (CAD) scripts, thereby ensuring precision, and reducing human error.
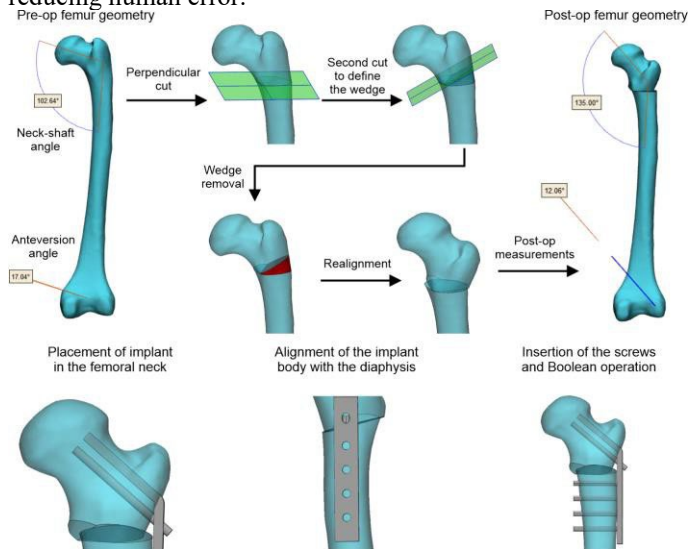
Figure 1: Pipeline for virtual PFO using an automated toolbox for systematic variation of NSA for the post-op femur. For each patient, their walking gait analysis data were used to determine joint kinematics, joint kinetics, and muscle tendon unit actuators in OpenSim [2]. Then, a scaled NMSK model was calibrated and executed to estimate lower limb muscle and joint

contact forces. Then, these muscle and joint contact forces were used as loading conditions within the FEA of the isolated femur. The CT imaging was used to map the material properties of the femoral bone for each patient. The femur FE models were subjected to a benchmarked 'biomechanical constraint' [3] to ensure physiological constraint during simulation. For each femur, the prescribed NSA set was applied systematically (Figure 1), implanted with the OrthoPediatrics blade plate, and the simulation conducted across the walking gait cycle. IF strain was extracted and compared to the mechanical stimulus range known to promote callus formation and calcification [4]. Analysis of variance and paired t-test statistical testing were performed to determine if NSA affected IF strains.

RESULTS AND DISCUSSION

Significant differences between the IF strain values for 128°, 135°, and 143° NSA were found with larger NSA resulting in larger IF strain. Further, IF strain varied significantly across stance phase of walking. Although the NSA assessed here were within normal range for an adolescent femur, simulations suggest only NSA of 143° would result in an optimal healing rate from the mechanobiological point of view.
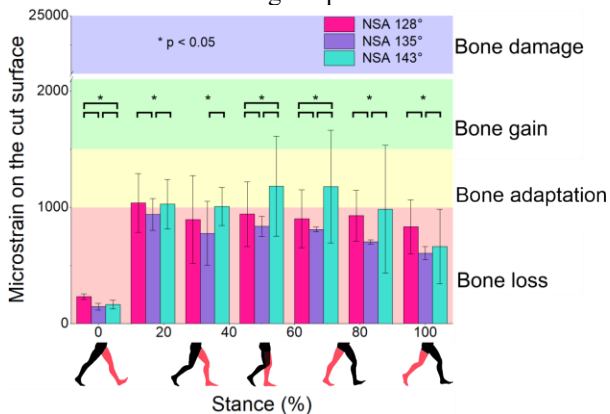
Figure 2: IF strains throughout the stance phase of gait.

CONCLUSIONS

Findings suggest IF strain is sensitive to NSA and varied across walking stance. Results highlights importance of PFO planning and using FEA throughout an activity rather than isolated time instances.

REFERENCES

1. Wang, et al., *IEEE Access.* 7 (1) 9827-9835, 2019.
2. Delp, et al. *IEEE Trans Biomed.* 54 (11) 1940, 2007
3. Bavil, et al., *Sci Rep*, 14 (1) 10808, 2024.
4. Mehboob, et al., *Ad in Dent Im*, 13(12) 7097, 2023

CIRCULATING microRNA IN ARTHROFIBROSIS PATIENTS OF POST TOTAL KNEE ARTHROPLASTY

[1]Jack Gong, [1]YiXuan Li, [1,2]Paul N. Smith and [1,2]Rachel W. Li

[1]School of Medicine and Psychology, Australian National University, ACT
[2]The Canberra Hospital, ACT
email: rachel.li@anu.edu..au

INTRODUCTION

Arthrofibrosis has been described in most joints like knee, hip, ankle, foot joints, shoulder, elbow (stiff elbow), wrist, hand joints as well as spinal vertebrae. It can occur after injury or surgical procedures of Total knee arthroplasty (TKA), which causes significant disability and limitation in daily living (1). There is no preventative care for arthrofibrosis. It poses a significant unsolved clinical challenge, which involves implant and materials, surgical technique, and patients' genetic responses. Some patients have to be performed manipulation under anaesthesia (MUA) or revision surgery. We hypothesized that the bridge among the data of bioinformatics analyses of blood miRNA and tissue mRNA, and clinical scenarios will yield exceptional predictive molecules for prognosis, prevention, and drug discovery, which will benefit the patients.

METHODS

This study includes two experimental groups. Group 1, patients who received primary TKA (n=10), and Group 2, patients were operated primary TKA and developed Arthrofibrosis (n=10). We have ethic approved protocols (ID: ACT HREC ETH.9.865). We collected blood samples for microRNA isolation and bone tissue for mRNA isolation. Whole blood samples were centrifuged using two cycles to separate plasma and remove cellular debris. Centrifuge speed is 3000 rmp, 10min each time. miRNA isolation using the miRNeasy serum/plasma kit (QIAGEN, USA) according to manufacturer's instructions. The miRNA samples were sequenced using the NovaSeq 6000 Sequencing System (Illumina, USA), the sequencing length was 100bp.

RESULTS AND DISCUSSION

While our sampling from the patients who were under MUA procedures are still ongoing, we have found significant genetic responses which involve the coordination of inflammatory cytokine release and growth factors, etc (Figure 1). We have recognized the regulatory factors from blood which might be responsible for abnormally expressed RNAs and proteins in the knee/skin tissue. The results provide information - a role for TGFβ1-SMAD signalling in the pathogenesis of development of Fb post TKA (2). Identified potential therapeutic targets in this pathway shall help development of gene therapy or compound for inhibition myofibroblast activation.
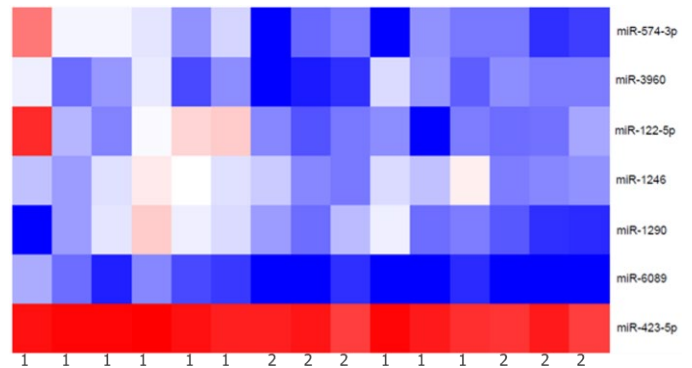
Figure 1: Differentially expressed plasma miRNA.

CONCLUSIONS

This is a prospective study. We are trying to address potential approaches based on the profibrotic actions of genetic factors for drug development. The results might be commercialized to fill a significant market gap for the prevention and treatment of arthrofibrosis.

ACKNOWLEDGEMENTS

REFERENCES

1. McAlister I., Sems, SA., Orthop Clin N edics. 2022 Sep;45(5):270.
2. Thorsteinsson H et al., Acta Orthopaedica. 2019:34(5)

Development of bioactive bone substitute (PearlBone™) using Mother-of-Pearl sourced from Broome, Western Australia

[1,2]Rui Ruan, [1,2]Behzad Shiroud Heidari

[1] Centre for Orthopaedic Research, Medical School, The University of Western Australia, Perth, WA
[2] Marine Biomedical Pty LTD, Broome, WA

INTRODUCTION

Bone substitutes are the most promising solution to address the shortage of bone grafts for dental and orthopedic conditions. However, slow resorption rates and poor osseointegration have resulted in less satisfactory clinical outcomes compared to using autografts and allografts. Nacre, commonly known Mother-of-Pearl, has been highlighted as a potentially suitable resource for bone implant material for decades but has yet to be translated into a clinically usable bone substitute. In this study, we converted nacre, a surplus by-product from the Western Australian pearling industry, into a bone substitute that meets clinical standards. We hypothesize that the bone substitute developed from nacre (pearl shell) has better bone integration and bioactivity and thereby promoting bone regeneration.

METHODS

The bone substitute material was prepared through a patented method (WO/2018/218305) involving two steps of self-setting chemical reactions that occur at low temperatures and ambient pressure. Using this method, a series of products in different forms, such as granules and moldable putty, trademarked as PearlBone™, were produced. The products were characterized by XRD, SEM, and mechanical testing. In vitro bioactivity was tested through SEM, XRD, FTIR, and mechanical testing by immersing the material into simulated body fluid at different time points. MC3T3-E1 cells were then seeded on the material, and cytocompatibility and osteostimulative properties were examined through the MTS method, confocal microscopy, and the expression of osteogenic markers. In vivo studies tested biodegradation by implanting PearlBone™ pellets into rabbit back fascia and examined bone healing efficacy by implanting PearlBone™ particles and putty into rabbit distal femoral critical bone defects, followed by analysis with Micro-CT and histology.

RESULTS AND DISCUSSION

The results show that the bone substitute material has unreacted nacre particles tightly integrated into the composite, which contains multiple biocompatible and osteoconductive calcium orthophosphates. The compression strength of the composite achieved 10.12 MPa, superior to human trabecular bone. The in vitro bioactivity tests demonstrated the formation of apatite with progressive nano-porous flake-like crystals on the surface of the composite over 28 days (Figure 1). Furthermore, the composite showed the capability to host the attachment and proliferation of osteoblast cells and to promote their osteogenic

differentiation. Confocal microscopy evidenced significantly high expressions of RUNX2 on day 1 and OPN on day 7. PearlBone™ material demonstrated a more efficient in vivo degradation rate without compromising physical structure. Finally, PearlBone™ particles demonstrated enhanced bone healing efficacy and biocompatibility in the healing of rabbit critical bone defect models compared to conventional bone substitutes (Hydroxyapatite). PearlBone™ putty showed equivalence in early-stage bone healing when compared to commercial bone putty products (MagnetOs™ and MasterGraft®) (Figure 2).

Figure 1: the surface topography change in *in vitro* bioactivity tests, (Ai) Day 0, (Bi) Day 7, (Ci) Day 28 after immersing PearlBone™ in SBF. (Aii) Day 0, (Bii) Day 7, (Cii) Day 28 after immersing calcite composite in SBF

Figure 2: PearlBone™ putty showed equivalence in early-stage bone healing when compared to commercial bone putty products, MasterGraft™ and MagnetOs™

CONCLUSIONS

PearlBone™, prepared through self-setting reactions, possesses advantages including faster biodegradation and osteostimulative properties, offering a promising alternative to traditional bone substitute for bone regeneration. Further clinical study is needed to demonstrate safety and efficacy of bone healing.

THE EFFICACY OF A NOVEL PORCINE-DERIVED COLLAGEN MEMBRANE ON GUIDED BONE REGENERATION: A COMPARATIVE STUDY IN CANINE MODEL

Anh Thi Mai Nguyen[1#], Euphemie Landao-Bassonga[1,2#], Elias D. Kontogiorgos[3#], Clair Lee[1], Tak Cheng[1], Hien Chi Ngo[4], Brent Allan[4], Mithran Goonewardene[4] Lynne A. Opperman[3], Minghao Zheng[1,2]

[1]Centre for Orthopaedic Research, Medical School, The University of Western Australia, Nedlands, Western Australia, Australia
[2]Perron Institute for Neurological and Translational Science, Nedlands, Western Australia, Australia
[3]Texas A&M College of Dentistry, Dallas, Texas, USA
[4]Dental School, Faculty of Health and Medical Sciences, The University of Western Australia, Nedlands, Western Australia, Australia

INTRODUCTION
Guided bone regeneration (GBR) is commonly used in dentistry, and it involves the use of bone substitutes and a barrier membrane [1]. This study aimed to evaluate the performance of the novel Striate+™ collagen membrane in a canine model of GBR with dental implant placement.

METHODS
Eighteen mature beagle dogs were used in this split-mouth design study. After having their premolar extracted, immediate implants with GBR techniques were carried out on all study subjects. The study treatments were: control group (implant + no membrane); BG-group (implant + Bio-Gide® membrane); and SG-group (implant + Striate+™ membrane). Six dogs were sacrificed at 4-, 8- and, 12-weeks post-treatment for radiographic (μCT) assessment, histological examination and histomorphometric analysis.

Figure 1. Histological assessment of osteoblast and osteoclast activities using Goldner Trichrome stained sections at 4-, 8- and 12-weeks post-treatment.

RESULTS AND DISCUSSION
μCT assessment showed that all groups exhibited increased bone formation from 4-weeks to 12-weeks post-treatment. There was no statistically significant difference in mean BV/TV between all 3 groups at weeks 4 and 8. But at week 12, BV/TV was significantly higher in SG and BG-groups compared to control group.

Assessment of bone microarchitectural parameters showed that animals in SG-group exhibited significantly higher Tb.N, O.Wi and lower Tb.Sp, suggesting more favorable mature bone structure. A significant increase in the number of osteoblasts on bone surface was also seen in SG-group (Figure 1).

Histological assessment showed that SG-group displays early signs of bone-to-implant contact at 8 weeks. While control sites showed early ingrowth of epithelium and connective tissue into the defects, infiltration of inflammatory cells, incomplete bone formation and limited bone to implant contact; significant bone infill, mature bone with good implant contact and limited soft tissue invasion were observed in SG- and BG- groups. Several studies have indicated that use of collagen membranes as a barrier structure is capable of soft tissue invasion and thereby increase the height of bone formation to the shoulder of implant [2]. A recent study also showed that both Striate+™ and Bio-Gide® membranes can block 0.2–16.4 μm beads from passing through them [3]. Thus, it is suggested that both membranes exhibit adequate space maintenance ability and favorable barrier characteristics to prevent unwanted epithelial and inflammatory infiltration.

CONCLUSIONS
This study demonstrated superiority of Striate+™ collagen membrane in GBR and prevention of unwanted epithelial infiltration in a canine model. Our studies suggest that Striate+™ collagen membrane is an ideal barrier scaffold for GBR.

REFERENCES
1. Urban IA, Monje A. Guided Bone Regeneration in Alveolar Bone Reconstruction. *Oral Maxillofac Surg Clin North Am*. 2019 May;**31(2):**331-338. doi: 10.1016/j.coms.2019.01.003.
2. Jung UW, Cha JK, Vignoletti F, Nuñez J, Sanz J, Sanz M. Simultaneous lateral bone augmentation and implant placement using a particulated synthetic bone substitute around chronic peri-implant dehiscence defects in dogs. J *Clin Periodontol*. 2017 Nov;**44(11):**1172-1180. doi: 10.1111/jcpe.12802.
3. Tai A, Landao-Bassonga E, Chen Z, Tran M, Allan B, Ruan R, et al. Systematic evaluation of three porcine-derived collagen membranes for guided bone regeneration. *Biomater Transl*. 2023 Mar 28;**4(1):**41-50. doi: 10.12336/biomatertransl.2023.01.006.

Monday, December 2

ANZORS Podium 4

MECHANICAL LOAD DISTRIBUTION IN EQUINE METACARPAL CONDYLES: A COMPUTATIONAL MODEL USING STANDING CT IMAGES

[1]Fatemeh Malekipour, [2]Chris Whitton, [1]Peter V.S. Lee

[1]Faculty of Engineering and Information Technology, The University of Melbourne, Melbourne, VIC
[2]Equine Centre, Faculty of Science, The University of Melbourne, Werribee, VIC
email: fmal@unimelb.edu.au

INTRODUCTION

Stress fractures are prevalent in both humans and animals engaged in athletic activities. Factors like joint structure, bone mineral density (BMD), and biomechanical strains contribute to their development. The third metacarpophalangeal joint (MC3) in racehorses is particularly susceptible due to rapid and high-magnitude cyclic loads during training/racing. Post-mortem examinations have revealed microcracks, densification of the subchondral bone (SCB), i.e. sclerosis and/or focal lysis with lower BMD. Standing computed tomography (sCT) can detect early changes in bone shape and BMD. This study aims to develop sCT-based finite element (FE) models for three horses with varying levels of sclerosis and lysis to investigate SCB strains. We hypothesize that the FE model will identify distinct SCB strain patterns in areas with sclerosis and lysis under simulated gallop loads in the MC3 joints of the three horses.

METHODS

CT images of right limbs from three live Thoroughbred racehorses were obtained in a standing position, each exhibiting different SCB conditions: bilateral sclerosis (BS), a lateral parasagittal groove lesion with surrounding sclerosis (LGL), and bilateral condylar lesions (BCL). CT images were aligned to simulate a galloping position, and 3D segmentation included distal MC3 bone, articular cartilage (AC), proximal sesamoid bones (PSBs), intersesamoidian ligament (ISL), and the proximal phalanx. Heterogeneous FE models were created by mapping BMD-based elastic modulus (E) to MC3: $E = -8196.7 + 5880.6\rho$, ρ: actual density [1]. An elastic modulus of 4GPa was assigned to PSBs and P1, and a hyperelastic neo-Hookean model with a shear modulus G=40 MPa and Poisson's ratio of 0.4999 to AC and ISL [2]. A surface pressure of 30 MPa was applied to simulate tendon compression during midstance. The models were analyzed in ABAQUS/Standard to evaluate SCB strain.

RESULTS AND DISCUSSION

The FE results showed peak surface pressure in the palmar section of the MC3-PSB, with higher pressure over the condyles and almost zero in the sagittal ridge, consistent with the literature [3]. In the horses with BS and LGL, tensile strain peaked at the PSGs (avg ± SD of 0.85 ± 0.2). In the horse with BCL, tensile strain peaked in the lytic condyles (0.86 lateral,

0.99 medial). The compressive strain was high in the most 2-3 mm superficial SCB for all subjects (1.82 ± 0.99) but peaked in the lytic condyles of the BCL horse (2.09 lateral, 2.90 medial). These compressive strains may explain the observed microcracks in the superficial SCB, commonly identified in specimens from similar sites, while tensile strains in the PSG may lead to crack propagation and failure.
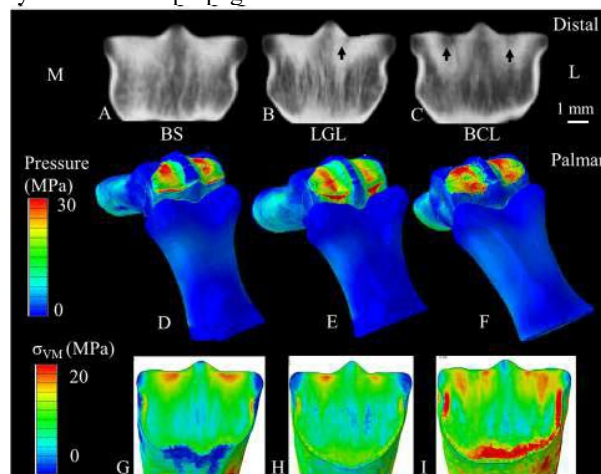
Figure: Dorsal oblique CT slices of the distal MC3 (A-C), contour of AC pressure from corresponding FE models of each horse (D-E) and von Mises stress within SCB for a section matching the CT slice (G-H).

CONCLUSIONS

The FE models highlighted the PSGs and MC3 condyles as critical regions at risk for mechanical failure due to elevated strain, consistent with clinical observations. Future research should involve a larger sample size and longitudinal imaging to improve understanding of SCB stress fractures.

REFERENCES

1. Martig et al., *Bone,* **57**, 392–8, 2013.
2. Malekipour et al., J Biomech, **49,** 2053-9, 2016.
3. Easton KL, ProQuest Theses, 99, 2012.

KNEE JOINT MOMENT CHANGES FOLLOWING A STRUCTURED EDUCATION AND EXERCISE PROGRAM (GLA:D®) FOR KNEE OSTEOARTHRITIS AND THE RELATIONSHIP TO RADIOLOGICAL OA SEVERITY AND BODY WEIGHT

[1]Jacqui Couldrick, [1]Andrew Woodward, [1 2 3]Joseph Lynch, [4]Nicholas Brown, [5]Christian Barton and [1]Jennie Scarvell

[1]Faculty of Health, The University of Canberra, Canberra, ACT
[2]College of Medicine and Health Sciences, Australian National University, Canberra, ACT
[3]Trauma Orthopaedic Research Unit, Canberra Hospital (TORU), Canberra, ACT
[4]Faculty of Health, Queensland University of Technology, Brisbane, QLD
[5]La Trobe University, Melbourne, VIC
email: Jacqui.couldrick@canberra.edu.au

INTRODUCTION

Evidence suggests the knee adduction moment (KAM), an indicator of medial to lateral joint load, does not change following exercise therapy [1,2]. However, studies focus on medial knee osteoarthritis and gait and the knee flexion moment (KFM) is less reported. KFM and more demanding tasks like chair-rise may be sensitive to change. Patient characteristics, including radiological compartment severity and body weight, might moderate knee joint load changes after exercise therapy. This study aimed to determine whether knee joint moments change following a structured education and exercise therapy program (GLA:D®) for knee osteoarthritis (OA) and the relationship with body weight and OA severity in each compartment.

METHODS

31 participants with knee OA underwent three-dimensional biomechanical analysis during walking and chair-rise at baseline and week 8 following GLA:D®. Multilevel models were used to calculate the changes in KAM and KFM and the relationships to body weight and radiological OA severity in the medial, lateral and patellofemoral compartments.

RESULTS AND DISCUSSION

Following GLA:D®, larger reductions were observed in knee joint moments for chair rise compared to walking (Table 1).

There was no evidence of a strong relationship between a person's body weight and any biomechanical following GLA:D® except for KAM in walking, where those with higher body weight tended to increase KAM at week 8. Different relationships were observed for OA severity depending on the task or outcome. A key finding was that the GLA:D® intervention had no effect on the relationship between compartment severity (medial, lateral or PF) and peak KAM 1 (see overlapping lines, Figure 1). A positive relationship was observed between medial compartment severity and KAM 1 and a negative relationship between lateral and PF compartment severity and KAM 1 (Figure 1).
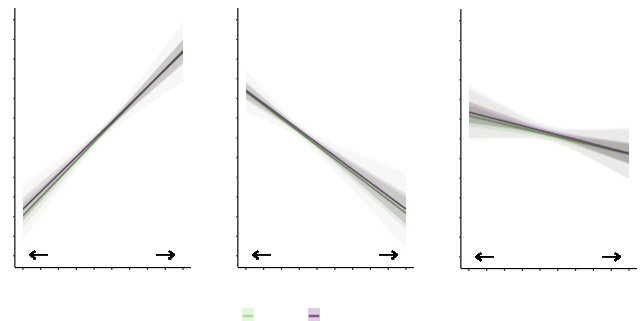
CONCLUSIONS

Greater reductions in KAM and KFM were found for the more demanding task of chair rise. For OA severity, different relationships were found depending on the task and the biomechanical measure. There was no relationship between body weight, and KAM, or KFM in walking or chair rise. Heavier people had similar joint moment changes following GLA:D®.

REFERENCES

1. Cottmeyer D, et al., *Clin Biomech.* **109**:106064, 2023.
2. Yokoyama M, et al., *Clin Rheum.* **42**:1737-1752, 2023

Table 1: Change in KAM and KFM following GLA:D® for walking and chair rise

Measure	Week 0 (n=31) Point estimate (90% Crl)	Week 8 (n=31) Point estimate (90% Crl)	Percent change
Task: Walking			
KAM 1 (Nm)	41.9 (37.9, 45.9)	43.0 (39.0, 47.0)	↑ 3%
KAM impulse (Nm sec)	1312 (1160,1498)	1357 (1209,1517)	↑ 3%
KFM 1 (Nm)	57.2 (50.8, 63.7)	55.9 (49.8, 61.9)	↓ 2%
KFM impulse (Nm sec)	1648 (1512,1795)	1540 (1391,1702)	↓ 7%
Task: Chair rise			
|Peak KAM| (Nm)	13.7 (11.6, 16.1)	10.3 (8.6, 12.4)	↓ 25%
KAM impulse (Nm sec)	1088.2 (922,1283)	806.1 (666, 974)	↓ 25%
Peak KFM (Nm)	61.3 (55.7, 66.8)	52.6 (46.4, 58.8)	↓ 14%
KFM impulse (Nm sec)	3196 (2847, 3577)	2880 (2589, 3198)	↓ 11%

Figure 2: Relationship between 1st peak KAM and OA compartment severity in walking

OVINE VERTEBRAL BONE STRAIN ANALYSIS AFTER OVERLOAD BY COMBINING MECHANICAL TESTING AND MICTO-CT

[1,2]Sara Montanari, [3]Michael P. Russo, [2]Sophie Rapagna, [1]Luca Cristofolini, [3]John J. Costi and [2]Egon Perilli

[1]Department of Industrial Engineering, Alma Mater Studiorum – University of Bologna, Bologna, Italy
[2]Medical Device Research Institute, College of Science and Engineering, Flinders University, Adelaide, SA, Australia
[3]Biomechanics and Implants Laboratory, Medical Device Research Institute, College of Science and Engineering, Flinders University, Adelaide, SA, Australia
email: sara.montanari.23@gmail.com

INTRODUCTION

Disc herniation can be replicated in an *ex-vivo* experiment through compressive overloading in a flexed or flexed and axial rotated posture [1]. While internal disc strains have been quantified to understand the mechanisms of progressive herniation during simulated lifting [2], these measurements have not yet been performed in the vertebra. Thus, this study aimed to compare internal vertebral strains in lumbar functional spinal units (FSUs) subjected to increasing compressive overload displacements, in a flexed and axially rotated posture.

METHODS

Fifteen ovine lumbar FSUs were prepared, subdivided into three groups, and overloaded in a Hexapod robot [3]. All the specimens were postured at 13° flexion and 2° left axial rotation and then compressed to either 1 mm, 2 mm, or 3 mm, at 400 mm/min [1]. Micro-CT scans (Nikon XTH 225 ST) of each FSU were performed (22 µm/pixel) before and after compression. Micro-CT datasets of each specimen after compression were co-registered to the intact dataset and DVC analysis (DaVis, v8.3.1, LaVision, 3-step progression, final subvolume side length 1.4 mm) was performed [4]. A zero-strain analysis was performed to assess the accuracy (mean) and precision (standard deviation) of the DVC process. The median Correlation Value (CV) was recorded as an indicator of DVC's ability to correlate datasets. The minimum principal strain (ε_{min}) was extracted on the bone vertebral area across each specimen.

RESULTS AND DISCUSSION

The zero-strain accuracy was 690 µε, precision 590 µε, with a CV of 0.99. Visual inspection of the FSU after each test did not find any gross vertebral fractures. Posterolateral annulus rupture was seen in the 3 mm group. In all specimens, both the growth plates (adjacent to the intervertebral disc) showed higher values of ε_{min} compared to their central vertebral body (-770±520 µε, median ± interquartile range, for all specimens) (Figure 1, Table 1). Micro-CT images also revealed clearly visible permanent bone deformations in the lower growth plate of the caudal vertebrae in the 2 mm group, and a fracture with visible fracture lines in the upper growth plate of caudal vertebra for all the specimens in the 3 mm group.
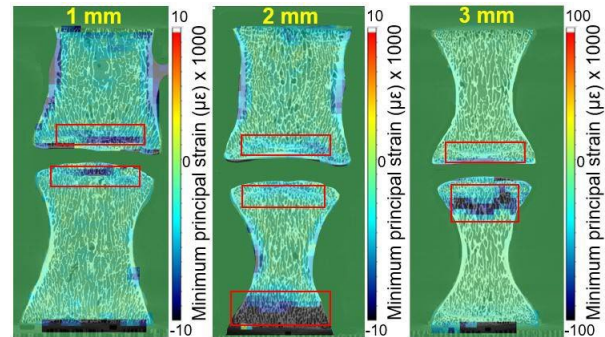
Figure 1: Minimum principal strain of an example specimen in each group compressed to 1 mm, 2 mm, or 3 mm, respectively. Red boxes: growth plates with higher strain values than in the vertebral body.

Table 1: Minimum principal strain (µε) in the growth plates adjacent to the disc of the cranial and caudal vertebrae; median±interquartile range values for each group are reported.

Compressive endpoint	1 mm	2 mm	3 mm
Cranial vertebra	-5,900 ±6,300	-3,400 ±2,200	-6,700 ±6,500
Caudal vertebra	-2,900 ±2,600	-3,500 ±250	-10,500 ±11,100

CONCLUSIONS

The findings of this ongoing study showed permanent strain in the growth plates following compressive overload to set compressive endpoints (1-3 mm). Although no significant visible damage to the vertebral bone was observed after each test, internal permanent deformation was detected by micro-CT imaging and DVC analysis, in the growth plates adjacent to the intervertebral disc, in all specimens. This confirms that, although herniation studies primarily focus on the disc, high strains are also generated within the vertebral bone, potentially leading to permanent bone deformation and fractures [5].

REFERENCES

1. Wade et al, *Spine,* **40**(12): 891-901, 2015.
2. Amin et al, *Spine,* **45**(6):357-367, 2020
3. Tavakoli et al, *Ann Biomed Eng*, **46**(9): 1280-1291, 2018.
4. Wearne et al, *JMBBM* **134**, 105336, 2022.

5. Rajasekaran et al, Spine, **38**, 1491-500, 2013

REDUCED MICROMOTION OF CEMENTLESS TIBIAL IMPLANTS IS RELATED TO INCREASED INTERFERENCE FIT: A MICRO-CT AND DVC STUDY

[1]Lauren S Wearne, [1]Sophie Rapagna, [1]Maged Awadalla, [2]Greg Keene, [1]Mark Taylor and [1]Egon Perilli

[1] Medical Device Research Institution, College of Science and Engineering, Flinders University, Adelaide, SA, Australia
[2] Orthopaedics Department, SportsMed, Adelaide, SA, Australia
email: lauren.wearne@bme.lth.se

INTRODUCTION

Sufficient primary stability is crucial to facilitate bony ingrowth for cementless tibial components in total knee arthroplasty (TKA). However, due to previous experimental limitations, little is known about the interplay between interference fit and micromotion across the entire bone-implant interface [1]. The aim of this study was 1) to experimentally quantify the micromotion across the entire interface of a cementless tibial component and underlying bone for seven cadaveric tibiae through micro-CT imaging and digital volume correlation (DVC) and 2) to assess the relationship between actual interference fit and observed micromotion.

METHODS

Micro-CT scans (46µm/pixel) were taken of seven cadaveric tibiae, first when resected, then once implanted with a cementless TKA component, and then during two time-elapsed mechanical load sequences, that replicated stair descent (SD, 0.0 – 2.5 bodyweight, BW) and deep knee bend (DKB, 0.0-3.5BW) [2]. Resected and loaded scans were rigidly co-registered to the unloaded scan in each activity. Actual interference fit was quantified as the distance between the resected surface of the tibiae after TKA preparation and the surface of the impacted implant, with positive values denoting interference and negative values a gap [1].

DVC was performed on loaded scans (DaVis v8.3.1, algorithmic masking to remove air, 5-step progression, final subvolume sidelength 1.56mm (34pixels)) [2] and the internal displacement vectors were extracted. Micromotion was defined as the absolute relative difference in displacement vectors for implant-to-bone subvolumes across the interface. Median actual interference and micromotion was calculated for eleven volumes of interest (VOIs) across the bone-implant interface: 4 across the pegs, the keel, and 6 VOIs across the tray (Fig.1A, dashed lines). For VOIs of the tray, the median vertical micromotion was also calculated. A linear regression was performed to test relationships between the micromotion (predicted variable) and actual interference (predictor variable) for each load case.

RESULTS AND DISCUSSION

Micromotion magnitude varied amongst the tibiae, but for all specimens there was a comparable regional distribution (Fig.1A). A sagittal rocking motion of the tray during both SD and DKB was apparent from micro-CT images, with anterior lift-off and posterior subsidence. This was enhanced during DKB in comparison to SD, particularly in the anterior-lateral region of the tray. Micromotion magnitude increased at progressive loads, however, even at highest applied loads (SD 2.5BW and DKB 3.5BW) at least 78.6% of the implant surface across all implants had a micromotion less than 150µm.

The actual interference (median ± std dev) was 0.70±0.25mm for the pegs, 0.95±0.50mm for the keel and 0.02±0.12mm for the 6 VOIs of the tray. Actual interference was a predictor of implant micromotion for all bar one load case (R^2 = 0.109 - 0.248, p< 0.035), with greater interference corresponding to reduced micromotion (Fig.1 B).
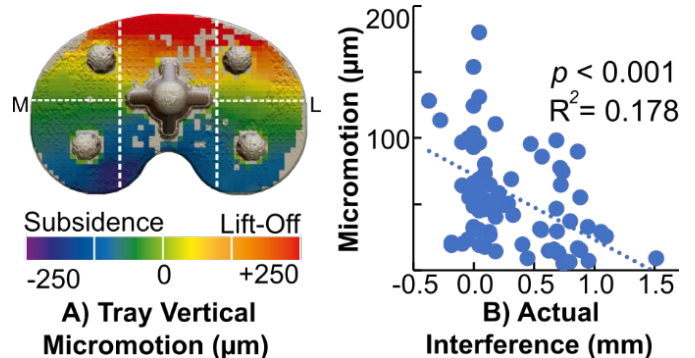
Figure 1: During DKB at 3.5BW: A) Vertical micromotion distribution across the tray of one tibia, and, B) regression analysis of micromotion vs. actual interference for all 7 tibiae.

CONCLUSIONS

The micromotion across the entire bone-implant interface was quantified experimentally for 7 cadaveric tibiae during activities replicating SD and DKB, by using time-elapsed micro-CT and DVC analysis. A sagittal rocking motion of the implant was revealed for both activities. Regions with reduced micromotion were related to increased interference. This supports the conjecture that including an interference fit during surgery may increase primary stability, enabling osseointegration of cementless tibial trays.

ACKNOWLEDGEMENTS

REFERENCES

1. Berahmani S et al., Clin Biomech. **51**:1-9, 2018.
2. Wearne LS et al., J Mech Behav Biomed Mater, **151**:

106347, 2024.

UNDERSTANDING CARDIAC CO-MORBIDITY WITH OSTEOARTHRITIS IN MICE

[1,2]Harrison Johansen, [1]John Mach, [1]Bryony Winters, [1]Yo Otsu, [1]Sarah Hilmer, [1,2]Christopher Little, [1,2,3]Carina Blaker

[1]Kolling Institute, Faculty of Medicine & Health, University of Sydney and Northern Sydney Local Health District, Sydney, NSW
[2]Sydney Musculoskeletal Health, University of Sydney, Sydney, NSW
[3]Sydney School of Veterinary Science, Faculty of Science, University of Sydney, Sydney, NSW
email: hjoh2985@uni.sydney.edu.au

INTRODUCTION

Osteoarthritis (OA) affects ~590 million individuals globally as of 2020, and is 1.4x more prevalent in females than males [1]. While OA is an established degenerative disease of the joints, the systemic effects of OA remain unclear. Recent meta-analyses and longitudinal clinical cohort studies have shown that OA is correlated with an increased risk of co-morbid cardiovascular diseases (e.g. hypertension), [2] which particularly affects females [3]. Co-morbidity worsens both individual and societal burdens and substantially increases mortality risk. Identifying the causal link/s between OA and chronic heart conditions could alter how we evaluate and treat OA and its comorbid diseases. Our current understanding is limited by patient confounders which are also independently attributed to the development of cardiovascular disorders (e.g. obesity, aging, smoking), however, these can be controlled in preclinical models. The study aimed to quantify cardiac tissue pathology in a murine model of induced-knee OA.

METHODS

Middle-aged (12-month-old) male and female C57Bl6 mice were randomly allocated to either an induced-OA or naïve control group (n=9-14/sex/group). OA was induced by a closed, ACL rupture, a common injury associated with post-traumatic OA and increased cardiovascular risks [4]. At 15-17 weeks after ACL rupture (or age-matched controls), the heart was fixed and stained with picrosirius red (PSR) for fibrosis quantification; or haematoxylin and eosin (H&E) for semi-quantitative scoring of cardiopathies (myocyte necrosis, cellular infiltration). Cardiac fibrosis was analysed using a colour thresholding and segmentation workflow on PSR sections in QuPath. The percentage of fibrosis was then quantified across the subregions of the heart (left ventricular wall, right ventricular wall, and interventricular septum). Differences between sex and OA groups were analysed using mixed model regression.

RESULTS AND DISCUSSION

PSR fibrosis staining was observed across the whole heart cross-section in both male and female mice, and both control and OA groups (Figure 1). In female mice, there were no differences between control and OA groups. Interestingly, there was a significant reduction in whole tissue cardiac fibrosis in male OA mice compared with male controls (P = 0.028; Figure 1A). From the region-specific analyses (Figure 1B), there was a significant reduction in the fibrosis of the right ventricular

wall in particular in the male OA vs control mice (P = 0.029). The reduction in middle-age OA male mice may have implications for sex-specific cardiovascular risk factors in OA.
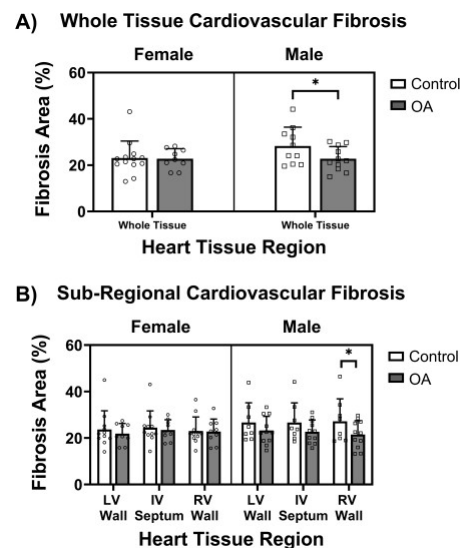
Figure 1: Fibrosis area percentage in cardiac tissue of aged male/female control and induced-OA mice: A) whole heart; B) heart subregions (left ventricular (LV) wall, right ventricular (RV) wall, and interventricular (IV) septum). Mean ± SD.

CONCLUSIONS

ACL-rupture induced knee-OA caused a sex-specific reduction in myocardial fibrosis staining, particularly the right ventricular wall. Additional cardiac histopathology will be evaluated to determine broader structural changes across older male and female mice with OA. Future studies will also evaluate effects in younger mice and with different OA-inducing injuries (e.g. meniscus) and age-associated OA.

ACKNOWLEDGEMENTS

REFERENCES

1. Haile L et al., *Lancet. Rheumatol.* **5**:e508-e522, 2023
2. Wang H et al., *Sci Rep.* **6**:39672-39672, 2016
3. Kovari E et al., *Semin Arthritis Rheum.* **50**:183-191, 2020
4. Meehan WP, et al. *Am J Cardiol* **122**: 1879-1884, 2018

EXPERIMENTAL-COMPUTATIONAL PLATFORM TO STUDY CORTICAL BONE REMODELLING

[1]Natalia M. Castoldi, [2]David Cooper, [1]Peter Pivonka

[1] School of Mech., Medical & Process Eng, Queensland University of Technology, Brisbane, QLD; [2] Department of Anatomy Physiology and Pharmacology, College of Medicine University of Saskatchewan, Saskatoon, Canada;
email: n.muhlcastoldi@qut.edu.au

INTRODUCTION

Osteoporosis affects over 200 million people globally, with 80% being women [1]. The incidence of osteoporosis increases the risk of bone fractures–where 80% of all fractures occur at weakened, thinned cortical bone sites [2]–leading to chronic pain and disability [3]. The root cause of osteoporosis is linked to the bone remodelling process, i.e. resorption of bone followed by bone formation and subsequent mineralisation. Basic multicellular units (BMUs) are responsible for the coordinated execution of bone remodelling. Currently, not much is known about BMU remodelling and how this is linked to changes in bone microarchitecture. We have developed an experimental-computational platform to investigate BMU remodelling in cortical bone. The experimental part of the platform is based on in-vivo μCT imaging of rabbit bone [5, 6]. The computational part of this platform is an extension of a discrete spatio-temporal model of trabecular bone [7]. In this work, we use this platform to test the hypothesis regarding BMU and mineralisation kinetics and their effect on cortical bone porosity and mineral density distribution (BMDD).

METHODS

Experimental data: In-vivo SR-μCT experimental data of rabbit cortical BMUs under different conditions was used [5, 6] *Discrete bone remodelling model:* We introduce BMUs discretely on a homogeneous representative volume of 0.5 mm² depending on the activation frequency (BMUs/year/mm²). The model follows bone fractions evolution: osteoid (ϕ_o), water (ϕ_w) and mineral (ϕ_m). Each activated BMU undergo typical bone remodelling periods and evolves in time (t) and space (r), as shown in Figure 1. During resorption, the osteon radius proceeds radially up to a distance R_{On}, creating a pore. After a quiescent reversal period, formation takes place radially from the osteonal wall towards the Harversian's canal, where the laid down bone is unmineralised: $\phi_m = 0$, $\phi_o = 0.33$ [7]. Once mineralisation starts, mineral content continuously increases to a maximum of 30 wt% of calcium [8].
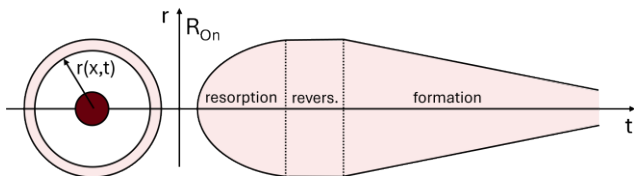
Figure 1: Osteonal geometry and time course of the radius of the region where modelling takes place.

RESULTS AND DISCUSSION

We analysed the influence of parathyroid hormone (PTH) on bone remodelling in the rabbit tibia. Figure 2A shows the experimental results indicating a high clustering of BMUs and a significant increase in activation frequency from 1.8 (control) to 30.1 (PTH treated) [5]. Our computational results show that PTH leads to a shift in BMDD (Figure 2B). The increased activation frequency leads to a significant increase in cortical porosity.
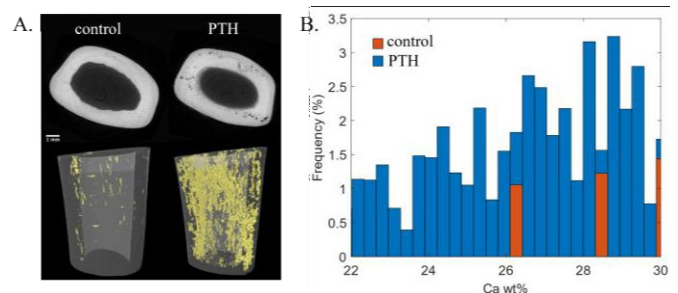
Figure 2: A. Cross-section and porosity of control and PTH treated rabbit tibia [5]; B. BMDD

CONCLUSIONS

Our computational results show that both BMU activation frequency and mineralisation kinetics contribute to the inhomogeneous distribution of minerals in bone, which may be useful for gaining insights into bone diseases such as osteoporosis. Future work aims to use our model to design novel experiments, such as using an inverse analysis of bone turnover/activation frequency. Using an in-silico approach will help to narrow down new animal experiments.

ACKNOWLEDGEMENTS

REFERENCES

1. Kanis, J. *WHO Scientific Group Technical Report*, 2007.
2. Zebaze et al, *J Bone Miner Res*, **30**(1):24, 2015
3. Sözen, et al, *Eur. J. Rheumatol.*, **4**(1), 46, 2017
4. Poole et al, *PLoS One*, **7**(6):e38466, 2017.
5. Harrison et al, *J Bone Miner Res*, **35**.11:2211-2228, 2020.
6. Cooper et al, *Bone*, **176**:116864, 2023
7. Castoldi et al, *Biomech Mechanobiol*, **23**:893-909, 2024.
8. Ruffoni et al, *Bone*, **40**(5):1308-1319, 2007

ANALYSIS OF BONE MINERALISATION USING DISCRETE AND CONTINUOUS MODELS OF BONE REMODELLING

[1]Corinna Modiz, [1]Natalia Muhl Castoldi, [1]Saulo Martelli, [2]Javier Reina-Martinez, [3]Stefan Scheiner, [4]Vittorio Sansalone and [1]Peter Pivonka

[1]School of Mechanical, Medical and Process Engineering, Queensland University of Technology, Brisbane, QLD
[2]Departmento de Ingeniería Mecánica y Fabricación, Universidad de Sevilla, Seville, Spain
[3]Institute of Mechanics of Materials and Structures, TU Wien, Vienna, Austria
[4]Faculté des Sciences et Technologie, Université Paris-Est Créteil (UPEC), Créteil, France
email: corinna.modiz@hdr.qut.edu.au

INTRODUCTION

Bone remodelling, essential for bone health and calcium homeostasis, involves four main stages: activation, resorption, formation, and mineralisation. This process is controlled by basic multicellular units (BMUs), which consist primarily of osteoblasts and osteoclasts. Diseases such as osteoporosis disrupt the balance of activity of these cells, leading to increased bone resorption and loss of bone mass.

Mathematical models have provided effective analyses of bone remodelling mechanisms, but many overlook mineralisation, which is crucial for understanding microcracks and anti-resorptive osteoporosis treatments [1]. Modelling mineralisation is complex due to its dependence on tissue age and biphasic kinetics: a rapid primary mineral development followed by a prolonged secondary phase that extends over years. This requires tracking and updating the age of each tissue patch, which significantly increases the computational and memory requirements for both discrete and continuous models. Thus, this study investigates different model strategies for mineralisation [1,2] to determine optimal mineralisation update intervals, improving efficiency and providing cross-methodological validation.

METHODS

The selected continuous bone cell population model (BCPM) considers average mineralisation in a representative volume element (RVE) of trabecular bone [1]. BMUs are not modelled explicitly, instead, the number of cells is aggregated over the entire RVE, and an iterative queue is used to track aging tissue patches. Mineral content is calculated based on patch age and averaged over the RVE to assess overall mineralisation. In contrast, the chosen discrete model activates individual BMUs on the trabecular surface and explicitly considers each remodelling phase for a given BMU [2]. It analyses the effects of bone turnover and mineralisation kinetics on the calcium content in the RVE without explicitly modelling cell dynamics.

Our methodology is represented in Figure 1. For the continuous model, we use cumulative cell counts over time and histomorphometric data [3] to calculate the number of active BMUs in an RVE. For the discrete model, individual BMUs are modelled directly. We compare the number of BMUs from both models at specific time points, ensuring a validated basis for further analysis. Using these aligned models, we compare mineralisation results for identical trabecular RVEs. This comparison allows us to improve the iterative queuing algorithm of the continuous model and reduce computational costs.
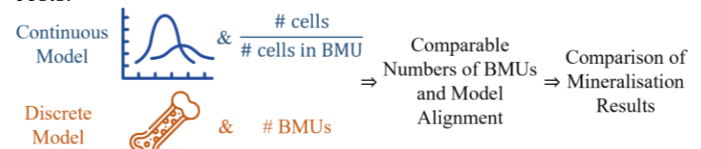
Figure 1: Illustration of the methodology.

RESULTS AND DISCUSSION

We developed a continuous model that integrates bone cell dynamics and mineralisation. By comparing it to the discrete model, we identified extended update intervals to reduce computational effort, justified by the prolonged secondary mineralisation phase. Additionally, the discrete model indicates an activation frequency of 1 to 8 BMUs/mm²/year. Since the BCPM analyses dynamics over years, daily updates to the iterative queuing algorithm are not required for accurate mineralisation and remodelling representation. In addition, the model is validated against histomorphometric measurements of BMUs and bone cells in the RVE.

CONCLUSIONS

Mineralisation can be efficiently integrated into a continuous BCPM by determining optimal update intervals. Future studies on e.g., mechanical loading can be facilitated by this model.

ACKNOWLEDGEMENTS

REFERENCES

1. Martinez-Reina J, et al., *Bone.* **125**:87-95, 2019.
2. Castoldi NM, et al., *Biomechanics and Modeling in Mechanobiology.* **23**:893-909, 2024.
3. Recker R, *Bone Histomorphometry: Techniques and Interpretation.* 1983.

ACOUSTIC AND TORSIONAL FACTORS AS PREDICTORS OF BONE QUALITY AND SCREW PURCHASE

[1] Tyra Lange, [1,2] Egon Perilli, [1,2] Sophie Rapagna, [1] John J. Costi and [1] Karen J. Reynolds

[1] Medical Device Research Institute (MDRI), College of Science and Engineering, Flinders University, Adelaide, Australia
[2] Flinders Microscopy and Microanalysis, College of Science and Engineering, Flinders University, Adelaide, Australia
email: tyra.lange@flinders.edu.au

INTRODUCTION

Pedicle screw insertion is heavily reliant on surgical expertise in conjunction with *sense perception*. Surgeons are able to *feel* and even *hear* the quality and types of bone tissues under fixation [1]. Acoustic emission is vibrations heard by surgeons' ears during drilling and insertion torque is the feeling in surgeons' hands during screw insertion [2, 3]. In clinical settings, surgeons use auditory (acoustic emission) and tactile (torque) perceptions to identify breach, to judge the quality of bone under fixation and the extent of screw purchase. These auditory and tactile cues are well-known to surgeons, yet they remain largely unexplored and are not currently monitored numerically, in theatres. This study aimed to quantify acoustic emission (AE) and insertion torque (T) as predictors of bone quality (in terms of morphometric parameters) and screw fixation strength (indicated by pullout force).

METHODS

In vitro experimental testing was conducted on 22 ovine lumbar vertebrae (L1–L6). Pilot holes were drilled at 1250 rpm into bones utilising an orthopaedic drill. AE was captured at 48 kHz by a sound sensor module and maximum AE (AE_{max}) extracted. Titanium, self-tapping pedicle screws (4.5 x 32 mm) were inserted with a custom rig at 6 rpm following predrilled trajectories, whilst torque was sampled at 20 Hz. Maximum, average and plateau torques (T_{max}, $T_{average}$, $T_{plateau}$) were determined. Specimens were scanned in a large-volume micro-CT system (Nikon XT H 225 ST) at 20 μm isotropic voxel size (Fig. 1A). Screws were virtually removed from micro-CT images through masking. Bone morphometric parameters (bone volume fraction (BV/TV), bone surface to bone volume (BS/BV), trabecular thickness (Tb.Th), trabecular separation (Tb.Sp), bone surface to total volume (BS/TV)) were calculated (CTAnalyser, Skyscan) within a cylindrical volume of interest (VOI: 9 mm x 25 mm) around the centre of each screw (Fig. 1B). After scanning, an electromechanical test machine pulled screws out of vertebrae. Screws were evulsed and concurrently force recorded, from which pullout force (F_{max}) was obtained. Relationships between acoustic emission and torsional factors versus bone morphometric parameters as well as pullout force, were determined using linear regression.
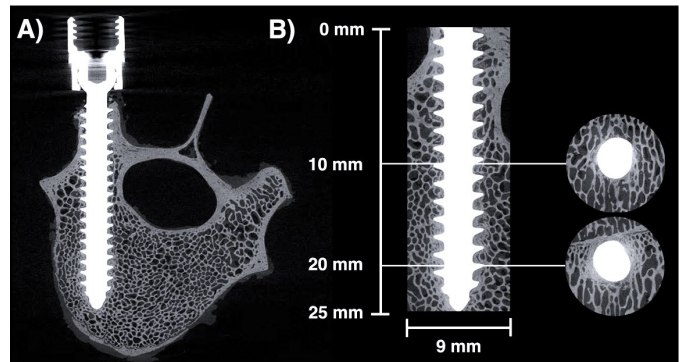
Figure 1: A) Micro-CT Cross-Sectional Image at 20 μm/pixel B) 9 mm x 25 mm Cylindrical VOI

RESULTS AND DISCUSSION

AE_{max} was a weak predictor of bone morphometric parameters, showing significant ($p < 0.05$) relationships only with BS/BV and BS/TV ($R^2 = 0.21$ and 0.23, respectively), see Table 1. The torque parameter $T_{average}$ was the strongest predictor of BV/TV, followed by $T_{plateau}$ and T_{max} ($R^2 = 0.58$, 0.41 and 0.38, respectively, $p < 0.05$). $T_{average}$ was also the strongest predictor of pullout force ($R^2 = 0.45$, $p < 0.05$), followed by T_{max} and $T_{plateau}$ ($R^2 = 0.38$ and 0.22, respectively, $p < 0.05$). AE_{max} was not significantly related to pullout force.

CONCLUSIONS

AE_{max} was a weak predictor of bone morphometric parameters and was unrelated to screw fixation strength. Conversely, torsional properties were significant and stronger predictors of both bone quality and fixation strength. These results highlight the utility of intraoperative torque measurements, which could provide numerical indications of bone quality and degree of screw anchorage. Despite this, torque-indicating devices are not routinely used in surgical theatre during spinal interventions.

REFERENCES

1. A. Massalimova et al. 2022. *Front surg.* PMID: 35990097.
2. Z. Zhang. 2020. *J Orthop surg.* DOI: 10.1111/os.12599.
3. M. Praamsma et al. 2008. *Can J Surg.* PMID: 19057732.

Table 1: Coefficient of Determination and Significance (R^2, p-value)

Factors	BV/TV	BS/BV	Tb.Th	Tb.Sp	BS/TV	F_{max}
AE_{max}	0.05, p =0.360	**0.21, p =0.042**	0.13, p =0.117	0.02, p =0.594	**0.23, p =0.034**	0.01, p =0.693
T_{max}	**0.38, p =0.003**	0.15, p =0.084	0.04, p =0.370	0.14, p =0.094	0.04, p =0.388	**0.38, p =0.003**
$T_{average}$	**0.58, p <0.001**	**0.34, p =0.006**	**0.27, p =0.015**	0.13, p =0.108	0.01, p =0.760	**0.45, p <0.001**

| $T_{plateau}$ | **0.41, *p* =0.002** | **0.42, *p* =0.001** | **0.39, *p* =0.002** | 0.06, *p* =0.294 | 0.05, *p* =0.355 | **0.22, *p* =0.033** |

Monday, December 2

ANZ Clinical Motion Analysis Group

THE EFFECT OF CLUSTERS AND INVERSE KINEMATICS ON A COHORT WITH IDIOPATHIC TORSIONAL DEFORMITIES

[1,2]Britney Kerr, [1,2]Jessie Mackay, [1,2]Pam Thomason, [1,2,3]Erich Rutz and [1,2,3]Elyse Passmore

[1]Hugh Williamson Gait Analysis Laboratory, The Royal Children's Hospital, Melbourne, VIC
[2] Murdoch Children's Research Institute, The Royal Children's Hospital, Melbourne, VIC
[3] Dept. of Paediatrics, University of Melbourne, VIC, Australia
email: britney.kerr@rch.org.au

INTRODUCTION
Idiopathic torsional deformities (ITD) of the lower limb bones (femur and tibia) in children and adolescents can lead to pain, gait impairments and reduced participation [1]. 3D gait analysis is commonly used to assess the functional impact of ITD on gait, with increased internal hip rotation being a key indicator for corrective surgery [2]. However, differences in marker sets, model definitions, and processing techniques can impact calculated kinematics and kinetics. This study aimed to evaluate the effect of modelling choices on gait kinematics and kinetics for children with ITD.

METHODS
This is a secondary analysis of data collected as part of two previous studies from our institute on 42 children with ITD [1] and 32 children with no pathology (NP) [3]. The ITD cohort had an average (SD) femoral torsion of 38° (13°) and tibial torsion of 39° (12°). In both cohorts, the data was reprocessed with different variants of the Python-based conventional gait model II (pyCGM2) [4], see Table 1. These model variants were chosen to evaluate differences related to using either a single lateral marker versus a marker cluster to track thigh and shank rotations and calculate joint kinematics using either direct or inverse kinematics.

| Model	Tracking	Kinematics
pyCGM2.1	single	direct
pyCGM2.2IKW	single	inverse
pyCGM2.3	cluster	direct
pyCGM2.3IKW	cluster	inverse

Table 1. Different pyCGM2 model variants.

Gait kinematics and kinetics were compared between models using 1D statistical parametric mapping with a two-tailed paired t-test with Bonferroni correction (α=0.002 with correction). The root mean squared difference (RMSD) for kinematics and kinetics was calculated between models for each child. We evaluated if each limb in the ITD cohort was within or outside of the 2SD band of the NP cohort throughout the gait cycle.

RESULTS AND DISCUSSION
The RMSD in hip rotation kinematics for the ITD cohort between the single marker and marker clusters was 8.4° when direct kinematics was used, Fig 1. When inverse kinematics was used, the RMSD was reduced to 4.9°. The RMSD between direct and inverse kinematics when using a single marker for tracking was 6.4°, whereas for marker clusters, the RMSD was 2.4°.
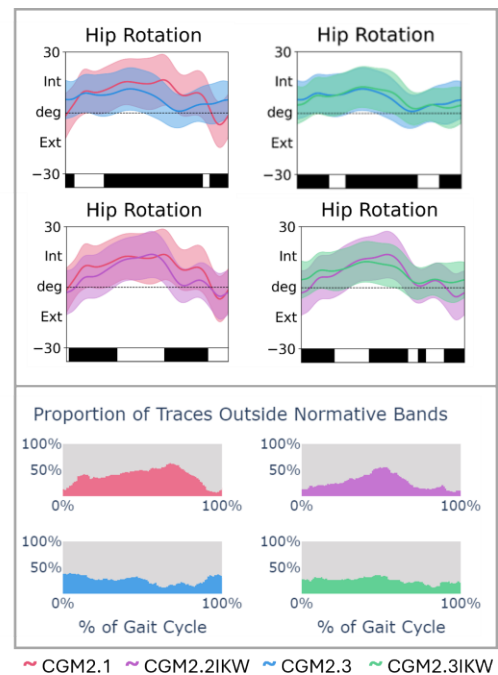
Fig 1: Hip rotation kinematics for pyCGM2 variants for ITD cohort (Top). The proportion of ITD traces outside NP 2SD normative bands by pyCGM2 variant (Bottom).

CONCLUSIONS
The choice of the pyCGM2 model affected the hip rotation kinematics. However, when the typically developing normative bands are processed with the same model as the ITD cohort, the effect of the pyCGM2 model version would likely not change clinical decision-making. Normative bands must be derived from the same model variant as decisions for surgical correction in children with ITD rely on comparisons to normative reference data.

REFERENCES
1. Mackay J, et al., *Gait & Posture.* **86**:144-149, 2021
2. Schwartz M, et al., *Gait & Posture.* **39**:778-783, 2014
3. Tirosh O, et al., *J Electro & Kine.* **23**: 1451-1459, 2013

4. Leboeuf F, et al., *Gait & Posture.* **69**:235-241, 2019

PREDICTIVE SIMULATIONS REVEAL MECHANISTIC LINKS BETWEEN ALTERED MUSCLE-TENDON FORM AND LOCOMOTOR FUNCTION IN AGING

[1]Taylor J. M. Dick, [1]Benjamin Kelley, [2]Friedl De Groote, [3]Christofer Clemente

[1] School of Biomedical Sciences, The University of Queensland, Australia
[2] Department of Movement Sciences, KU Leuven, Belgium
[3] School of Engineering and Science, University of the Sunshine Coast, Queensland, Australia
email: t.dick@uq.edu.au

INTRODUCTION

Aging is associated with a range of locomotor deficits. Older adults walk slower, consume more energy, and are more likely to fall compared to younger adults [1]. Aging is also accompanied by changes in the structure and function of the lower limb muscle-tendon units that limit their ability to generate ankle power [2]. Despite our ability to characterize age-related changes in locomotion with experimental tools, the mechanisms that link changes in form and function with aging remain poorly understood.

Recent advances in musculoskeletal simulation have opened new paradigms to study the consequences of aging on movement without the reliance on experimental data at computational speeds faster than ever before [3]. The aim of this study is to use whole body predictive musculoskeletal simulations to explore the influence of age-related changes in ankle muscle-tendon properties on walking performance. We hypothesised that decreases in muscle strength and tendon stiffness would independently lead to increases in cost of transport, but that the locomotor consequences will be greatest when muscle and tendon properties change in combination

METHODS

To simulate human locomotion, we used a full body OpenSim musculoskeletal model with 29 DoF, 92 muscle-tendon units, 8 ideal torque actuators, and 6 contact spheres per foot. To simulate the effects of age-related changes in triceps surae muscle strength and tendon stiffness, the maximum isometric strength (PF_{Max}) of the soleus (SOL), medial gastrocnemius (MG), and lateral gastrocnemius (LG) were varied from 50-120% of the base model's PF_{Max}. Achilles tendon stiffness (K_t) was varied from 60-120% of the base model's K_t. We solved for steady state (i.e. periodic) gaits based on a musculoskeletal model that captured the dependency of muscle forces on excitation, cross sectional area, fiber length and contraction velocity over gait speeds from 0.67-2.01m s^{-1}. We evaluated the individual and combined impacts of PF_{Max} and K_t on the biomechanics and energetics at the whole body-, joint-, and muscle- level using linear mixed effects models (RStudio, V2023.03)

RESULTS AND DISCUSSION

Our predictive simulations captured the magnitude and bowl-shaped pattern of cost of transport (COT) owing to changes in gait speed (Fig. 1). Our results demonstrated that weaker triceps surae muscles and reductions in Achilles tendon stiffness (both p<0.001) led to higher COT across walking speeds (Fig. 1), with the "oldest" model having a COT that was, on average, 4.1% higher than the "young" model. These whole body energetic trends were reflected at the muscle level, with both reductions in strength and stiffness (both p<0.001) associated with increases in SOL energy use. Weaker plantar flexors also led to a distal-to-proximal shift in walking workload, from the ankle joint to the hip joint. Additionally, we found that weaker muscles and more compliant tendons were compensated with increases in muscle activation in the SOL, MG, and LG (all p>0.001)—supporting neuromuscular fatigue as a driver of age-related gait deficits.
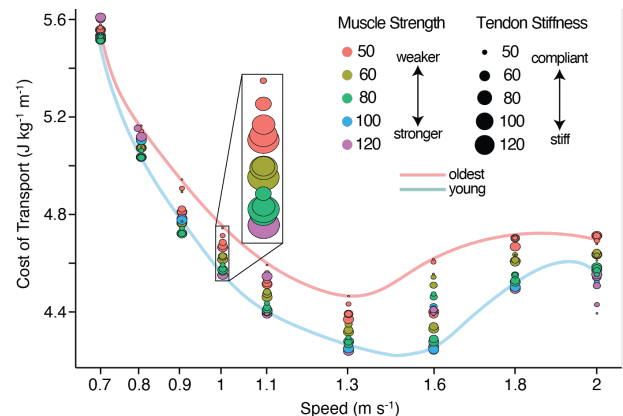
Fig.1: Influence of muscle strength and tendon stiffness on predicted cost of transport across the aging phenotype models.

CONCLUSIONS

Musculoskeletal simulations that emulated age-related reductions in triceps surae strength and Achilles tendon stiffness lead to poorer walking economy, and altered neuromotor control across scales from the joint to the individual muscle. Predictive simulations provide a powerful framework to examine cause-effect relationships between altered form and function that remain challenging to establish using experiments. The ability to personalize models provides a future avenue to direct targeted exercise interventions or rehabilitation strategies to lessen the impacts of aging on locomotor performance.

REFERENCES
[1] McCrum, C. et al (2018) Front physiol, 9, 150
[2] Franz, J.R. (2016) Exerc Sport Sci Rev,. 44(4)
[3] Falisse, A. et al (2019) Interface, 16(157)

DEFINING THE KNEE JOINT AXIS FOR CLINICAL GAIT ANALYSIS IN A PAEDIATRIC POPULATION

[1,2]Jinella Lopez, [1,2]Pam Thomason, [1,2,3]Erich Rutz and [1,2,3]Elyse Passmore

[1]Hugh Williamson Gait Analysis Laboratory, The Royal Children's Hospital, Melbourne, VIC
[2]Murdoch Children's Research Institute, The Royal Children's Hospital, Melbourne, VIC
[3]Dept. of Paediatrics, University of Melbourne, VIC, Australia
email: jinella.lopez@rch.org.au

INTRODUCTION

In the clinical setting, three-dimensional gait analysis (3DGA) provides quantitative information on a person's gait pattern, informing surgical decision-making. Accurately defining the knee joint axis (KJA) is crucial for accurate hip and knee kinematics, with hip rotation being a major determinant for femoral derotation osteotomy [1]. Anatomical or functional calibration methods are used to define the KJA. Anatomical methods use either a knee alignment device (KAD) or markers placed on the knee epicondyles. Functional methods rely on movement between the thigh and shank to determine the KJA. Imaging, such as freehand three-dimensional ultrasound (3DU) of the femoral condyles offers a method to define an anatomical axis, that is highly repeatable [2]. The aim of this study is to determine the accuracy of KADs, epicondyle markers, and functional calibration for defining the KJA compared to the condylar axis from 3DU in children with a range of gait pathologies.
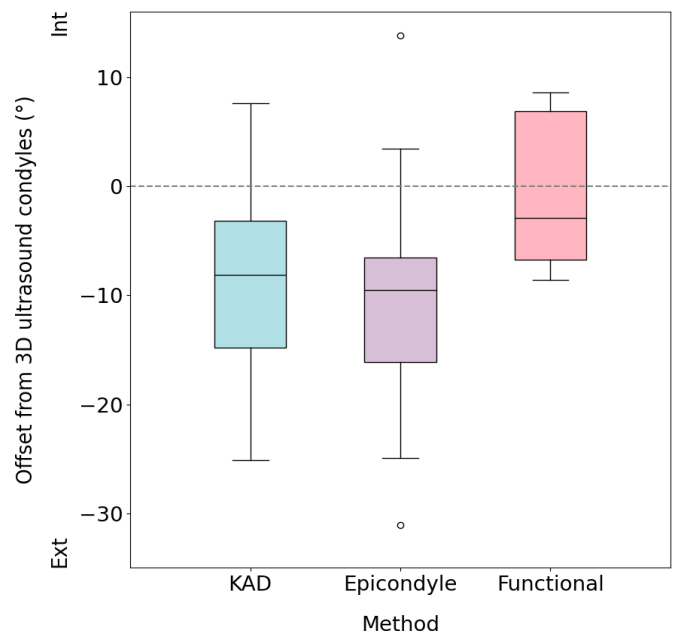
METHODS

Thirty children (13 female) with gait pathology (cerebral palsy (CP) (n=21), rotational malalignment (n=4), developmental dysplasia of the hip (DDH) (n=3), and other (n=2)), mean age 12.07 ± 3.17 years, underwent 3DGA following a standard protocol with the addition of 3DU of the femoral condyles. Thirty-six reflective markers were placed on the lower-limbs according to the pyCGM2.3 marker-set, consisting of clusters on the thigh and shank [3]. The KJA was defined using the following methods: KAD, epicondyle markers, and functional calibration from five repetitions of knee flexion-extension. 3DU was used to determine the condylar axis and provide the reference KJA. Each method was assessed by comparing its offset relative to the 3DU condylar axis.

RESULTS AND DISCUSSION

The KJA obtained from the KAD and epicondyle methods was on average more external compared to the 3DU condylar axis, (8.1° and 9.5° respectively), with both having large variability in their results (SD: 7.8° and 7.9° respectively), Fig 1. The functional calibration method was the closest to the ultrasound condylar axis, 2.9° external on average, and showed the least variability (SD: 6.6°).

Fig 1: Angular offset from 3DU condylar axis for KAD, epicondyle markers, and functional calibration methods.

CONCLUSIONS

Three methods were used to define the KJA and compared to 3DU imaging. The functional knee flexion-extension method showed the closest alignment to the 3DU condylar axis and was the most consistent. This study assessed children capable of standing for 3DU imaging and performing the functional knee flexion-extension activity. Further work is required in a larger population and in those with more severe pathology.

REFERENCES

1. Schwartz M, et al., *Gait & Posture.* **39**:778-783, 2014.
2. Passmore E, et al., *Gait & Posture.* **45**:211-216, 2016.
3. Leboeuf F, et al., *Gait & Posture.* **69**:126-129, 2019.

Tuesday, December 3

International Keynote 2 – Prof Jess Snedeker
Multiscale biomechanics and the cell-matrix interactions behind tendon adaptation to exercise

The field of tendon biology, long understudied, is rapidly gaining ground. On one hand, the tendon field is profiting from ever increasing mechanistic clarity within the broader disciplines of immunology, biophysics, matrix biology and mechanobiology. On the other hand, powerful technologies in molecular biology, biotechnology, bioimaging and data science are opening unprecedented experimental possibilities for labs everywhere.

Our research group employs multi-scale imaging to identify novel mechanisms of cellular mechano-transduction (mechanical stimuli that regulate biological processes and their cellular sensors). Our scientific efforts aim to unwind multi-scale and multi-tissue complexity that lies both upstream and downstream of these sensors.

This lecture aims to introduce important insights we have derived from cell and tissue engineering approaches that we have devised to disentangle cell-system cross-talk in tissue homeostasis, damage repair, and adaptation to exercise. More broadly, we will map the tendon as a complex physiological system with tightly coordinated interplay between a mechanically regulated core and an "extrinsic tendon compartment" that consists of synovium-like tissues interfacing the immune, vascular, and nervous systems. This conceptual framework interconnects diverse aspects of tendon physiology and pathophysiology and provides a unifying picture that may help in understanding human how mechanics regulate tendon biology, including functional adaptation to exercise.

Tuesday, December 3

ABC & David Findlay ECR Award Final

ROBUST WORKFLOW FOR DIAPHYSEAL CORTICAL BONE THICKNESS CALCULATION IN LONG BONES

[1]Julie Kim, [1]Ted Yeung, [1]Roshni Raghvani, [1]Julie Choisne, [1]Harnoor Saini and [1]Thor Besier

[1]Auckland Bioengineering Institute, University of Auckland, Auckland, New Zealand
email: hkim375@aucklanduni.ac.nz

INTRODUCTION

Cortical bone, prominently found in the diaphyseal area of long bones, can resist higher ultimate stresses compared to trabecular bone [1]. As a result, a considerable portion of the mechanical loading received by the skeleton is borne by the cortical bone. Its thickness is one of the major determinants of bone strength and plays a crucial role in the success of medical implants [2].

Treece et al. [3] introduced a novel technique for measuring cortical thickness from clinical CT scans in the sub-millimetre range. This was achieved by fitting a mathematical model to match the anticipated change in Hounsfield Units across the cortical bone boundary. However, the method fails across regions with high curvature and thick cortical bone, due to the need for surface normal projections. Building upon the work of Treece et al, a robust workflow is proposed, which calculates the cortical thickness and accurately reconstructs the inner cortical surface for a range of long bones.

METHODS

Consistent with the previous approach, the proposed workflow begins with the outer surface mesh of the cortical bone. The next step re-slices the CT image stack to the anatomical axes of the bone, which are systematically determined through principal component analysis.

For each of the axial slices from the re-sliced CT scans, a line of search for the mesh points belonging to the slice is projected radially from the centre of mass. This differs from the previous approach, which projected in the normal direction, and ensures that transitions from the surrounding soft tissue to the cortical bone, and to the trabecular bone or medullary cavity, are captured when the CT values are sampled along the line of search. By fitting a mathematical model, which approximates these transitions through step functions, to the sampled CT values, valid calculations of the inner surface are made including the outer mesh points that are situated at high-curvature areas with a thick cortex.

The entire process is repeated as an automated workflow written in the Python programming language, resulting in the inner surface mesh of the cortical bone.

RESULTS AND DISCUSSION

The workflow was successfully applied to the femur, tibia, fibula, humerus, radius, and ulna. This resulted in the reconstruction of their diaphyseal inner cortical bone surfaces (Figure 1). Notably, these included the mesh points for which the previous approach failed to generate valid measurements, with failure rates ranging from 0.7% for the fibula to 8.5% for the radius.
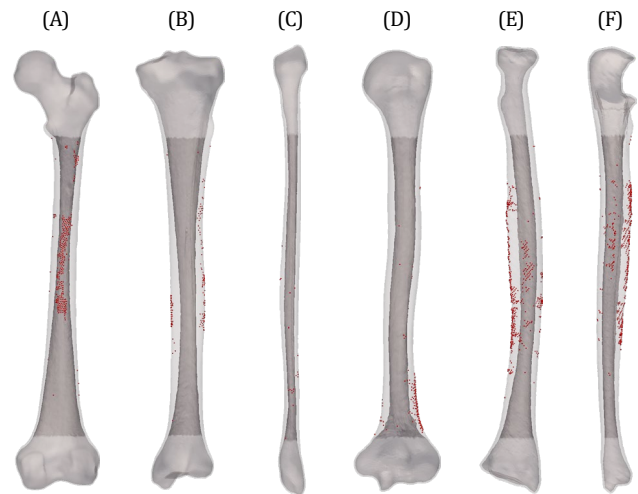
Figure 1: Diaphyseal inner cortical bone surfaces of (A) femur, (B) tibia, (C) fibula, (D) humerus, (E) radius, and (F) ulna calculated by the proposed workflow. Mesh points with invalid measurements from the previous approach are highlighted in red.

CONCLUSIONS

The proposed workflow successfully addressed the limitations of the previous technique, demonstrating its robustness and versatility across a range of morphologies observed in long bones. The tool opens a new avenue for broader applications in biomechanics, exemplified by its potential to analyze large cohorts of data for studying various osteogenic phenomena in population studies.

ACKNOWLEDGEMENTS

REFERENCES

1. Osterhoff G, et al., *Injury.* **47**:S11-S20, 2017.
2. Moschos A, et al., *Skeletal Anchorage in Orthodontic Treatment of Class II Malocclusion.* 258-273, 2015.
3. Treece G, et al., *Medical Image Analysis.* **16**:952-965, 2012.

TARGETING WNT INHIBITORS TO IMPROVE BONE MASS AFTER SPINAL CORD INJURY

[1]Hui Jean Kok, [1]April Hoggatt, [1]Daniel Horan, [1]Christen Mumaw, [1]Meredith Mitchell, [1]Chandler Walker and [1,2]Alexander Robling

[1]Department of Anatomy, Cell Biology & Physiology, Indiana University School of Medicine, Indianapolis, IN, US
[2]Richard L. Roudebush Veterans Affairs Medical Center, Indianapolis, IN, US
email: jeankok@iu.edu

INTRODUCTION

Spinal cord injury (SCI) is one of the most debilitating medical conditions among the veteran population. A major complication associated with SCI, beyond motor, sensory, and visceral deficits induced by the primary insult, is the rampant bone loss (i.e., neurogenic osteopenia) that ensues soon after injury. Neurogenic osteopenia represents a significant hurdle for overall SCI rehabilitation efforts. Major progress has been made in spinal cord repair strategies and neuromuscular rehabilitation (e.g., harnessing motoneuron plasticity and sprouting/regeneration mechanisms) for restoring neuronal function and control. But those rehabilitative advances are, in practice, nullified if concomitant restoration of bone structure and strength is not addressed, as fractures can bring neuromuscular rehabilitation to an abrupt halt. There is currently a paucity of options for treating bone wasting associated with SCI. Thus, an urgent need exists to develop new rehabilitative strategies for preserving and/or restoring bone lost following SCI. Our lab has previously shown that targeting the Wnt signaling pathway improves skeletal fragility in old mice [1]. However, whether this strategy provides similar anabolic response in mice after SCI is unknown. The goal of this project is to enhance the anabolic action of Wnt signaling in the skeleton after SCI.

METHODS

Four-month-old male mice received SHAM (T10 laminectomy) or SCI contusion surgery. SCI animals were further stratified to receive vehicle (SCI-V), anti-Sclerostin (SCI-S), or anti-Sclerostin plus anti-Dkk1 (SCI-S+D) monoclonal antibody treatment (n=10/group) from week 2 to week 5 post-SCI. Animals were assessed for locomotor function using the Basso Mouse Scale (BMS) and body weight was measured on a weekly basis. Skeletal muscle function was measured before surgery and harvest. Muscles and bones were harvested on 8 weeks post-surgery and radiographic analysis was performed.

RESULTS AND DISCUSSION

Hindlimb paralysis in SCI mice were confirmed by BMS scores. There were significant decreases in body weight after SCI when compared to SHAM mice from week 1 to week 8 post-surgery, regardless of treatment. Skeletal muscle mass and function were also lower in SCI mice compared to SHAM regardless of treatment. In both femur and tibia, cortical thickness was significantly lower in SCI-V mice when compared to SHAM mice. Importantly, both SCI-S and SCI-S+D had higher cortical thickness when compared to SHAM and SCI-V mice. Interestingly, SCI-S+D had the highest trabecular bone volume and thickness and are significantly higher than all groups, an indication that S+D has the most potential in restoring bone mass after SCI.

CONCLUSIONS

Overall, we identified a novel therapeutic target combining sclerostin and Dkk1 inhibitors to increase bone mass after SCI. Our future goals include assessing the mineralization levels of the periosteum and endocortical region at different timepoints using dynamic histomorphometry as well as measuring bone strength to compare different drug targets to restore bone mass after SCI.

REFERENCES

1. Choi RB, et al., *Aging Dis.* **13(6)**:1891-1900, 2022.

INTERNAL TIBIAL BONE DISPLACEMENTS AND STRAINS DUE TO IMPLANTATION WITH CEMENTLESS TIBIAL TRAYS

[1]Kieran J Bennett, [1]Lauren S Wearne, [1]Sophie Rapagna, [2,3]Sunil P Reddy, [4,5]Julius Dohm, [4]Christoph Schilling, [4]Berna Richter, [4,5]Thomas M Grupp and [1]Egon Perilli

[1]Medical Device Research Institute, College of Science and Engineering, Flinders University, Adelaide, SA, Australia
[2]The Joint Replacement Clinic, Adelaide, SA, Australia
[3]Department of Orthopaedics, Lyell McEwin Hospital, Adelaide, SA, Australia
[4]Aesculap AG, Research & Development, Tuttlingen, Germany
[5]Department of Orthopaedic and Trauma Surgery, Musculoskeletal University Center Munich (MUM), LMU Munich, Munich, Germany
email: kieran.bennett@flinders.edu.au

INTRODUCTION

Primary fixation of a cementless total knee replacement (TKR) component is achieved through an interference fit [1], with implant manufacturers typically recommending 300–1000μm interference for tibial trays [1]. During implantation, the tibial tray is impacted into a contour prepared resection, making its way into the resected bone, however, the resultant whole-bone internal displacements are currently unknown. As part of an ongoing study, we present the quantification of *in-situ* internal bone displacements and strains within the proximal tibia due to tibial tray implantation, using micro-CT imaging and digital volume correlation (DVC).

METHODS

Six human cadaver tibiae were resected and implanted with in-development cementless tibial components (Aesculap AG) by a specialist consultant orthopaedic surgeon following the surgical guide (ethics HREC 223.23). The proximal tibiae were micro-CT scanned at two time points at 46μm/pixel resolution (Nikon XT H 225ST) [2], first after resection and then following implantation. Implanted micro-CT image datasets were co-registered to the resected ones, median filtered, and residual bone deformations and strains due to implantation were determined using DVC (DaVis v8.4, final subvolume side length of 34pixels, 1.56mm).

RESULTS AND DISCUSSION

Across all six specimens, the peak bone displacement due to implantation ranged from 265μm to 780μm (median range across the entire tibia: 30-114μm). The bone adjacent to the implant surface was displaced and, interestingly, this displacement extended radially through the trabecular bone bed up to the periphery (Figure 1). Median compressive strains across the entire tibiae ranged from -2200μϵ to -2960μϵ, with the highest strains adjacent to and in between the geometric features (tray, keel, pegs) of the implants.

CONCLUSIONS

During the implantation process of cementless tibial components, bone is permanently displaced to fit the implant, and as found in this study, this displacement extends to the bone periphery. The peak displacements (360μm) are less than the typical spatial resolution of clinical CT scanners (e.g., 0.5-0.7 mm), and are unlikely to be detected in routine clinical CT scans. The residual strains within the proximal tibia were greatest in regions adjacent to the implant. This cadaveric study experimentally quantifies displacements and strains, which will help to inform cementless tibial tray implant design and surgical technique, with implications for understanding and modelling the immediate postoperative state of bone following TKR.
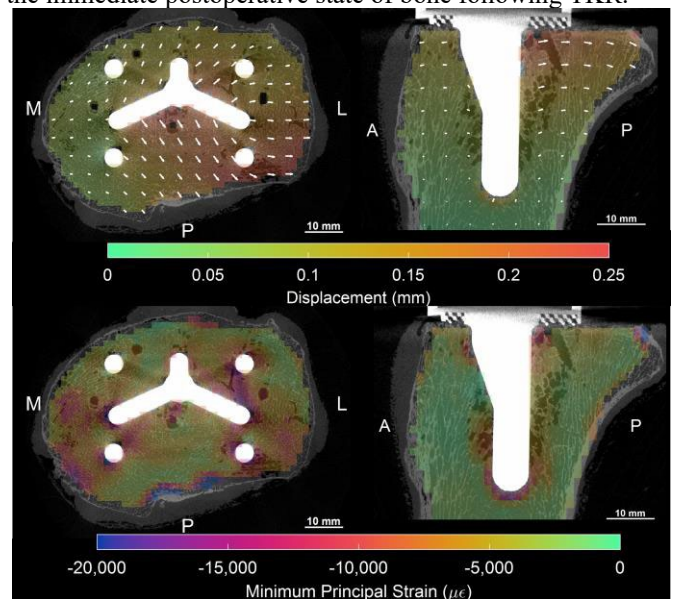
Figure 1: (Top) Displacements and (Bottom) strains due to implantation for one proximal tibia directly beneath the implant tray. Displacement vectors show the mean direction of displacement in 3x3 blocks and are scaled by a factor of 10.

REFERENCES
1. Sánchez E, et al., *JMBBM*. **118**:104435, 2021.

2. Wearne LS, et al., *JMBBM*. **134**:105336, 2022.

CARBOXYLATED OSTEOCALCIN- A POTENTIAL BIOMARKER OF IMPROVED CORTICAL AND TRABECULAR BONE PROPERTIES

[1,2]Deepti K Sharma, [3]Chris Schultz, [4]Rebecca Bahnisch, [5]Chloe Furst, [1,2]Bogdan Solomon, [1,2]Stuart Callary, [1,2]Boopalan Ramasamy
[1]Department of Orthopaedics and Trauma, Royal Adelaide Hospital, Adelaide, SA
[2]Centre for Orthopaedic and Trauma Research, The University of Adelaide, Adelaide, SA
[3]Nucleae Medicine, PET and Bone Densitometry, Royal Adelaide Hospital
[4]Metabolic Unit Head, Chemical Pathology, SA Pathology
email: Deepti.sharma@sa.gov.au

INTRODUCTION

Osteocalcin, the most abundant non-collagenous protein synthesized by osteoblast, is a Vitamin K dependent protein which is known to play an important role in bone metabolism. Osteocalcin contains three gamma-carboxyglutamic acid residues which are responsible for the calcium-binding properties of the molecule and Vitamin K is an essential cofactor for this carboxylation step. Deficiency of Vitamin K is associated with higher levels of undercarboxylated osteocalcin and increased hip fracture risk (1). The levels of Vitamin K required for effective carboxylation of osteocalcin are not known and recommended intake of vitamin K are based on the hepatic vitamin K requirements for blood clotting. Randomized controlled studies of vitamin K supplementation have shown significant improvement in carboxylated osteocalcin levels but the effect on bone parameters have not been consistent (2-4). Hence, we aimed to investigate the interaction of carboxylated and under-carboxylated forms of osteocalcin and Vitamin K levels with cortical and trabecular bone microarchitecture, hip geometry and bone turnover markers.

METHODS

Fifty patients scheduled to undergo hip replacement surgery due to hip osteoarthritis or avascular necrosis at the Royal Adelaide Hospital (2022-2024) with normal kidney functions, not on warfarin therapy or medications that may affect bone metabolism, were prospectively recruited (HREC #15811). All patients underwent DXA scans prior to surgery to determine the cortical bone parameters and hip geometry. Intertrochanteric femoral biopsies and serum specimens were obtained intraoperatively. Trabecular bone microarchitecture was analysed by microCT. Bone turnover markers (PINP; crosslaps and total osteocalcin) were measured using standard assays. Carboxylated and undercarboxylated osteocalcin were measured with ELISA kits (Takara Biosciences) and vitamin K1 and K2-7 levels were measured with HPLC.

RESULTS AND DISCUSSION

The mean age of this cohort was 68 years (48-88.6 years). Patients with high carboxylated osteocalcin had higher section modulus, lower buckling ratio, higher cortical width with cross-sectional area statistically different when compared to patients with low carboxylated osteocalcin levels (p=0.04, table 1).

P1NP, CTX and bone alkaline phosphatase were also significantly different between the two groups (p<0.01, for all). Interestingly, higher Vitamin K2-7 levels were associated with better hip geometry, with higher K2-7 levels associated with lower Hip Axis Length (HAL, p=0.003) and remained significant after controlling for height in multiple regression. No correlation was observed between vitamin K1 or patient age with HAL in this cohort.

Table 1: Median (range) for cortical bone parameters and bone turnover markers in low and high carboxylated osteocalcin groups

	Low cOC group (n=21)	High cOC (n=22)	P-value (one sided)
Cortical thickness shaft (mm)	5.06 (2.6-8.5)	5.98 (2.1-13.5)	0.08
Section modulus (mm³)	922 (529-1564)	1085 (477-2319)	0.07
Cross-section moment of Inertia (mm⁴)	18846 (8131-36497)	24497 (9334-65691)	0.09
Cross-sectional area (mm²)	185.3 (137-286)	204.9 (100-463)	0.04
Bone ALP (ug/L)	11.3 (6.48-19.5)	15.5 (7.04-25)	<0.001
CTX (ng/L)	388.5 (81-1020)	542 (237-1449)	<0.001
PINP (ug/L))	32 (15-79)	57 (21-257)	<0.001

CONCLUSIONS

This study provides first evidence on the relationship between carboxylated osteocalcin and bone structure. The differences in bone parameters seems to be driven by differences in bone turnover.

REFERENCES

1. Szulc P et al., *Bone*. 1996 May;18(5):487-8.
2. Knapen MH et al., *Osteoporos Int*. 2013 Sep;24(9):2499-507
3. Knapen MH et al., Osteoporos Int. 2007 Jul;18(7):963-72.
4. Rønn SH et al., *Osteoporos Int.* 2021 Jan;32(1):185-191.

VALIDATION OF WEARABLE SENSORS AGAINST THREE-DIMENSIONAL GAIT ANALYSIS

[1,2]Elizabeth Wojciechowski, [1,2]Kayla Cornett, [1,2]Gabrielle Donlevy, [1,2]Leanne Dwan and [1,2,3]Joshua Burns

[1]The Children's Hospital at Westmead, Westmead, NSW
[2]Faculty of Medicine and Health, University of Sydney, Sydney, NSW
[3]St. Jude Children's Research Hospital, Memphis, TN, USA
email: elizabeth.wojciechowski@sydney.edu.au

INTRODUCTION

Three-dimensional gait analysis (3DGA) is the gold standard measure for evaluating gait and is routinely used to assess children with walking impairments to help determine treatment strategies. However, 3DGA is resource-intensive, time consuming, and performed in a controlled laboratory environment. The use of wearable sensors or inertial measurement units (accelerometers, gyroscopes, ±magnetometer) provides a potentially more efficient, cost-effective assessment tool that can be used outside a laboratory setting, reducing in person visits and associated costs. Therefore, the aim of this study is to validate the APDM Opal Sensors and Moveo Explorer system against 3DGA in children with movement disorders.

METHODS

Data was captured simultaneously from 3DGA and APDM Opal sensors during barefoot walking, at a self-selected pace in 10 children with either Charcot-Marie-Tooth disease (n=9) or Cerebral Palsy (n=1) (5 male, 5 female, mean age 13±3.8yrs). 3DGA was captured with an 8-camera Vicon Nexus motion capture system using the lower body Plug-in Gait model. The APDM Opal sensors were positioned with one on each foot, lower leg and upper leg and one on the 5th lumbar vertebra. The average of 5 non-consecutive strides from one side was used for analyses using the same strides from each system. Temporal-spatial parameters and key kinematic parameters at the ankle, knee and hip in the sagittal plane were compared using the Bland-Altman method and Pearsons correlation coefficient (r).

RESULTS AND DISCUSSION

There was strong correlation (r > 0.9) in all temporal spatial measures (walking speed, stride length, cadence, stride time and step time). The Bland-Altman plots also showed no or limited bias and narrow limits of agreement in temporal spatial measures suggesting a good agreement between the two systems. All key ankle dorsi/plantarflexion measures showed a strong correlation (r > 0.79) however the APDM Opal sensors showed large bias in maximum ankle plantarflexion (bias 11.1°) and ankle dorsiflexion range of motion (bias -8.2°) (Figure 1a.). A strong correlation (r > 0.84) and small bias were observed for peak knee extension in stance (bias 0.8°), knee flexion range of motion (bias -0.2°) and peak knee flexion at loading response (bias 1.3°) (Figure 2b.). However, peak knee flexion in swing showed a medium correlation (r = 0.34) and knee flexion at initial contact showed a positive bias (bias 6.1°). At the hip there was strong correlation (r = 0.85) and small bias in hip flexion range of motion (bias 1.4°). However, there was a large bias in peak hip extension (bias 7.9°), peak hip extension in swing (bias 9.6°) and hip flexion at initial contact (bias 9.1°) (Figure 3c.).
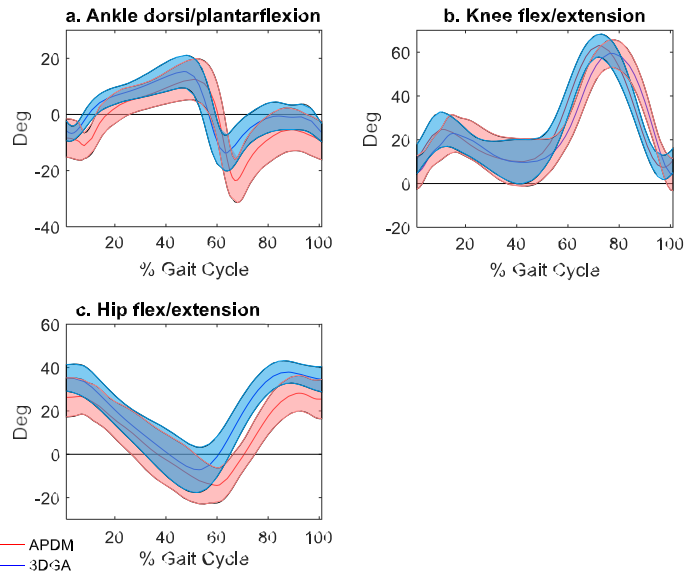
Figure 1: 3DGA (blue, ±1SD) and APDM Opal sensors (red, ±1SD) a. ankle dorsiflexion angle b. knee flexion angle c. hip flexion angle

CONCLUSIONS

In conclusion, temporal spatial measures and sagittal plane knee kinematics calculated using wearable sensors showed a potentially good agreement to 3DGA data. Further data will be collected from children with Cerebral Palsy and typically developing children.

ACKNOWLEDGEMENTS

OPTIMISING MUSCLE MECHANICS AND ENERGETICS IN HUMAN CYCLING: A PRESCRIBED AND EMG-ASSISTED APPROACH ACROSS SADDLE VARIATIONS

[1]Cristian D. Riveros-Matthey, [2]Glen A. Lichtwark

[1] School of Health and Rehabilitation Sciences, The University of Queensland, Brisbane, QLD
[2]School of Exercise and Nutrition Sciences, Queensland University of Technology, Brisbane, QLD
email: c.riverosmatthey@uq.edu.au

INTRODUCTION

Understanding energy expenditure is crucial for optimizing human performance and designing equipment the humans interact with, including bicycles. However, quantifying energy expenditure of activities with indirect calorimetry requires people to work for extended periods at a steady state, is costly, and lacks portability. An alternative approach is to calculate muscle mechanics through prescriptive modelling and estimate energy consumption using an energetic model [1]. In this study, we tested two prescriptive methods to compute energy expenditure and examined how they are influenced by variations in cadence and saddle height during simulated submaximal cycling.

METHODS

Twelve level 3-4 cyclists participated in the study, cycling for 3 minutes each at cadences of 50, 65, 80, 95, 110 rpm and two self-selected cadence conditions, all at a fixed power output of $2.5\ W \cdot kg^{-1}$ in a randomized order. The assessments on the second and third days included similar protocols with additional low and high saddle variations. Measurements taken during the experiments included 3D motion capture, breath-by-breath gas analysis, radial tangential pedal force, crank angle, and electromyographic (EMG) activity of eight muscles. A lower extremity model of right limb was driven by 40 Hill-type muscle-tendon unit actuators [2], incorporating muscular energetic probes [3]. Following an inverse dynamics approach, two prescribed simulations (OpenSim *MocoInverse* and *MocoSolver*) were implemented to address the muscular redundancy problem. *MocoSolver* used muscle EMG from muscles used to constrain the activation solution. Model validation involved comparing experimental metabolic power with predicted values using second-order polynomial regressions and linear mixed-effects models. We present data from two individuals with the remaining individuals to be presented when analysed fully.

RESULTS AND DISCUSSION

Both the experimental data and simulated outputs of metabolic power exhibit a U-shaped relationship with cadence (Fig 1). Preliminary qualitative results indicate that the simulations align closely with the experimental metabolic power data (Table 1), however using EMG data to constrain the solution typically increased the metabolic power predictions across all cadences tested.
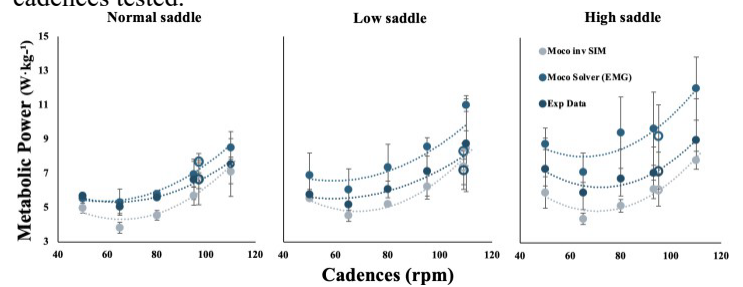
Figure 1: Experimental and simulated metabolic power across cadences (n=2) across normal, low and high saddle variations at $2.5\ W \cdot kg^{-1}$. Empty circles represent the self-selected cadence.

CONCLUSIONS

Preliminary results suggest that both methods show promising predictive capabilities across varying cadences and saddle-constrained conditions. Ongoing data analysis will provide a more comprehensive understanding, and the full data set will be prepared for presentation, including mechanical sources that contribute to changes in energy consumption with varying movement patterns.

REFERENCES

1. Dembia, C., *PLoS Comput. Biol.,* **16**, e1008493, 2020.
2. Millard, M., *J Biomech Eng.,* **135**, 1–11, 2013.
3. Umberger, B., *J Roy. Soc. Inter.,* **7**, 1329–1340, 2013.

Table 1: Mean experimental and predicted metabolic power at 50, 80, and 110rpm across saddle variations. Grey-filled cells indicate normal, black-filled cells indicate low and unfilled cells indicate high saddle variation.

	50rpm			80rpm			110rpm		
MocoInverse	5.0 ± 0.3	5.5 ± 0.1	5.9 ± 0.9	4.5 ± 0.3	5.2 ± 0.1	5.2 ± 0.4	7.1 ± 0.7	8.5 ± 1.0	7.8 ± 0.5
MocoSolver	5.5 ± 0.3	6.9 ± 1.3	8.8 ± 0.3	5.8 ± 0.2	7.4 ± 1.3	9.4 ± 2.1	8.5 ± 0.5	11.0 ± 0.4	12.0 ± 1.8
Exp. Data	5.7 ± 0.1	5.8 ± 0.3	7.3 ± 2.4	5.6 ± 0.1	6.1 ± 0.5	6.7 ± 1.7	7.5 ± 1.9	8.7 ± 2.8	9.0 ± 2.4

THE ACUTE EFFECTS OF GAIT AND FOOTWEAR INTERVENTIONS ON TIBIAL STRAIN DURING RUNNING

[1,2] Meghan Keast, [1]Jason Bonacci, [1]Aaron Fox

[1] Centre for Sport Research, School of Exercise and Nutrition Sciences, Deakin University, Waurn Ponds, VIC, Australia
[2] Queensland Academy of Sport, Nathan, QLD, Australia
email: mf.keast@gmail.com

INTRODUCTION

Those who engage in high volumes of running are at an elevated risk for lower limb bone stress injuries, with a common site for injury being the tibia [1]. It is hypothesised that the magnitude of bone loads is strongly related to damage accumulation rate [2]. Identifying strategies to reduce the magnitude of strain on the tibia during running may reduce the risk of developing a tibial stress injury for those who run regularly. The purpose of this work is to examine the effect of acute gait interventions on tibial bone strain magnitude using subject-specific finite element analysis.

METHODS

Ten naturally rear foot striking recreational runners (4/6 male/female; mean ± SD age, 28.5 ± 1.7y; height, 175.1 ± 8.6cm; body mass, 67.9 ± 7.6kg) ran on an instrumented treadmill under seven running conditions: (i) self-selected running speed; (ii) self-selected running speed +10%; (iii) preferred running speed +20%; (iv) induced forefoot strike; (v) wearing minimalist shoes; (vi) self-selected running speed with +10% cadence; and (vii) self-selected running speed with -10% cadence. During each of the seven running conditions, 3D kinematics and kinetics were collected over a 30 second period. Muscle and joint contact forces were estimated and applied to participant-specific finite element models of the tibia created from computed tomography images. The 50th and 95th percentile effective strain was extracted from the tibial shaft for analysis [3,4]. Paired t-tests were conducted to evaluate the differences in effective strain during all manipulated running conditions relative to the self-selected preferred speed condition.

RESULTS AND DISCUSSION

There was no statistically significant difference observed for 50th or 95th percentile effective strain for any of the running conditions when compared to the self-selected speed condition (Table 1). Previous literature supports the lack of significant change observed in tibial strain when running in minimalist shoes when compared to standard cushioned shoes [5]. Contrary to previous literature, we found no increases in strain with increases in speed [4]. There are limited studies conducted evaluating the effect of the other conditions on tibial strain. There was considerable inter-individual variation in tibial strain response to several running conditions. Modifications to running gait that acutely change technique may have different outcomes on tibial strain dependent on the individual. Interventions that aim to change tibial strain magnitude may therefore not be 'one size fits all'.

Table 1: Mean and standard deviation of the 50th and 95th percentile effective strain for all seven running conditions.

Condition	Effective Strain (µε)	
	50th Percentile	95th Percentile
Self-selected speed	3160 ± 1012	4838 ± 1491
Self-selected speed +10%	3228 ± 1224	4940 ± 1812
Self-selected speed +20%	2989 ± 1465	4550 ± 2140
Induced forefoot strike	3398 ± 1341	5205 ± 1946
Minimalist shoes	3227 ± 1739	4958 ± 2628
Self-selected speed with +10% cadence	2491 ± 847	3809 ± 1233
Self-selected speed with -10% cadence	3702 ± 1278	5666 ± 1842

CONCLUSIONS

Modifications to running gait such as changes to speed; foot strike and cadence did not induce statistically significant changes in effective strain along the tibial shaft. Footwear also had no significant effect on tibial strain. Strain responses to each condition were variable between participants, suggesting that interventions aiming to modify tibial strain magnitude may not have the same effect for all individuals. Further research needs be conducted to identify the factors underpinning individualised tibial strain responses to different running gait modifications.

REFERENCES

1. Rizzone K, et al., *J Athl Train.* **52**(10):966-975, 2017.
2. Carter et al., *Acta Orthopaedica* **52**:481–490, 1981
3. Haider I, et al., *J Biomech.* **122**, 2021.
4. Baggaley M, et al., *J Exp Biol.* **227**(10), 2024
5. Sinclar J et al., *Computation.* **11**(12), 248, 2023

BIOMECHANICS OF LOAD CARRIAGE WALKING AT MILITARY-RELEVANT SPEEDS AND LOADS – DIFFERENCES BETWEEN MALES AND FEMALES

[1]Danielle Vickery-Howe, [2]Ben Dascombe, [4]Jace Drain, [1]Anthea Clarke, [3]Brooke Hoolihan, and [1]Kane Middleton

[1]Sport, Performance, and Nutrition Research Group, La Trobe University, Melbourne, VIC
[2]School of Health Sciences, Western Sydney University, Campbelltown, NSW
[3]Applied Sport Science and Exercise Testing Laboratory, University of Newcastle, Ourimbah, NSW
[4]Human and Decision Science Division, Defence Science and Technology Group, Fishermans Bend, VIC

email: d.vickery-howe@latrobe.edu.au

INTRODUCTION

Australian Army personnel are required to carry loads up to and above 35 kg, depending on their trade [1]. There has been a consistent increase in the proportion of females in the Australian Defence Force [2], in addition to females serving in more diverse occupations including combat-centric roles which highlights the need to include both males and females in research. Females tend to have similar kinematics, or exhibit shorter stride lengths and different trunk and hip kinematics during load carriage when assessed at set speeds or loads in isolation [3], however the interaction between speed, load, and sex is not well understood. Understanding sex-specific responses is crucial for optimising training and injury prevention strategies during load-carriage tasks. This study aimed to examine the biomechanical responses of males and females during treadmill walking with military-relevant loads and speeds.

METHODS

Twelve males (1.83 ± 0.08 m, 84.9 ± 14.0 kg) and eleven females (1.68 ± 0.05 m, 68.6 ± 10.9 kg) completed nine 12-minute loaded walking trials on an instrumented treadmill. Trials were completed at three military-relevant speeds (3.5, 5.5, 6.5 km/h) and loads (7.2, 23.2, 35.2 kg). Retroreflective markers were attached to the pelvis and lower-limbs. Marker trajectories were collected using an 18-camera Vantage Vicon Motion System (120 Hz). Raw marker trajectories were reconstructed within Vicon Nexus. Marker trajectories were filtered using a dual-pass second-order low-pass Butterworth filter (12 Hz). Data were modelled to determine pelvis, hip, knee, and ankle angles [4]. Foot contact and spatiotemporal variables were calculated from foot trajectories. Ground reaction forces (GRF) were measured with the treadmill-embedded force plates (1000 Hz) and normalised to body weight (in Newtons). Linear mixed-effects models examined interactions of sex, load, and speed (Jamovi).

RESULTS AND DISCUSSION

Females exhibited greater step width relative to body height compared with males (1.7% of height, p = .011), which may be due to females attempting to increase stability resulting from carrying a higher relative load [5]. This wider step width may relate to the greater pelvis frontal range of motion (ROM, p = .031), hip frontal ROM (p = .003), and hip adduction ROM (p = .044) that were exhibited by the females, also likely in response to the greater relative load. It is unknown whether these differences emerged due to anatomical differences of the pelvis [6], or as a result of females having, on average, a shorter stature and lower body mass.

Females also had a greater stride length relative to body height compared with males (3.8% of height, p = .006), reflecting that the foot traverses a greater relative distance from the centre of mass [7], and greater vertical GRF (p = .013) during the 35.2-kg load. This is reflected in greater hip sagittal ROM (stride, p = .003) and knee sagittal ROM (stance phase, p = .017) due to overstriding. This overstriding may increase lower-limb muscular demands per stride and place additional shearing stress on the pelvis.

These kinematic differences may provide insight into the mechanisms of why females have a higher incidence of stress fractures [8].

CONCLUSIONS

These biomechanical variations during load carriage are indicative of different physical characteristics between sexes that could contribute to the observed differences in injury risk. Quantifying these differences can guide future research and help Defence in tailoring training programs and policy to address specific training needs based on sex to enhance performance and reduce injury risk.

REFERENCES

1. Drain J, et al., *Appl Erg*. **52**:85-94, 2016.
2. Australian Government, D*efence Report*, 2022.
3. Hudson S, et al., *Appl Erg*. **114**:104123, 2024.
4. Wu G, et al., *J Biomech*. **35**:543-548, 2002.
5. McAndrew Young P, et al., *Natl Inst Heal*. **36**:219-224, 2013
6. Kelly E, et al., *Mil Med*. **165**:142-146, 2000
7. Lim Y, et al., *J Biomech*. **57**:1-7, 2017.
8. Orr R, et al., *Int J Inj Contr Saf Promot*. **21**:388-396,2014.

Tuesday, December 3

ABC Student & ANZORS PhD Award Final

ANZSB
anzsb.asn.au

QUANTIFYING THE CONTRALATERAL REPEATED BOUT EFFECT OF THE TRICEPS SURAE

[1,2]Nicole S. Jones, [1,2,3]Dean E. Mills, [1]Patricio A. Pincheira and [1,2]Ben W. Hoffman

[1] Centre for Health Research, Institute for Resilient Regions, University of Southern Queensland, Toowoomba, QLD

[2] School of Health and Medical Sciences, University of Southern Queensland, Ipswich, QLD

[3] Respiratory and Exercise Physiology Research Group, School of Health and Medical Sciences, University of Southern Queensland, Ipswich, QLD

email: Nicole.Jones@unisq.edu.au

INTRODUCTION

Unaccustomed eccentric exercise typically leads to temporary strength loss and delayed-onset muscle soreness (DOMS), collectively termed exercise-induced muscle damage (EIMD). Skeletal muscle adapts to a single exposure of EIMD, providing partial resistance to future EIMD in both the exercised and opposite limbs [1]. Known as the ipsilateral and contralateral repeated bout effects (IL-RBE, CL-RBE), these have been observed in muscle groups with significant EIMD, such as the elbow and knee flexors [2]. However, the EIMD in the triceps surae is considerably smaller [3], and since the CL-RBE is about 50% of the IL-RBE [4], the existence of the CL-RBE in the triceps surae is uncertain. Identifying the CL-RBE could help exercise professionals better prescribe eccentric exercises for individuals more affected by EIMD, such as the elderly [5]. This study aimed to determine the presence and duration of the CL-RBE in the triceps surae by comparing two groups performing exercise bouts with either a 2-day or 7-day interbout timing.

METHODS

Healthy adults (30.0 ± 10.0 yr.) were pseudo-randomly assigned to 2-d or 7-d interbout timing groups (n = 12/group). Participants performed 225 heel drops (ECC1) with a random leg, followed by the same exercise (ECC2) using the opposite leg after 2-d or 7-d. Heel drops were performed through a 50^0 range of motion while wearing a weighted vest (10% body mass). Plantar flexor torque and DOMS, markers of EIMD and CL-RBE, were measured before (PRE) and at 2H, 24H, and 48H after each exercise bout on both limbs. Peak active plantar flexor torque was defined as the highest torque achieved during three maximal voluntary isometric contractions (MVCs) measured using an isokinetic dynamometer. Muscle soreness was rated 0-10 (visual analogue scale) during three muscle belly palpations and three functional tasks, for a total rating out of 60. The magnitude of the CL-RBE (index of protection) was calculated for both variables at 48H using (ECC2-ECC1)/ECC1×100 [6]. Changes in plantar flexor torque and DOMS following ECC1 and ECC2 were compared between bouts and among groups using a mixed-design three-way ANOVA.

RESULTS AND DISCUSSION

DOMS significantly decreased after ECC2 in the 2-d group ($F_{(1,11)}$=4.90, p=0.05), with a ~30% protection index, while the 7-d group showed no change between ECC1 and ECC2 ($F_{(1,11)}$=0.50, p=0.49). Interbout timing had no significant effect on DOMS between the 2-d and 7-d groups ($F_{(1,22)}$=0.23, p=0.64).

Post-ECC1, plantar flexor torque significantly declined at 2H, 24H, and 48H compared to PRE for both the 2-day ($F_{(3,33)}$=6.86, p<0.01) and 7-day ($F_{(3,33)}$=6.86, p<0.01) interbout timings. Post-ECC2, a significant main effect of bout on MVC torque was observed for both the 2-d ($F_{(1,11)}$=6.45, p=0.03) and 7-d ($F_{(1,10)}$=5.66, p=0.04) groups. These results indicate a significant reduction in torque drop post-ECC2, demonstrating the presence of the CL-RBE. No significant main effect of interbout timing was observed between the 2-d and 7-d groups for torque decrement ($F_{(1,22)}$=1.47, p=0.24), with protection indices of approximately 13% and 15%, respectively.
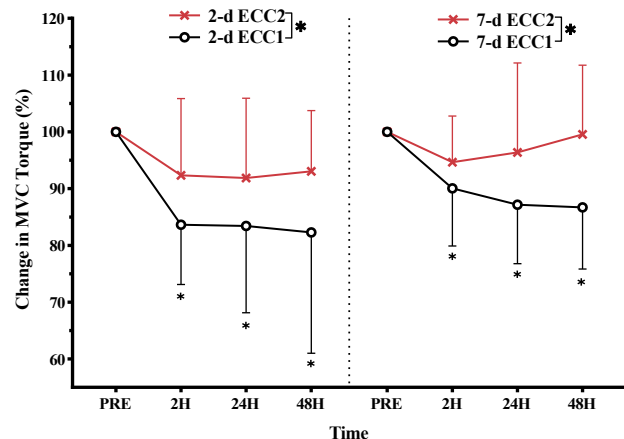
Figure 1: Normalized changes (mean ± SD) in MVC torque pre- and post-ECC1 (black line) and ECC2 (red line) on the contralateral leg 2 or 7 days later. Asterisks (*) denote significant differences (p < 0.05) between bouts based on the three-way ANOVA interaction effect and between PRE and 2H, 24H, and 48H within a bout per post hoc tests.

CONCLUSIONS

An initial bout of eccentric exercise that induces muscle damage in one leg's triceps surae confers protection during a subsequent bout of eccentric exercise in the contralateral limb. As such, the CL-RBE is present in the triceps surae and persists for at least 7 days. Future research could explore optimal eccentric exercise prescriptions to leverage CL-RBE in stroke/unilateral-immobilisation recovery and promote adherence to newly initiated exercise programs.

REFERENCES

1. Howatson G, et al., *Eur. J. Appl. Physiol.* **101**:207–214, 2007.
2. Chen T, et al., *MSSE.* **50**(3):542–550, 2018.
3. Pincheira P, et al., *Eur. J. Appl. Physiol.* **123**(8):1801-1808, 2018.
4. Chen T, et al., *Scand J Med Sci Sports.* **33**(12):2548-2560, 2023.
5. Baxter B, et al., *Eur. J. Appl. Physiol.* **123**(10):2131–2143, 2023.

6.   Chen T, et al., *MSSE.* **48**(10):2030–9, 2016.

RAPID CALIBRATION OF EMG-INFORMED NMS MODELS USING DIFFERENTIABLE PHYSICS

[1]Matthew Hambly, [1]Matthew Worsey, [1]David Lloyd and [1]Claudio Pizzolato

[1]Griffith Centre of Biomedical & Rehabilitation Engineering, Griffith University, Gold Coast, QLD
email: matthew.hambly@griffithuni.edu.au

INTRODUCTION

Electromyography (EMG) informed neuromusculoskeletal (NMS) models can predict physiologically valid individualised muscle and joint contact forces. However, the level-of-accuracy depends on the model's neuromuscular parameters (e.g., optimal fibre length, tendon slack length) that vary across individuals and cannot be easily measured. Similar to any other engineering models, calibration of NMS model parameters is required to minimise the error between model predictions and experimental data [1]. However, NMS model calibration uses optimisation that converges very slowly (hours), limiting deployment in time-critical applications.

Dramatic reduction in calibration time may be possible with differentiable physics. This combines physics-based modelling with backpropagation using automatic differentiation for fast gradient-based optimisation [2]. We implemented an EMG-informed NMS model in this differentiable physics framework and evaluated its reduced calibration time while producing physiologically valid predictions.

METHODS

We created an auto-differentiable Hill-type muscle model with an elastic tendon in LibTorch, and implemented it as a new calibration method (gradient-based) in CEINMS [1]. The reformulation of the muscle model enabled backpropagation to calculate gradients of the calibration loss function with respect to each model parameter. For the gradient-based calibration, the AdamW optimiser was used to adjust the model parameters.

Upper-limb EMG and marker data from one participant [3] were processed using OpenSim (v4.4), estimating musculotendon lengths, moment arms, and joint moments. An uncalibrated NMS model containing three degrees of freedom (shoulder abduction and rotation, and elbow flexion) and 16 muscles was constructed using initial parameters from the linearly scaled OpenSim model.

The differentiable physics calibration was compared to the simulated annealing calibration currently implemented in CEINMS. Both calibrations were performed across the same three trials, adjusting optimal fibre length, tendon slack length, strength coefficient and three activation dynamics parameters. The loss function minimised error between predicted and experimental joint moments (determined using inverse dynamics), while penalising non-physiologically valid solutions. After each type of calibration their models were executed in CEINMS EMG-driven mode [1] on the same trials, which were not used within the calibrations. Predicted and experimental joint moments were compared using root mean squared error (RMSE) and coefficient of determination (R^2).

RESULTS AND DISCUSSION

The differentiable physics method achieved joint moment tracking accuracy comparable to the traditional CEINMS approach (Figure 1), but calibration time decreased from 111 to 5 minutes, a 22-fold speedup. This new formulation enables rapid calibration for deployment in time-sensitive applications, including real-time biomechanical analyses and personalised rehabilitation.
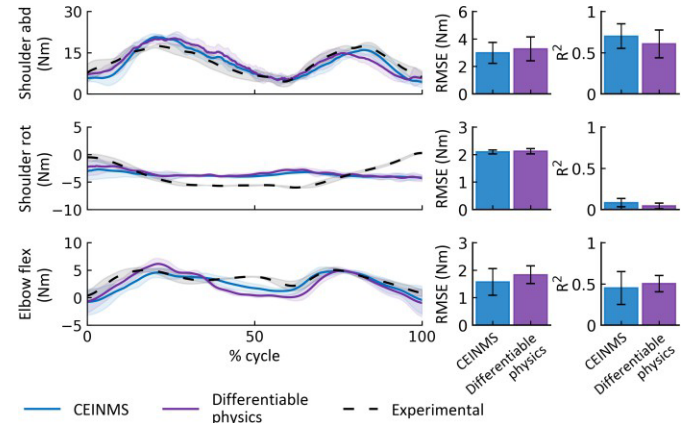
Figure 1: Joint moment tracking for the calibrated models compared to the experimental values across all cycles.

CONCLUSIONS

An auto-differentiable Hill-type model with gradient-based optimisation and backpropagation reduced calibration time of NMS model parameters. This differentiable physics approach is seamlessly compatible with neural network methods and facilitates the future implementation of hybrid physics-informed neural networks for EMG-informed NMS modelling.

ACKNOWLEDGEMENTS

REFERENCES

1. Pizzolato C, et al., *J Biomech.* **48**:3929-3936, 2015.
2. Ramsundar B, et al., *arXiv preprint*. 2109.07573, 2021.
3. Bolsterlee B, et al., *Med Biol Eng Comput.* **52**:283-291, 2014.

Using Predictive Musculoskeletal Simulations to Explore the Effect of Altered Gravity on Locomotor Performance

[1]Ioana Oprescu, [2]Christofer Clemente, [1]Taylor Dick

[1]School of Biomedical Science, University of Queensland, Brisbane, QLD
[2]School of Science, Engineering and Technology, University of the Sunshine Coast, Sippy Downs, QLD
email: i.oprescu@student.uq.edu.au

INTRODUCTION

For centuries, humans have been captivated by space and the prospect of space exploration, but there is limited research on the effects of altered gravity on our movement patterns. Theoretical and experimental studies have explored gait choice or the mechanical energetics of moving in altered gravity environments. For example, simulations revealed that different gaits emerge at different gravities [1]. Empirical data shows that duty factor and cost of transport (COT) are impacted by gravity [2]. However, these studies are limited by highly simplified musculoskeletal models and constraints on experimentally altering gravity. The aim of this research is to use physics-based predictive musculoskeletal simulations to determine the effect of altered gravity on locomotor performance across different body masses. To illuminate how locomotor performance varies with gravity, we created 3D computational models of the human musculoskeletal system across body masses ranging from 1 kg to 900 kg. We generated predictive muscle-driven simulations in these models across a range of gravities and gait speeds. We hypothesized that gravity would alter gait choice and the shape of the speed-mass relationship, such that optimum body mass for maximum speed would vary with gravity.

METHODS

We used an OpenSim musculoskeletal model (31 DoF, 92 muscles, 12 foot contact spheres) within a predictive simulation framework [3]. We scaled the generic musculoskeletal model to create 15 models ranging from 1 kg to 900kg. Musculoskeletal properties were scaled according to geometric similarity. Segment mass, inertia, and linear dimensions were scaled as $m^{1.0}$, $m^{1.67}$ and $m^{0.33}$, respectively. Maximum isometric force, F_{max}, was scaled with $m^{0.67}$. We solved for steady state (i.e. periodic) gaits across speeds from 0.1 to 6.5ms^{-1} based on a musculoskeletal model that captured the dependency of muscle forces on excitation (constrained to be between zero and maximum possible excitation), cross sectional area, fiber length and contraction velocity [3]. A separate model of each body mass was then made for each of the 5 gravities investigated, -1.62, -3.71, -9.81, -11.48 and -18.64 ms^{-2} by changing the gravitational value in the model. These values represent the gravities of earth-like planets and other extraterrestrial bodies including the Moon, Mars, Earth, Kepler186f and Kepler452b respectively. Based on the simulated gaits, we extracted variables related to locomotor performance that ranged from the whole body (stride parameters, ground reaction forces, COT),

to the joint (range of motion, angular velocity), and the individual muscle (forces, activation).

RESULTS AND DISCUSSION

Our current simulations have demonstrated a curvilinear speed-mass relationship whereby maximum locomotor speed occurs at an intermediate body mass, but the shape of the curve was influenced by gravity. Furthermore, duty factor (Fig. 1) and the relationship between lower limb kinetics and body mass differed across gravity levels such that locomotion in lower gravity environments was associated with differing speed transitions between gaits and different chosen gaits at certain speeds depending on gravity. For example, in lower gravities we observed an increased ariel phase across a range of speeds while at higher gravities grounded running appears more often.
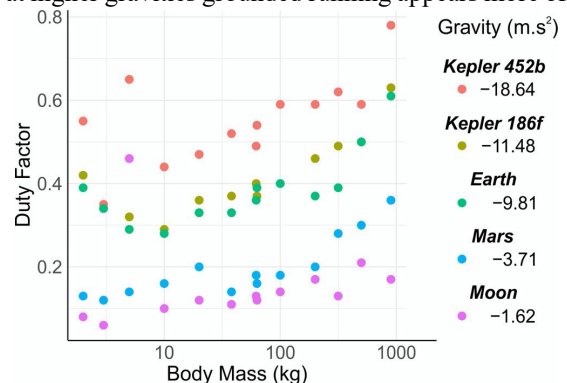
Fig 1. Duty Factor as determined by a predictive simulation framework across multiple body masses and gravities at the maximum feasible locomotor speed in each model.

CONCLUSIONS

This research helps to fill the knowledge gap regarding how gravity influences movement across varying body masses using cutting edge computational approaches. We have determined a change in the curvi-linear relationship between body mass and speed with altered gravity, which appears related to alterations in locomotor kinematics and kinetics. Further research is underway to investigate the patterns of these changes, with implications for the design of spacesuits or exercise regimes for persons undertaking space travel.

REFERENCES

[1] Ackermann M, van den Bogert AJ.J Biomech. 2012;45(7):1293-8.
[2] Pavei G, Biancardi CM, Minetti AE. J Appl Physiol. 2015;119(1):93-100.
[3] Falisse A, Serrancoli G, Dembia C, Gillis J, Jonkers I, De

Groote F. J R SOC Interface. 2019;16(157): 20190402.

EXPLORING THE NEUROMECHANICS OF THE ANKLE PLANTAR- AND DORSI-FLEXORS DURING SLIP PERTURBATIONS TO HUMAN WALKING

[1]India Lindemann, [1]Taylor Dick

[1]School of Biomedical Sciences, Faculty of Medicine, University of Queensland, QLD
email: uqilinde@uq.edu.au

INTRODUCTION

In Australia alone, falls result in over 200,000 hospitalisations and 6000 deaths annually [1]. It is therefore vital for public health that we understand the mechanisms by which humans stay upright when moving through real world environments. Previous perturbation research has explored kinetics and kinematics at the whole-body level as well as muscle-level activation responses. However, our understanding of *in vivo* lower limb muscle neuromechanical behaviour during unexpected perturbations remains largely unknown. Most previous studies extrapolate skeletal muscle dynamics from joint motions, which is not typically representative of muscle-level behaviour [2]).

The aim of this study is to determine how neuromuscular control and muscle-tendon dynamics are modulated in the ankle plantarflexors and dorsiflexors to maintain stability during unexpected slip-induced perturbations to human walking.

METHODS

Sixteen healthy young adults (23.6±3.5 yrs; 9 M 7 F) participated in the study. Participants were exposed to unexpected slip perturbations delivered to the right lower limb while walking at their preferred speed on a split-belt instrumented treadmill (Bertec). The perturbations consisted of a rapid acceleration and deceleration of the right belt at 10%, 20%, and 30% of the gait cycle, lasting 50% of the stance phase duration and reaching a maximum velocity of 0.7 m s^{-1} above their walking speed. During the perturbations, lower limb kinematics and kinetics were obtained using 3D motion capture (Qualisys) and force plates (Bertec); muscle activity in the triceps surae and tibialis anterior (TA) using surface electromyography (Trigno Delsys); and fascicle lengths in the medial gastrocnemius (MG) and TA using dual probe B-mode ultrasound (ArtUS, Telemed). Comparisons in muscle activation and fascicle dynamics were made between normal walking, the perturbation, and the recovery step (one step after perturbation) using a linear mixed effects model.

RESULTS AND DISCUSSION

Lower limb joint angles were unaffected during the perturbation (P) but varied in the recovery stride (P+1), compared to normal walking. Muscle activity increased across all four muscles during both the perturbed and the recovery stride (Fig. 1A/B). We found medial gastrocnemius and (likely) tibialis anterior fascicle length change was greater during the perturbation (Fig. 1C/D). An increase in muscle coactivation

during the slipped stride combined with increased fascicle shortening in the ankle plantarflexor and dorsiflexor muscles suggests that the ankle's response to a slip may be a neuromechanical clutch-like mechanism.
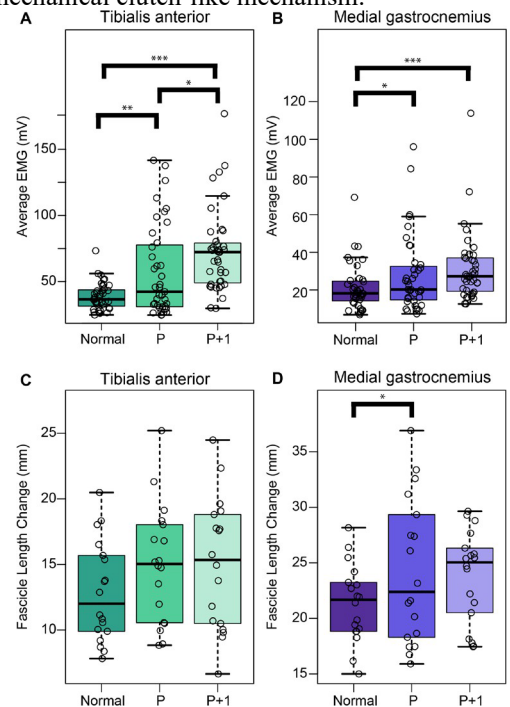
Figure 1: Tibialis Anterior and Medial Gastrocnemius average EMG amplitude (A, B) (n=16 participants) and fascicle length changes (C, D) (n=7 participants) of the right leg over normal walking, the perturbed stride (P), and the stride after the perturbation (P+1) over three slip trials.

CONCLUSIONS

Our results suggest that the human reaction to a slip may function to stiffen the ankle joint, potentially applying a braking effect to slow the velocity of the bodies centre of mass and thereby prevent a fall. Future analysis of the relationship between time-varying changes in muscle activation and fascicle length changes will further reveal the ankle's neuro-mechanical response towards unexpected slips.

REFERENCES

1. Australian Institute of Health and Welfare, 2024
2. Dick, T.J.M, et al., *Journal of Experimental Biology*. **220(9)**: 1643-1653, 2017.

LOWER LIMB JOINT WORK IN RUNNERS WITH AND WITHOUT A HISTORY OF KNEE SURGERY

[1]Brody McCarthy, [1]Danilo De Oliveira Silva, [1]Prasanna Sritharan, [1]David Carey, [1]Kay Crossley, [1]Melissa Haberfield, [1]Michael Girdwood, [1]Fernanda Serighelli, [1]Josh Hill, [1]Paula Pappalardo, [1]Richard Johnston and [1]Benjamin Mentiplay

[1]La Trobe Sport and Exercise Medicine Research Centre, La Trobe University, Melbourne, VIC
email: brody.mccarthy@latrobe.edu.au

INTRODUCTION

Running has increased in popularity in recent decades, likely due to its well-known health benefits, accessibility, and affordability. While traumatic knee injuries are rare for runners, following knee surgery, many people will opt for running as a safer form of exercise instead of pivoting activities. Post-surgical alterations in running biomechanics (i.e., underloading at the knee joint) may be associated with the development of post-traumatic knee osteoarthritis [1]. It remains unclear whether this load shifts to other lower limb joints, such as the hip or ankle.

We aimed to compare the total positive and negative work done by the lower limb during the stance phase of running between runners with and without a history of knee surgery, as well as the proportion of positive and negative work done by the hip, knee, and ankle to the total work done by the lower limb.

METHODS

This study was part of a larger prospective cohort study (Trajectory of Knee Health in Runners - TRAIL) with the full protocol published recently [2]. 102 participants from the TRAIL cohort were included, 52 with a history of knee surgery (46% females) and 50 controls (52% females).

Biomechanical overground running data were collected at two set paces (3-3.5 m/s and 5-6 m/s) using a 10 Vicon camera, 3D motion capture system and two embedded AMTI force plates. A generic whole-body biomechanical model was created in OpenSim 4.3 for each participant to calculate joint power (product of angular velocity and moment) which was then integrated over the stance phase to calculate positive and negative work. Joint work data were then compared between control and surgical groups, and between injured limbs and uninjured limbs in the surgical group. Linear mixed effect models split by sex were used for both absolute work variables (Joules) and relative work variables (% contribution to total lower limb work) to observe any meaningful differences.

RESULTS AND DISCUSSION

The surgical group displayed lower work done at the knee joint at both running paces for both positive (3-3.5 m/s= -5.2 J, 95%CI= -8.1 to -2.3; 5-6 m/s= -9.9 J, 95%CI= -13.9 to -5.9) and negative (4.4 J, 95%CI= 2.4 to 6.4; 7.4 J, 95%CI= 4.9 to 9.9)

work done. The total work done by the lower limb followed this same pattern where the injured limb 'underloaded' when compared to the control group limbs, and uninjured limb. When converted to percentage-based relative contributions, a shift of load away from the knee (-1.34% to -2.63%) and towards the ankle (1.06% to 2.51%) and hip (0.23%) joints was observed.
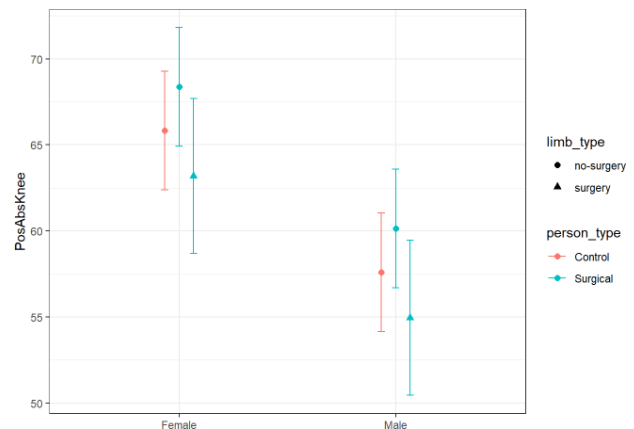
Figure 1: Differences in positive knee joint work for an average 70kg runner between sexes and surgical, non-surgical, and control limbs at the 3 to 3.5 m/s running pace.

CONCLUSIONS

Runners with a history of knee surgery performed significantly less work at the knee joint and across the whole lower limb when compared to their uninjured limb and healthy controls. Load shifted to the hip and ankle joints and uninjured limb, however understanding the meaningfulness of these findings requires further research.

Our results highlight the permanency of post-surgical gait alterations and emphasise a need for gait retraining solutions to manage potential future osteoarthritis risk.

REFERENCES

1. Sritharan P, et al., *American Journal of Sports Medicine.* **48**:1711-1719, 2020.
2. De Oliveira Silva D, et al., *BMJ Open.* **13**:e068040, 2023.

Reduced radiation dose enables multi-positional high resolution computed tomography wrist data for computational modelling without substantial geometric inaccuracy

[1]Zhengxu Cheng, [2]Carl Howard, and [2]Claire F. Jones

[1] Adelaide Medical School, The University of Adelaide, Adelaide, SA
[2]School of Electrical and Mechanical Engineering, The University of Adelaide, Adelaide, SA
email: zhengxu.cheng@adelaide.edu.au

INTRODUCTION

Multi-positional computed tomography (CT) images can be used to define three-dimensional (3D) bone geometries to study carpal "kinematics". Image sets for young, healthy participants, must minimise total radiation exposure while maintaining sufficient image quality. The aim of this study was to determine a lower CT dose that provides definition of carpal bone envelopes sufficiently similar to that of the full clinical dosage.

METHODS

CT images of five cadaveric wrists (54-77yr; 3 male; HREC H-2023-104) in a neutral position, were obtained at full clinical dose [80 keV (0.017 mSv)], and at 60, 40, 30, 20, 15, 10, and 5 keV, with in-plane resolution 0.195 mm, slice thickness 0.2 mm (Naeotom Alpha® photon-counting CT, Siemens; Sn filter). The current, dose-length product and dose index were automatically adjusted. Signal-to-noise ratio (SNR) and contrast-to-noise ratio (CNR) were determined for the thickest cortical boundary within the hand. Carpal bones were segmented, using identical automatic steps for all doses (Materialise Mimics). The full clinical dose bone geometries were the reference set. The volume of each carpal bone geometry was determined. The deviation of each bone geometry from the reference (termed "surface disparity") was determined as the minimum distance between the test and reference (80 keV) point clouds. The median of the disparity distribution (P50) was calculated for each carpal bone. Paired Friedman tests (alpha=0.05) were used to compare SNR and CNR at each dose, to the 80 keV reference set. Linear mixed models (alpha=0.05) with fixed effects of dose and carpal bone, and a random effect of donor, were used to examine the effect of dose on surface disparity and volume (SPSS, IBM). Post-hoc pairwise comparisons were made. Natural log transformations were applied and LMM estimates were back-transformed and interpreted as percentage difference between the means of two samples [1].

RESULTS AND DISCUSSION

All outcome variables were dose-dependent (Table 1). At 15 keV and below, SNR and CNR were lower than that of the reference set ($p<0.014$). Bone volume was significantly different at 5 keV compared to reference ($p<0.003$). Surface disparity was greater at 30 keV and below, compared to 60 keV ($p<0.001$) (Fig. 1).
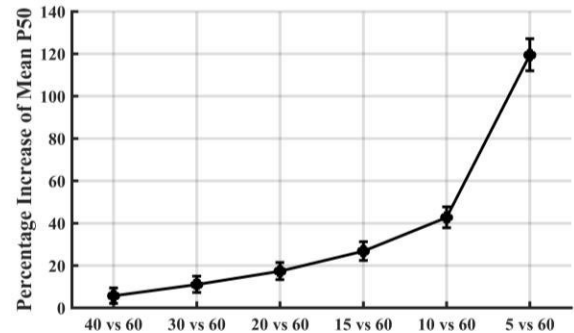
Figure 1: Percentage increase in mean P50 surface disparity ($\pm95\%$ confidence interval) for all dose levels vs. 60 keV.

CONCLUSIONS

SNR, CNR and geometric accuracy were substantially reduced at 5 keV. Below 5 keV (6.25% of standard clinical dose) all defined measures were statistically different to the reference, although the change in geometric quality was not substantial. Geometric deviations of ≈50μm are unlikely to cause image registration inconsistencies that substantially impact pose and kinematics calculations. Multi-positional wrist CTs obtained at <20% full clinical radiation dose (i.e., 0.00213 mSv; 10 keV) can produce carpal bone geometry of suitable quality for kinematics modelling.

REFERENCES

1. DK Lee, *Korean J Anesthesiol.* **73(6)**:503-508, 2020

Table 1: Surface disparity (P50), volume difference, SNR and CNR (mean±SD) for all specimens and bones; **bold:** $p<0.05$.

CT Dose (keV)	5	10	15	20	30	40	60	80
Surface disparity (μm)	**90.6±17.4**	**58.7±10.2**	**52.0±8.0**	**48.1±6.9**	**45.5±6.3**	43.3±5.7	40.9±4.8	NA
Volume (cm³)	**2.40±1.08**	2.31±1.04	2.29±1.03	2.28±1.03	2.29±1.03	2.29±1.03	2.29±1.03	2.27±1.02
SNR	**13.5±4.3**	**18.3±5.1**	**21.5±6.7**	24.9±7.7	29.9±8.8	33.1±8.8	38.0±10.6	41.3±11.6
CNR	**12.8±4.5**	**17.3±5.4**	**20.3±6.9**	23.5±7.9	28.4±9.2	31.4±9.3	36.0±11.0	38.8±12.2

USING SONOGRAPHY TO ASSESS THE CONDITION OF THE LUMBAR MULTIFIDUS FOLLOWING RESTORATIVE NEUROSTIMULATION: A PRELIMINARY ANALYSIS

[1,2]Patrick Beaumont; [1,3]Patricio Pincheira Miranda; [1]Paul Hodges

[1]School of Health and Rehabilitation Sciences, University of Queensland, St Lucia, Australia
[2]SpinePlus, Brisbane Private Hospital Spine Research Group, Brisbane Private Hospital, Spring Hill, Australia
[3]School of Health and Medical Sciences, University of Southern Queensland, Ipswich, Australia
Email: p.beaumont@uq.edu.au

INTRODUCTION

Chronic pain relating to back problems remains one of the most common and most costly conditions in Australia. Although the mechanisms of chronic low back pain (LBP) are multifactorial, research suggests the structure of the paraspinal muscles might contribute to this condition in some individuals. Accumulation of adipose and connective tissue within the lumbar multifidus muscle (LM) has been related to symptoms and its reduction is related to recovery. Recently, a novel implantable restorative neurostimulation device (ReActiv8[®], Mainstay Medical, and USA) which elicits targeted contraction of the LM has demonstrated significant reductions in pain and disability in people suffering from persistent mechanical LBP. Although studies in animals have shown that this stimulation can reduce accumulation of connective tissue after an experimental spinal injury, there is not yet data from human studies to show how this relates to changes in pain and disability. Conventional muscle imaging with MRI has not been possible because of the device's incompatibility with this technique. Ultrasound imaging provides a safe, non-invasive, and cost-effective alternative. Recent work has suggested new methods to quantify connective tissue structure within the multifidus muscle using ultrasound texture analysis methods [1]. The aim of this preliminary study was threefold: to assess the utility of ultrasound texture analysis in detecting changes in connective tissue over time, to evaluate whether restorative neurostimulation could induce changes in connective tissue distribution, and to determine if these changes correlate with clinical metrics.

METHODS

A prospective study was conducted on patients presenting with mechanical LBP (defined as LBP persisting for longer than 3-months which could not be attributed to a specific pathology) who were scheduled to undergo implantation of ReActiv8 through a single private surgical practice were invited to participate in the study. The data from the first 10 participants (10 males and 5 females; mean age of 57 ± 13 years, mean body mass index of $27.9 \pm 4.3 kg/m^2$, and mean back pain duration of 18.5 ± 13.1 years) enrolled in the study was used for this analysis. Measures were made prior to implantation and at 6-months post-implantation. Outcome measures included subjective scores of back pain and disability using the visual analogue score (VAS; 0 -10 points; representative of average

pain over the last week) and Oswestry Disability Index (ODI; 0-100%; representative of an average over the last week). B-Mode ultrasound images from the L3 level (the level immediately below the site of stimulation) on the predominantly painful side were analysed pre- and post-intervention. Texture analysis involved the selection of known pixels representing connective tissue within the image (thoracolumbar fascia). Using this region of interest, a support vector machine model was trained to classify individual pixels containing connective tissue-like texture from within the region of the LM muscle. A single researcher, who was blinded to the timepoint of the scan, performed the LM segmentation and analysis. The primary outcome was the proportion of connective tissue-like texture within the segmented muscle. Measures were compared between timepoints using a paired t- test. Further, the linear relationship between the overall change in pain, disability, and presence of connective tissue were also analysed (Pearson Correlation). Significance was set at $p<0.05$.

RESULTS AND DISCUSSION

At 6-months post-intervention, participants reported significantly less pain (6.4 ± 1.6 to 4.2 ± 2.6; p = 0.027) and
disability (36 ± 11% to 24 ± 16%; p = 0.038). Texture analysis revealed a reduction in the proportion of connective tissue in the multifidus at L3 (pre = 23 ± 6% to 6-months post = 20 ± 4%; p=0.013). We found no significant linear correlations between change in pain (R^2= 0.027; p=0.650) or disability (R^2=0.034; p=0.612) and the change in the proportion of connective tissue.

CONCLUSIONS

The results of this preliminary study show that the proportion of LM connective tissue is reduced following restorative neurostimulation. However, this change is not related in a simple linear manner to clinical outcomes. These results suggest promising utility of texture analysis to detect change in muscle quality over time, and a potential metric to represent the effects of restorative neurostimulation for specific cases of LBP. Future work should consider a larger sample and potential non-linear relationships between this biological parameter and clinical outcomes.

REFERENCES

1. Paris M et al. *Ultrasound Med Biol* **47(4)**: 880-95, 2021

Artificial Intelligence in the Prediction of Persistent Foot Drop in Children with Cerebral Palsy after Gastroc-soleus Lengthening.

[1]Mohammad Yavari, [2,3]Elyse Passmore, [2,3]Erich Rutz, [2,3]Pam Thomason and [1]David Ackland

[1]Faculty of Engineering and Information Technology, The University of Melbourne, Melbourne, VIC
[2]Murdoch Children's Research Institute, The Royal Children's Hospital, Melbourne, VIC
[3]Hugh Williamson Gait Analysis Laboratory, The Royal Children's Hospital, Melbourne, VIC
email: myavari@student.unimelb.edu.au

INTRODUCTION

Equinus is the most common deformity in children with Cerebral Palsy (CP) [1]. Gastroc-soleus lengthening surgery (GSL) is known to be an effective surgical procedure in treating this condition with improvement in stance phase kinematics; however, persistent ankle plantar flexion during swing, (known as foot drop), can occur in up to 42% of children with hemiplegia and 19% of children with diplegia [1,2]. Persistent foot drop, which occurs during the swing phase of gait, increases the risk of tripping or falling during walking. The aim of this study was to develop an artificial neural network model to predict post-operative ankle dorsiflexion angles, and hence footdrop, from pre-operative gait and clinical examination data.

METHODS

Gait data were obtained from 109 children, which included lower limb joint kinematics and kinetics from 5 over-ground walking trials collected before and between 12 and 24 months after GSL. Pre-operative physical examination data were collected, which included topography, ankle dorsiflexion range of motion (soleus and gastrocnemius length), dorsiflexor strength, and selective motor control. An artificial neural network model was trained to predict post-operative ankle dorsiflexion kinematics using pre-operative gait data and clinical examination as input. It included a feed-forward neural network for processing clinical examination and a multi-headed convolutional neural network for analysing time-series gait data. Univariate logistic regression was then used to assess the associations between pre-surgery clinical data variables and presence of foot drop post operatively, and correlation coefficient (β) used as a measure of strength and direction of these associations. The definition of foot drop used in this study was a maximum ankle dorsiflexion in mid-swing that was greater than two SD below the mean of typically developing children (TDC), which was > 2.2∘ of ankle plantarflexion in our cohort [1,2]. SHAP (Shapley additive explanations) was used to identify the contribution of each parameter (gait variable and clinical examination) to model predictions of post-operative ankle dorsiflexion kinematics.

RESULTS AND DISCUSSION

The RMS difference between the predicted and actual post-operative ankle dorsiflexion angles across the entire gait cycle was 5.1° (RMS difference for stance and swing phases were 5.1° and 5.0°, respectively). The predicted mean ankle dorsiflexion angle underestimated the measured post-operative ankle, though the trends were similar (Fig 1). Post-operative foot drop was predicted with 87% accuracy. Soleus muscle length (β: -0.74, SHAP value: 0.4), maximum dorsiflexion in mid-swing (β: -0.87, SHAP value: 0.32), and the ankle dorsiflexion gait variable score (GVS) (β: 0.59, SHAP value: 0.15) were identified as key features associated with post-surgery dorsiflexion and presence of foot drop, according to both logistic regression and SHAP analysis (Table 1). The deep learning model also highlighted CP topography (β: 0.18, SHAP value: 0.17) as a parameter that may be linked with occurrence of foot drop following GSL.
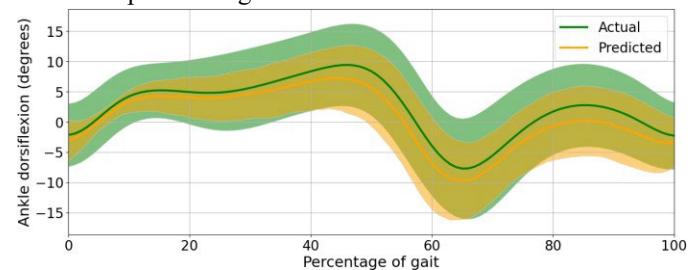
Figure 1: Predicted (orange) and measured (green) mean post-operative ankle dorsiflexion angles, with shaded regions showing ±1 standard deviation.

CONCLUSIONS

This study presents a deep learning framework capable of predicting post operative foot drop in CP children with 87% certainty. The model outputs, which were supported by regression and SHAP analysis, showed that soleus muscle length and maximum ankle dorsiflexion angle in mid-swing were strong contributors to post-operative swing dorsiflexion and foot drop. This study highlights that pre-surgery kinematics and clinical examination may be useful in assessing the risk of post-surgery foot drop. This will help inform directions for future research.

REFERENCES

1. Lofterød B, et al., *The Journal of foot and ankle surgery.* **48**: 631-636, 2009.
2. Sclavos N, et al., *Gait & Posture.* **100**: 254-260, 2023.

Influence of anterior cruciate ligament reconstruction parameters on kinematics and cartilage stresses in pediatric knee

[1]Ayda Karimi Dastgerdi, [2]Amir Esrafilian, [1]Christopher P. Carty, [1]Azadeh Nasseri, [2]Rami K. Korhonen, [3]Ivan Astori, [4]Wayne Hall, and [1]David John Saxby

[1]Griffith Centre of Biomedical and Rehabilitation Engineering, Griffith University, Australia; [2]Department of Technical Physics, University of Eastern Finland, Finland; [3]Department of Orthopedics, Children's Health Queensland Hospital and Health Service, Australia; [4]School of Engineering and Built Environment, Griffith University, Australia.
email: ayda.karimidastgerdi@griffithuni.edu.au

INTRODUCTION

Anterior cruciate ligament (ACL) rupture is increasingly common among physically active children and adolescents. Reconstruction of the ACL (ACLR) aims to restore knee stability by using grafts to replace the failed ACL. However, post-ACLR knee laxity and altered biomechanics can lead to early-onset knee osteoarthritis [1]. Surgical parameters such as graft type, diameter, pre-tension, and femoral tunnel location significantly impact ACLR knee biomechanics, yet their complex interactions are underexplored. This study used a linked neuromusculoskeletal (NMSK)-finite element (FE) model to determine combinations of four critical ACLR surgical parameters (graft type, diameter, location, and pre-tension) that minimized deviations of knee kinematics and articular cartilage stresses during walking compared to corresponding ACL-intact knee.

METHODS

Lower-limb anatomy from an 8-month post-op ACLR adolescent patient (aged 16 years, mass 55.5 kg) was acquired using magnetic resonance imaging. For this patient, 135 FE knee models were created, each consisting of a surgically plausible combination of three variations for graft type (gracilis, semitendinosus, patellar tendon), diameter (6, 8, 9 mm), and pre-tension (0, 40, 100 N) as well as five femoral graft locations (±5 mm deviation from the native ACL footprint in medial, lateral, anterior, and posterior directions). Three-dimensional motion (Vicon Motion Systems Ltd, UK), ground reaction forces (AMTI, MA, USA), and 12 lower-limb muscle electromyograms (EMG) were recorded during walking at a self-selected pace. Patient-specific FE motion, loading, and boundary conditions were estimated using OpenSim and a calibrated EMG-assisted model. Tibiofemoral flexion angle, abduction-adduction and internal-external rotation moments (summed generalized joint and muscle moments), as well as tibiofemoral and patellofemoral joint contact forces, were used to drive FE models. From the set of 135 FE simulations, absolute error of the kinematics (anteroposterior and mediolateral translations, abduction/adduction and internal/external rotations) and tibial cartilage stress compared to the corresponding intact knee FE model were computed. Optimal surgical configurations were those with clinically acceptable deviations within the clinical thresholds for both kinematics and stress compared to the intact model.

RESULTS AND DISCUSSION

Approximately 21.5% of the surgical combinations resulted in sub-optimal anteroposterior kinematics (Fig. 1), while mediolateral translations were restored for all surgical combinations. All surgical parameter combinations restored abduction/adduction rotations; however, only ~9% restored internal/external rotations. Approximately 94% of surgical combinations induced medial cartilage stresses exceeding 4 MPa compared to the intact model, while ~28% resulted in significant deviations in lateral tibial cartilage stress. Although optimal surgical configurations were identified, deviations from the normal knee persist, warranting caution when selecting surgical parameters.
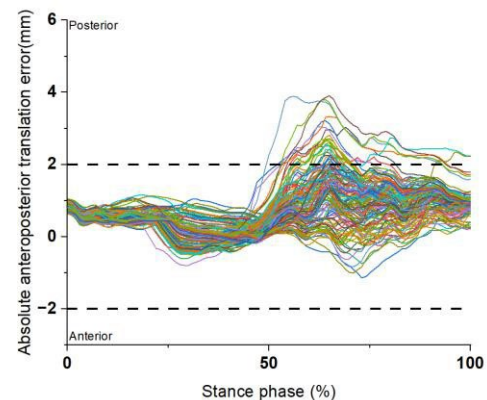
Figure 1: Absolute error of anteroposterior translation between the 135 distinct ACLR FE models and the corresponding intact FE model. The dashed lines represent the threshold for clinically acceptable deviation from the intact model, indicating the ACLR knee behaves similarly to the intact knee for anteroposterior translations.

CONCLUSIONS

The study findings highlight the patient-specific complexities in ACLR biomechanics, emphasizing the need for personalized surgical planning to effectively restore both motion and tissue mechanics. Future studies should include additional subjects to investigate the impact of patient-specific parameters on optimal surgical outcomes.

REFERENCES

1. L. Benos, et al., Frontiers in Bioeng and Biotech, vol. 8,

2020.

Optimising early acetabular implant migration thresholds

[1]Chan Hee Cho, [2]John Abrahams, [2]Lucian Solomon, [3]Bart Pijls, [4]Elise Laende, and [1,2]Stuart Callary
[1]Centre for Orthopaedics and Trauma and Research, The University of Adelaide, Adelaide, SA
[2]Department of Orthopaedics and Trauma, The Royal Adelaide Hospital, Adelaide, SA
[3] Department of Orthopaedics, Leiden University Medical Centre, Leiden, Netherlands
[4]Systems Design Engineering, University of Waterloo, Ontario, Canada
email: chanhee.cho@adelaide.edu.au

INTRODUCTION

Radiostereometric analysis (RSA) is currently the most sensitive method to measure acetabular cup migration *in vivo* [1]. The earliest form of implant surveillance are two year RSA migration studies which have been validated to predict long-term loosening at ten years [2]. However, the current acceptable thresholds were established more than a decade ago, which may not be representative of modern prostheses.

A recent systematic review of RSA studies on acetabular cups has identified that the majority of implant migration occurs within the first 6 months [3]. The migration pattern of the acetabular implant resembles a Michaelis-Menten curve, where migration of the implant increases and then plateaus after 6 months post-operation. This indicates that poor-performing implants could potentially be identified at an earlier time point.

Therefore, the aim of Study 1 was to establish acceptable thresholds of migration by matching early RSA data with long-term registry survivorship data. The aim of Study 2 was to develop a predictive measure to differentiate implants that either stabilise over time or have continuous migration.

METHODS

Study 1: Our previous systematic review of RSA studies was used to identify implants with early proximal acetabular cup migration data [3]. The 10-year revision rate of the same acetabular cup designs were requested from the Australian Orthopaedic Association National Joint Replacement Registry (AOANJRR). The mean 6-, 12- and 24-month proximal migration was compared with long-term registry rate. Thresholds for acceptable migration was classified at <5% revision at 10 years.

Study 2: The Michaelis-Menten curve was used to model RSA acetabular implant migration data. The point of maximum migration of each cup design (EMax) was generated by inputting ≤1-year RSA migration results into the Michaelis-Menten curve. The predive values were then compared to the matching 5-year RSA migration results, often reported in follow-up publications.

RESULTS AND DISCUSSION

Study 1: 15 acetabular implants had both 12-months migration and 10-year revision rate for all-cause revision. Six implants had greater than 5% revision rate at 10-year follow-up.

Migration of implant ≥0.08mm at 1-year were considered to be at risk of long-term revision.

Study 2: 83 cohorts from 47 RSA studies were extracted to produce Michalis Menten Curve. 51 of which Michalis Menten Curve was successfully made using ≤1 year RSA data. Of the 10 cohorts that had matching 5-year RSA results, 7 implant designs had a predicted EMax that matched (defined as <0.08mm) 5-year in vivo data. Only 2 implant designs (3 cohorts: Opticup (n=2) and E1 Biomet (n=1)) had predicted EMax lower than actual 5-year RSA results (Figure 1) and both of cups were known to have excessive long-term failure rates.
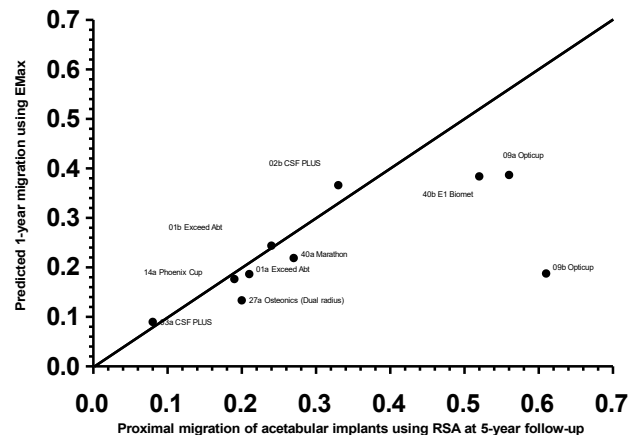
Figure 1: Comparison of proximal migration of acetabular implants with predicted EMax using early migration (≤ 1year) results against 5-year RSA data.

CONCLUSIONS

Our study refined acceptable migration thresholds for modern acetabular cup designs. The use of EMax predictive migration curves demonstrate promising results to identify outlier implants with continuous long-term migration.

ACKNOWLEDGEMENTS

REFERENCES

1. Nelissen RG, et al. JBJS Am. 2011;93 Suppl 3: 62-5.
2. Pijls BG, et al. Acta Orthop. 2012;83(6): 583-91.
3. Cho CH, et al. Acta Orthop. 2023; 94: 626–634.

Wednesday, December 4

National Keynote 3 – Prof Kay Crossley
Biomechanics and early OA – is underloading the new black?

Early-onset (early in life – young adults < 50 years) and early-stage (early in the disease process) osteoarthritis (OA) develops quickly after knee (e.g. anterior cruciate ligament (ACL)) and hip (e.g. femoroacetabular impingement (FAI)) injury, and is burdensome for young active adults.

While the mechanism underpinning early-OA development and worsening may differ for the hip and the knee, it is possible that biomechanics might contribute to the worsening OA after injury. Activity related loading is integral to joint health, and it was traditionally thought that OA progression is driven by higher joint loads (e.g. over-loading). In contrast, joint underloading is a feature of older people with established hip OA, and is a sequalae of ACL injury.

This presentation will explore whether joint loading in younger, active individuals with hip pain or following ACL injury is associated with features of early-onset and early-stage OA. It will discuss possible strategies that might be targets for future research, in efforts to reduce or slow early-OA.

Wednesday, December 4

ABC Podium 5
Locomotion and human movement

DYNAMIC SIMULATION OF TRUNK MUSCLE FUNCTION DURING VERTICAL JUMPING

[1]Harry G. Driscoll, [2]Olga Panagiotopoulou, and [1]Marcus G. Pandy

[1]Faculty of Engineering and Information Technology, The University of Melbourne, Melbourne, VIC
[2]Department of Anatomy and Evolutionary Biology, Monash University, Melbourne, Australia
email: hdriscoll@student.unimelb.edu.au

INTRODUCTION

A model of the human musculoskeletal system that includes a detailed representation of the torso has not yet been used to perform dynamic simulations of sporting activities like running and jumping. Such simulations would allow for a better understanding of trunk muscle function during activities that entail a wide range of trunk movement, thereby lending insight into the relationships between trunk muscle strength and athletic performance. The main aim of the present study was to build on previous dynamic simulations of medium-paced running performed with a new full-body model [1], and to then implement this model in a dynamic simulation of vertical jumping.

METHODS

The newly developed model is an updated version of that reported on by Driscoll et al. [1], with 80 muscle-tendon units modelled in the lower limbs and 38 in the trunk. The model has been updated to work on the most recent version of OpenSim 4.5 [2]. The model is formed in part from the lower limb model from Lai et al [3], as well as a modified torso model derived from that published by Raabe and Chaudhari [4]. Unlike early versions of the model developed by Driscoll for running, the new model retains the constraints controlling lumbar spine motion present in Raabe and Chaudhari. This is due to the high range of lumbar motion present in vertical jumping that necessitates smooth curvature in the lumbar spine for appropriate kinematic tracking and muscle path wrapping. The range of motion of the lumbar spine has been increased from Raabe and Chaudhari to allow for tracking of jumping kinematics [3]. Kinematic data for squat jumping were taken from a previous unpublished study. The subject was instructed to perform a maximum height vertical jump from a stationary squat position with their arms crossed over their torso. The model was scaled in OpenSim 4.5 [4] and used to perform inverse kinematics and computed muscle control (CMC). The simulation was run from the lowest point of the squat, through take-off, flight and landing.

RESULTS AND DISCUSSION

RMS errors for kinematic tracking using CMC are given in Table 1 below. This study presented novel model-predicted activations for a three-dimensional simulation of trunk muscle function during vertical jumping, for a single subject performing a squat jump from lowest point to take-off.

Predicted muscle activations clearly demonstrate the role of the lumbar-spanning muscles, particularly the Erector Spinae, in supporting the torso when crouched and accelerating it into an upright position during extension. Further work is in progress to validate model-predicted activations against data from EMG, and to investigate the effect of the inclusion of the torso muscles on ground reaction forces generated by major lower-limb muscle groups.
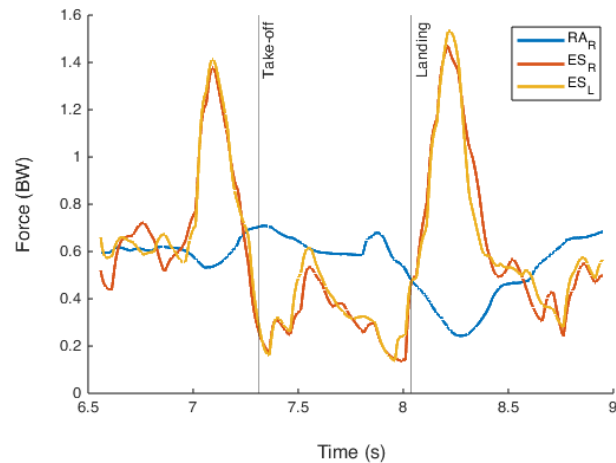
Figure 1: Predicted muscle forces for Rectus Abdominis right (RA_R) and the left and right Erector Spinae muscle groups (ES_R, ES_L) for vertical jumping. Body weight (BW) is ~588N.

CONCLUSIONS

A full-body model incorporating 118 muscles, including 38 trunk muscles, was used to perform a dynamic simulation of vertical jumping. The model reproduced measured 3D joint motion and validation is underway to compare predicted muscle activation patterns with measured EMG.

REFERENCES

1. Driscoll H, et al., XX*IX Congress of ISB,* 2023.
2. Delp et al. IEEE transactions on biomedical engineering 54(11): 1940-1950, 2007.
3. Lai et al. *Annals of biomedical engineering* **45(12)**: 2762-2774, 2017.
4. Raabe M & Chaudhari A. *J Biomech* **49(7)**: 1238-1243, 2016

Table 1: Root-mean-squared errors between model-predicted and measured motion for a dynamic simulation of vertical jumping.

	R-Hip Flex.	R-Hip Add.	R-Hip Rot.	R-Knee Angle	R-Ankle Angle	L5-S1 Flex.	L5-S1 Bend.	L5-S1 Rot.	T12-L1 Flex.	T12-L1 Bend.	T12-L1 Rot.
RMSE	2.4203	0.4624	0.8006	2.2286	2.3574	2.5602	0.4037	0.7490	2.4609	2.6062	1.4146

134

Normalized	0.0291	0.0485	0.0505	0.0270	0.0354	0.0308	0.0508	0.0352	0.0315	0.0366	0.1308

Stride Length Significantly Decreases in a Fatigued State of a Jerry Can Carry

[1,2]Ayden McCarthy, [1,2]Jodie Wills, [3]Bradley Nindl, and [1,2]Tim Doyle

[1]Faculty of Medicine, Health and Human Sciences, Macquarie University, NSW 2109, Australia.
[2]Biomechanics, Physical Performance, and Exercise Research Group, Macquarie University, NSW 2109, Australia.
[3]Department of Sports Medicine and Nutrition in the School of Health and Rehabilitation Sciences University of Pittsburgh, Neuromuscular Research Laboratory/Warrior Human Performance Research Laboratory
email: ayden.mccarthy@hdr.mq.edu.au

INTRODUCTION

Understanding the effects of physical fatigue on military personnel is critical during demanding military tasks. Casualty evacuation is among the most fatiguing and demanding tasks in a military setting [1]. The Australian Defense Force (ADF) Army requires all active personnel to complete a simulated casualty evacuation assessment by carrying jerry cans for a minimum of 150 m. Although a high correlation is present with the jerry can carry to a casualty evacuation event, often in real-life scenarios, personnel are required to carry victims for distances greater than 150 m [1]. Exploring spatiotemporal gait metrics during real-life or simulated casualty evacuation to a fatigued state may indicate key metrics that show an individual is near failure. Thus, this study aimed to identify spatiotemporal metrics indicating fatigue during a maximal jerry can carry assessment.

METHODS

19 participants completed the ADF jerry can carry assessment to fatigue with two 22 kg jerry cans and body armour (23.5 kg) being donned. Standardised instructions and demonstrations were provided before the test. A cadence audio track was played on a loop so that participants completed 25 m laps in a time of 20 seconds until volitional fatigue. FLIR Blackfly cameras integrated into a Vicon motion analysis system to capture motion data at 100 Hz. Motion capture data for each lap was captured in a standardised 8 m volume capture area within the lap. The participants' recorded data were then analysed using Theia software. A 6 Hz, fourth-order, double-pass Butterworth filter was applied. Proprietary algorithms then calculated all joint angles that Theia outputs. In Visual 3D, foot progression angles were used to calculate toe-off and heel strikes via local minima and maxima. The temporal distance gait pipeline computed the spatiotemporal metrics. In the Jamovi environment, mean differences and paired t-tests ($p < 0.05$) were calculated between the participant's first and last lap for stride length, cycle time, stance and swing time.

RESULTS AND DISCUSSION

Table 1 displays mean differences and p values. Stride length was the only metric with a significant difference, showing a decrease of 8 cm and a p-value of 0.035. Although not significant, cycle, stance, and swing time did decrease between the first and last laps.

Table 1. Paired t-test results of gait metrics

Paired t-tests		MD	t	p
Stride_Length_First	Stride_Length_Last	0.08 m	2.28	0.04
Cycle_Time_First	Cycle_Time_Last	0.03 s	1.03	0.32
Stance_Time_First	Stance_Time_Last	0.02 s	1.04	0.31
Swing_Time_First	Swing_Time_Last	0.004 s	0.95	0.36

p value significance at 0.05, MD = mean difference

Participants in a fatigued state had a minimal cadence increase with shorter strides than those in a fresh state. To our knowledge, this study is the first to explore spatiotemporal gait metrics during a simulated casualty evacuation military task to fatigue. Similar military gait studies have explored these metrics and found varying results. A systematic review by Walsh and Low [2] explored how load carriage affects gait in military personnel. Five out of the eight studies showed no changes in spatiotemporal gait metrics. A study by Fellin, Seay [3] found similar findings to this research when an external load of > 20 kg was donned, cadence increased, and stride length decreased. The results from this study demonstrate that when individuals start to decrease stride length significantly, they enter a fatigued state while cadence has minimal change. Although this multifactorial task involves total body physical fitness, stride length may be used as an indicator of fatigue.

CONCLUSIONS

Casualty evacuation is a highly demanding task in the military, often performed in highly dangerous situations like active combat. When military personnel perform this task in the field, a decreased stride length must be closely monitored to identify fatiguing personnel. Strategies such as rest intervals or rotating personnel carrying an injured comrade can be used when a fatigued state is identified.

ACKNOWLEDGEMENTS

REFERENCES

1. Beck, B., et al., Ergonomics, 2016. 59(6): p. 813-20.
2. S Walsh, G.S. and D.C. Low, Appl Ergon, 2021. 93: p. 103376.
3. Fellin, R.E., et al., J Hum Kinet, 2016. 50(1): p. 27-35.

PATELLOFEMORAL JOINT CONTACT AREA DEPENDS PRIMARILY UPON THE KNEE FLEXION ANGLE DURING DAILY ACTIVITIES

Shanyuanye Guan and Marcus G. Pandy

Department of Mechanical Engineering, The University of Melbourne, Parkville, VIC
email: shanyuanye.guan@unimelb.edu.au

INTRODUCTION

Patellofemoral (PF) joint contact area, a key parameter characterizing PF joint contact, has been measured both *in vitro* and *in vivo* [1, 2]. *In vivo* measurements of PF joint contact area have been acquired only under static conditions, with the knee held at fixed flexion angles between 0 and 60° [2]. No previous study has measured PF contact area *in vivo* during any dynamic activity. The aim of this study was to measure and compare PF contact area in healthy individuals across a range of activities of daily living.

METHODS

Ten healthy young people (29.8 ± 6.1 years) with no history of lower-limb surgery or knee pain participated in this study. Mobile biplane X-ray imaging [3], combined with magnetic resonance imaging, was used to measure the area of articular cartilage contact at the PF joint during six dynamic activities: level walking, downhill walking, stair ascent, stair descent, open-chain (non-weightbearing) knee flexion, and open-chain knee extension. The measured PF contact area was normalized using the ratio of the patellar cartilage area of each participant to the average patellar cartilage area of all ten participants. Third-order polynomial functions were fitted to the normalized data to quantify the dependence of PF contact area on the knee flexion angle and to describe changes in PF contact area as the knee flexion increased from full extension.

RESULTS AND DISCUSSION

PF contact area was strongly associated with the knee flexion angle for all six activities with coefficient of determination (r^2 in Figure 1) values ranging from 0.77 to 0.89 for individual activities. When pooling all six activities together (Figure 1C, black line), 83% of the variation in the PF contact area was explained by the knee flexion angle, indicating that the PF contact area was primarily determined by knee flexion. The PF contact area increased as the knee flexed from full extension to approximately 60-70° and then decreased as the flexion angle increased further, up to around 120°.

CONCLUSIONS

In conclusion, this study presents the first *in vivo* measurements of the PF contact area across a wide range of daily activities. The PF contact area was found to be primarily determined by the knee flexion angle and was relatively insensitive to the type of activity. Accurate knowledge of *in vivo* PF contact area during daily activities, combined with joint loading data from computational models of the PF joint, may provide more reliable estimates of PF joint stress.
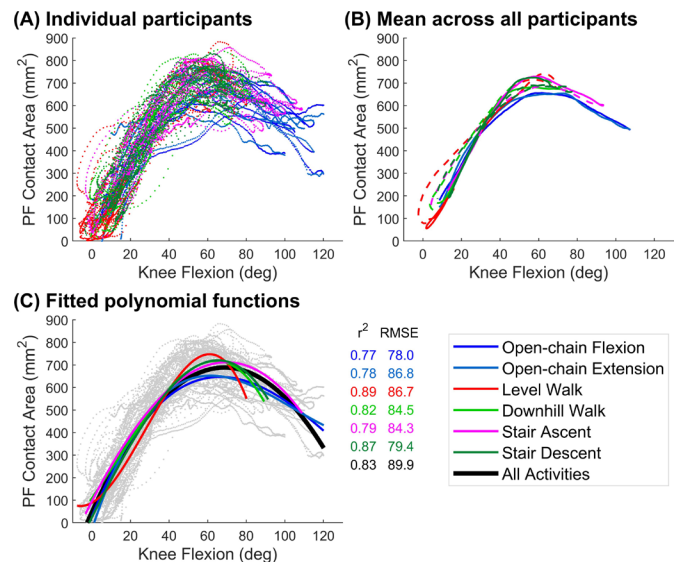
Figure 1: Normalized PF contact area plotted against the knee flexion angle for all ten participants and all six activities. (A) PF contact area for individual participants. (B) Mean PF contact area across all participants for each activity. The solid and dashed lines for the four gait activities represent the stance and swing phases, respectively. (C) Third-order polynomial functions fitted to the data of all ten participants for each activity (colored lines) and for all six activities pooled (black line).

ACKNOWLEDGEMENTS

REFERENCES

1. Ahmed AM, et al., *J. Biomech. Eng.* **105**:226-236, 1983.
2. Besier TF, et al., *J. Orthop. Res.* **23**:345-350, 2005.
3. Thomeer L, et al., *Ann. Biomed. Eng.* **49**:1183-1198, 2021.

HOSE DRAG TASK DEMANDS OF AVIATION FIREFIGHTERS

[1,2]Jodie A. Wills, [1,2]Rhiannon A. Campbell, [3]Paul J. Tofari, [3]Stuart J. Cormack and [1,2]Tim L.A. Doyle

[1]Macquarie University, Department of Health Sciences, Faculty of Medicine, Health and Human Sciences, Sydney, NSW
[2]Biomechanics, Physical Performance, and Exercise (BioPPEx) Research Group, Macquarie University, Sydney, NSW
[3]School of Behavioural and Health Sciences, Australian Catholic University, Melbourne, VIC

INTRODUCTION

Occupational firefighting requires short intense bouts of physical work including handling, dragging, and supporting charged hoses, climbing stairs /ladders, performing search and rescue missions, and carrying heavy equipment [1]. Aviation rescue firefighters (ARFFs) are specialised first responders dedicated to managing emergency aviation-related incidents. Rapid responses are often required to prevent potentially explosive situations, such as fuel spills and aircraft-related fires [2]; hose drag tasks are deemed a critical firefighting task in this instance.

Due to the highly specific nature of aviation firefighting, there is limited information regarding the physical capacities of ARFF personnel and criterion task demands. This study provides a descriptive analysis of the physical loads experienced by ARFFs completing a hose drag task.

METHODS

Twenty-nine operational ARFF (mean±standard deviation (SD); sex 27 male, 2 female; age 38.9±8.3 years; height 1.8±0.1 m; body mass 88.9±15.9 kg; service duration 9.0±6.1 years) were recruited from a firefighting organisation. Firefighters who volunteered to participate provided written, informed consent prior to testing. Research was approved by the Macquarie University Human Research Ethics Committee (Project ID: 52021993530114). The ARFF organisation was not involved in the analysis or interpretation of results.

Fitness testing was completed to profile ARFF physical capacities. A force platform (VALD ForceDecks; FDLite V.1, VALD Performance, AUS) was used for countermovement (CMJ) and squat (SJ) jump assessments of lower body explosive power, and isometric mid-thigh pull and push-up tests for lower and upper body maximum strength. A 20m multistage fitness test was used to assess aerobic capacity. Participants then completed a hose drag task; ARFFs advanced a 38mm charged hose to its full 30m length. The hose was connected to a branch nozzle (FB10X) via a strain gauge (EXSURGO GStrength, Sterling, VA). The task duration (s) and peak force exerted (kg) were used to quantify external load, maximum heart rate (HR_{max}) and relative heart rate ($HR_{max}\%$) during the task, and the rating of perceived exertion (RPE, BORG CR100 scale) after the task were used to quantify internal load.

Descriptive statistics for ARFF physical characteristics and the hose drag task were calculated using Jamovi (version 2.4.8). Results are presented as mean±SD, range (min, max), standard error of mean (SEM).

RESULTS AND DISCUSSION

Aerobic capacity was determined by predicted $\dot{V}O2_{max}$. Results aligned with the recommended minimum standard (45 ml/kg/min) required for incumbent firefighting activities [3] (Table 1).

Table 1. Physical characteristics of Aviation Rescue Firefighters.

Physical Test / Measure	N	Mean±SD	Range	SEM
20 m Multistage Fitness Test Level (AU)	28			
20 m Multistage Fitness Test Distance (m)	28	1586±530	540-2660	100
Predicted V O2max (ml/kg/min)	28	45.4±8.4	27.6-61.2	1.58
HRmax (bpm)	26	189±10.2	169-208	2.01
CMJ Peak Jump Height (cm)	29	33.6±5.5	23.6-45.1	1.01
SJ Peak Jump Height (cm)	29	29.4+5.5	19.0-40.1	1.02
EUR	29	1.2±0.1	0.9-1.5	0.02
IMTP Peak Force (N)	29	3552±698	1993-4891	130
IPU Peak Force (N)	29	1207±245	744-1697	42.6

HRmax, maximum heart rate; AU, Arbitrary unit; V̇ O2max, maximum oxygen consumption; CMJ, countermovement jump; SJ, squat jump; EUR, eccentric utilisation ratio; IMTP, isometric mid-thigh pull; IPU, isometric push up; Range, minimum to maximum value; SEM, standard error of mean.

Interestingly, external load metrics demonstrated quicker task completion and lower internal load responses (HR_{max} and RPE) compared to previous research [4] that investigated the demands of a similar hose drag task.

Table 2. External (task duration and exerted force) and internal (physiological and perceptual responses) load metrics measured during a 30m hose drag task.

Hose Drag Task	N	Mean±SD	Range	SEM
External Load				
Duration (s)	29	22.9±6.58	16.32-39.22	1.22
Average Force (kg)	29	18.34±14.0	14.95-21.26	1.34
Internal Load				
Task HRmax (bpm)	29	152±17	119-184	3.08
HRmax% (bpm)	26	79.4±6.5	64.8-88.9	1.27
RPE (AU)	29	34±14	15-70	2.64

s, seconds; kg, kilograms; HRmax, maximum heart rate; HRmax%, relative maximum heart rate; bpm, beats per minute; RPE, rating of perceived exertion; AU, arbitrary unit

CONCLUSIONS

This work investigated the loads associated with an aviation firefighting hose drag task. Results indicate that ARFF personnel physical capacities sufficiently meet task demands of discrete hose drag tasks. These findings offer valuable insights for developing the physical capacities of personnel to successfully perform ARFF criterion tasks.

ACKNOWLEDGEMENTS

REFERENCES

1. Skinner TL, et al., *JSAMS*. **23**:1228-1233, 2020.
2. Jagim AR, et al. *J. Funct. Morphol*. **8**: 21, 2023.
3. Gledhill N & Jamnik VK. *Can J Sport Sci*, **17**(3): 207-213, 1992.

4. Nazari G, et al., *Rehabil Res Pract,* 1: 323-417, 2018.

ANZSB
anzsb.asn.au

BACK IN ACTION: ASYMMETRY IN PARASPINAL MUSCLE SIZE, COMPOSITION AND ACTIVATION IN ADOLESCENT IDIOPATHIC SCOLIOSIS

[1]Kylie Tucker, [1]Phoebe Duncombe, [2]Phoebe Ng, [3]Frederique Dupius, [4]Maree Izatt, [4]Robert Labrom,
[1]Wolbert van den Hoorn, and [1]Taylor Dick

[1]School of Biomedical Sciences, Faculty of Medicine, The University of Queensland, Brisbane, QLD
[2]Physiotherapy Department, KK Women's and Children's Hospital, Singapore
[3]Faculty of Medicine, Laval University, Quebec, Canada
[4]Biomechanics and Spine Research Group (QUT) at the Centre for Children's Health Research and Queensland Children's Hospital; and School of Mechanical, Medical and Process Engineering, Queensland University of Technology, Brisbane, QLD

email: k.tucker1@uq.edu.au

INTRODUCTION

Adolescent idiopathic scoliosis (AIS) describes a three-dimensional curvature of the spine and ribcage that occurs in 2-4% of adolescents between 10-18 years with otherwise healthy musculoskeletal structures and can progress rapidly. Many biological factors have been attributed to the presence and progression of AIS; however, as the term idiopathic suggests, the pathogenesis of this condition remains unclear [1]. It is well known that forces applied to bones and vertebral discs, including from muscles, are substantial moderators of growth and adaptation [2,3]. The aim of this study is to quantify muscle activation, volume, intramuscular fat, fat-free volume asymmetry in AIS and determine if this differs from age and gender matched controls.

METHODS

Data is presented from 29 female adolescents with primary-right-thoracic scoliosis (range: Cobb angle 16-80°; age mean: 13.8(1.5) years) and 19 age-matched female control participants without scoliosis (age: 13.1(1.8) years).

Participants (i) completed a series of maximal and submaximal movement tasks while muscle activation was recorded paraspinal muscles adjacent to C7, T9/curve apex, T12, and L5 vertebra, and (ii) underwent magnetic resonance imaging scans from which multifidus, longissimus, iliocostalis, spinalis, and psoas muscle volume, intramuscular fat, and fat-free muscle were measured across 11 vertebral levels (from T4 to L4/5).

RESULTS AND DISCUSSION

AIS participants had greater asymmetry in paraspinal muscle activation, particularly at the level of the apex/T9 vertebra, compared to controls. For example, during a bilateral rapid arm flexion task, activation was 6ms (95%CI: 2-10ms) earlier on the right (convex) than left side of the spine in AIS, and 8ms (95%CI: 3-13ms) earlier on the left than right side in controls (p<0.05). Muscle volume, intramuscular fat, and fat-free muscle were more asymmetrical in AIS compared to controls (p<0.05, example data from multifidus, Figure 1). The regions of muscle volume and fat asymmetry varied between muscles.
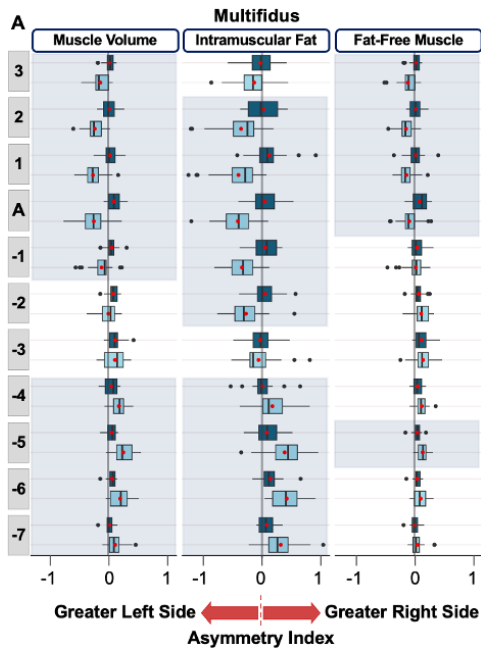
Figure 1: Data from 3 vertebrae above to 7 below the level of the curve apex (A). Shaded area: sig difference between AIS (light) and control (dark) asymmetry.

CONCLUSIONS

These findings provide evidence that asymmetries in superficial paraspinal muscle activation are localized to near the level of the curve apex, and asymmetries in muscle size and composition exist along the length of the soloistic spine. Further work that considers the activation of deep muscles; and the link between these asymmetries and curve progression is warranted.

REFERENCES
1. Nigrini et al., Scoliosis and Spinal Disorders. **13**(1), 2018.
2. Wolf. *The Law of Bone Remodeling,* 1892.

How Does Motor Unit Recruitment Differ Across Knee Extension Tasks? A preliminary analysis.

[1]Robert Lees, [1]Wolbert Van Den Hoorn, [1,2]Francios Hug, [1]Kylie Tucker and [1,3]Jacob Thorstensen

[1]School of Biomedical Sciences, The University of Queensland, Brisbane, Australia
[2]Laboratory EA 4334 'Movement, Interaction, Performance', University of Nantes, Nantes, France
[3]Faculty of Health Sciences and Medicine, Bond University, Gold Coast, Australia

email: robert.lees@student.uq.edu.au

INTRODUCTION

Neural control of movement and posture is a complex process orchestrated by the central nervous system (CNS) [1]. It involves the integration of sensory information, generation of motor commands, and execution of these commands via motor units. Motor units, comprising a motoneuron and the muscle fibers it innervates, are the fundamental units of motor control [1]. The recruitment and firing of motor units is modulated by descending pathways from the brain and brainstem, for example the corticospinal tract [2]. These pathways convey commands for movement to the spinal cord, which influences the activity of motoneurons, and allows the CNS to regulate body posture and execute a wide range of movements [2]. This study aims to assess motor unit discharge patterns of the Vastus Lateralis (VL) and Vastus Medialis (VM) during knee extension tasks with varying postural demands, and to determine if motoneuron synergies within and between VL and VM are affected. It is hypothesized that motor unit discharge rates will be higher during tasks with greater postural demand, but coherence will be higher during tasks with lower postural demand.

METHODS

We recruited 5 male participants (age 23.6 ± 4.2 years old) without significant lower limb injuries or neurological issues. High-density surface EMG (HDsEMG) was recorded from the VL and VM using four grids over VL and two over VM. Signals were recorded at 2048Hz with a bandpass filter of 20Hz to 500Hz. Participants performed three tasks: a single leg squat (dynamic postural condition), a dynamic isometric contraction, and a static isometric contraction. The single leg squat involved squatting to a 60° knee angle and was completed first to match muscle activation across tasks. The static isometric task required a knee extension at a fixed 60° knee joint angle. The dynamic isometric task involved pulling against a pulley system to maintain a 60° knee angle. Each task was repeated three times for 20 seconds, with a minute rest between repetitions. Raw HDsEMG recordings were blind source separated into individual motor unit pulse trains, and manually inspected to ensure accurate decomposition results. Motor unit coherence analyses involved transforming pulse trains into the frequency domain and calculating the magnitude squared coherence within and between muscles.

RESULTS AND DISCUSSION
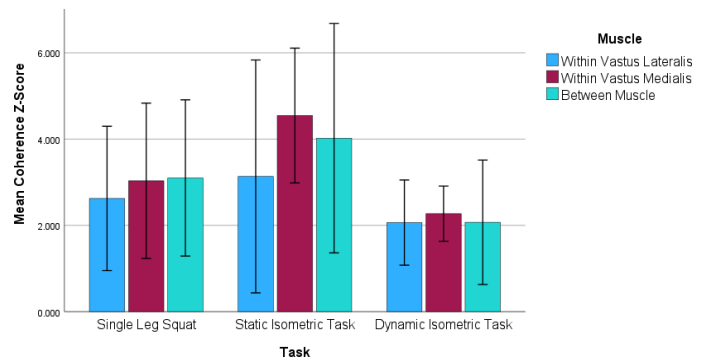
Figure 1: Coherence Z Scores across tasks completed. Average coherence scores and standard deviation for each task (N = 5). Each bar represents the coherence analysis conducted within the VL and VM muscles, as well as the coherence between these muscles.

Motor unit coherence was highest for the static isometric condition, followed by the single leg squat task, with the lowest coherence observed during the dynamic isometric condition. This suggests that performing different knee extension contraction types with different postural requirements affects neuromuscular control and muscle activation strategies for the VL and VM. Motor unit coherence is largest during EMG and joint angle matched static isometric contractions and smallest during dynamic isometric contractions (whereby participants actively maintain their joint angle). However, as this is a preliminary analysis of data collected to date, we acknowledge that our results could differ when we recruit more participants.

CONCLUSIONS

In conclusion, our preliminary motor unit coherence analysis showed higher coherence values during static isometric task compared to the other completed tasks. These insights can help enhance our understanding of neuromuscular function.

REFERENCES

1. Pearson K.G, *Review of Neuroscience* **16** 265 – 297, 1993
2. Nichols T.R, Journal *of Neurophysiology* **119** 1186 -1200, 2018

Wednesday, December 4

ANZORS Podium 5

Septic vs Aseptic: A Cost-Analysis of Revision THA at a Tertiary Referral Centre

[1]Aaron Hammat, [1]Taisha D'Apollonio, [2]Marieke Hopman, [3]Kerry Costi, [4]Renjy Nelson, [5]David Campbell, [1,3]Lucian B. Solomon, [6]Emmanuel Gnanamanickam, [1,3]Stuart Callary

[1]Centre of Orthopaedic and Trauma Research, The University of Adelaide, Adelaide, SA
[2]Faculty of Medicine, Vrije Universiteit Amsterdam, Amsterdam, Neatherlands
[3]Department of Orthopaedics and Trauma, Royal Adelaide Hospital, Adelaide, SA, Australia
[4]Department of Infectious Diseases, Royal Adelaide Hospital, Adelaide, SA, Australia
[5]Wakefield Orthopaedic Clinic, Calvary Adelaide Hospital, Adelaide, SA, Australia
[6]Adelaide Centre for Clinical Epidemiology, The University of Adelaide, Adelaide, SA, Australia
email: aaron.hammat@adelaide.edu.au

INTRODUCTION

Revision total hip arthroplasty (rTHA) poses substantial clinical and economic challenges for patients, healthcare providers, and the healthcare system. However, rTHA is subject to substantial variation due to different diagnoses and various types of treatment, particularly for periprosthetic joint infections (PJI). We previously had estimated hospital costs of PJI by treatment pathways beyond first admission with the PIANO cohort [1] using activity-based costing, estimating the Australian burden of PJI to be $250 million.[2] However, these are only estimates and understanding the true cost burden is important for appropriate servicing, resource allocation and sustainable healthcare access to patients.

Hence, we aimed to investigate (1) the hospital costs of revision THA by diagnosis in a tertiary referral centre per episode of care (EoC) and (2) the influence of treatment type of revision THA on hospital costs for patients treated for PJI.
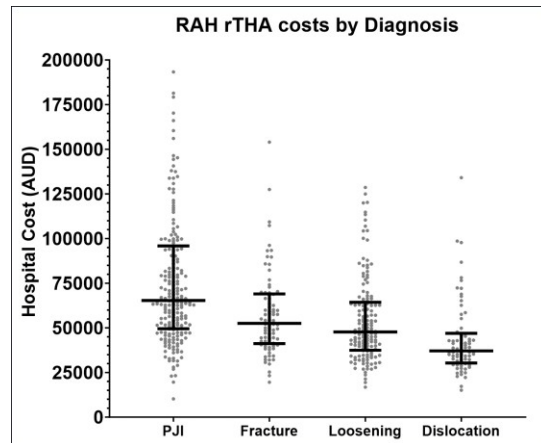
METHODS

For patients who underwent a rTHA procedure at the Royal Adelaide Hospital (RAH) between 2014 and 2022, hospital finance records were matched with procedural and admission records. Hospital costs of rTHA were analysed by diagnosis, and PJI patient costs were analysed according to treatment type and resultant treatment pathway post initial admission.

RESULTS AND DISCUSSION

A total of 396 patients with 529 EoCs were included. The PJI rTHA median costs of $65,325 (Figure 1) were significantly higher than the aseptic rTHA costs $45,850 (p<0.001). The costs for fracture, loosening and recurrent dislocation were $52,521, $47,708 and $37,072 respectively (Figure 1). For PJI patients, two-staged rTHA was the costliest initial treatment, and additional surgery (two-stage + re-revision, first-stage + repeat first stage) increased costs substantially (Table 1).

Figure 1: rTHA hospital costs by diagnosis

Substantial variation was shown in the costs of the PJI cohort (Figure 1); however, these costs are better represented when categorized by treatment type (Table 1). This study reports the true costs of PJI to be on average 33% higher than our estimates from the PIANO cohort [1], suggesting that the true cost burden is significantly greater, in excess of $330 million.

CONCLUSIONS

Costs were incrementally higher across dislocation, loosening, fracture and PJI diagnoses. We estimate the true annual burden of PJI to the Australian healthcare system is more than $330 million.

ACKNOWLEDGEMENTS

REFERENCES

1. Manning L et al., Open Forum Infect Dis. 2020
2. Hammat et al., (In Print), Bone and Joint Journal, 2024

Table 1: Hospital costs of PJI by Treatment Type (AUD, '000)

	Two-stage rTHA only	Two-stage + re-revision	First Stage rTHA only	First-stage + repeat First-stage	Single stage rTHA	DAIR
Hospital Costs (Median, IQR)	$134.9 ($113-$225)	$210 ($177-$255)	$69.2 ($45-$92)	$262.2 ($176-$456)	$78.3 ($52-$118)	$55.9 ($36-$80)

| EoC | 1-3 | 3-5 | 1 | 1-4 | 1 | 1 |

KNEE JOINT REACTION FORCES ARE POSITIVELY CORRELATED WITH CHANGES IN THE BONE OF THE PROXIMAL TIBIA FOLLOWING PRIMARY TOTAL KNEE REPLACEMENT SURGERY

[1]Salindi P. Herath, [1]David Hobbs, [2]Dominic Thewlis, [3]Christopher Wilson, [1]Mark Taylor

[1]Medical Device Research Institute, Flinders University, Adelaide, SA, Australia
[2]Faculty of Health and Medical Sciences, University of Adelaide, Adelaide, SA, Australia
[3]College of Medicine and Public Health, Flinders University, Adelaide, SA, Australia
email: salindi.herath@flinders.edu.au

INTRODUCTION

One of the most common reasons for revision of a cemented primary total knee replacement surgery is aseptic loosening of the tibial component [1]. Aseptic loosening can be attributed to a loss of fixation between the bone and the implant, secondary to bone loss [1]. Stress shielding is a mechanism by which bone loss can occur where load passes primarily through the implant due to its higher stiffness compared to the surrounding bone. Previous literature has shown that bone mineral density (BMD) decreases in the periprosthetic region around the tibial component [2]. The relationship between mechanical factors that affect bone remodeling and the changes in the bone are unknown, however.

According to Wolff's Law, bone remodels based on the loads that are applied to it, but there are currently no longitudinal studies that have estimated knee joint loads following a total knee replacement surgery. The aim of this study was to investigate the relationship between knee joint loads from pre-operation up to 12 Months post-operation and changes in the BMD of the proximal tibia.

METHODS

This study included 22 primary total knee replacement patients (10 male). All participants received DEXA BMD scans of the proximal tibia preoperatively, and then at 3, 6, and 12 months post-operatively. At these same timepoints, motion capture data (marker trajectories and ground reaction forces) was collected using a 10 camera Vicon system (Vicon Motion Systems, Oxford, UK) during activities of daily living. BMD was measured using Hologic software in the medial and lateral proximal tibia near the wings of the tibial component, firstly under the baseplate, and then further distally away from the baseplate. Modified Gait2392 model [3] and OpenSim were used to estimate the knee JRFs using static optimization to calculate muscle forces.

Linear regressions were used to determine the relationship between knee JRF and BMD changes. Statistical significance was defined as $p < 0.05$.

RESULTS AND DISCUSSION

Most participants experienced a decrease in their total knee JRF (n = 20) at 3 Months and a decrease in their lateral BMD (n = 21) from 3 to 6 months following surgery. The changes in total knee JRF between surgery and 3 months were significantly positively correlated with changes in the BMD from 3 – 6 months (Figure 1).
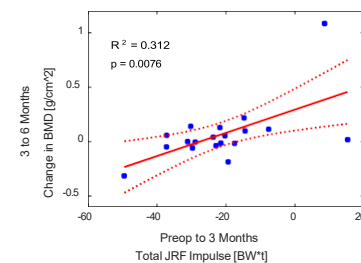
Figure 1: Linear regressions showing correlations between changes in the BMD from 3 to 6 months in the proximal lateral region with changes in knee JRF.

The correlation between the changes in the knee JRF and the changes in the lateral BMD suggest a relationship between knee loading and bone remodeling. Bone remodeling takes time to occur in response to changes to the mechanical load indicating that early changes to knee loading may result in BMD changes that occur later. Changes to the BMD up to 12 months are yet to be calculated at the time of this abstract submission, but this study aims to test the hypothesis that changes in the bone from 6 to 12 months may follow a similar correlation to the earlier changes in the knee JRF. These results suggest that increased knee loading may lead to less bone loss in the proximal tibia.

CONCLUSIONS

Bone loss in the proximal tibia following a primary total knee replacement surgery has been previously reported but no other study has investigated changes in the knee JRF at the same timepoints. Although there are patient and cellular factors that also contribute to bone remodeling, the results of this study demonstrate that increasing loading following a primary total knee replacement surgery could be beneficial for retaining bone in the proximal tibia.

ACKNOWLEDGEMENTS

REFERENCES

1. AOANJRR, A.O.A.N.J.R.R., 2020   .
2. Jaroma A., *Acta Orthopaedica*, **87**. 2016.
3. Saxby D, et al., *Gait and Posture*. **49**. 2016.

DOES THE NUMBER OF PREVIOUS REVISION SURGERIES INFLUENCE THE SURVIVORSHIP OF IMPLANTS USED AT REVISION TOTAL HIP ARTHROPLASTY?

[1,2]Taisha D'Appolonio, [3]Marieke Hopman, [1,2]John Abrahams, [1,2]Kerry Costi, [4]Thomas Sullivan, [1,2]Boopalan Ramasamy [1,2]Bogdan Solomon, [1,2]Stuart Callary

[1]Centre for Orthopaedic and Trauma Research, The University of Adelaide, Adelaide, SA
[2]Department of Orthopaedics and Trauma, Royal Adelaide Hospital, Adelaide, SA
[3]Faculty of Medicine, Vrije Universiteit Amsterdam, Amsterdam, Netherlands
[4]South Australian Health & Medical Research Institute, Adelaide, SA, Australia
email: stuart.callary@adelaide.edu.au

INTRODUCTION

Revision total hip arthroplasty (rTHA) is known to have inferior survivorship to primary THA and patients often require multiple re-revision surgeries during their lifetime. The Australian National Joint Replacement Registry results are limited to survivorship following first revision only due to difficulties matching each individual's index primary procedure. Tertiary referral centres specialize in treating these complex cases, and it would be valuable for surgeons to inform patients of the risks of further surgery when undergoing rTHA, often after multiple previous surgeries.

Our study aimed to investigate the effect of the number of previous surgeries on the survivorship of implants used at rTHA.

METHODS

This retrospective observational study analyzed all rTHA procedures performed at the Royal Adelaide Hospital between January 2003 and December 2023. The Local Ethics Board approved the study. To determine the index primary THA procedure date and any subsequent revision and reoperations, data were collected from multiple hospital databases and follow-up radiographs were screened. Patient and surgical information were prospectively collated in a hospital arthroplasty register. Each rTHA was categorized into aseptic and septic diagnostic groups; and decade time period groups. Kaplan-Meier estimates of survivorship and Cox proportional hazards modeling were performed to assess revision and re-revision probabilities based on the number of previous surgeries.

RESULTS AND DISCUSSION

1406 rTHA procedures were performed on 961 patients. The cases were stratified by the number of previous surgeries on the same hip into four groups (R1, R2, R3, R4+). Most cases were identified as R1 (808, 57.5%), with subsequent rTHA procedures accounting for 22.2% (R2, 312), 9.8% (R3, 138), and 10.5% (R4+, 148), respectively. An increased incidence of re-revision was observed with each subsequent rTHA surgery. Within two years, the risk of re-revision after the first, second,

third, and fourth or higher revisions was 12%, 17%, 17%, and 30%, respectively. The time period-based analysis indicated an increased risk of re-revision of rTHAs treated within 2013-23 compared to 2003-12, predominately due to early dislocation and periprosthetic fracture.
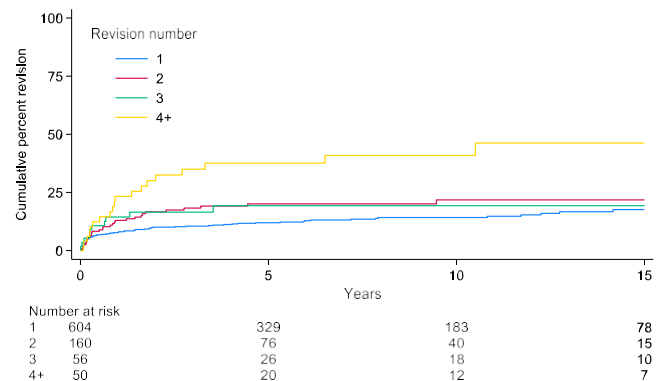
Figure 1: Cumulative percent revision by revision number (Aseptic diagnoses only)

CONCLUSIONS

This study reveals that the risk of re-revision increases with each subsequent rTHA. The survivorship of rTHA at our institution was improved when compared to a UK registry study of first, second and third rTHAs [1] and an Australian registry study of first aseptic rTHAs [2]. Recent increased early failures due to dislocation and fracture need further investigation and a review of treatment protocols.

ACKNOWLEDGEMENTS

REFERENCES

1. Deere K, et al., *Lancet Rheumatol.* 2022;4(7):e468-e79.
2. AOANJRR, Revision of Hip and Knee Arthroplasty Supplementary Report in Hip, Knee & Shoulder Arthroplasty: 2023 Annual Report. Adelaide: AOA; 2023

EFFECT OF BLADE PLATE IMPLANT SIZE SELECTION ON BIOMECHANICAL SURGICAL OUTCOMES FOLLOWING PROXIMAL FEMORAL OSTEOTOMY

[1]Emmanuel Eghan-Acquah, [1]Alireza Yahyaiee, [1]Azadeh Nasseri, [1]Martina Barzan, [1]David Bade, [1]Stefanie Feih, [1]Chris Carty

[1]Griffith Centre of Biomedical & Rehabilitation Engineering, Griffith University, Gold Coast, QLD
Presenting author's email: emmanuel.eghan-acquah@griffithuni.edu.au

INTRODUCTION

The blade plate is the most widely used implant for bony fixation following proximal femoral osteotomy (PFO) and is considered the standard for this procedure [1]. While numerous studies have examined the effects of surgical methods and implant types on PFO outcomes, the specific impact of implant size on the postoperative bone-implant mechanical environment remains unclear. One study recommended a blade plate with a width-to-femoral neck diameter (W-D) ratio between 50% and 75% [1], though this lacked rigorous mechanical analysis. Consequently, current practice is based on manufacturer recommendations and/or surgeon experience. Implant selection should be guided by biomechanical factors ensuring patient safety and implant efficacy, such as structural integrity and minimizing micromotion. This study compares the implant factor of safety (FoS) and bone-implant micromotion for W-D ratios of 30%, 40%, 50%, and 60% for four patients.
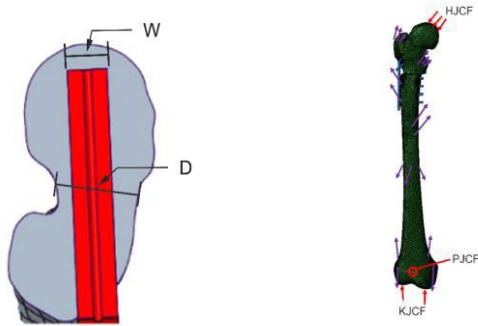
METHODS

Figure 1. W-D ratios were varied and compared (left). Post-op FE model (right).

A neuromusculoskeletal finite element (FE) modelling framework was developed for this study, using postoperative CT images and gait laboratory data from the participating cohort (age = 10.75±2.75 years; height = 1.52±0.17 m; weight = 23.68±26.66 kg). The gait data included 3D whole-body motion, ground reaction forces (GRF), and surface electromyography (EMG) recorded during self-paced walking. A customized OpenSim [2] model, tailored to the patients' anthropometry, calculated joint angles, moments, muscle-tendon lengths, and moment arms. Combined with EMG data in a calibrated EMG-assisted model (CEINMS) [3], these outputs estimated muscle and joint contact forces during the stance phase of the gait cycle. FE models of the patient-specific femurs were constructed in Abaqus (v2022.1, DS, US) from

148

segmented postoperative CT images. Four surgical FE models were created by adjusting implant dimensions to achieve W-D ratios of 30%, 40%, 50%, and 60% based on the manufacturer's brochure (Figure 1a). Hip, knee, patellofemoral contact, and muscle forces were applied as loading conditions (Figure 1b). The respective patient-specific implant FoS was calculated using Soderberg and Basquin's equations, while custom Python scripts quantified average bone-implant micromotion at discrete time points during the stance phase of the gait cycle.
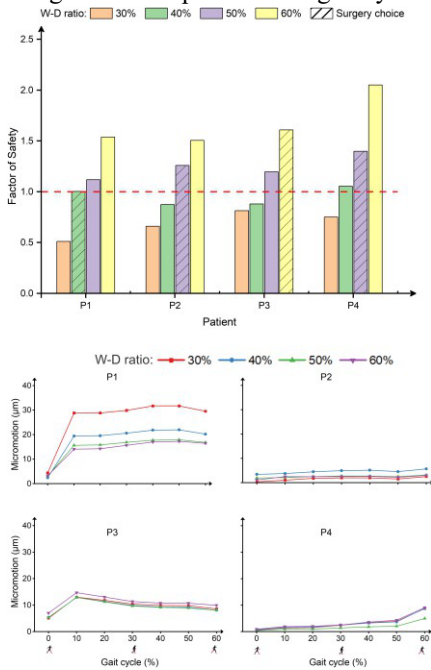
Figure 2. (a) Implant factor of safety after 2 million cyclic loadings. The red dashed line represents Fos =1, below which the implant is considered to have failed. (b) Average bone-implant micromotion across the stance phase of gait.

RESULTS AND DISCUSSION
The FoS increased with an increasing W-D ratio whereas the average micromotion showed patient-specific outcomes with an increasing W-D ratio (Figure 2).

CONCLUSIONS
Our analysis indicates that larger implants (W-D ratio > 40%) reduce the likelihood of implant failure and enhance initial implant stability.

REFERENCES
1. Beauchesne R et al. J Pediatr Orthop, **12(6)**, 735, 1992
2. Delp SL et al. IEEE Trans. BME **54**:1940–1950, 2007
3. Pizzolato C et al., JBiomech, **48**(14):3929-3936, 2015

A Fully Automated Pipeline for Medical Image Reconstruction, Surgical Planning and Simulation of Post-operative Joint Function Following Revision Hip Arthroplasty Involving Acetabular Defects

[1]Daniel Hopkins, [2,3]Stuart A. Callary, [2,3]L. Bogdan Solomon, [1]Peter V.S. Lee, [1]David C. Ackland

[1]Department of Biomedical Engineering, University of Melbourne, VIC, AUSTRALIA; [2]Centre for Orthopaedic and Trauma Research, University of Adelaide, Adelaide, SA, AUSTRALIA; [3]Department of Orthopaedics and Trauma, Royal Adelaide Hospital, Adelaide, SA, AUSTRALIA

email: dchopkins@student.unimelb.edu.au

INTRODUCTION

Revision total hip arthroplasty (rTHA) involving acetabular defects (THAd) is a complex procedure associated with lower rates of success than primary THA [1]. Computational models that predict post-operative joint function following THAd are time-consuming to develop due to highly variable anatomy and the presence of metal artefact in pre-operative computed tomography (CT) scans (Fig. 1). The aim of this study was twofold. Firstly, to develop a fully automated and rapid modelling framework to convert pre-operative CT images of THAd to anatomical models, perform surgical planning of revision arthroplasty, and run simulations of post-operative joint loading; and secondly, to use this pipeline to assess the effect of screw number and placement on bone-implant micromotion and osseointegration (OI) potential.

METHODS

Sixty patients (aged 50-93 yrs.) with acetabular defects who underwent rTHA at the Royal Adelaide Hospital (RAH) by a single surgeon (LBS) were recruited. Each had pre- and post-operative CT scans. An automated neural network, statistical shape modelling and FEM (finite element modelling) framework was developed to estimate post-operative implant primary stability utilizing the pre-operative CT images. The pipeline employed artificial neural network auto-segmentation of the remaining pelvic anatomy and 3D model development of the pelvis and bone defect. Model accuracy was evaluated by calculating the dice coefficient and volume comparison between the fully automated and manually generated models. An automated custom virtual surgery algorithm was then developed for implant selection, bone preparation and implant placement and fixation based on surgical technique employed at the RAH. The algorithm was applied to each patient, with the resultant models being employed in automated FEM, with simulations performed using screws placed in the following regions: (1) superior acetabulum (2) superior and posterior acetabulum (3) superior and anterior acetabulum (4) superior, posterior and anterior acetabulum. Bone-implant micromotion and potential osseointegration area was calculated in each case in the superior, posterior and anterior acetabulum (Fig. 1).

RESULTS AND DISCUSSION

Acetabular defect models were automatically generated from artificial neural networks with an overall mean dice coefficient of 0.827 and a mean absolute relative volume error of 16.4%. Simulation results indicate that case 4 (all 3 screws) resulted in the lowest overall micromotion. Relative to case 4, removing the posterior screw (cases 1 & 3) increased mean micromotion in the posterior acetabulum (mean difference: 97.0μm, $p<0.001$). Removing the anterior screw (cases 1 & 2) increased mean micromotion in the anterior acetabulum (mean difference: 39.2μm, $p<0.01$). Mean micromotion in the superior acetabulum was consistent across all four cases. Reduced micromotion did not always result in an increase in OI potential since certain screw trajectories can decrease implant-bone contact. The entire automated pipeline takes approximately 2 hours to complete utilizing 16 processors and 1 GPU. Model validation via micro-CT cadaveric testing has been undertaken.
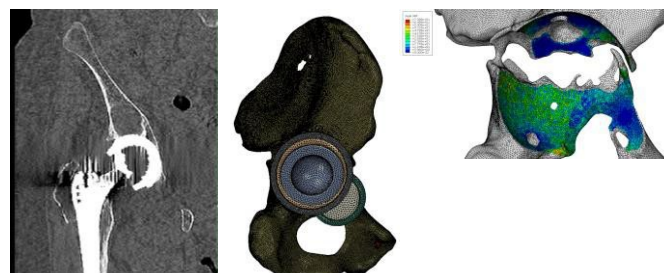
Figure 1: Pre-operative CT image used as pipeline input (left) and automatically generated FE model (middle) and corresponding acetabular distribution map of implant micromotion (right).

CONCLUSIONS

A rapid automated pipeline was developed that was successfully able to convert pre-operative CT images into a detailed finite element model for surgical planning and estimation of post-operative functional performance. The results indicate that regional micromotion of rTHA implants in the acetabulum is highly dependent on local screw fixation and that an appropriate screw trajectory must be selected to maximize osseointegration potential. This pipeline will be useful for planning the surgical treatment of these complex cases and evaluating implant-bone fixation post-operatively.

REFERENCES

1. Ong, K, et al., *Clin Orthop Rel Res.* **468**:3070-3076, 2011.

OBJECTIVE KNEELING ASSESSMENTS MAY HELP DISCERN DIFFERENCES IN PATIENT OUTCOMES BETWEEN TIBIAL NAILING APPROACHES: INTERIM RESULTS FROM A PILOT RCT

[1]Simon Thwaites, [1,2]Mark Rickman, [1,2]Dominic Thewlis

[1]Centre for Orthopaedic & Trauma Research, University of Adelaide, Adelaide, SA, Australia
[2] Department of Orthopaedics & Trauma, Royal Adelaide Hospital, Adelaide, SA, Australia
email: simon.thwaites@adelaide.edu.au

INTRODUCTION
Tibial shaft fractures are the most common long bone fracture and kneeling is known to be the most painful activity amongst this cohort [1]. Intramedullary nailing is the preferred method of fixation to treat these fractures, yet only one study investigating differences in patient outcomes following infrapatellar (IP) and suprapatellar (SP) nailing has reported an objective outcome [2]. The study used the ratio of bodyweight transmitted through each knee in an upright kneeling posture for 60 s as a surrogate measure for anterior knee pain [3]. We have previously reported [4] the reliability of a laboratory-based extension of the original analogue Aberdeen Weight-Bearing Test (AWT), additionally showing kneeling loading patterns. This study aimed to investigate the utility of a variety of objective kneeling assessments to discern differences in patient outcomes between tibial nailing approaches.

METHODS
Patients were recruited from an active pilot RCT (ANZCTR: ACTRN 12620000109909) investigating tibial shaft fractures treated with IP and SP nails at 3-, 6-, 12-, and 18-month follow-ups [5]. A healthy case-matched cohort was also recruited. Participants completed the Knee Injury and Osteoarthritis Outcome Score (KOOS) and KOOS patellofemoral (KOOS-PF) subscales then performed six kneeling tasks on two in-ground force platforms. Knee loading patterns were recorded with eight force sensitive resistors (FSRs) affixed to the knee using the tibial tuberosity (TT) and inferior pole of the patella (IPP) as reference points. A binary outcome of FSR activation was used to calculate the overall proportion ($\hat{p}$) of activated FSRs for each kneeling task, which included: AWT in upright and flexed kneeling positions, and reaching forward, left, right, and backwards. For AWT ratios, Kruskal-Wallis tests compared multiple groups and pairwise comparisons were calculated using Dunn's test ($\alpha = 0.05$). Two-tailed Kendall's Tau (τ) correlations were calculated between KOOS-Sport and KOOS-PF, as well as their component kneeling questions, with the total percentage of kneeling trials completed.

RESULTS AND DISCUSSION
Twenty tibial nailing patients (nIP = 9; nSP = 11) and 18 healthy participants were recruited. The IP group showed increased bodyweight transmitted through the contralateral limb compared to the SP group for upright kneeling at three months at all AWT timepoints (0, 15, 30, 45, 60 s). The IP group

showed most knee loading at the superior patella tendon (SPT) (mean $\hat{p} = 0.79$); the inferior patella tendon (IPT) was most loaded in the SP group (mean $\hat{p} = 0.90$) (Figure 1). SP patients completed more kneeling trials compared to the IP group at all follow-ups (3-month: IP = 39%, SP = 40%; 6-month: IP = 50%, SP = 81%; 12-month: IP = 80%, SP = 98%; 18-month: IP = 77%, SP = 97%; healthy = 95%). KOOS-Sport ($\tau = 0.36$) and KOOS-PF ($\tau = 0.38$) showed weak positive correlations to the total percentage of completed kneeling trials; their component kneeling questions showed moderate negative correlations ($\tau = -0.41$ and $\tau = -0.4$, respectively).
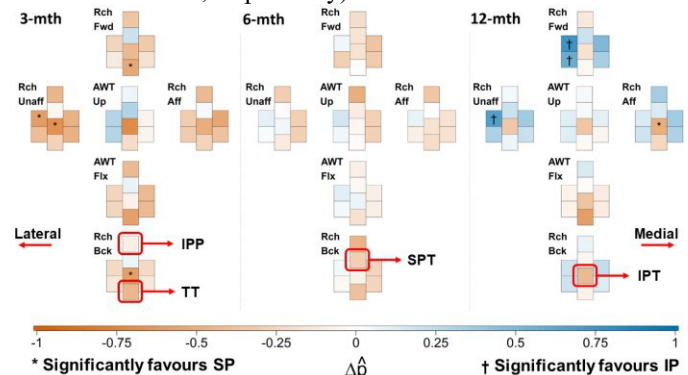
Figure 1: Difference in proportion of FSR activation ($\Delta\hat{p}$) up to 12-months between nailing groups. Heatmaps show anterior view of right knee loading (left knees are mirrored med./lat.).

CONCLUSIONS
A combination of subjective and objective measures may be required following tibial nailing. Objective kneeling assessments may help discern differences in patient outcomes between intramedullary nailing approaches, providing clinicians with important information regarding patient recovery previously limited to mostly subjective measures.

REFERENCES
1. Song S, et al., *J Orthop Trauma.* **26**(3):172-177, 2012.
2. Thwaites S, et al., *Eur J Tr Em Sur.* **50**: 59-70, 2023.
3. MacDonald, D. et al., *BJJ.* **101-B**(9):1138-1143, 2019.
4. Thwaites S, et al., *Knee.* **38**: 201-211, 2022.

5. Thwaites S, et al., *Pilot Feas Stud* **8**:110-122, 2022.

Wednesday, December 4

ABC Podium 6
Clinical biomechanics

LEG STIFFNESS DURING RUNNING IN ADULTS WITH TRAUMATIC BRAIN INJURY

[1]Benjamin Mentiplay, [2]Clara Jobic-Deprez, [3]Annie Chappell and [2,4]Gavin Williams

[1]School of Allied Health, Human Services and Sport, La Trobe University, Melbourne, VIC
[2]School of Medicine, Dentistry and Health Sciences, The University of Melbourne, Melbourne VIC
[3]Western Kids Health, Perth, WA
[4]Physiotherapy Department, Epworth Healthcare, Melbourne, VIC
email: b.mentiplay@latrobe.edu.au

INTRODUCTION

Traumatic brain injury (TBI) is one of the leading causes of death and long-term disability among young adults around the world. Given the prevalence of TBI amongst young adults (aged 18-35), restoration of running is a common treatment goal. One important biomechanical measure of running is leg stiffness, which provides an indication of the spring-like characteristics of the leg as it stores and releases energy. While leg stiffness during running has been studied in other neurological cohorts such as cerebral palsy [1], leg stiffness during running in adults with TBI has yet to be investigated.

The primary aim of this study was to compare leg stiffness during running in adults with TBI and healthy controls. The secondary aims of this research were to: 1) compare leg stiffness in the affected and less affected leg in adults with TBI; and 2) determine whether differences in leg stiffness exist in people with TBI that either have lower limb spasticity compared to those without or that have lower limb muscle weakness compared to those without.

METHODS

Sixty-one adults with TBI and 20 healthy controls were included. Participants ran overground on a 20m runway while three-dimensional kinematic and kinetic data were recorded via an eight camera VICON system with AMTI force plates embedded in the laboratory floor. The TBI group were asked to run at a self-selected speed, while the controls were asked to run at a speed comparable to the mean (±5%) of the TBI group given the known impact running speed has on leg stiffness [2].
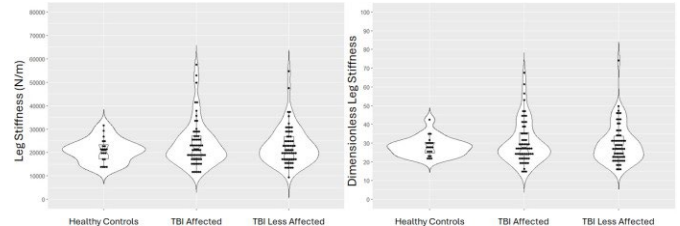
In the adults with TBI, affected limb spasticity was assessed using the Modified Tardieu scale (quadriceps, soleus, and gastrocnemius) and muscle weakness vis hand-held dynamometry for both limbs (knee extensors). Participants were classified as having spasticity if they scored 2-4 for any muscle examined and having weakness if the affected knee extensors were ≥10% weaker than the less affected side.

Leg stiffness [3] was calculated as the ground reaction force in line with the leg vector [N] divided by the change in leg length [m] during stance. Dimensionless leg stiffness was also calculated to account for differences in body size.

Statistical analyses to compare leg stiffness between limbs and between groups, and between those with and without spasticity or weakness, were conducted using t-tests with effect sizes.

RESULTS AND DISCUSSION

There was a large range of leg stiffness (Figure 1) in adults with TBI during running (affected leg median = 21,562 [range 11,074 to 57,436] N/m; less affected leg = 20,870 [9,378 to 54,720] N/m) compared to healthy controls (20,943 [13,402 to 31,502] N/m). However, there were no statistically significant differences in leg stiffness between the affected and less affected limbs of the TBI group (p=0.59, effect size [ES]=0.08) nor between both the TBI limbs and healthy controls (affected limb; p=0.44, ES=0.12; less affected limb; p=0.47, ES=0.11).

Figure 1: Leg stiffness (left) and dimensionless leg stiffness (right) during running in the affected and less affected limb for adults with TBI (n = 61) and for healthy controls (n = 20).

Additionally, there were no statistically significant differences in affected leg stiffness during running between those with and without spasticity (p=0.64, ES=0.07) or between those with or without muscle weakness (p=0.31, ES=0.17).

CONCLUSIONS

Although no statistical significance was found on a group level, results demonstrated high variability in leg stiffness in adults with TBI compared to controls. Further research is needed to determine which factors influence leg stiffness during running and how stiffness relates to clinical outcomes in TBI.

REFERENCES

1. Chappell A, et al., *Clinical Biomechanics*. **84**, 2021.
2. Kuzmeski J, et al., *Journal of Applied Biomechanics*. **37**:327-332, 2021.
3. Chappell A, et al., *Gait and Posture*. **90**:441-448, 2021.

POSTURAL ALIGNMENT DURING UNSUPPORTED WALKING FOLLOWING ACQUIRED BRAIN INJURY: APPLICATION OF A NEW MEASURE

[1,2]Jack Beard, [1,2]Gavin Williams, [3]Benjamin Mentiplay, [4]Simon Mills and [1,2]Michelle Kahn

[1]Physiotherapy Department, Epworth Healthcare, Melbourne, VIC
[2]School of Medicine, Dentistry and Health Sciences, The University of Melbourne, Melbourne VIC
[3]School of Allied Health, Human Services and Sport, La Trobe University, Melbourne, VIC
[4]South Australian Brain Injury Rehabilitation Service, Adelaide, SA
email: jack.beard@epworth.org.au

INTRODUCTION

Impaired postural alignment is commonly observed following acquired brain injury (ABI). The Postural Alignment and Dispersion (PAD) score has been proposed as a measure of postural alignment. The PAD score quantifies the extent of dispersion of body segments in relation to the base of support (BoS). Improved alignment is associated with mobility recovery in the pre-ambulant phase (i.e. sitting and standing) following ABI [1]. It is unknown whether this association exists for walking.

This study aimed to; i) determine whether the postural alignment and dispersion (PAD) score, previously validated in sitting and standing, can be applied to measure postural alignment during walking in people with ABI, and ii) whether the PAD discriminates those with slower and faster walking speeds.

METHODS

Forty-two adults with mobility limitations following ABI, who could walk without assistance for 10m, and 34 healthy controls (HC) underwent three-dimensional gait analysis at their self-selected walking speed. Outcome measures were the PAD score (whole-body postural alignment), walking speed (m/s), lateral centre of mass displacement (dynamic postural control), and the Gait Profile Score (walking quality). The ABI cohort was dichotomised by walking speed into those with better and worse functional capacity [2]. Outcome measures were evaluated for between-group differences (t-tests and Cohen's d effect size) and individual incidence of abnormality.

RESULTS AND DISCUSSION

Adults with ABI had significantly higher PAD scores compared to HCs ($p<0.05$; ES > 0.49) (Fig. 1). Within the ABI cohort, PAD scores were not significantly different at both more affected ($p>0.05$; ES 0.37) and less affected ($p>0.05$; ES 0) midstance between faster ($\geq$ 0.8m/s) and slower walkers (< 0.8m/s) (Table 1). In contrast, dynamic postural control and walking quality were significantly worse in those participants who walked slower ($p<0.01$; ES 1.05). Prevalence of abnormality was low on an individual participant level, capturing 19% and 26% of participants for the more affected and less affected lower limb PAD scores.
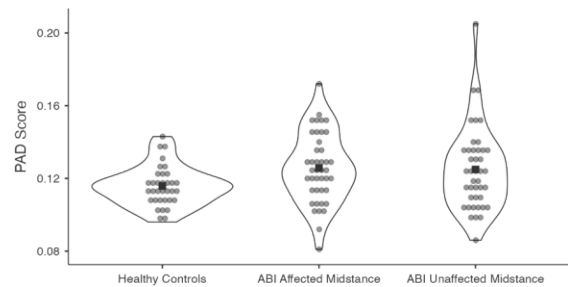
Figure 1: Distribution of PAD score data for HC and ABI patient cohorts.

CONCLUSIONS

Preliminary evidence suggests postural alignment may be impaired during walking in people with ABI. The PAD did not discriminate between slower or faster walkers within the ABI cohort. Further research is required to determine the optimal method for measuring postural alignment during walking.

ACKNOWLEDGEMENTS

REFERENCES

1. Mills S et al. *Phys Theor Prac*. 39:1274-86, 2023
2. Perry J et al. *Stroke*. 26(6):982-9,

Table 1: Outcome Variables Dichotomised by Walking Speed for the ABI cohort

	Limited Community Ambulator <0.8*m/s* (n=21)	Community Ambulator ≥0.8*m/s* (n=21)	Between Group Difference	
			p-value	Cohens "*d*" ES
Walking Speed, *m/s*	0.63 ± 0.17	1.07 ± 0.21	<0.01*	2.25
Gait Profile Score More Affected	11.57 ± 2.76	8.61 ± 2.86	<0.01*	1.05
Lateral CoM Displacement, *cm*	10.10 ± 4.06	6.47 ± 2.75	<0.01*	1.05

| PAD Midstance More Affected, *m* | 0.122 ± 0.019 | 0.129 ± 0.019 | 0.268 | 0.37 |

ARE ALTERED KNEE JOINT BIOMECHANICS ASSOCIATED WITH THE ONSET AND PROGRESSION OF POST-TRAUMATIC OSTEOARTHRITIS? A SYSTEMATIC REVIEW OF LONGITUDINAL STUDIES.

Savage, Matthew[1]; Culvenor, Adam[1]; Hedger, Michael[1]; Matt, April-Rose[1]; O'Brien, Michael[1]; McMillan, Rachael[1]; Mentiplay, Benjamin[1]

[1]La Trobe University, La Trobe Sport and Exercise Medicine Research Centre, School of Allied Health, Bundoora, Australia
email: matt.savage@latrobe.edu.au

INTRODUCTION

Post-traumatic knee osteoarthritis (PTOA) affects one in two athletes within a decade of knee injury, especially in those following surgery[1]. Altered biomechanics following knee surgery are thought to underpin the rapid onset and progression of PTOA but the evidence on this relationship has not yet been synthesised. We aimed to conduct a systematic review of the association between lower limb biomechanics and future joint structure and symptoms in individuals following surgery for traumatic knee injuries.

METHODS

Our systematic review followed the PRISMA guidelines and was prospectively registered (PROSPERO: CRD42024504099). Five electronic databases were searched from inception until May 2024 for peer-reviewed longitudinal studies reporting on the relationship between lower limb biomechanics and joint structure (imaging) or patient-reported outcome measures in individuals with a history of knee surgery for a traumatic injury. Meta-analyses were completed where possible, with the remaining studies synthesised narratively due to large heterogeneity precluding meta-analysis.

RESULTS AND DISCUSSION

We included 18 studies (12 examined structure, six examined symptoms). Meta-analyses demonstrated that lower patellofemoral contact force up to one-year post-ACLR was associated with worse future cartilage structure in the trochlea (r = -0.48, 95% CI -0.62 to -0.32) (Figure 1) and in the patella (r = -0.27, 95% CI -0.52 to 0.01) (Figure 2).

We found inconsistent evidence for the association between kinetic measures and tibiofemoral joint structure, and between kinematic measures and patellofemoral and tibiofemoral structure and symptoms. Lower vGRF during walking up to six months post-ACLR was associated with worse symptoms at one year, but lower vGRF at two years post-ACLR was associated with better symptoms at 10 years, suggesting time post-surgery may influence the association between mechanical loading and self-reported symptoms. Surrogate measures for lower medial compartment load (KAM and medial GRF) up to six months and two years post-ACLR were associated with better future symptoms.

CONCLUSIONS

Our research highlights the complex interplay between knee joint loading, biomechanics and the onset and progression of post-traumatic OA. Underloading the PFJ in the first year post-ACLR is associated with structural deterioration of PF cartilage.

REFERENCES

1. Culvenor, A. et al., *BJSM*, **47**(2): 66-70, 2013.
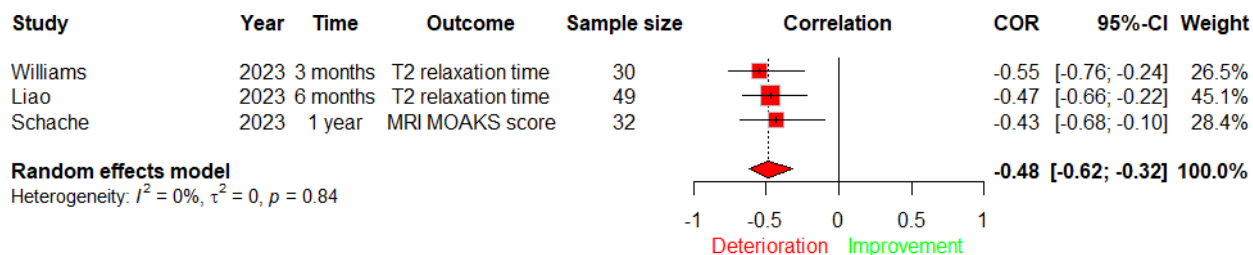
Figure 1: The association between patellofemoral contact force and structural changes in trochlea cartilage.
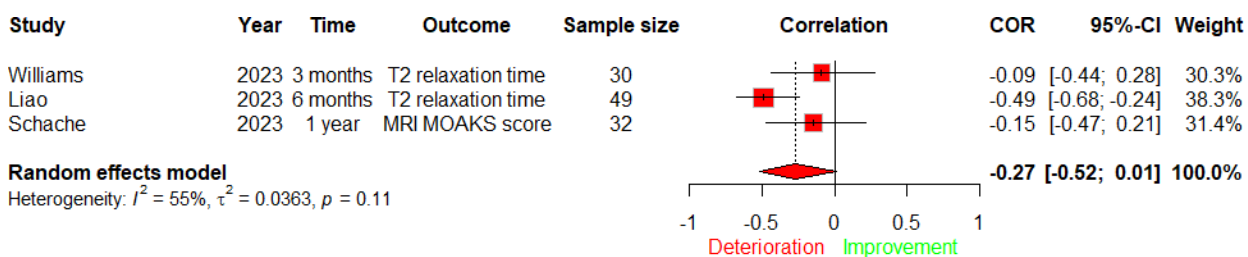
Figure 2: The association between patellofemoral contact force and structural changes in patellar cartilage.

ALTERED TRUNK MOVEMENTS AND LOWER LIMB MOMENTS DURING RUNNING AFTER ANTERIOR CRUCIATE LIGAMENT RECONSTRUCTION

[1]Jodie A. McClelland, [2]Julian A. Feller, [2]Michael Maes, [3]Anna Nilsson, [3]Gustaf Gauffin and [1]Kate E. Webster

[1]School of Allied Health, Human Services and Sport, La Trobe University, Melbourne, VIC
[2]OrthoSport Victoria, Epworth Health, Melbourne, VIC
[3]Linköping University, Linköping, Sweden
email: j.mcclelland@latrobe.edu.au

INTRODUCTION

Successful return to sport following anterior cruciate ligament reconstruction (ACLR) almost always requires that patients successfully return to running. However, despite the need for patients to attenuate high-impact forces through a single limb, little is known about the biomechanics of overground running in patients following anterior cruciate ligament reconstruction, and particularly the movement of joints and segments other than the knee. The aim of this study was to compare the overground running biomechanics of the lower limb and trunk between patients who had returned to sport following anterior cruciate ligament reconstruction with that of healthy controls.

METHODS

Three dimensional biomechanics were assessed in 30 participants as they ran along a 50 metre walkway at two speeds: 50% and 80% of self-determined maximum pace. Fifteen of these participants had received an anterior cruciate ligament reconstruction using hamstring autograft from a single orthopaedic surgeon at least twelve months earlier and all had returned to sport. Data was collected from at least six trials of running at each speed, and data from trials where the speed varied by more than 5% of the average were discarded. A 10 camera Vicon Motion Analysis system with 4 embedded forceplates (AMTI, Kistler, Bertec) were used to collect data. Reflective markers were attached to key bony landmarks and in clusters to allow calculation of kinematics and kinetics using the Conventional Gait Model II. Maximum angles and moments of the ankle, knee, hip, pelvis and trunk (relative to the laboratory) in the sagittal plane during the stance phase of running were extracted for both the operated and non-operated limbs of the patients and for both limbs of the comparison group. These data were compared between groups using an Analysis of Covariance where running speed was entered as a covariate to control for subtle between-group differences.

RESULTS AND DISCUSSION

As expected, ACLR participants ran with significantly lower knee flexion, ankle dorsiflexion and hip flexion moments than controls at both 50% and 80% pace, despite there being no difference in the magnitude of the vertical ground reaction force (Table 1). With increased speed, the ankle dorsiflexion moment did not increase in ACLR participants, as it did in the controls.

The only kinematic difference between groups was that ACLR participants ran with less trunk excursion than the control cohort through stance (p=0.05). The peak ankle dorsiflexion moment was also lower in ACLR participants.

CONCLUSIONS

The findings of this study demonstrate that patients with anterior cruciate ligament reconstruction return to sport with deficits in running mechanics compared to an active comparison group. Deficits in joint moments were accentuated with faster running speed. ACLR Patients appeared to run with a more upright trunk position, which may be a mechanism to protect the operated limb[1]. Although this difference was minimal, greater rigidity of trunk movements in dynamic tasks has been associated with increased risk of anterior cruciate ligament injury[2,3], and further investigation are necessary to understand the implications of these findings on risk of further injury.

REFERENCES

1. Kulas AS, J Athletic Training. **45**(1): 5-15.
2. Hewett TE, BJSM. **43**(6): 417-22.
3. Pairot-de-Fonteny, **49**(9): 1411-24.

Table 1 Maximum external joint moments during stance phase

	50% pace			80% pace		
	ACLR	Controls		ACLR	Controls	
Ankle dorsiflexion moment (%bw*ht)	2.21 +0.58	2.61 +0.49	**p=0.03**	2.16 +0.85	2.74 +0.44	**p=0.04**
Knee flexion moment (%bw*ht)	2.41 +0.45	3.17 +0.46	**p<0.01**	2.69 +0.42	3.27 +0.41	**p<0.01**
Hip flexion moment (%bw*ht)	1.69 +0.61	2.02 +0.54	p=0.09	2.04 +0.89	2.30 +0.62	**p=0.02**
Vertical GRF (N)	248.41 +27.61	254.71 +18.15	p=0.45	260.78 +40.77	251.74 +39.44	p=0.66

BIOMECHANICAL RISK FACTORS ASSOCIATED WITH ANTERIOR CRUCIATE LIGAMENT INJURY AND THE LINK TO PUBERTAL MATURATION: A SYSTEMATIC REVIEW

[1]Anna Butcher, [2]Sarah Ward, [3]Tracey Clissold, [4]Jim Richards, and [1]Kim Hebert-Losier

[1]Division of Health, Engineering, Computing and Science, *Te Huataki Waiora* School of Health, University of Waikato, Adams Centre for High Performance, Tauranga, NZ
[2]Department of Exercise Sciences, University of Auckland, Auckland, NZ
[3]Faculty of Health, Education and Environment, Toi Ohomai Institute of Technology, Windermere Campus, Tauranga, NZ
[4]Allied Health Research Unit, University of Central Lancashire, Preston, England, UK
email: anna.butcher@waikato.ac.nz

INTRODUCTION

Anterior cruciate ligament (ACL) injury incidence rate exponentially increases following pubertal onset[1]. Research has shown that females have a greater incidence and younger average age of non-contact ACL injury compared to males, peaking between ages 15 to 19[2]. Changes with maturation in lower-extremity mechanics and postural control during landing tasks have been suggested as a contributing factor to increased ACL injury risk, particularly in females[3]. Consideration of sex and task differences are required to better understand biomechanical differences associated with ACL injury risk across maturational phases. This study aimed to systematically review the literature to determine whether changes in biomechanics associated with ACL injury occur between different maturation phases and different sexes.

METHODS

Five databases (CINHAL®, Cochrane Library, PubMed®, Scopus®, and SPORTDiscus) were searched. Studies including one or more biomechanical variables linked with ACL injury and exploring participants across two or more maturation phases were considered eligible. Risk of bias and study quality were assessed using a modified version of the Newcastle Ottawa Scale (NOS) and Grading of Recommendations Assessment, Development and Evaluation (GRADE).

RESULTS AND DISCUSSION

The 18 included studies examined 400 males (19.1%), 1377 females (65.8%), and 315 individuals of undefined sex (15.1%). Maturation phases included pre-pubertal, early-pubertal, mid-pubertal, late-pubertal, post-pubertal, and young adult. The NOS rankings of methodological quality was considered good for most studies (n = 16, 89%), and satisfactory for two (11%). Nine of the 18 studies used a drop vertical jump task (50%), four used a cutting task (22.2%), two used a single-leg drop landing task (11.1%), one used a drop and cut task (5.5%) and one used a horizontal jump task (5.5%). Studies most often examined knee abduction angle, knee abduction moment, knee flexion, and ground reaction forces and were classified as having a low or medium overall quality of evidence according to the GRADE. Knee abduction angles and moments, and knee

flexion angles were generally greater in late and post-pubertal

females compared to pre-pubertal females and males across all maturation groups during both landing and cutting tasks. Normalised ground reaction forces were generally greater in less mature participants.

Figure 1: Summary of the observed links between maturation and changes in biomechanics associated with ACL injury as reported in the literature. Note: Arrow indicates and increase or decrease with maturation.

CONCLUSIONS

Late and post-pubertal females demonstrate biomechanics associated with increased ACL injury risk during landing and cutting tasks. Specifically, in response to maturational development, females demonstrated increased knee abduction angles and moments, and decreased knee flexion angles and ranges of motion. Our findings highlight sex and maturation need consideration when selecting tasks in injury risk identification processes and exercises for ACL injury prevention strategy development.

REFERENCES

1. Renstrom P, et al. *BJSM*. **42(6)**:394-412, 2008.
2. Maniar N, et al. *The Lancet Regional Health– Western Pacific.* **21**, 2022.
3. Ramachandran AK, et al. *Sports Med*. **1-26**, 2024.

Biomechanical risk factors associated with ACL injury and the link to pubertal maturation

Knee abduction angle
- double leg drop jump tasks and cutting tasks overall and in females
- with maturation in single leg landing study in males and females.

Knee abduction moment
- double leg drop jump, cutting, single leg landing, and horizontal jump tasks.
- double leg drop jump and cutting tasks in pubertal and post-pubertal females compared to males.

Knee flexion angle
- double leg drop jump and vertical jump tasks.
- cutting, single leg drop landing, and horizontal leap task.
- double leg drop jump at initial contact and smaller range of motion.

Ground reaction forces
- double leg jump upon landing in males but not females.
- double leg drop jump upon take-off in females but not males.
- cutting and vertical jump upon landing for both sexes.

Wednesday, December 4

<u>ANZORS Podium 6</u>

A parametric finite-element model of the femur spanning the entire adulthood.

[1]Natali Uribe, , [1]Dermot O'Rourke, [1]Peter Pivonka, and [1,2]Saulo Martelli
[1]School of Mechanical, Medical and Process Engineering, Queensland University of Technology, Brisbane, Australia
[2]Medical Device Research Institute, College of Science and Engineering, Flinders University, Adelaide, Australia
email: natali.uribeacosta@hdr.qut.edu.au

INTRODUCTION

The human femur is a complex structure with significant individual variation and intricate microarchitectural organization. Existing parametric models that incorporate cortical and microarchitectural details are typically based on data from older populations [1]. This study presents the development of a parametric model that implements both isotropic and anisotropic material properties, encompassing the entire adult population. These parameters are used to create a statistical model (SM) for individuals spanning the entire adult range, utilizing Principal Component Analysis (PCA).

METHODS

HR-ρQCT images (SCANCO Medical, 82 µm/pixel Switzerland) of the proximal femur in 84 patients aged 20-92 years were obtained from a public database [2]. Automatic segmentation was performed using MATLAB (The MathWorks Inc., MA, USA). The surface was meshed and smoothed with nine iterations of Laplacian smoothing in MeshLab. A template solid mesh from a previous study [3] was morphed to fit all specimens through a three-step process: rigid registration with an ICP algorithm, non-rigid ICP based registration to locally deform the baseline model, and elastic registration by applying calculated displacements to the superficial nodes, at the end of the process, a mesh with 205233 elements was obtained. For microarchitectural analysis, the entire femur was subdivided into 5x5x5 mm³ cubes, and the analysis was done using CT analyzer software (Skyscan, Kontich, Belgium) automatically run in batch for all the cubes, obtained the elastic properties. A single threshold value was used to segment all the cubes, with threshold calibration performed to ensure that the Bone Mineral Density (BMD) obtained for people aged between 60 to 92 years matched the BMD expected for the entire population. The elastic properties map in the 5mm grid was interpolated to element mesh level, between the barycenter of the cubes and the centroid elements of the bones. For the parametric model the elements were analyzed based on density and spatial location. Elements with a density value greater than 0.5 g/cm³ and positioned outside the barycenter of the cubes were designated as cortical. For the local isotropic analysis, the ash density and elastic modulus were calculated using an empirical relationship, with shear moduli derived accordingly. Anisotropic material properties were determined using the formulation established by Zysset and Curnier [4]. The validity of the model was quantified by element quality of mesh. The statistical model was obtained using PCA decomposition of the entire dataset.

RESULTS AND DISCUSION

For the microarchitectural analysis a single threshold of 82 was used to segment all the samples, resulting in a bone mineral density of 0.20 g/cm³ which aligns with values reported in the literature for aged individuals [5] (Figure 1a). The main direction of the trabeculae, indicated by the third eigenvector (largest eigenvalue of fabric tensor), demonstrates the integrity

of the cubes (fig1b). The elastic properties were mapped in the 5mm grid cubes through interpolation of the results at the element level, as detailed in Fig1c. Preliminary results showed that the mesh element sizes were above 0.6mm, which is adequate for performing finite element simulations (fig1d). For the statistical model the first mode explains the 8.7% of the variance in appearance, and 66 bones were required to account for 90% of the variance. The model displayed variations in the intertrochanteric distance, overall length and angles (fig1e)
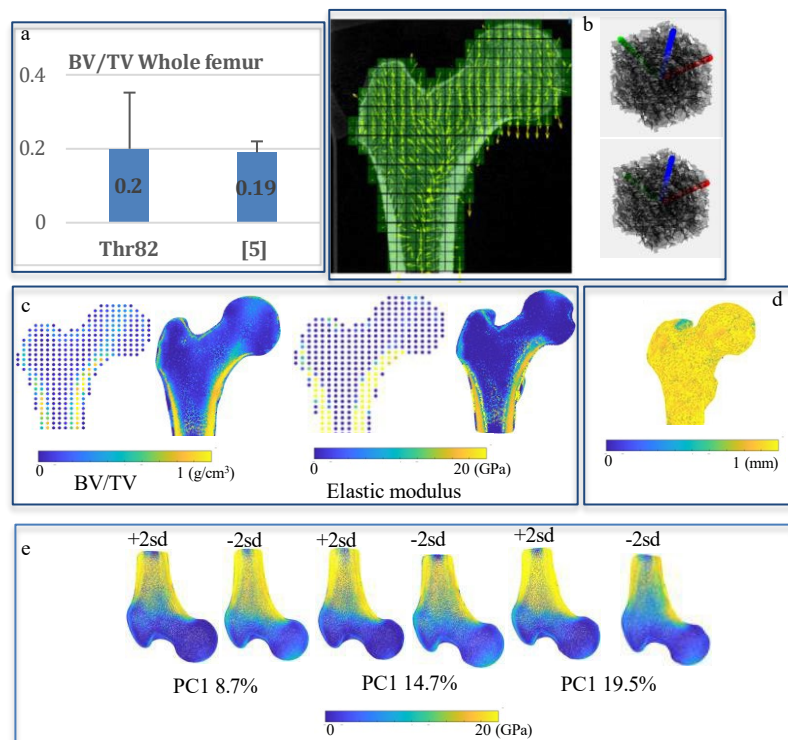

Fig. 1. *a. calibration of the threshold value with literature. b integrity of the volume of cubes and the third eigenvector, visualizing direction of the trabecular and elastic properties. c different microstructural parameters at cube level (dot plot) and element level. d, mesh quality check, e. statistical shape and appearance model using 84 subjects.*

CONCLUSIONS

The parametric model enables the mapping of mechanical anisotropy across the entire bone for the entire population. The utilization of the principal modes of variation can provide further insights from finite element analysis on the prediction of fracture load under parametric loading conditions.

USIONS

REFERENCES
1. O. Ariza et al. medengphy *rep* **38**:1339-1347, 2016
2. Clement J. Melbourne Femur Collection, 2016
3. O' Rourke et al. *J Biomech* **119**:1-13, 2021.
4. P. Zysset et al., mechanic of materials **21**:243-250, 1995.
5. J, Hazrati et al. *Bone* **60**:213-220, 2014

FINITE ELEMENT ANALYSIS OF A CUSTOMIZED PELVIC FRACTURE IMPLANT TO MONITOR FRACTURE HEALING

[1]Fuyuan Liu, [1]Dale Robinson, [1]Sarah Woodford, [1]David Ackland and [1]Peter Vee Sin Lee
[1]Department of Biomedical Engineering, The University of Melbourne, Melbourne, VIC
email: fuyuanl@student.unimelb.edu.au

INTRODUCTION

The pelvis is a ring-shaped bone situated in the middle of the human body that accommodates the attachment of numerous abdominal and lower limb muscles. While pelvic fracture incidence is not severe, affecting 23 per 100,000 people in Australia, secondary injuries to the surrounding abdominal organs lead to it being amongst the deadliest fracture types, with mortality up to 23% [1]. In cases where fracture plate implantation is needed to secure fractured bone in position, non-union or slow fracture healing remains a persistent issue [2]. Previous research using instrumented fracture plates has demonstrated that implant strain decreases during healing and new bone formation; data that can be used to guide rehabilitation and additional treatment [3]. However, this innovative approach has not been previously considered for the pelvis. This research aims to determine implant strain for a range of different fracture sizes representative of the various phases of fracture healing. Understanding this relationship will help to inform implant design as well as providing better understanding of load transmission through the pelvis and fracture plate during the fracture healing process.

METHODS

A custom pelvis fracture plate was designed to stabilize a composite hemi-pelvis with a virtual iliac wing fracture. A 3D surface model of the hemi-pelvis was constructed from a 3D surface scan and imported and meshed in a commercial finite element modelling package (Abaqus, Dassault Systems). The material properties of the bone were assigned as, whereas the fracture plate and screws were assigned as Ti–6Al–4V. Clamped boundary conditions were applied to the pubic symphysis and sacroiliac joint. A total load of 800 N was applied to the surface of the acetabulum to simulate the peak walking load [4]. To model the varying phases of fracture healing, three fracture states were modelled, complete fracture of the iliac crest, partial fracture of the iliac crest and intact bone. Strains were quantified across the fracture plate and compared between each fracture condition.

RESULTS AND DISCUSSION

The finite element simulation results indicate that as the fracture size was decreased, the strain on the implants decreased. For example, comparing completely fractured bone to intact bone, the maximum principal strain site A decreased from 203.4 με to 10.8 με (Figure 1; Table 1). Similarly, at site B the maximum principal strain decreased from 144.5 με to 47.2 με. These changes demonstrate that the implant strain is highly sensitive to the extent of the fracture and that sites A and B are suitable for accommodating strain gauges that monitor fracture healing.
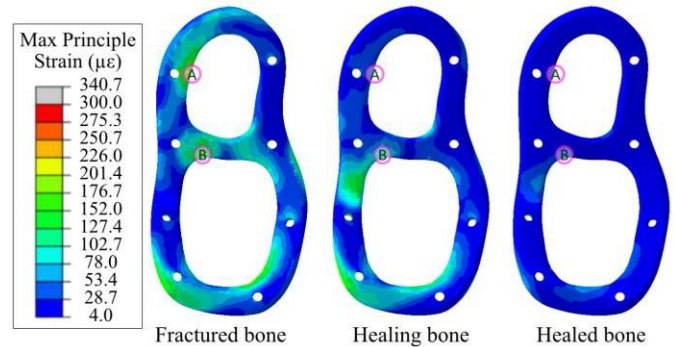
Figure 1: Maximum principal strains of fracture plate for a completely fractured, partially fractured and intact hemi-pelvis. Sites A and B are indicated.

CONCLUSIONS

This study shows the feasibility of using a pelvic fracture plate capable of monitoring fracture healing via measurements of fracture plate strain. This system has the potential to detect and treat non-unions early and guide safe rehabilitation exercises. In future work, cadaveric studies will be used to validate these models, more pelvic fracture types will be studied, and a smart implant will be developed and tested to monitor bone healing.

REFERENCES

1. Balogh Z et al., *The Journal of Trauma: Injury, Infection, and Critical Care,* **63(5)** **p**: 1066-1073, 2007.
2. Ghiasi M et al., *Bone Reports*, **6**: 87-100, 2017.
3. Cunningham J et al., *Engineering in Medicine*, **16(4)**: 229-232, 1987.
4. Bergmann G et al., *PloS one*, **11(5)**: e0155612, 2016.

Table 1: Strain change of point A and B from finite element simulation.

Point Number	Maximum Principal Strain (με)		
	Completely Fractured Hemi-pelvis	**Partially Fractured Hemi-pelvis**	**Intact Hemi-pelvis**
A	203.4	37.2	10.8
B	144.5	122.4	47.2

Can Statistical Shape and Density Models Predict Femoral and Tibial Stress in a Paediatric Population?

[1]Yidan Xu, [1]Laura Carman, [1,2]Thor Besier and [1]Julie Choisne

[1]Auckland Bioengineering Institute, The University of Auckland, Auckland, NZ
[2]Department of Engineering Science and Biomedical Engineering, The University of Auckland, Auckland, NZ
email: j.choisne@auckland.ac.nz

INTRODUCTION

Finite Element Analysis (FEA) is a mathematical representation of geometry, materials and forces to non-invasively understand the mechanical properties of bone. Such models have been used to examine fracture risk in osteoporosis patients, fracture healing, bone development and bone remodeling. However, FEA models for paediatric bones are lacking. We have developed a statistical shape and density model to predict bone geometry and density in a population of typically developed children aged 4 to 18 years [1]. Geometry and material properties/densities are critical factors influencing the stress and strain distributions in bone. However, the influence of prediction errors from shape-density models on FE results remains understudied. To this end, we evaluated bone stress distributions from a shape-density model of the paediatric femur and tibia.

METHODS

CT scans of 330 children (136 F, 12 ±5 years old, H: 148 ±24cm and W: 49 ±22 kg) were obtained from the Victorian Institute of Forensic Medicine (VIFM). Femora (657) and tibiae (652) were manually segmented, fitted to a surface template mesh and morphed to a volumetric template mesh. The shape-density model was built using Principal Component Analysis of the nodal coordinates and bone mineral density (BMD). BMD was extracted from a calibration phantom and assigned to the mesh using *Bonemat* software. Partial least square regression was used to predict bone shape and BMD using demographic data and bone length and width. Young's Modulus (E) was assigned to each element based on existing BMD-E relationships [2,3]. Forces from single leg stance (OrthoLoad [4,5]) were applied to the proximal end, whilst the distal end was fixed (6DoF). Von Mises stress from the shape-density model was compared to the "gold standard" CT-based model using R^2 and element-element normalized root mean square error (NRMSE) for each region.

RESULTS AND DISCUSSION

Stress predictions from the shape-density model were close to those estimated from a CT-based model with mean ±SD R^2 = 0.83±0.06 for the femur and 0.80±0.07 for the tibia (Figure 1).

Regional stress prediction was less than 12% NRMSE (Table 1). Lower R^2 was found when the geometry was not well predicted.
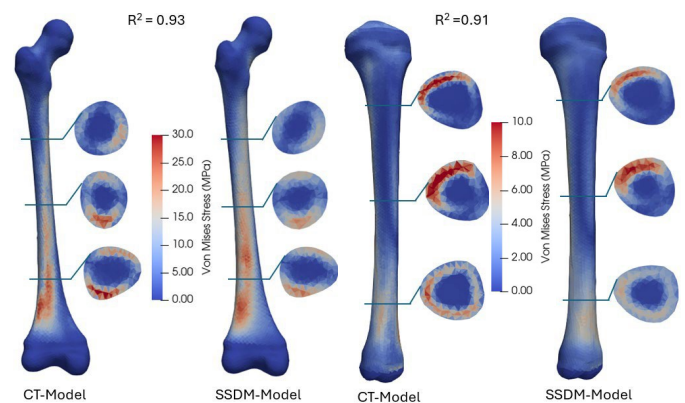
Figure 1: Von Mises stress distributions in posterior femur and anterior tibia for CT-based and shape-density models (SSDM). Cross-sections at 25%, 50%, and 75% of bone total length.

CONCLUSIONS

This study revealed that our paediatric shape-density model can predict stress distributions within the femur and tibia, similar to those from gold-standard CT models. Future work will investigate partial imaging to enhance geometry prediction.

ACKNOWLEDGEMENTS

REFERENCES

1. Provyn S, et al., *Ergonomics.* **104**:757-759, 2011.
2. Morgan EF, et al., *J Biomech.* **36**(7): 897-904, 2003.
3. Keyak JH, et al., *J Biomed Mater Res.* **28**: 1329-36, 1994.
4. Bergmann G, et al., *Biomed Mater Eng.* **20**: 65-75, 2010.
5. Kutner I, et al., *J Biomech.* **43**(11): 2164-73, 2010.

Table 1: Normalized root means square error (NRMSE) between the CT based and shape-density predict FE models by region

	Femoral head	Femoral neck	Trochanter	Femoral shaft	Distal femur	Proximal tibia	Tibia shaft	Distal tibia

| NRMSE (%) | 4.6 | 7.4 | 7.6 | 10.2 | 4.2 | 5.3 | 11.1 | 7.9 |

BIOMECHANICAL ADVANTAGES OF A PARTIAL FACETECTOMY IN THE SURGICAL MANAGEMENT OF PARS INTERARTICULARIS FRACTURES

[1]Reza Arjmandi, [2]Rowan Schouten and [1]Ashvin Thambyah

[1]Department of Chemical and Materials Engineering, University of Auckland, Auckland, New Zealand
[2]Forte Orthopaedics, Christchurch, New Zealand
email: r.arjmandi@auckland.ac.nz

INTRODUCTION

Lumbar stress injuries are a common cause of low back pain in athletes, particularly professional cricketers (fast bowlers) [1,2]. These lumbar stress fractures typically occur in the pars interarticularis located between the superior and inferior processes (Fig. 1A). In treating such injuries, the second author (an orthopaedic surgeon) has proposed that an osteotomy of the distal part of the inferior facet may neutralize the tensile forces implicated in the causation of these injuries. We explore the biomechanical rationale for the above intervention using computational modelling.

METHODS

An open-source human lumbar spine motion segment finite element (FE) model [3], constructed from CT scans, was used in this study.
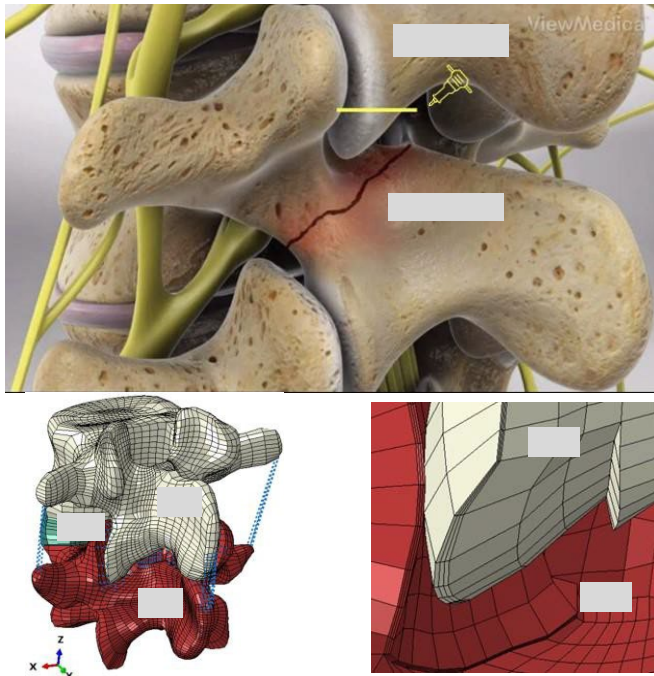
Figure 1: (A) A typical pars articularis fracture. The yellow line indicates the lip of the facet that is to be removed. (B) FE model of a motion segment. (C) Partial facet removal to replicate the osteotomy procedure.

The geometry of the L4-L5 functional spinal unit (FSU) was imported to ABAQUS CAE, as-meshed (Fig. 1B). A linear elastic material model was assigned to vertebral bodies, while a hyperplastic Mooney-Rivlin model was assigned to disc. All ligaments were modelled using tension-only connector elements. A 500N axial load was applied (L4) to simulate upper body weight, and the inferior endplate of the lower vertebral body (L5) was rigidly fixed. With this initial condition, pure flexion-extension bending moments ranging from -10Nm to 7.5Nm, with 2.5Nm increments, were applied, and the resulting range of motion (RoM) was obtained. The resulting plots were compared with those obtained from an in-vitro study [4]. Upon validation, the distal part of the inferior facet of the L4 vertebra was removed from the intact model (Fig. 1C) to replicate the osteotomy procedure and the mechanical simulation was repeated.

RESULTS AND DISCUSSION

The bending moment versus RoM plot for the intact model showed good agreement with the experimental data, with an RMSE of 0.68°. With the partial removal of the facet, there were no significant differences in the RoM. The material stress response showed that when subject to extension, in the intact model, there were large regions of principal *tensile* stresses in the pars articularis as the region of interest (ROI). Such stresses were, however, not present when the facet was partially removed. Instead, there were primarily compressive stresses (~5MPa) at the RoI when the extension bending moment was applied.

CONCLUSIONS

By removing the distal part of the suprajacent facet, the extent of tensile stresses on the pars interarticularis appears to be reduced. This, in turn, might contribute to lowering the risk of further or recurring stress fracture injuries in this region of the spine.

REFERENCES

1. Annear PT, et al., *Aust N Z J Surg.* **62**(10):768-73, 1992.
2. Farhat P., BMC Sports Sci Med Rehabil. 15(1): 114, 2023
3. Finley, S. M., et al., *Comp Methods Biomech Biomed Eng.* **21**(6): 444–452, 2018.
4. Schmidt H, et al., *Clin Biomech.* **21**(4):337-344, 2006.

TIBIA AND FIBULA BONES PREDICTION FROM EXTERNAL SHANK SKIN SHAPE IN A PAEDIATRIC POPULATION

[1]Enzo Allevard, [1]Thor Besier and [1]Julie Choisne

[1]Auckland Bioengineering Institute, The University of Auckland, New Zealand
email: eall036@aucklanduni.ac.nz

INTRODUCTION

Several devices and software solutions enable low-cost 3D body scanning using LiDAR sensors, laser scanners, and photogrammetry [1]. This creates opportunity to measure musculoskeletal parameters directly from 3D surface scans for clinical and orthopaedic applications. Statistical shape models (SSMs) have shown promise in predicting bone morphology in paediatric populations from sparse anatomical landmarks and demographic data [2]. Coupling surface skin to the underlying bone would enable direct prediction of bone morphology from a 3D body scan. To this end, we evaluated the capability of a SSM to predict tibia and fibula bone geometry using shank skin surface data as input in a typically developed paediatric population.

METHODS

Forty-eight post-mortem CT scans of children (20F; 10 ± 4 [4-18] years; 40 ± 18 [14-84] kg; 140 ± 25 [97-185] cm) were segmented to extract the left shank skin and left tibia/fibula bones meshes. Each mesh was non-rigidly registered and fitted to a template mesh, using radial basis functions to achieve nodal correspondence, then rigidly aligned after merging bones and skin meshes. A Principal Component (PC) Analysis [3] was performed to determine the coupled morphological variation of skin surface of the shank to the underlying tibia/fibula bone morphology. The accuracy of the SSM was assessed using fitting error, compactness, specificity, and generality using a leave-one-out (LOO) analysis. The LOO analysis was conducted five times, with PC fitting performed using different numbers of PCs (5, 15, 25, 35, and 45). The optimisation criterion was based on the root mean square (RMS) distance error of the predicted bone surface, selecting the configuration where the PC fit error of the skin was minimized across the five PC configuration.

RESULTS AND DISCUSSION

The PC-optimised LOO analysis resulted in an average RMS distance error of 1.76 ± 1.14 mm between the CT reconstructed and the PC fitting of the shank to predict the tibia/fibula geometry (Table 1) and a dice score of 0.87 ± 0.06. The best and worst bone prediction showed an average point-to-cloud distance errors of 0.73 mm and 8.64 mm respectively (Figure 1).
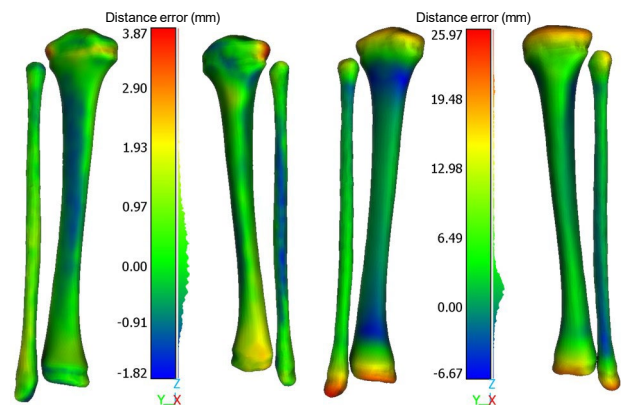
Figure 1: Distance error for the best (Left) and worst (Right) prediction.

CONCLUSIONS

This study demonstrated the potential to predict bone structures from surface skin geometry. The accuracy of these predictions was influenced by the shank shape, and height with extreme height or shape showing the highest error. Including joint articulations in the model is anticipated to improve the fitting process with additional constraints.

ACKNOWLEDGEMENTS

REFERENCES

1. Bartol K et al., *IEEE Access,* **9**: 67281-67301, 2021.
2. Carman L et al., *Sci. Rep.,* **12**, 3251, 2022.
3. Zhang J et al., *Med. Eng. Phys.*, **38**: 450–457, 2016.

Table 1: RMS distance error for the 5 different number of PCs used for the LOO PC fitting and the optimisation using the lowest fitting error across the 5 configurations.

	5 PCs	15 PCs	25 PCs	35 PCs	45 PCs	Optimisation
RMSE Skin (mm)	2.58 ± 1.57	2.54 ± 2.36	2.47 ± 2.32	2.18 ± 2.22	2.57 ± 3.53	1.86 ± 1.26

| RMSE Bones (mm) | 2.03 ± 1.60 | 2.28 ± 2.44 | 2.30 ± 2.40 | 2.07 ± 2.19 | 2.49 ± 3.44 | 1.76 ± 1.14 |

Wednesday, December 4

National Keynote 4 – Dr Bart Bolsterlee
Quantitative magnetic resonance imaging to study skeletal muscle during childhood development

Magnetic resonance imaging is well known for its ability to visualize anatomical structures in exquisite three-dimensional detail. However, MRI is less frequently used as a quantitative measurement tool, even though the MR signal contains a wealth of quantitative information about tissue structure and composition. MRI provides especially strong contrast in soft tissues, such as skeletal muscle – the most abundant and most plastic tissue in the human body.

The first part of this presentation will introduce the key quantitative MRI methods to measure the size, structure and composition of skeletal muscles in living humans in unprecedented detail. The second part of this talk will show how these methods can be used in large-scale research, and potentially in clinical routine. Data from a 6-year longitudinal quantitative MRI study on 200 typically developing children and 80 children with cerebral palsy will be used to describe how lower leg muscles change their size and structure during typical childhood development, and to determine how cerebral palsy affects muscle growth.

Wednesday, December 4

ABC Podium 7
Emerging technology

THE TASK DEPENDENT NEUROMUSCULAR RESPONSE OF OLDER ADULTS TO EXOSKELETON ASSISTANCE DURING STANDING BALANCE TASKS

[1]**James L. Williamson**, [1]Jemima C. N. Po, [1]Connor Clark, [2,3]Ruth E. Hubbard, [4,5,6]Alejandro Melendez-Calderon, [4]Antonio Padilha Lanari Bo, [7]Camila Shirota, [2]Phil Aitken, [1]Taylor J. M. Dick

[1] School of Biomedical Sciences, The University of Queensland, Brisbane, Australia
[2] Princess Alexandra Hospital, Metro South Hospital and Health Service, Brisbane, Australia
[3] Centre for Health Services Research, The University of Queensland, Brisbane, Australia
[4] School of Electrical Engineering and Computer Science, The University of Queensland, Brisbane, Australia
[5] School of Health and Rehabilitation Sciences, The University of Queensland, Brisbane, Australia
[6] Jamieson Trauma Institute, Metro North Health, Brisbane, Australia
[7] The Hopkins Centre, Menzies Health Institute Queensland, Griffith University, Brisbane, Australia
email: j.williamson@uq.edu.au

INTRODUCTION

Aging is associated with motor deficits that limit ones' ability to maintain independent movement [1]. Age-related alterations to plantarflexor muscle-tendon unit function result in reduced positive power generation at the ankle, leading slower walking speeds, elevated energetic demands and an increased fall risk [1,2]. Passive ankle exoskeletons are wearable assistive devices that add structural stiffness in parallel to the ankle plantarflexors and have recently been suggested as potential aids to restore ankle function in older adults [3]. Yet, we have limited information regarding the feasibility and immediate effects of these devices on locomotor performance in older adults. This knowledge is required for designing and applying the next generation of assistive technologies to combat against frailty and the loss of independent mobility with age. The aim of this study was to assess the short-term impact of wearable assistive exoskeletons as potential aids to improve neuromuscular function of older adults during balance tasks.

METHODS

A total of 28 older adults (11 M, 17 F, age: 71±5 years, 72.1±15.6 kg) participated in this study (UQ HREC approval #2021/HE000943). Participants conducted a series of balance tasks (**Fig. 1a**), with and without passive ankle exoskeleton assistance at a range of stiffnesses (0, 42, 85 Nm rad^{-1}) (**Fig. 1b**). We used inertial measurement units (IMUs) to determine ankle, knee, and hip kinematics and surface electromyography (EMG) to characterize muscle activation of ankle plantar- and dorsi-flexors (Noraxon Inc., USA). Muscle activation was normalized to a 0 Nm rad^{-1} walking condition. Whole body sway was estimated from the standard deviation of a marker placed on the greater trochanter of the femur.

RESULTS AND DISCUSSION

There was no effect of exoskeleton assistance on whole body sway during any balance task. Average ankle angles were influenced by exoskeleton assistance in a task dependant manner, where simpler tasks were associated with a more dorsiflexed ankle, while more complex tasks were associated with a more plantarflexed ankle (p=0.023). There was no influence of exoskeleton assistance on knee or hip kinematics. During simpler standing balance tasks (neutral stance and

active sway), plantarflexor muscle activity (soleus, medial

gastrocnemius and lateral gastrocnemius) was reduced with exoskeleton assistance (all: $p \leq 0.04$). Conversely, during more challenging balance tasks (foam and single leg stance) the activation of tibialis anterior (TA), a key dorsiflexor, increased with increasing exoskeleton assistance ($p < 0.001$; **Fig. 1c**).
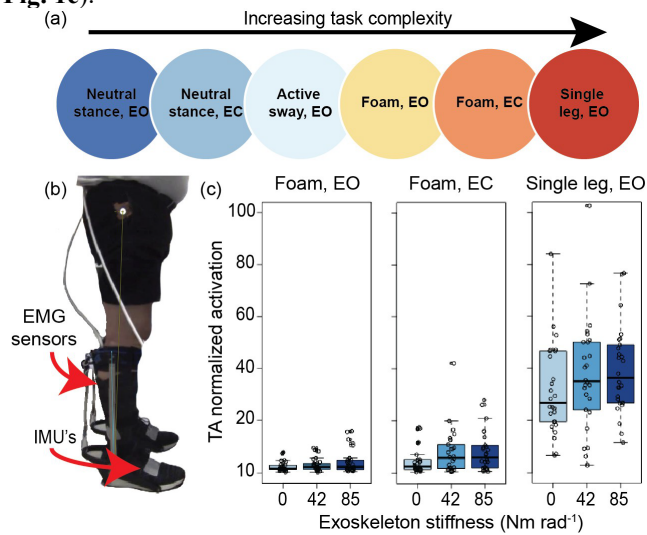
Figure 1. (a) Balance tasks descriptions (EO: Eyes Open; EC: Eyes closed). **(b)** Experimental set-up for balance trials. **(c)** TA activation during foam and single leg balance conditions.

CONCLUSIONS

Passive exoskeleton devices may improve standing balance via reductions in muscular effort, without disruptions to whole body sway. However, these devices may not be suitable for more challenging tasks owing to increases in activity of antagonist muscles. Additional experiments which aim to explore the limits of assisted-balance performance in clinical or frail populations may aid the design of standards for the prescription of assistive technologies.

ACKNOWLEDGEMENTS

REFERENCES

1. Grimmer M, et al., *J. Neuroeng. Rehabilitat.* **16(1):**2, 2019.
2. Franz J, et al., *Exerc. Sport Sci. Rev.* **44(4):**129-136, 2016.
3. Krupenevich R, et al., *Gerontology.* **68(3):**241-251, 2022.

173

PREDICTIVE MUSCULOSKELETAL SIMULATIONS TO EXPLORE THE ENERGETICS OF HOPPING WITH A JOEY IN MACROPODS

[1]Miyuki Chamberlain, [2]Assoc/Prof Christofer Clemente, [2]Lauren Thornton and [1]Dr Taylor Dick

[1] School of Biomedical Science, University of Queensland, Brisbane, QLD
[2] School of Science, Technology and Engineering, University of Sunshine Coast, Sippy Downs, QLD
email: miyuki.chamberlain@uq.net.au

INTRODUCTION

Wallabies incur no additional metabolic cost when hopping with a fully developed joey (15% of the mother's body mass) [1]. Macropods (kangaroos and their relatives) are also able to uncouple their hopping speed from energy use, meaning they can hop faster while their energy use remains constant [2]. These energetic phenomena oppose the trends observed in all other terrestrial mammals whereby increases in load-carriage or speed during locomotion both incur an increase in metabolic cost [3, 4]. However, establishing the mechanisms that underpin these energetic phenomena remains challenging with experimental approaches along. Hence, we have developed an experimentally-informed musculoskeletal modelling framework to simulate wallaby hopping with a joey such that we can explore how energetics is altered over a range of joey masses and speeds.

METHODS

To date, we have built a whole-body musculoskeletal model of a 7.9 kg swamp wallaby using open-source modelling software by combining CT imaging and anatomical dissection data. We are currently informing our model with locomotor kinematic and kinetic data collected from wallaby hopping experiments.

Skeletal geometry and muscle morphology data were collected from two female swamp wallabies (*wallabia bicolour*) collected under the permit WA0042488 (QLD). Skeletal geometry was extracted from CT scans and modelled into a system of rigid 3D mesh segments. Joints were characterised in OpenSim Creator. In OpenSim, muscle-tendon units were characterized in line with the Hill-type muscle model with a series elastic tendon and informed by muscle dissection data. Experimental hopping data was collected at WildLife HQ, Woombye, QLD. Body mass, contact duration and ground reaction forces (GRFs) were captured using a force plate (AMTI AccuGait). 3D joint angles were estimated using a 2-camera 3D motion capture camera system (Fastec Imaging) and DLTr software [5]. Subsequently, inverse kinematics will be performed to compute joint moments and muscle control to estimate tendon dynamics, muscle forces and excitations at the measured movement speeds. We performed a pilot simulation study using an OpenSim model of a 27.5kg Western Grey kangaroo. Joeys were modelled as a sphere segment and attached to pelvis via a flexible join. Hopping was simulated at 3.5, 6 and 8.5 ms^{-1} while loaded with joeys of masses that were 10, 15 and 50% of the models mass (MM).

RESULTS AND DISCUSSION

COT was reduced with increasing speed and joey mass (Fig. 1). During faster hopping, models carrying larger joeys took more frequent and shorter hops, while increasing duty factor (ie: spending more time on the ground). Additionally, heavier joeys resulted in reduced propulsive and vertical GRFs but increased breaking GRFs.
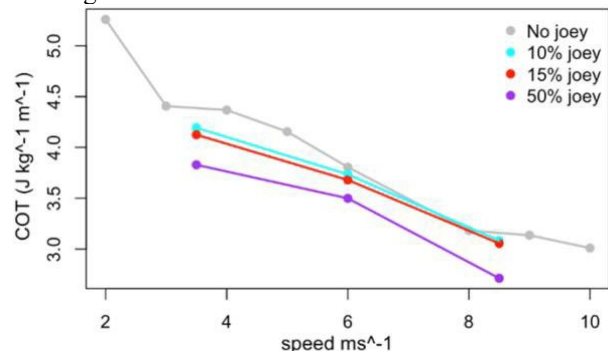
Figure 1: *Cost of transport (J kg^{-1} m^{-1}) across 3.5, 6 and 8.5 ms^{-1} while hopping with no joey (grey), 10% MM joey (aqua), 15% MM joey (red) and 50% MM joey (purple) based on simulation of a 27.5kg Western Grey kangaroo.*

CONCLUSIONS

This pilot study demonstrated that our modeling pipeline will be able to replicate the energetic savings observed in Baudinette and Biewener [1]. Translating this to our wallaby model and performing further anaylsis at the muscle-tendon stress level could elucidate wallaby's mechanism of load-carriage efficiency.

REFERENCES
1. Baudinette & Biewener. *Nature.* **395**:653-654, 1998.
2. Dawson & Taylor. *Nature.* **246**:313-314, 1973.
3. Taylor et al. *J Exp Biol.* **86**:9-18, 1980.
4. Dick & Clemente. *PLoS Biol.* **15**:e2000473, 2017.
5. Hendrick. *Bioinspir. Biomim.* **3**:034001-034001, 2008.

OPTIMAL CONTROL SIMULATION OF FULL HAND FLEXION MOVEMENTS EXPLOITING OPTICAL MARKERTRACKING

[1]Simon Heinrich, [2,3]Birte Coppers, [2,3]Anna-Maria Liphardt and [1]Sigrid Leyendecker

[1]Institute of Applied Dynamics, Friedrich-Alexander-Universität (FAU) Erlangen-Nürnberg, Erlangen, GER
[2]Department of Internal Medicine 3 – Rheumatology & Immunology, Universitätsklinikum Erlangen & FAU Erlangen-Nürnberg, Erlangen, GER
[3]Deutsches Zentrum Immuntherapie, Universitätsklinikum Erlangen & FAU Erlangen-Nürnberg, Erlangen, GER
email: simon96.heinrich@fau.de

INTRODUCTION

Investigating immeasurable internal states of biomechanical systems, such as joint torques, muscle forces, or joint reactions, depends strongly on dynamic simulations. These simulations usually rely on tracking measurement data, often realized as an inverse dynamics simulation, where the difference between measured data and the simulated counterpart is minimized. Alternatively, optimal control problem (OCP) simulations can be used to recreate human motions, while also taking into account known postures and physiological fundamentals of movement [1,2]. They minimize an objective function while fulfilling a set of constraints. It is yet to be investigated, whether it is advantageous to use the data as part of an objective or as part of the constraints. A previous investigation [2] for arm motions indicated, that there are advantages to formulating the OCP with a physiological and goal-motivated objective and to use the measurement data in the constraints rather than adding them in the objective. To better understand how to formulate the OCP for biomechanical simulations optimally, we are investigating different approaches to include marker-based optical motion capture data in OCP simulations of hand movement.

METHODS

We collected marker position data of hand movements using an optical motion capture system comprising 9 cameras (Oqus 7+, Qualisys AB, Sweden) and a marker set of 29 reflective markers (diameter 6.5mm) on the hand dorsum, similar to [3]. A personalized, torque-driven, rigid body model of the human hand (excluding the thumb) consisting of 18 bodies with 24 degrees of freedom is created. The OCP is formulated in the framework of Discrete Mechanics and Optimal Control for Constrained Systems (DMOCC) [4] as a finite-dimensional constrained optimization problem and can be written as

$$\min_{\tau, u} J(u, \tau, X)$$
$$\text{s.t.} \quad \text{DEL}(u, \tau) = 0, \quad g(u, \tau, X) = 0, \quad h(u, X) \leq \varepsilon$$

The joint torques τ are the controls, u are the states, and the dynamics are imposed via the discrete Euler Lagrange equations DEL. The data X is either used as part of the objective $J(\tau, u, X)$ or in the inequality constraints $h(u, X)$ together with a tolerance parameter ε. Additional equality constraints on the movement are imposed via $g(u, X)$. This optimization problem is solved using standard optimization algorithms. We are investigating five different ways to include data with different physiological objective functions for multiple subjects. The data inclusions are either via the objective function or four different variants of constraints, with a varying number of constraints.

RESULTS AND DISCUSSION

A preliminary investigation based on 41 OCP simulations resulted in the following results. There was, as expected, a strong inverse relation between marker data residual and physiological objective function values. The simulation duration between different variations was similar, but surprisingly the fastest simulations were the OCP with data in the objective followed by data as inequality constraints with the highest number of constraints, indicating that computational performance is not solely tied to the size of the optimization problem. Also, there was a relation between two of the physiological objective functions, i.e., minimizing for control change did reduce the control, but the same is not true vice versa.

CONCLUSIONS

Our results emphasize that the formulation of the OCP strongly affects the objective function values and marker residuals, as well as the computational performance. Our next step will be to extend this investigation to more study participants and movements to investigate this further.

ACKNOWLEDGEMENTS

REFERENCES

1. Umberger B R, et. al. *In: Handbook of Human Motion, Springer, Cham,* 2017.
2. Hoffmann R, et al. *Multibody Syst Dyn*. **48**, 105-126, 2020.
3. Phutane U, et al. *Sensors* **21**, 1208, 2021
4. Leyendecker S, et al. *Optim. Control Appl. Meth.* **31**, 505-

528, 2010.

ANZSB
anzsb.asn.au

**Quantitative Fall Risk Assessment via an Enhanced Timed Up and Go Test
with Markerless Motion Capture and Machine Learning**

[1,2]Longbin Zhang, [1]Ananda Sidarta, [1]Tsung-Lin Wu, [1]Prayook Jatesiktat,
[1,2]Hao Wang, [1,2]Lei Li, [4]Patrick Wai-Hang Kwong, [5]Aoyang Long, [5]Xiangyu Long and [1,3]Wei Tech Ang

[1]Rehabilitation Research Institute of Singapore, Nanyang Technological University, Singapore.
[2]Guangdong Zhongxin Intelligent Rehabilitation Institute affiliated with Jian Xiang Hospital Group, China
[3]School of Mechanical and Aerospace Engineering, Nanyang Technological University, Singapore
[4]Department of Rehabilitation Sciences, The Hong Kong Polytechnic University, China
[5]Jian Xiang Hospital Group, China
email: longbin.zhang@ntu.edu.sg

INTRODUCTION

Falls among older adults pose a significant global health challenge, affecting one in three individuals aged 65 and above annually, leading to substantial injuries and healthcare costs [1]. Effective fall risk assessment is crucial for guiding preventive strategies. Traditionally, the Berg Balance Scale (BBS) and the Timed Up and Go (TUG) test are standard methods for assessment, but they are time-intensive and require specialized clinicians. Our objective is to develop an enhanced fall risk assessment for older adults by integrating a markerless motion capture (Mocap) system and machine learning with the TUG test. This framework aims to accurately predict fall risk (BBS scores) while providing detailed gait analysis, including spatiotemporal parameters and joint kinematics.

METHODS

Seventy participants (age: 52.3 ± 18.7 years, sex: 46F/24M) were involved in the study. They were asked to perform TUG movements within the capture range of a markerless Mocap system, with BBS assessments conducted by professional physical therapists. TUG features were extracted using an auto-segmentation approach (115 features) and then served as inputs for machine learning models to predict BBS scores. Regression models, including LR, Lasso, RF, GBDT, XGBoost, KNN, and SVR, were employed for this prediction. Additionally, a comparison of lower limb joint kinematics between marker-based and markerless Mocap systems during the gait phase of the TUG motion was performed.

RESULTS AND DISCUSSION

All regression models demonstrated high prediction accuracy (RMSE ≤ 1.62, MAE ≤ 1.38, $R^2 \geq 0.82$, Fig. 1). RF, GBDT, and KNN exhibited low prediction error and high explanatory power, while LR and XGBoost had higher prediction errors and lower explanatory power. RF had the lowest RMSE, with GBDT showing similar performance, whereas XGBoost had higher prediction errors possibly due to hyperparameter complexities. These findings align with Lin et al. (2022) [2], who also found RF to have the lowest RMSE among models predicting BBS scores.

The lower limb joint kinematics captured by our markerless Mocap system exhibited similar patterns and ranges of motion

to marker-based systems, with an average RMSE $\leq 9.14°$. Our system showed better prediction accuracy for ankle D/P (3.03°). The accuracy is comparable to state-of-the-art technologies like Theia 3D (RMSE $\leq 13.2°$) in a recent study [3].
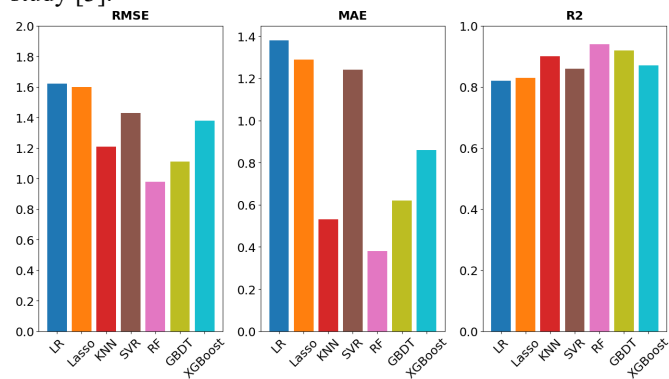
Figure 1: Root mean square error (RMSE), absolute mean error (MAE), and R-squared (R^2) between predicted by machine learning models and actual BBS scores.

CONCLUSIONS

Our enhanced TUG Test, incorporating a markerless motion capture system and a machine learning model, accurately predicts BBS scores while providing comprehensive gait analysis. High-fall-risk individuals showed longer completion times, lower performance velocities, and smaller lower-limb joint ranges of motion. The RF model excelled in predicting BBS scores, and our markerless system matched state-of-the-art accuracy without requiring markers or sensors. This study advances fall prevention strategies in older adults by offering an innovative and quantitative approach to assessing fall risk.

ACKNOWLEDGEMENTS

REFERENCES

[1] Zecevic et al., *The Gerontologis.* **46(3)**:367-376, 2006.
[2] Lin et al., *IEEE Sens. J.* **22(20)**:19919-19930, 2022.
[3] Kanko et al., *J. Biomech.* **127**:1-7, 2021.

LiDAR-based Scaling of OpenSim Human Models is a Viable Alternative to Marker-Based Approaches

[1]Grace McConnochie, [3]Aaron Fox, [2]Clint Bellenger, [1]Dominic Thewlis

[1]Centre for Orthopaedic Trauma and Research, Adelaide Medical School, University of Adelaide
[2]Alliance for Research in Exercise, Nutrition and Activity (ARENA); University of South Australia
[3]Institute for Physical Activity and Nutrition Research, School of Exercise and Nutrition Sciences, Deakin University
Email: g.e.mcconnochie@gmail.com

INTRODUCTION

Accurate scaling of biomechanical models is crucial for accurate motion analysis, particularly in dynamic simulations. Existing methods, such as marker-based scaling or MRI/CT scans, often use specialized equipment, can be subjective [1], and may not be practical for analysis in field settings. LiDAR scanning offers a non-invasive, portable, and efficient alternative, capable of producing high-resolution 3D surface geometries with everyday devices.

This study aimed to test a novel approach using LiDAR scans to inform the scaling of OpenSim models, comparing outcomes with traditional marker-based scaling. We hypothesized that the LiDAR-based method would demonstrate reliability and comparable scaling factors and marker-based joint kinematics to traditional marker-based scaled models.

METHODS

The study protocol was approved by our local HREC (H-2022-120). All participants (n=16) provided written informed consent. Participants underwent LiDAR scanning using an iPad Pro (Apple Inc., 2022). Eight participants were scanned twice for reliability testing, and the rest had scaling factors compared with a marker-based method. For six participants, joint kinematics over three running speeds were compared using marker and LiDAR scaled models. Skinned Multi-Person Linear (SMPL) surface geometries were fit to the LiDAR scans, from which anatomical skeletons were derived [2]. Pelvis, femur, and tibia scaling factors were calculated in MAPClient using statistical shape models informed by key skeletal landmarks [3] (Figure 1). Statistical analyses, including Bland-Altman and ICC, evaluated reliability and compared outcomes with marker-based optical motion capture. [2].
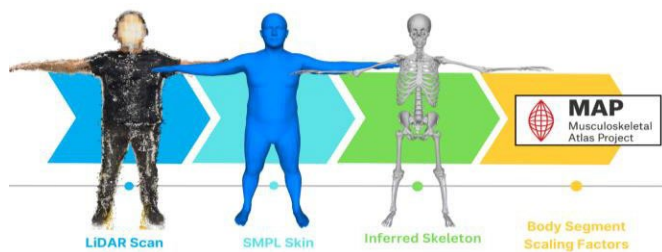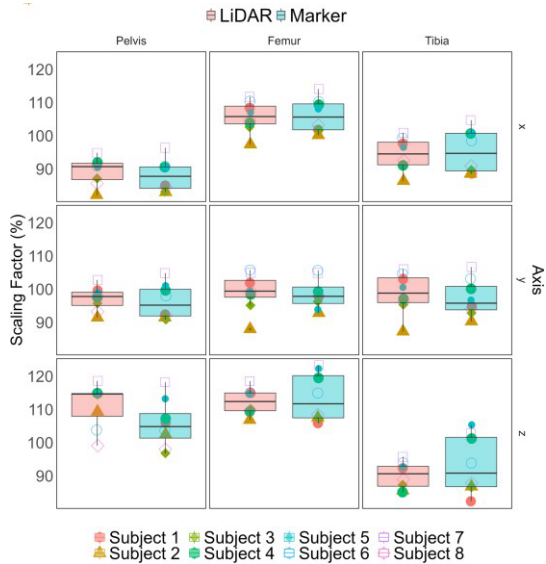
factors.

Figure 1: Workflow from point cloud to body segment scaling

RESULTS AND DISCUSSION

LiDAR-based scaling showed excellent reliability for scaling factors from repeat scans (ICC=0.961). Compared to marker-based methods, Bland-Altman analysis revealed LiDAR-based scaling factors had a mean difference of -0.5% ± 5.3%, with larger differences along the long axis of body segments. (Figure 2). Differences in joint kinematics computed using marker based inverse kinematics with the two differently scaled models were minor, with an average RMSE of 3.7° ± 0.1°.

Figure 2: LiDAR and marker based scaling factors separated by body segment and axis

CONCLUSIONS

LiDAR scanning is a valid and reliable alternative for scaling musculoskeletal models, suitable for field-based applications. This approach could significantly alter how we scale biomechanical, making it more accessible and efficient, especially in the context of wearable sensors. Further research will enhance its applicability across diverse populations, using additional body segments and the effects of varied locations or devices.

REFERENCES
1. Uchida K, et al., *Front. bioeng. biotechnol*. 10, 2022
2. Keller M, et al., *IEEE/CVF Conference*, 2022
3. Zhang J, et al., *LNCS*, 182–192, 2014

Wednesday, December 4

ANZORS Podium 7

A PHYSICS-INFORMED NEURAL NETWORK FOR ESTIMATION OF HIP BIOMECHANICS

Bradley Cornish, Zhengliang Xia, David John Saxby, Claudio Pizzolato, and Laura E Diamond

Griffith Centre of Biomedical and Rehabilitation Engineering (GCORE), Griffith University, QLD, Australia
email: bradley.cornish@griffith.edu.au

INTRODUCTION
Tissue loads and localized stresses and strains are key mechanical drivers of tissue adaptation and offer potential targets for treatment of musculoskeletal conditions. Currently, estimating these internal biomechanics is time-consuming and restricted to laboratories, preventing implementation of movement retraining strategies in everyday life, when they matter the most. To develop accessible treatments that produce sustained movement adaptions, prediction of internal biomechanics must move from laboratory to the real-world *via* affordable and easy-to-use technologies, such as inertial measurement units (IMU). We propose a novel treatment method for people with hip pathologies that aims to modify hip contact forces (HCF) *via* real-time biofeedback assisted movement retraining [1]. To achieve real-time estimations of internal and external biomechanics, we combined wearable sensors with physics-informed neural networks (PINN) [2] that adhere to physical and physiological laws of human motion. This study aimed to develop a PINN to predict hip angles, hip moments, and HCF from IMU data combined with electromyography (EMG) across a broad range of movements.

METHODS
Three-dimensional optical motion capture (Vicon, UK), ground reaction forces (AMTI, USA), 9-axis IMU (XSENS, Netherlands), and EMG (Cometa, Italy) from 14 lower-limb muscles were recorded synchronously from 20 healthy participants (aged 18-45 years) during 11 tasks: treadmill walk (level, incline, and decline), treadmill run (level, incline), bilateral squat, split squat, counter-movement jump (CMJ), forward jump, sit-to-stand, and side-step cut. A validated neuromusculoskeletal modelling pipeline (NMSK) using OpenSim and calibrated EMG-informed (CEINMS) [3] modelling estimated lower-limb joint angles, moments, muscle forces, and HCF from body motions, ground reaction forces, and EMG linear envelopes, providing ground-truth estimates to develop and train the PINN. The PINN was developed in TensorFlow (v2.6) and trained to estimate hip angles, hip moments, and HCF from 3 IMU (pelvis and thighs) and 4 EMG linear envelopes (gluteus maximus, gluteus medius, rectus femoris, and semitendinosus). The PINN consisted of a long short-term memory network and used a previously validated feed-forward NN to solve muscle-tendon unit kinematics [4]. The PINN solved for individual muscle forces while respecting muscle contractile mechanics, and then computed HCF. Additional loss functions were used to ensure internal consistency between predicted moments and muscle forces as well as smooth physiologically plausible predictions. Hip angles, hip moments, and HCF estimations were compared between PINN and NMSK models using coefficient of determination (r^2) and root mean square error normalised to trial range (nRMSE) within a leave-one-subject-out and leave-one-task-out cross-validation process.

RESULTS AND DISCUSSION
Using leave-one-subject-out validation, the PINN well predicted sagittal plane hip kinematics (median $r^2 > 0.95$; nRMSE < 10%), hip moments (median $r^2 > 0.85$; nRMSE ranged 10-17%), and HCF (median $r^2 = 0.84$; nRMSE < 9.5%) across all tasks (Figure 1). The computation time per prediction was <25ms on an Intel i9-12900K CPU.
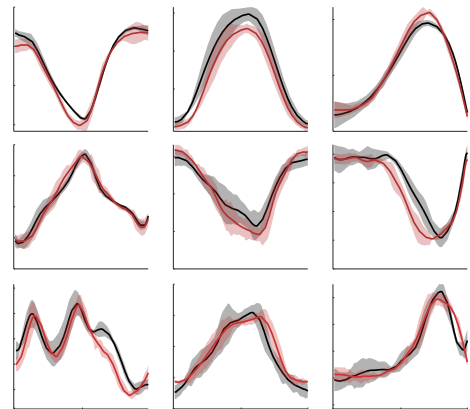
Figure 1: Sagittal plane hip angle (top), moment (middle), and HCF magnitude (bottom) for walking (left), split squat (centre), and forward jump (right) for 1 participant. The NMSK (black-line) and NN (red-line) model estimates ±1 standard deviation (shaded).

CONCLUSIONS
The PINN accurately predicted hip angles, hip moments, and HCF using 3 IMU and 4 EMG. The developed PINN enables real-time estimation of HCF outside the laboratory and supports use of novel tissue-targeting movement modification strategies for management of hip pathologies.

REFERENCES
1. Diamond LE et al. *Osteo Cartilage*, **28**:921-31, 2020.
2. Raissi M et al. *J Comput Phys*, **378**:686-707, 2019.
3. Pizzolato C et al, *J Biomech*, **48**:3929-36, 2015.

4. Cornish BM et al. *TechRxiv*, Feb 27, 2024.

MEDIAL GASTROCNEMIUS MUSCLE AND FASCICLE DYNAMICS *IN VIVO* DURING ECCENTRIC CONTRACTIONS

[1]Matheus D Pinto, [1]Kazunori Nosaka, [1]João Pedro Nunes, [1]Anthony J Blazevich

[1]Centre for Human Performance, School of Medical and Health Sciences, Edith Cowan University, Perth, WA
email: m.pinto@ecu.com.au

INTRODUCTION

In both rehabilitation and resistance training of the calf muscles, eccentric (ECC) training is commonly prescribed using various contraction intensities and slow velocity isokinetic contractions [1]. However, our understanding of how muscles behave during voluntary submaximal eccentric contractions remains limited. This is important for optimising training and rehabilitation prescriptions, and to further understand the mechanisms underpinning muscle damage and hypertrophy. This study examined human medial gastrocnemius (MG) muscle and fascicles dynamics *in vivo* during slow isokinetic ECC contractions performed at different contraction intensities.

METHODS

Thirteen subjects (27.2±5.1 y) attended two familiarisation sessions and one experimental session. Testing consisted of maximal (100%) and submaximal (40% and 60% of maximum) voluntary eccentric plantar flexor contractions on an isokinetic dynamometer from 20° plantarflexion to 20° dorsiflexion at 5°/s. B-mode sonography was used to capture videos of the MG belly. This allowed for fascicle length (FL), fascicle angle (FA), and muscle thickness (MT) to be measured, whilst simultaneous imaging of the muscle-tendon junction and digital motion capture allowed whole MG length to be measured *post-hoc* [2] Changes in fascicle length (ΔFL), angle (ΔFA), thickness, (ΔMT) and muscle length ΔMG length were determined and allowed for belly gear ratio to be computed as ΔMG length/ΔFL through each 5° of movement. Linear-mixed models were used to examine the effect of ECC intensity (40%, 60%, and 100%) and joint angle on FL, FA, MT, MG length (and their changes), and torque using 'individual' as a random factor.

RESULTS

FL was longer at contraction onset and ΔFL was greater in 40% than 60% and 100% ECC (P<0.01). However, FA was smaller in 40% but showed greater ΔFA in 60% and 100% ECC (P<0.01) (Figure. 1). MT and ΔMT were both greater in 40% than 100% ECC (P<0.01). MG length and its change were greater during 40% than 60% and 100% ECC (P<0.01). A higher gear ratio was observed in high-intensity contractions, while a low gear ratio was found in low-intensity contractions (P≤0.04). Torque increased with higher contraction intensities (P<0.01).
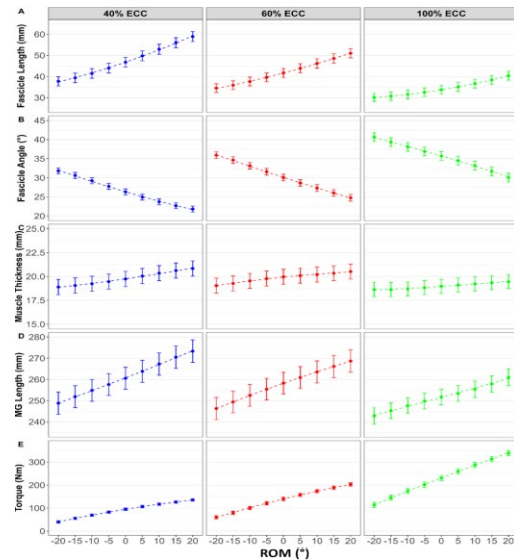
Figure 1: Marginal means ± SE for (A) fascicle length, (B) fascicle angle, (C) muscle thickness, (D) medial gastrocnemius length, and (E) torque across the range of motion and contraction intensities (40%, 60%, and 100%).

CONCLUSIONS

Low-intensity ECC resulted in larger ΔFL than maximal ECC, yet similar ΔFA. However, the higher initial FA during maximal ECC ensured that any ΔFA contributed more to overall muscle length change than during low-intensity ECC. This resulted in less ΔFL for a given ΔMG length during maximal ECC and a higher gear ratio. Larger ΔFL during low-intensity ECC may provide a greater mechanical stimulus for muscle damage and longitudinal muscle growth [2]. The mechanical behaviour observed herein may stem from muscle shortening against the stretched series elastic structures, allowing shorter MG length and higher FA, and longer MG length and FA at the start of the maximal and submaximal ECC contractions, respectively. These findings have important implications for ECC training prescription, suggesting that varying contraction intensities can be strategically used to target different training and rehabilitation outcomes.

REFERENCES

1. Couppé, C, et al., *J Orthop Sports Phys Ther*. **45**:853−63, 2015.
2. Pinto, MD, et al., *J Biomechanics.* **162**:111895, 2024.

3. Lieber, RL., Fridén, J. *J Appl Physiol*. 74:520-26, 1993.

A COMPREHENSIVE PIPELINE FOR IN VIVO DETERMINATION OF SKELETAL MUSCLE AND CONNECTIVE TISSUE ANATOMY USING MAGNETIC RESONANCE IMAGING

[1,2]Manuela Zimmer, [1]Filiz Ates, [2,3]Geoffrey Handsfield

[1]Institute of Structural Mechanics and Dynamics in Aerospace Engineering, University of Stuttgart, Stuttgart, Germany
[2]Auckland Bioengineering Institute, The University of Auckland, Auckland, New Zealand
[3]Department of Orthopaedics and Joint Department of Biomedical Engineering, The University of North Carolina, Chapel Hill, US
email: manuela.zimmer@isd.uni-stuttgart.de

INTRODUCTION

Skeletal muscle function is tightly coupled to its structure. Thus, accurate probing of muscle mechanics, e.g. through finite element modeling (FEM), requires a precise representation of anatomy. Muscle geometries can be imaged in 3D using conventional magnetic resonance imaging (MRI), while diffusion-weighted MRI enables estimation of muscle fiber architecture [1]. Recent developments in ultrashort echo time (UTE) MRI have been proposed to determine connective tissue structure [2]. However, technical challenges remain in applying these to musculoskeletal tissues, and this suite of sequences has yet to be applied to whole muscle groups such as the triceps surae. In this work, we combine advanced MRI sequences and present a pipeline to image the triceps surae muscle, aponeuroses, and Achilles tendon structures. We highlight previously unknown pitfalls in diffusion-weighted MRI of skeletal muscle along with recommendations to overcome these. In combining advanced MRI sequences, we demonstrate a detailed reconstruction of in vivo anatomy for the development of a high-fidelity image-based FEM.

METHODS

We acquired images in multiple slabs from knee to calcaneus using three MRI sequences: anatomical (TSE sequence, TR/TE 625/8.6 ms), diffusion-weighted (DT-EPI sequence, TR/TE 4801/50.9 ms, 16 gradient directions, b-value 500 s/mm^2), and dual-echo UTE (TR/TE 150.6/0.028 ms and 150.6/2.2 ms) using a 3T MRI scanner (Signa Premier, GE Healthcare). We compared diffusion-weighted images with different settings regarding field-of-view (FOV) size, phase-encoding direction, image acceleration technique ("Hyperband"), and shimming routine. Divided echo subtraction images (dES) were obtained by a voxel-by-voxel subtraction, followed by division by the sum of the two dual-echo images [2]. Susceptibility-induced distortions were corrected in the diffusion-weighted images and affine image registration to the anatomical images was performed. Muscles, aponeuroses, and tendons were manually segmented on the anatomical and dES images. Muscle fiber architecture was reconstructed using deterministic tractography with anatomical constraints based on aponeurosis location [3].

RESULTS AND DISCUSSION

High-signal images with clear muscle boundaries were obtained from anatomical images, while aponeurosis and tendon were visible on the dES images with high intensities (Fig. 1). Diffusion-weighted images produced obvious errors in the form of (a) substantial distortions when slices were acquired away from isocenter, (b) opposite phase-encoding directions demonstrated susceptibility-induced distortions and chemical shift, (c) Hyperband led to increased imaging artifacts. Higher-order shimming reduced distortions, resulting in continuous and consistent images and fiber tracts across slabs (Fig. 1). Following the analysis pipeline, we generated a model of the triceps surae including connective tissue and fiber directions.
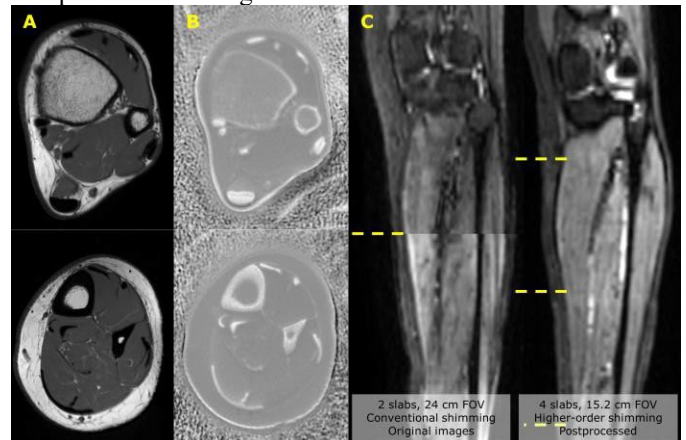
Figure 1: Examples of the three imaging sequences: (A) anatomical, (B) dES, and (C) diffusion-weighted images.

CONCLUSIONS

Combining the three MRI sequences with the proposed settings and post-processing enables imaging and reconstruction of muscle and connective tissue of the triceps surae group. This will allow us to comprehensively study muscle mechanics using a high-fidelity FEM.

ACKNOWLEDGEMENTS

REFERENCES

1. Damon B, et al., *NMR Biomed*. **30**:e3563, 2017
2. Cornfeld D, et al., *bioengineering*. **11(5)**: 441, 2024.

3. Bolsterlee B, et al., *J Appl Physiol*. **122**:727–738, 2017.

The effect of intramuscular fat on the anisotropic viscoelastic properties of human skeletal muscle in vivo

[1]Alice Hatt, [1,2]Robert Lloyd, [1,2]Bart Bolsterlee and [1,2]Lynne Bilston

[1]Neuroscience Research Australia, PO Box 1165, Randwick, NSW
[2]University of New South Wales, Graduate School of Biomedical Engineering, Kensington, NSW
email: a.hatt@neura.edu.au

INTRODUCTION

Skeletal muscle is a tissue with complex strain and direction-dependent viscoelastic properties. The functional performance of muscle (including whole muscle force) is affected by these properties, as well as by its architecture and composition [1]. For instance, a high proportion of intramuscular fat (IMfat) is associated with reduced muscle strength [2], but how IMfat affects the mechanical properties of muscle is not fully understood. IMfat proportions typically increase with age, obesity, inactivity or neuromuscular disease. Knowledge of the relationship between IMfat and muscle mechanical properties may help produce accurate and widely applicable computational models of skeletal muscle.

We aimed to investigate the effect of IMfat percentage and loading condition on the anisotropic viscoelasticity (stiffness) of the medial gastrocnemius (MG) and soleus (Sol) muscles using multimodal magnetic resonance (MR) imaging.

METHODS

Eighteen healthy adults (10F, 19-68 years) with a wide range of BMI (18-40kg/m^2) participated in this study. The right calf of participants were scanned at 3T using a Philips Achieva TX MR scanner. MR elastography (50Hz, voxel=3mm^3, 9slices) and diffusion tensor imaging (b-factor=500s/mm^2, 32dir) were acquired in a mid-sagittal plane under four conditions: foot plantarflexed (Slack), foot dorsiflexed (Stretch), foot in the neutral position (Neutral) and under 10% of maximal voluntary plantarflexor contraction (10%MVC, Active). Axial, two-point gradient-echo mDixon imaging (420x420, 200slices), was performed to quantify intramuscular fat fraction. The diffusion and MR elastography images were used to calculate shear stiffness parallel ($G'_\parallel$) and perpendicular ($G'_\perp$) to the muscle fibres [3]. The mean fat fraction, $G'_\parallel$, $G'_\perp$ and pennation angle (relative to the angle of the tibial shaft visible in scans), were measured in MG and Sol for all conditions. Pennation angle was selected as a proxy for fibre strain, which could not be reliably measured due to the complex large deformations selected for this study. Linear mixed models were used to test the effect of IMfat percentage and pennation angle on shear stiffness with increasing passive tension (between Slack and Stretch conditions), and of IMfat percentage and muscle activation on shear stiffness in isometrically contracting muscle (between Neutral and Active).

RESULTS AND DISCUSSION

In passively stretched muscle (Fig 1A), there was a significant association between shear stiffness and pennation angle ($G'_\parallel$ slope = -13.2 Pa/deg, p=0.004; $G'_\perp$ slope = -14.8 Pa/deg, p<0.001). In isometrically contracting (active) muscle (Fig. 1B), IMfat fraction was significantly correlated with $G'_\parallel$ (slope = -28.7 Pa/% MVC, p=0.008), but not with $G'_\perp$. Shear moduli were not affected by muscle activation, likely due to the relatively low level of activation selected for this study (10% MVC), a contraction level that was able to be held without fatigue by all participants over the length of each scan (up to 4 minutes). Future investigations should determine whether this effect becomes more pronounced at higher levels of contraction, and at higher IMfat percentages.

These results suggest that the viscoelastic properties of muscle are affected by both loading condition and IMfat fraction. The decline in shear stiffness of activated muscle with increasing intramuscular fat infiltration aligns with our previous findings that (subcutaneous) fat has a lower shear stiffness than the underlying muscle [4].
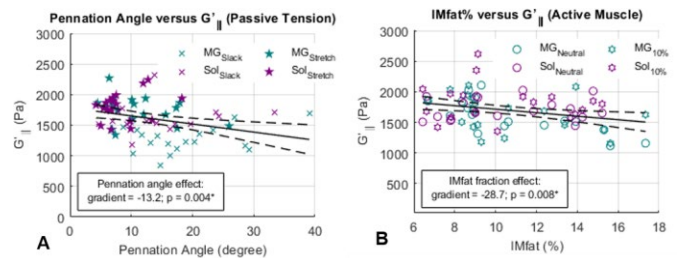
Figure 1: A) Pennation angle versus $G'_\parallel$ for passively stretched muscle. B) IMfat fraction versus $G'_\parallel$ for isometrically contracting muscle.

CONCLUSIONS

The viscoelastic properties of in vivo skeletal muscle are negatively correlated with intramuscular fat fraction under isometric contraction. These findings may be used to inform accurate computational models of skeletal muscles that account for viscoelasticity and muscle composition.

REFERENCES
1. Rahemi H, et al., *J. R. Soc. Interface.* **12:** 20150365
2. Giuliani HK, et al., *J Gerontol A Biol Sci Med Sci.* **75**:2286-2294, 2020
3. Babaei, B, et al., *Med Image Anal.* **74**: 102212
4. Hatt A, et al., *J Mech Behav Biomed Mater.* **143**: 105924

ASSESSMENT OF TWO MUSCLE MODELS WITH COUPLED ACTIVATION AND CONTRACTION DYNAMICS

[1]Andrea Sgarzi, [1]Théo Meranger, [3]Arnault Caillet, [3]Dario Farina, [1]Nigel Lovell [1,2]Bart Bolsterlee, [1]Luca Modenese

[1] Graduate School of Biomedical Engineering, UNSW, Sydney, NSW
[2] Neuroscience Research Australia (NeuRA), Sydney, NSW
[3] Dept of Bioengineering, Imperial College London, UK
email: l.modenese@unsw.edu.au

INTRODUCTION

Muscle models aim to simulate how skeletal muscles produce force in response to a neural signal, accounting for their architecture and contraction conditions. Hill-type muscle models are based on a phenomenological characterisation of the muscle contraction dynamics [1] and are commonly used in muscle physiology and computational biomechanics. Hill-type muscle models consistent with the popular framework proposed in [2], implement contraction dynamics neglecting its physiological dependence on the active state. When assessed experimentally, they demonstrated good accuracy in slow, nearly maximally-activated contractions, but were less accurate in faster, submaximal contractions more representative of *in vivo* muscle use [3] and for which the active state dependency might not be negligible. This study aims to quantify the accuracy of two computational muscle models that consider the non-linear coupling between activation and contraction dynamics by, in the first instance, predicting experimental measurements of forces in maximally stimulated muscles [4].

METHODS

We considered two computational muscle models. The first one is an implementation of the Hatze (HA) model [5] including the dependency of active state on fibre length, improved according to [6]. The second model is a motor-unit-level muscle model based on Caillet et al. (CA model) [7]: it considers the dependency on fibre length and active state of both the force-length and force-velocity relationships, differentiating between fast and slow motor unit (MU) types. Differently from [7], we implemented an elastic tendon, replaced the calcium-troponin binding dynamics with a simplified excitation-activation coupling, and controlled the muscle force using 27 MUs, three of which were fast-twitch [8]. The muscle models were benchmarked against force measurements from a maximally activated rat soleus undergoing six different displacements [3-4]. The curvature of the force-velocity relationship and maximum isometric force F_{iso} of the HA model were calibrated through a least-squared fit to the first trial of the benchmark, as in [3]. The CA model, developed using mammalian muscle parameters, was not calibrated except for setting F_{iso} equal to the HA model, and adjusting the elastic tendon stiffness (1.95 N/%ε) from rat-related literature [9]. The agreement between force measured experimentally and predicted by simulation was quantified in terms of maximum absolute error (MAE), mean absolute error (mAE) per trial and, as a global comparison metric, across all trials simulated by each model. Errors were expressed as percentage of F_{iso}.

RESULTS AND DISCUSSION

Both models predicted the experimental muscle forces remarkably well, with global errors comparable to [3] ([3]: 5.6±2.2%, HA: 5.1±1.0%, CA: 4.0±1.5%). The MAE increased with the amount of stretch applied to the muscle, reaching 68% for HA (CA: 25%) for the trial with maximum displacement amplitude (Figure 1). Similarly, the mAE for individual trials reached 7.0% for HA (CA: 6.6%). This suggests that muscle active stretch is not adequately modelled by either model.
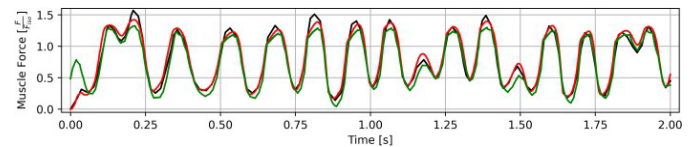
Figure 1: Measured (black line) and simulated muscle force (HA: green, CA: red) for maximum-stretch experimental trial.

Because the muscles were maximally activated, the considered benchmark predominantly tested the models' contraction dynamics. We are currently extending this partial assessment using a submaximal activation benchmark [3] and developing a novel verification procedure for the activation dynamics.

CONCLUSIONS

Muscle models with coupled contraction and activation dynamics and MU-level muscle dynamics can predict muscle force slightly more accurately than standard Hill-type models in maximally stimulated muscles.

ACKNOWLEDGEMENTS

REFERENCES

1. Hill AV, *Proc Royal Soc B*. **126**:136-195, 1938.
2. Zajac FE, *Crit Rev Biom Eng.* **17**:359-411, 1989.
3. Millard M et al., *J Biomech Eng.* 135: 021005, 2013.
4. Krylow AM et al. *J Biomech.* 30:27-33, 1997.
5. Hatze H, *Biol Cyber.* **28**:143-157, 1978.
6. Rockenfeller et al. *J Theor Biol.* **454**:240-252.
7. Caillet AH et al. *PLOS Comp Biol.* 19 e1011606, 2023.
8. Chamberlain S et al., *J Physiol.* **412**:1-21, 1989.

9. Monti RJ et al. *J Exp Biol*. 206(Pt 19):3437-3445, 2003.

A NEUROMECHANICAL MODEL FOR MUSCLE ENERGY USE IN VIVO

[1]Ryan N. Konno, [2]Glen A. Lichtwark, and [1]Taylor J.M. Dick

[1]School of Biomedical Science, The University of Queensland, Brisbane, QLD
[2]School of Exercise and Nutrition Sciences, Queensland University of Technology, Brisbane, QLD
email: r.konno@uq.edu.au

INTRODUCTION

Skeletal muscle energy use provides key insights into the role of muscle during complex motor tasks. The energy used depends on the muscle neuromechanical state, which includes the recruited motor units, muscle fascicle dynamics, and muscle force [1]. However, determining *in vivo* cause-effect relationships between specific muscle components and total energy use remains difficult; thus, modelling techniques are required. Here, we develop a mathematical framework to identify specific neuromechanical contributions to energy use.

METHODS

The proposed framework combines motor unit pool, excitation-activation, mechanical, and energetic models. The motor unit model follows the formulation by [2] with parameters (e.g. motor neuron size) based on subject-specific data and extrapolated using experimentally determined relationships (Figure 1). The outputs from the motor unit model (discharge times) are then used as input to an excitation-activation model predicting activation at the motor unit level. A Hill-type model determines the muscle mechanical state and corresponding energetics were calculated using the model by [3]. The model was validated using motor unit data collected with high density electromyography during isometric dorsiflexion contractions at a range of contraction rates.
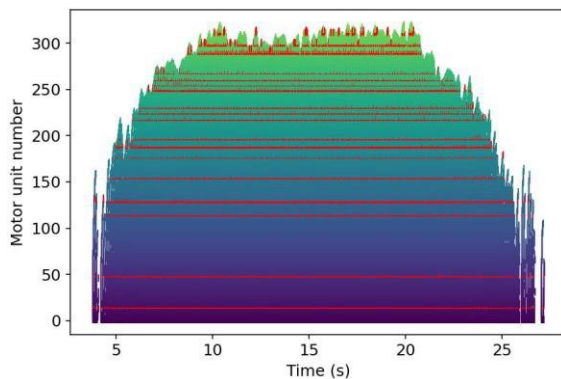
Figure 1: Simulated motor unit discharge times based on experimental data from [4] for the tibialis anterior at 35% maximum voluntary contraction (MVC). Red indicates experimentally identified motor units.

RESULTS AND DISCUSSION

The model shows how changes to the neuromechanical state, in this case faster contraction rates, lead to changes in energetic

cost (Figure 2). The increased energetic cost with contraction rate can be linked to faster shortening rates that require higher activation levels and more motor units recruited. This model captures the role of motor unit level properties, including fibre- type properties and distributions, on whole muscle energetics. Next steps include validating the modelling framework across a range of mechanical conditions.

Figure 2: Predictive isometric simulation of a tibialis anterior muscle contraction to 20% MVC. Discharge times and energetic cost are shown at slow (0.3125 MVC s⁻¹; green) and fast (2.5 MVC s⁻¹; purple) contraction rates. Time is normalized to contraction length: 0.8s and 3.6s, respectively.

CONCLUSIONS

Improving predictions of energy consumption can help to identify the role of targeted interventions, such as mobility aids, on neurological disorders where both motor unit and structural changes to muscle occur. The predictive capabilities of the modelling framework presented here highlight the independent and combined consequences of motor unit level and structural changes to whole muscle energetic cost.

REFERENCES

1. Barclay & Curtin., *J. Biomech.*, **156**, 111669, 2023.
2. Caillet et al., *PLOS Comp. Biol.*, **18**(9), e1010556, 2022.
3. Lichtwark & Wilson, *J. Exp. Biol.,* **208**, 2831-2843. 2005.
4. Del Vecchio et al., *J. Physiol.*, **597**, 1873-1887, 2019.
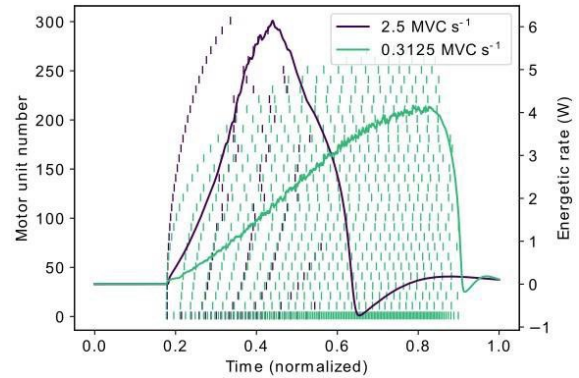
Monday, December 2

POSTERS DAY 1

Insights into patellofemoral kinematics and cartilage stresses following pediatric anterior cruciate ligament reconstruction

[1]Ayda Karimi Dastgerdi, [2]Amir Esrafilian, [1]Christopher P. Carty, [1]Azadeh Nasseri, [1]Alireza Yahyaiee Bavil, [1]Martina Barzan, [2]Rami K. Korhonen, [3]Ivan Astori, [4]Wayne Hall, and [1]David John Saxby

[1]Griffith Centre of Biomedical and Rehabilitation Engineering, Griffith University, Australia; [2]Department of Technical Physics, University of Eastern Finland, Finland; [3]Department of Orthopedics, Children's Health Queensland Hospital and Health Service, Australia; [4]School of Engineering and Built Environment, Griffith University, Australia.
email: ayda.karimidastgerdi@griffithuni.edu.au

INTRODUCTION

Anterior cruciate ligament (ACL) reconstruction (ACLR) is performed to restore knee stability following ACL rupture. However, post-ACLR complications such as patellofemoral joint (PFJ) pain and early onset osteoarthritis affect 6-26% of patients within two years and ~72% of patients within 15 years [1]. Surgical variations, including graft type, size, pre-tension, and femoral tunnel location, as well as patient-specific factors like knee size and neuromusculoskeletal function, may impact post-ACLR PFJ biomechanics. This study used a linked neuromusculoskeletal (NMSK) and finite element (FE) model to investigate the effects of ACLR surgical parameters on PFJ kinematics and cartilage stresses during walking gait in pediatric patients and assessed how knee phenotype and neuromusculoskeletal function influence these outcomes.

METHODS

Lower-limb anatomy from three typically developing adolescent patients (mass 60.6±7.7 kg) was acquired using magnetic resonance imaging. For each participant, 135 FE models of their knee were created, each consisting of a surgically plausible combination of three variations of graft type (gracilis, semitendinosus, patellar tendon), diameter (6, 8, 9 mm), and pre-tension (0, 40, 100 N), as well as five femoral graft locations (±5 mm deviation from the native ACL footprint in medial, lateral, anterior, and posterior directions). Three-dimensional motion (Vicon Motion Systems Ltd, UK), ground reaction forces (AMTI, MA, USA), and 10 lower-limb muscle electromyograms (EMG) were recorded during walking at a self-selected pace. Patient-specific FE motion, loading, and boundary conditions were estimated using OpenSim and a calibrated EMG-assisted model. The tibiofemoral joint (TFJ) flexion angle, abduction-adduction and internal-external rotation moments (summed generalized joint and muscle moments), as well as TFJ and PFJ contact forces, were used to drive FE models. Normalized root mean square error (nRMSE) was used to quantify deviation between ACLR and intact knee models in terms of PFJ kinematics (translations and rotations) and cartilage maximum principal stresses.

RESULTS AND DISCUSSION

Most of the surgical combinations successfully restored PFJ kinematics indicated by nRMSE<10% relative to the corresponding intact knee (Fig 1). However, a substantial proportion of these kinematically-acceptable surgical combinations had in large errors in maximum principal stresses on patellar cartilages. Moreover, the magnitudes and patterns of kinematics and maximum principal stresses in patella cartilages were contingent upon both surgical parameters and patient-specific features of knee anatomy, motion, and loading. Results suggest that despite ACLR restoring PFJ kinematics, the PFJ cartilage mechanics may be disturbed potentially prompting onset of degeneration.
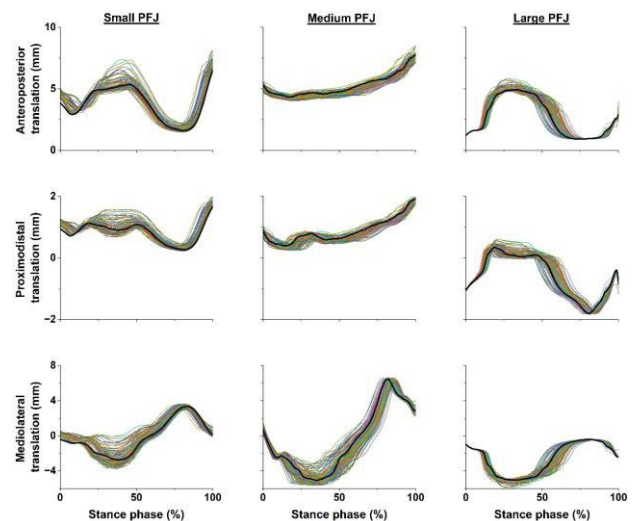
Fig 1: Patellofemoral joint (PFJ) translations for intact (black line) and 135 ACLR finite element models (colored lines) for small, medium, and large knees during walking stance.

CONCLUSIONS

Findings emphasize the importance of incorporating patient-specific geometry and neuromusculoskeletal factors when optimizing ACLR for biomechanical outcomes. Overall, this study represents the first comprehensive investigation into the influence of surgical parameters on pediatric PFJ biomechanics and contributes to advancing our understanding of PFJ biomechanics following ACLR.

REFERENCES

1. A. G. Culvenor, et al., British Journal of Sports Medicine, 47(2), 2013.

BETWEEN-DAY RELIABILITY OF GAIT VARIABILITY MEASURES CALCULATED FROM AN INERTIAL MEASUREMENT UNIT

[1,2] Ben Jones, [3] Jon Wheat, [1] Kane Middleton, [1] David Carey and [2] Ben Heller

[1] School of Allied Health, Human Services and Sport, La Trobe University, Melbourne, Victoria, Australia.
[2] Sport and Physical Activity Research Centre, Sheffield Hallam University, Sheffield, UK
[3] Sport and Human Performance Enhancement Research Centre, Nottingham Trent University, Nottingham, UK.
Corresponding author: benjamindavidmichael.jones@latrobe.edu.au

INTRODUCTION

High-order biomechanical signals, such as stride time or sacral acceleration time series, will contain variability that may reflect the ability of the body to utilise its abundant degrees of freedom [1]. This variability can be measured in terms of the magnitude and structure (complexity or regularity) of fluctuations within the signal. Such fluctuations have successfully distinguished between previously injured and uninjured groups [2] and between periods before and after functional overreaching [3]. Longitudinal assessment of gait variability measures, which can be facilitated by wearable devices such as inertial measurement units (IMUs), may therefore support injury management and prediction [1]. However, the between-day reliability of gait variability measures calculated from IMU data is unknown, and reliability may differ between measurement devices [4,5], This study investigated the between-day reliability of variability measures calculated from IMU data.

METHODS

Nineteen healthy recreational runners completed an ordered set of six trials (Figure 1) on two sessions 7 days apart. Trials lasted up to 8 minutes and were separated by a minimum of 2 minutes rest. Stride times (ST) were collected with and processed directly by commercial RunScribe™ IMUs that were placed in lace cradles. Raw sacral accelerometer data was collected using a third RunScribe™ IMU sampling at 200 Hz placed in a cradle secured onto the waistband. 512 strides were taken from each trial. The magnitude of ST variability was quantified using the coefficient of variation (CV). ST complexity was quantified by applying the average evenly spaced detrended fluctuation analysis (DFA) algorithm, with window sizes ranging from 4 to N/5 and detrending performed using a first-order polynomial. ST regularity was quantified using sample entropy (SE) for all combinations of m and r in the respective sets {2, 3, 4} and {0.10, 0.15, 0.20, 0.25, 0.30}. Resultant sacral acceleration (RSA) regularity was quantified by applying SE to 30 strides of resampled data. Reliability was assessed using the intraclass correlation coefficient (ICC), standard error of measurement (SEM) and minimum detectable change (MDC).
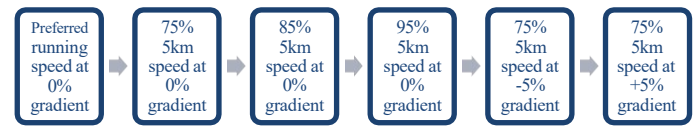
Figure 1: The ordered set of six treadmill running conditions completed by participants during each session.

RESULTS AND DISCUSSION

Mean ST displayed excellent relative reliability (ICC = 0.957) (Table 1). ST CV displayed moderate relative reliability (ICC = 0.664), although with an absolute MDC = 0.548%. ST DFA-α displayed lower relative reliability (ICC = 0.447; poor) than previously observed with other measurement devices [4,5], and yielded MDCs greater than between group differences and within participant changes previously reported [2,3]. ST SE also displayed poor relative reliability for all combinations of m and r (ICC ≤ 0.446). Conversely, RSA SE displayed moderate to good relative reliability for all combinations of m and r (0.641 ≤ ICC ≤ 0.798), although with relatively high MDCs.

CONCLUSIONS

DFA and SE displayed poor reliability when applied to pre-processed stride time data from an IMU. However, SE displayed moderate to good reliability when applied to raw RSA data. Between-day changes in stride-time variability measures should be interpreted with caution when using pre-processed stride time data from IMUs.

REFERENCES

1. Fonseca S, et al., *Sports Medicine* **50**: 1757-1770, 2020.
2. Meardon S, et al., *Gait & Posture* **33**: 36-40, 2011.
3. Bellenger C, et al*., Journal of Science and Medicine in Sport* **22**: 294-299, 2019.
4. Godin A, et al., *Gait & Posture* **111**: 37–43, 2024.
5. Fuller J, et al., *ISBS Proceedings Archive* **36**: 702, 2018.

Table 1: Between-day reliability of stride time (ST) mean, coefficient of variation (CV), detrended fluctuation analysis (DFA-α) and sample entropy (SE), and resultant sacral acceleration (RSA) sample entropy. For the two sample entropy measures, results are displayed for the combination of m and r that yielded that highest ICC (m = 2 and r = 0.25, and m = 3 and r = 0.20 respectively).

Variable	Visit 1 Mean (95% CI)	Visit 2 Mean (95% CI)	ICC (95% CI)	SEM	MDC
ST Mean (s)	0.729 (0.723, 0.736)	0.732 (0.726, 0.738)	0.957 (0.943, 0.967)	0.010	0.027
ST CV (%)	1.239 (1.191, 1.288)	1.209 (1.169, 1.249)	0.664 (0.584, 0.730)	0.198	0.548
ST DFA-*α*	0.751 (0.736, 0.766)	0.756 (0.740, 0.771)	0.447 (0.337, 0.545)	0.087	0.241
ST SE	1.763 (1.733, 1.794)	1.788 (1.760, 1.815)	0.446 (0.336, 0.544)	0.167	0.462

| RSA SE | 0.275 (0.261, 0.289) | 0.273 (0.258, 0.288) | 0.798 (0.720, 0.856) | 0.034 | 0.095 |

THE EFFECT OF BIOLOGICAL SEX ON LOWER-LIMB COUPLING VARIABILITY IN MILITARY PERSONNEL

[1]Brooke Hoolihan, [2]Jonathan Wheat, [3]Ben Dascombe, [4]Danielle Vickery-Howe and [4]Kane Middleton

[1]School of Biomedical Science and Pharmacy, University of Newcastle, Ourimbah, Australia
[2]Department of Sport Science, School of Science and Technology, Nottingham Trent University, Nottingham, UK
[3]School of Health Sciences, Western Sydney University, Campbelltown, Australia.
[4] Sport, Performance, and Nutrition Research Group, School of Allied Health, Human Services and Sport, La Trobe University, Melbourne, Australia
email: brooke.hoolihan@uon.edu.au

INTRODUCTION

Thirty-four percent of soldiers sustain at least one load-carriage injury during their career [1], with female personnel being more likely to sustain foot, hip, and lower-extremity overuse injuries [2]–[4]. Lower-limb coupling variability (CV) has been proposed as a mechanism of injury, with injured individuals demonstrating both higher and lower variability than healthy individuals [5]–[7]. Although our previous work has shown that load-related changes in CV are sex-dependent, [8], it included civilians without load-carriage experience and utilised loads relative to body mass. This study aims to investigate the effect of biological sex on lower-limb CV in military personnel during load carriage.

METHODS

Twenty-two Australian Army Soldiers (11 females) walked for 12 minutes at 5.5 km/h on an instrumented treadmill wearing body-borne load (23.2 kg). Marker trajectories were captured using a Vicon system, which was used to calculate segment angles in the sagittal (SAG), transverse (TRA), and frontal (FRO) planes. The standard deviation of continuous relative phase was used to quantify the CV of nine lower-limb couplings. Statistical parametric mapping paired t tests [9] with Cohen's d_z effect sizes were used to assess the effect of sex on CV.

RESULTS AND DISCUSSION

There were no significant ($p > .05$) sex differences in CV in any of the nine couplings. Effect sizes ranged from -0.42 (ThighTRA-ShankTRA at 100% of the gait cycle) to 0.65 (ThighTRA-ThighFRO at 17% of the gait cycle).

No significant differences were observed in lower-limb CV between biological sexes. Although there are many factors that may influence injury risk during load carriage between sexes, lower-limb CV while carrying 23.2 kg of load may not be one of these. Although the current results support our previous research that required civilians to carry relative loads of 20% and 40% of body mass [8], the female cohort in that study had significantly greater CV in the 40% compared to the 0% body-

mass condition. The external load in the current study equated to approximately 31% of body-mass and may not have been a sufficient perturbation to elicit a response in military personnel experienced in load carriage. Given that greater CV is thought to lead to increased movement adaptability and flexibility, the greater load carriage experience of military personnel may result in functional increases in variability at greater loads. Thus, investigating the impact of greater military-relevant loads on CV is recommended to further explore its links with injury risk. However, it should be noted that links between injury risk and CV are speculative and require prospective research to confirm potential causal relationships.

CONCLUSIONS

The current results suggest that there is no elevated CV-related injury risk in female personnel when carrying up to 23.2 kg of load, when compared to males. This suggests that current training for load carriage does not require amendments for either the male or female military population.

REFERENCES

1. Orr R, et al., *Int J Inj Contr Saf Promot.* **21**:388-396, 2014.
2. Knapik J, et al., *Med Sci Sport Exerc,* **33**:946-954, 2001.
3. Orr R & Pope R, *NMC Musculoskelet Disord,* **17**:1-8, 2016.
4. Wardle S, et al., *BMJ Mil Heal,* **169**:62-68, 2023.
5. Hamill J, et al., *Clin Biomech,* **14**:297-308, 1999.
6. Seay J, et al., *Clin Biomech,* **26**:572-578, 2011.
7. Heiderscheit B, et al., *J Appl Biomech,* **18**:110-121, 2002.
8. Hoolihan B, et al., *Gait Posture,* **100**:236-242, 2023.
9. Pataky T, *Comput Methods Biomech Biomed Engin,* **15**:295-301, 2012.

[1] R. Orr, J. Coyle, V. Johnston, and R. Pope, "Self-reported load carriage injuries of military soldiers," *Int. J. Inj. Contr. Saf. Promot.*, vol. 24, no. 2, pp. 189–197, 2017, doi: 10.1080/17457300.2015.1132731.

[2] J. Knapik, M. A. Sharp, M. Canham-Chervak, K. Hauret, J. F. Patton, and B. H. Jones, "Risk factors for training-related injuries among men and women in basic combat training," *Med. Sci. Sports Exerc.*, vol. 33, no. 6, pp. 946–954, 2001, doi: 10.1097/00005768-200106000-00014.

[3] R. Orr and R. Pope, "Gender differences in load carriage injuries of Australian army soldiers," *BMC Musculoskelet. Disord.*, vol. 17, no. 1, pp. 1–8, 2016, doi: 10.1186/s12891-016-1340-0.

[4] S. L. Wardle, T. J. O'Leary, S. Jackson, and J. P. Greeves, "Effect of sex and combat employment on musculoskeletal injuries and medical downgrading in trained military personnel: An observational cohort study," *BMJ Mil. Heal.*, vol. 169, no. 1, pp. 62–68, 2023, doi: 10.1136/military-2022-002284.

[5] J. Hamill, R. E. A. Van Emmerik, B. C. Heiderscheit, and L. Li, "A dynamical systems approach to lower extremity running injuries," *Clin. Biomech.*, vol. 14, no. 5, pp. 297–308, 1999, doi: 10.1016/S0268-0033(98)90092-4.

[6] J. F. Seay, R. E. A. Van Emmerik, and J. Hamill, "Low back pain status affects pelvis-trunk coordination and variability during walking and running," *Clin. Biomech.*, vol. 26, no. 6, pp. 572–578, 2011, doi: 10.1016/j.clinbiomech.2010.11.012.

[7] B. C. Heiderscheit, J. Hamill, and R. E. A. Van Emmerik, "Variability of stride characteristics and joint coordination among individuals with unilateral patellofemoral pain," *J. Appl. Biomech.*, vol. 18, no. 2, pp. 110–121, 2002, doi: 10.1123/jab.18.2.110.

[8] B. Hoolihan, J. Wheat, B. Dascombe, D. Vickery-Howe, and K. Middleton, "The effect of external loads and biological sex on coupling variability during load carriage," *Gait Posture*, vol. 100, pp. 236–242, 2023, doi: 10.1016/j.gaitpost.2023.01.002.

[9] T. C. Pataky, "One-dimensional statistical parametric mapping in Python," *Comput. Methods Biomech. Biomed. Engin.*, vol. 15, no. 3, pp. 295–301, 2012, doi: 10.1080/10255842.2010.527837.

REGIONAL EFFECTS OF RAPID ECCENTRIC STRETCH ON TIBIALIS ANTERIOR MUSCLE SHEAR MODULUS AND MOTOR UNIT DISCHARGE FREQUENCY DURING MODERATE ISOMETRIC CONTRACTIONS: PRELIMINARY RESULTS

[1]Cristian D. Riveros-Matthey, [2]Patricio A. Pincheira, [3]Glen A. Lichtwark

[1] School of Health and Rehabilitation Sciences, The University of Queensland, Brisbane, QLD
[2] School of Health and Medical Sciences, University of Southern Queensland, Ipswich, QLD
[3] School of Exercise and Nutrition Sciences, Queensland University of Technology, Brisbane, QLD
email: c.riverosmatthey@uq.edu.au

INTRODUCTION

Human muscles are structurally heterogeneous, leading to regional differences in stress during contraction and variations in motor unit discharge strategies for a given muscle stretch [1,2]. When exposed to unaccustomed high strain from eccentric activities, muscles may become damaged or injured. However, the mechanisms behind this damage remain poorly understood. Investigating the influence of structural and neural factors on stress and strain distribution within muscles is relevant for injury prevention strategies. Therefore, this study aimed to quantify muscle stress distribution and to determine how differences in stress and motor unit (MU) discharge rates are related to muscle strain during rapid stretching.

METHODS

Five participants were included in these preliminary results. Data from the Tibialis Anterior (TA) muscle was collected in two sessions: high-density EMG (HDEMG) session and ultrasound sessions. All measurements were made from two TA regions: proximal and distal portions. In each session, while the right foot (dominant) was attached to a custom-made dynamometer, participants performed two isometric contractions at 20% and 50% of their maximum voluntary contraction (MVC). Each trial required participants to maintain a constant isometric torque at the specified level for 5 seconds, aided by visual feedback displaying their actual EMG output. During the ultrasound session, supersonic shear wave elastography (SWE) maps and B-mode ultrasound images were recorded (Aixplorer V9, transducer SL10-2 MHz, SuperSonic Imagine, France) (Fig. 2). During the HDEMG session, EMG signals were recorded using two 2D grids of 8 x 4 equally spaced electrodes (inter-electrode distance of 10 mm, 2000Hz sampling rate)(Fig. 2). At the middle of each isometric contraction, a TA stretch was elicited by the dynamometer, by rapidly rotating the ankle at approximately 300 degrees per second. These stretches were performed with two different ankle ranges of motion so that a short and a long stretch of the TA was elicited. Three-way ANOVA was used to test the main effects of MVC levels, regions, and perturbation on SWE values and MU discharge rates with an alpha of $p = 0.05$.

RESULTS AND DISCUSSION

Preliminary results from SWE ($n=5$) and MU discharge ($n=2$) indicate that during the short stretch, SWE values tend to be higher in the distal region and increase further after rapid stretching. Conversely, MU discharge rates are lower in the distal region but rise following the perturbation (Fig. 1). While qualitatively SWE and MU show no changes between regions, both increase after perturbation during the long stretching (Fig. 1).
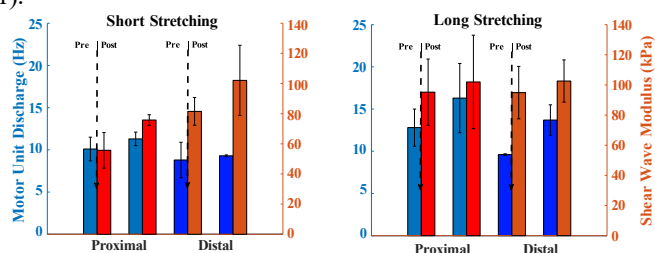
Figure 1: Motor unit discharge rate and shear wave modulus across regional (proximal/distal), stretching (short/long) and rapid perturbation (pre/post) conditions at 50% of MVC.
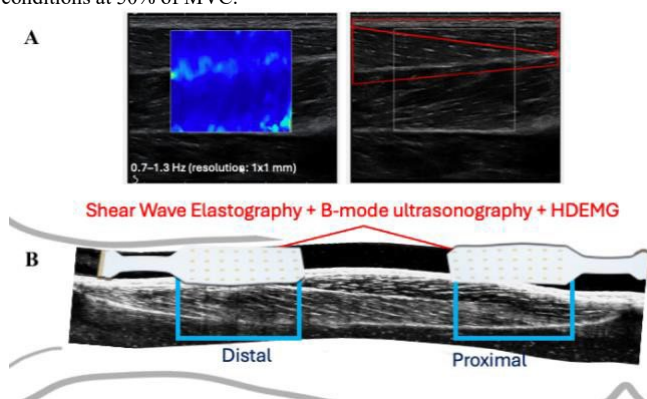
Figure 2: SWE and B-mode ultrasound images (A) and 2D grids from HDEMG (B).

CONCLUSIONS

The preliminary results suggest that regional responses might be influenced by differences in fascicle length, pennation angles, and MU discharge rates. Ongoing data analysis is expected to yield a more comprehensive understanding, and the complete dataset will be prepared for presentation.

REFERENCES

1. Bennett, H., *J Biomech.,* **47**, 3050-3055, 2014.

2. Wakeling, J., *Biol. Lett.,* **5**, 30-34, 2009.

PREDICTING HUMERAL VERSION ANGLE FOR SHOULDER SURGERY USING STATISTICAL POSE MODELS

François Bruyer-Montéléone[1], Maxence Lavaill[1,2] Natalia M. Castoldi[1], Graham Kerr[2,3], Ashish Gupta[1,2,4],
Kenneth Cutbush[1,2,4], Jeffrey Bischoff [1,5], Saulo Martelli[1,2] and Peter Pivonka[1,2]
[1] School of Mech., Medical & Process Eng, Queensland University of Technology, Brisbane, QLD; [2] Queensland Unit for
Advanced Shoulder Research, Brisbane, QLD; [3] School of Exercise and Nutrition Sciences, QUT, QLD; [4] Orthopaedic Surgery,
Sports Injury, Orthopaedics, Greenslopes Private Hospital, Brisbane, QLD, [5] Zimmer Biomet, Warsaw, IN
email: f2.bruyermonteleone@hdr.qut.edu.au

INTRODUCTION

Humerus version angle is used to position the humeral implant component during total shoulder arthroplasty. Humeral version angle can be determined either by (i) predicting it from the contralateral side assuming it is equivalent and healthy [1], or by (ii) applying a generic pre-defined value [2]. Statistical shape models (SSMs) can describe shoulder anatomical variation across a population and predict individual pre-injured bones [1,3]. Moreover, if changes in shape within the bone and in the shape of the adjacent bones are related, hence affecting bones' relative position, one could use statistical pose models (SPMs), which consider multiple bones within a joint, to estimate the humeral shape and version angle based on its adjacent bones. This approach represents a new direction in shoulder implant positioning, addressing a current gap in knowledge.

METHODS

Sixty-one healthy shoulder bones, i.e., humerus, scapula and clavicle, (29M and 32F, age: 36 ± 14 y.o.) were reconstructed from medical images (Mimics 26.0, Materialise NV, Belgium). Each bone was registered following a three-step method. First, a rigid registration step aligned the template axes with the target meshes. Then, a rigid Iterative Closest Point (ICP) algorithm rotated and scaled the template vertices. Finally, a non-rigid ICP algorithm deformed the template mesh to locally match the targets' shape. Registered bones were expressed in the clavicle coordinate system defined with the ISB's clavicular markers [4] and the most anterior and posterior points of the midplane between the ISB's markers. Considering bone shape co-variation, only inter-segment translations were used to position the bones. Humeral shape reconstruction was performed with the principal component (PC) analysis scores via a leave-one-out method. The root mean square errors (RMSE) of the point-by-point distance over the entire surface were based on the best-fitting prediction using the humeral adjacent segments, i.e., the scapula (entire shape – S, or damaged, i.e., without its glenoid - SG) or the clavicle (C). Shape errors were averaged over all the PCs and the bones. Finally, the version angle was calculated based on the transepicondylar line and the line perpendicular to the anatomical margin so the error between the prediction and the original bone was estimated [4]. Statistical analysis was performed with a 1-way ANOVA test (SPSS 29.0, IBM, USA)

while results were compared with the literature [1,3-6].

RESULTS AND DISCUSSION

The mean shape error reached 1.2 ± 0.3 mm with no significant differences between the SPMs (p>0.05) (Figure 1A). Compared with the literature, the shape prediction fell under the previously reported value of 4 mm [1,3]. The average version angle was 24.5 ± 5.6° which agreed with the literature [5,6]. The mean angle error was 0.1 ± 6.8° and did not significantly change across the SPMs (p>0.05) (Figure 1B). Likewise, the angle errors aligned with the existing literature [2.9-6.5°] [3].
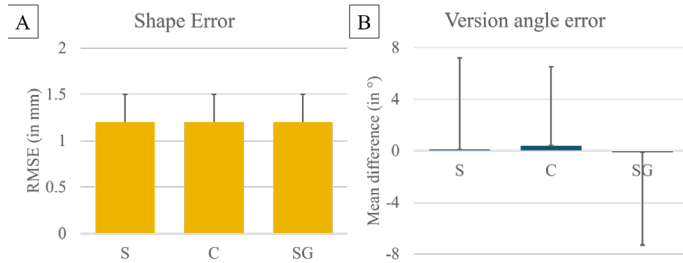
Figure 1: Mean humeral shape (A) differences presented as RMSE + SD and version angle (B) differences presented as mean difference ± SD for the SPM (i.e., the Scapula (S), the Clavicle (C), S without glenoid (SG)).

CONCLUSIONS

The SPM showed comparable results with the literature in predicting pre-injury shape and version angle. Its versatility can handle complex cases involving multiple bone damages or predict multiple bones simultaneously, improving the reconstruction process and reducing healthcare costs. Hence, the SPM represents a valuable tool in surgical planning like shoulder implant positioning or trauma surgery.

ACKNOWLEDGEMENTS

REFERENCES

1. Van Schaardenburgh F, et al., *Bioeng.* **10**:10, 2013
2. Berton A, et al., *J. Clin. Med.* **11**:24, 2022
3. Poltaretskyi S, et al., *BJJ* **99**:927-933, 2017
4. Wu G, et al., *J.* Biomech **38**:981-992, 2005
5. Johnson J, et al., *J. Bone Jt. Surg.* **95**:719-724, 2013
6. Goldberg R, et al., *JSES* **29**:1236-41, 2020

Enhancing Scientific Reproducibility in Biomechanical Studies with Google Colab

[1]Hossein Mokhtarzadeh

[1]Faculty of Engineering and Information Technology, The University of Melbourne, Melbourne, VIC
email: mokhtarzadeh.hossein@gmail.com

INTRODUCTION

Reproducibility is vital in scientific research, but many biomechanical studies struggle due to complex software setups. While data sharing has improved, clear and accessible methods are still lacking. This work highlights the need to share both data and methods in biomechanical research. We introduce a framework using Google Colab and OpenSim to create reproducible models and analyses, accessible online with just an internet connection and a Gmail account. An example project demonstrates the setup and execution of biomechanical simulations. This framework enhances transparency, collaboration, and the reliability of biomechanical research.

METHODS

We developed a reproducible biomechanical analysis framework using Google Colab and the open-source software OpenSim. Detailed in an IPython notebook on GitHub (freely available **here**, the workflow includes installing essential packages, downloading sample C3D files, extracting and printing data, and plotting ground reaction forces (GRFs). For simplicity, we show a basic example, but we have demonstrated OpenSim analyses elsewhere [1].

RESULTS AND DISCUSSION

Using Google Colab, users can analyze biomechanical data without installing software on their PCs. We validated our method by comparing results with Mokka, a free biomechanics analysis software (details in the notebook, not shown here). This approach ensures transparency and collaboration, enhancing the reliability and accessibility of biomechanical research. For more extensive results, see this paper [1] and the freely available notebook **here**. We used no other software; the web-based tools read C3D files, plotted GRFs (Figure 1), and performed complex biomechanical analyses like inverse kinematics, kinetic dynamics, muscle force estimation, and more [1].

CONCLUSIONS

The proposed framework using Google Colab and OpenSim enhances reproducibility in biomechanical studies. It allows researchers to share and access detailed methods and data online without the need for complex software installations.

This method promotes the advancement of biomechanical research through improved transparency and collaboration [1].
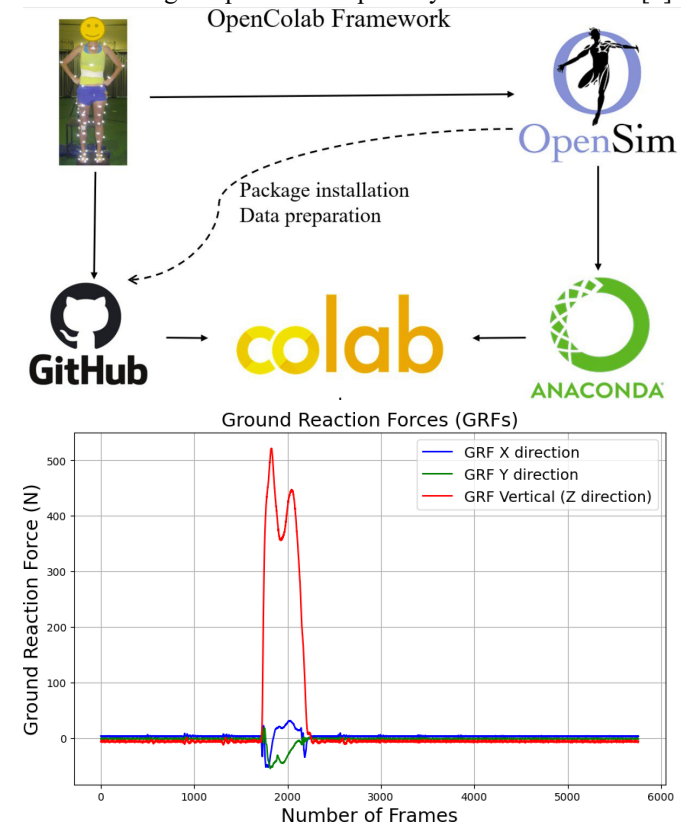
Figure 1: Top: The OpenColab framework integrates motion data analysis and sharing through Google Colab. Bottom: Plot of Ground Reaction Forces (GRFs) over time, showing forces in the X (blue), Y (green), and Z (red) directions across frames.

ACKNOWLEDGEMENTS

REFERENCES

1. Mokhtarzadeh, H, et al. *Computer Methods in Biomechanics and Biomedical Engineering* 26.9: 1055-1063, 2023.

THE BIOMECHANICS OF WALKING WITH MND: A JOINT-LEVEL PERSPECTIVE ON THE LOWER-LIMB

[1]**James L. Williamson***, [2]Cory J. Holdom*, [1]Georgia O'Reilly, [3,4]Robert D. Henderson, [2]Sally Neville, [1,4]Shyuan T. Ngo, and [1,4]Frederik J. Steyn#, [1]Taylor J. M. Dick#

*,#Equal contributions

[1] School of Biomedical Sciences, The University of Queensland, Brisbane, Australia

[2] Australian Institute for Bioengineering and Nanotechnology, The University of Queensland, Brisbane, Australia

[3] Centre for Clinical Research, The University of Queensland, Brisbane, Australia

[4] Department of Neurology, Royal Brisbane and Women's Hospital, Brisbane, Australia

email: j.williamson@uq.edu.au

INTRODUCTION

Motor neuron disease (MND) is a progressive neurodegenerative disease that leads to severe muscle weakness and loss of voluntary motor control [1]. Assessments of gait in people living with MND (plwMND) often focus on gross measures such as stride times and walking speed, which provide limited mechanistic insight into functional decline. Comprehensive gait measures that characterise the body's motions and forces can reveal distinct *movement signatures* that could serve as modifiable targets for future interventions. These measures could also enhance understanding and use of emerging technologies, including actigraphy, as clinical measures of disease progression. The aim of this study was to investigate differences in lower-limb mechanical energetics between plwMND and control populations.

METHODS

We have completed biomechanics assessments in 9 plwMND and 9 controls (UQ HREC approval #2022/HE001787). Participants walked at their preferred speed on an instrumented treadmill (FIT5, Bertec, USA) which measured ground reaction forces. Movements were tracked using a twelve-camera 3D optical motion capture system (Miqus, Qualisys, SWE) with reflective markers on participants' limbs and bony landmarks. OpenSim (v4.4) was used to perform inverse kinematics and kinetics to determine time-varying joint kinematics and kinetics, respectively [2,3]. Time-varying joint powers were determined as the product of joint angular velocities and moments. To determine joint work, the trapezium method was used to integrate joint power over periods of positive and negative work.

RESULTS AND DISCUSSION

plwMND walked at slower speeds (0.62 ± 0.40 vs 1.17 ± 0.14m s^{-1}), with shorter step lengths (0.39 ± 0.19 vs 0.64 ± 0.06m), and reduced step frequencies (41.1 ± 18.4 vs 55.3 ± 5.04 steps min^{-1}) compared to controls (all:$p<0.03$). Lower-limb kinematics were altered in plwMND. Peak ankle plantar-flexion, knee flexion and hip extension were all reduced in plwMND, compared to controls (all:$p\leq0.036$). Analysis of lower-limb mechanical energetics revealed altered ankle mechanics in MND. plwMND showed, on average, a 72% reduction in peak ankle propulsive power and a 67% reduction in positive ankle work, compared to controls (all:$p<0.001$). Despite an increased contribution of the hip to lower-limb total positive work (**Fig. 1**), alterations in knee and hip mechanics were limited in plwMND. Rather than

a redistribution of work across the lower-limb, plwMND may rely on their more proximal joints owing to a reduced capacity of the ankle to produce positive work and power.
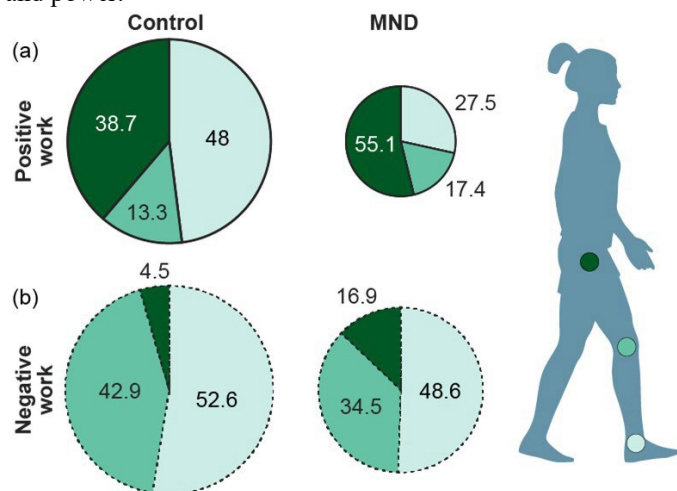
Fig 1. plwMND redistribute work from the distal ankle to the proximal hip, compared to controls. Relative contributions of the ankle, knee and hip to positive (**a**) and negative (**b**) work during preferred speed walking. Data presented is an average of the left and right legs. The size of pie charts is relative to controls.

CONCLUSIONS

We demonstrate unique biomechanical changes in gait in plwMND and identify the ankle as a locus of lower-limb deficits. These results highlight the ankle joint as a potential target for lower limb exoskeletons that aim to improve mobility, and establish unique changes in MND gait that could impact ongoing studies using movement as a biomarker for disease progression in plwMND.

REFERENCES

1. Masrori P, et al., *Eur. J. Neurol.* **27(10)**:1918-1929, 2020.
2. Delp S, et al., *IEEE. Trans. Biomed. Eng.* **54:**1940–1950, 2007.
3. Rajagopal A, et al., *IEEE. Trans. Biomed. Eng.* **63(10):**2068-2079, 2016.

Lower Limb Prosthesis User Gait Symmetry Across Multiple Walking Speeds

John Kerr[1,2], Luca Modenese[1], Key Nahan[1], Lucy Armitage[3], Lauren Kark[1] and Kirsty A. McDonald[1,2]

[1] University of New South Wales, Sydney, NSW, Australia.
[2]Neuroscience Research Australia, Sydney, NSW, Australia.
[3] University of Wollongong, Wollongong, NSW, Australia.
Email: john.kerr@unsw.edu.au

INTRODUCTION

Prosthesis users (PUs) generally exhibit higher metabolic cost of transport (CoT) during gait compared to able-bodied controls [1]. Asymmetric gait characteristics are the frequently postulated culprit. However, asymmetric strategies have been identified as more metabolically optimal in certain pathological populations [2]. When walking at their preferred walking speeds (PWSs), PUs optimise CoT via longer intact limb stance times [3]. Habitual asymmetries of 4.34% (95% CI: 3.54-5.15%) were observed [3], where 0% denotes perfect symmetry and positive values indicate larger intact limb stance time.

During walking, the CoT-speed relationship is generally U-shaped, with the minimum typically aligning with an individual's PWS [4]. It is unclear whether the asymmetries observed by Wedge et al. [3] are present across a range of walking speeds, or whether they are limited to the PWS. We therefore aimed to characterise stance time symmetry across a range of walking speeds in unilateral below-knee PUs.

METHODS

Three unilateral below-knee PUs provided written consent to participate in this study, approved by University of New South Wales Human Research Ethics Committee (HC220783).

Participants performed 5-min walking trials at 0.8 m/s, 1.0 m/s, 1.2 m/s, 1.4 m/s, 1.6 m/s and their assessed PWS on a split-belt, instrumented treadmill (Motek, Netherlands). Ground reaction forces for each limb were collected (1000 Hz). Net metabolic CoT was computed via gaseous exchange data (Cosmed, Italy).

The final minute of each trial was analysed to compute CoT and stance time. Stance time symmetry was calculated using the same symmetry index [5] implemented by Wedge et al., [3].

RESULTS AND DISCUSSION

Data collection is ongoing and will be complete by the time of the conference. As seen in Figure 1, preliminary results indicate a trend towards increased stance time symmetry as walking speed increases. Participant 1 (P1) and 2 (P2) both exhibited longer stance times on their intact limb, consistent with previous work [3], but the discrepancy between limbs was lower at greater speeds. Participant 3 (P3) demonstrated a more symmetrical pattern at all speeds and even favoured the

prosthesis limb more at higher speeds with a symmetry index

of -0.54% ± 1.12% at a walking speed of 1.6 m/s. Almost all stance time symmetry values were lower than the 95% CI interval found in Wedge et al. [3].

PWS of 1.43, 1.16 and 1.16 m/s were recorded for P1, P2 and P3, respectively. While participant PWS was found to align with the lowest experimentally recorded metabolic COT (2.6, 2.0 and 1.9 J/kg/m, respectively), we did not find comparable stance time symmetry observed in Wedge et al. [3]. Of note, P3 did exhibit their most symmetrical gait pattern at their PWS.

Figure 1: The stance time symmetry index was calculated for the last minute of walking data in each walking trial. The shaded region represents the 95% CI band (3.54-5.15%) from Wedge et al. [3].

CONCLUSIONS

The preliminary data suggest stance time symmetry may be influenced by walking speed. The mechanical demands of walking at higher speeds may require PUs to forgo more metabolically favourable stance time asymmetry in order to maintain speed and produce required propulsive forces. Further analysis will be completed on future participants.

REFERENCES

1. Waters R, et al., *J Bone Jt Surg.* **58 (1)**: 42-46, 1976.
2. Roemmich R, et al. *Neurorehab.* **33 (8)**: 602-613, 2019.
3. Wedge R, et al., *Clinical Biomechanics*. **94**, 2022.
4. Ralston HJ. *Int Z Angew Physiol*. **17 (4)**: 277-83, 1958.
5. Dingwell B, et al., *Prosthet Orthot Int.* pp. 101-110, 1996.
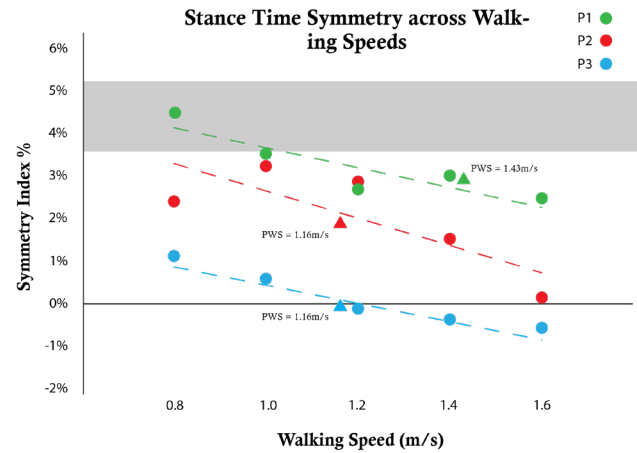
Automatic Segmentation of Shoulder Anatomy from Magnetic Resonance Imaging Using nnU-Net

[1]Maggie May-Hornigold, [1,*]Maxence Lavaill

[1]School of Mechanical, Medical and Process Engineering, Queensland University of Technology, Brisbane, QLD
*e-mail: maxence.lavaill@qut.edu.au

INTRODUCTION

Shoulder patient-specific 3D models empower surgeons with preoperative planning capabilities and facilitate the development of tailored medical devices. These 3D models, including bones and muscles, can be obtained through segmentation of medical images, especially of magnetic resonance images (MRI). However, the segmentation process has been known to be labour- and time-intensive when using usual manual and semi-automatic segmentation techniques [1]. Automatic segmentation methods based on deep learning have the potential to accurately and efficiently segment the whole shoulder musculoskeletal anatomy and democratise 3D shoulder models. Through this project, a range of segmentation methodologies will be investigated, spanning from common manual/semi-automatic approaches to automatic registration-based algorithm and deep learning algorithm (nnU-net [2]), moreover their accuracy and efficiency will be reported.

METHODS

Ten young and healthy individuals were recruited (3M, 7F, 29 ± 5 yo, 165.8 ± 8.2 cm and 58.5 ± 11.5 kg). Each participant underwent an MRI scan session where their right hemithorax (including cervical/thoracic spine and sternum) and right upper extremity were imaged using a 3 Tesla MR scanner (Ingenia, Koninklijke Philips N.V., The Netherlands) at voxel sizes of 0.4 × 0.4 × 0.8 mm using a T1 Dixon sequence.

Four bone (sternum, clavicle, scapula and humerus) and ten muscle (deltoid, trapezius, subscapularis, supraspinatus, infraspinatus/teres minor, latissimus dorsi/teres major, pectoralis major/minor, rhomboid, biceps, triceps) anatomies were semi-automatically segmented by an experienced operator using Mimics 24.0 (Materialise, Leuven, Belgium). The semi-automatic method involved manual segmentation of 1 out of 10 slices, the other 9 slices being interpolated.

Two automatic segmentation techniques were investigated. First, we used Mimics Muscle Segmentation Module (Materialise, Leuven, Belgium) that compares a medical volume against a manually segmented anatomical atlas and evaluates the probability of each voxel to be part of a specific segmentation class. The second automatic method used the 2D configuration of the deep-learning nnU-net algorithm [2]. This nnU-net framework involved prior training of the neural network using a segmented atlas. For both automatic segmentations methods, an atlas of nine manually segmented shoulders were used for training. Moreover, a random individual's (F, 32 yo, 160 cm, 48.3 kg) MRI volume (TEST) was selected for automatic segmentation. Accuracy of the automatic segmentations was assessed using Dice similarity coefficient compared against semi-automatic segmentation and efficiency was reported as total computation time.

RESULTS
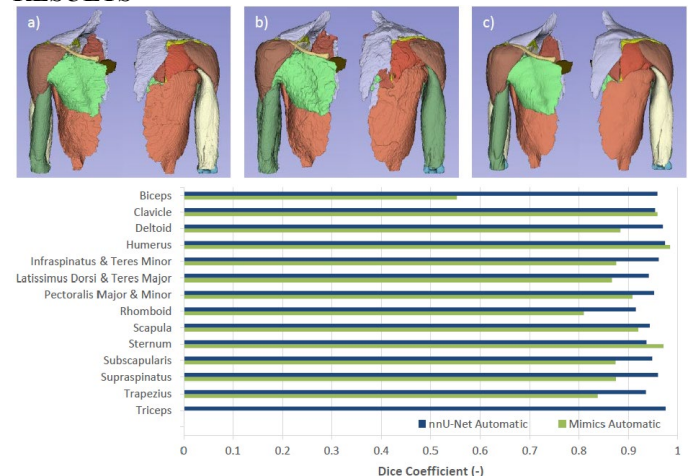
Figure 1: Accuracy of the Mimics and nnU-net automatic segmentation algorithms on the TEST individual. a, b and c) correspond to semi-automatic, Mimics and nnU-net, respectively.

All segmented anatomies exceeded a Dice coefficient of 0.9 using nnU-net as opposed to the Mimics method ranging from 0 (triceps, identified as being part of the biceps) to 0.96 (sternum). Manual/semi-automatic segmentation took 1800 minutes to segment a full shoulder anatomy, Mimics and nnU-net took 294 and 26 minutes, respectively.

CONCLUSIONS

Deep-learning-based nnU-net segmentations outperformed registration-based Mimics segmentation for the tested individual, both in terms of accuracy and efficiency. Future works will involve cross-validation among several individuals and investigating more advanced 3D-high res and cascaded nnU-net algorithms, that may allow complex, patient-specific and accurate 3D shoulder models to be routinely used in clinics.

REFERENCES
[1] Holzbaur et al., *J Biomech*, **40**: 742-749, 2007
[2] Isensee et al., *Nature Methods*, **18(2): 203-211**, 2021

MOVEMENT EFFICIENCY CAN BE MEASURED USING MIXED REALITY

[1]Nikolaos Darras, [1]Anna Murphy, [2]Corey Joseph

[1] Clinical Research Centre for Movement Disorders & Gait Monash Health, Melbourne, VIC
[2]Victorian Paediatric Rehabilitation Service, Monash Health, VIC
email: nikolaos.darras@monashhealth.org

INTRODUCTION
The Direction Translation Protocol (DTP) was proposed by the Gait & Motion Analysis Centre, Athens, Greece, in 2014 as a clinically applicable test to evaluate movement efficiency utilizing equipment commonly found in a gait laboratory [1]. The protocol assesses speed and variability of the centre of mass trajectory during straight line walking and turning which can be completed with a walking aid or done in a wheelchair. With the universal availability of mixed reality (MR) headsets at <$AUS800, adapting and developing protocols for the assessment of ambulation in a variety of environments outside of a gait laboratory will provide clinicians with the opportunity to quantitatively assess rehabilitation outcomes and potentially correlate with falls risk [2]. This initial pilot assessed the feasibility of using MR to apply the DTP.

METHODS
A Meta Quest 2 all-in-one MR headset with controllers, was programmed to create a 2.5 x 0.3 x 0.5m virtual box within a virtual boundary, replicating the DTP (Figure 1). A flexible strap was tied around the participant's waist and a controller positioned at the centre of their waist. The MR headset was comfortably positioned on the participants head who were then orientated to the MR environment. The participants were instructed to stand to the left/right and a step behind the midpoint of the virtual box and instructed to walk around and as close to the virtual box at a steady comfortable pace. Three rounds in a clockwise and anti-clockwise direction were allowed for practice. Data were collected for six full rounds in a clockwise direction followed by six full rounds in an anti-clockwise direction. This was then repeated. Five of the six rounds were extracted for the analysis.

Total, lap and half-lap X-Y trajectory length, total, lap and half-lap time and min/max XY values (medial-lateral and anterior-posterior) were calculated. An algorithm divided the trajectories into straight (2.0m) and turning divisions (0.5m total) to calculate straight time and turning times as a percentage of the half-lap time. Intra-subject Coefficient of Variation (CV) was calculated as a percentage for all variables.

RESULTS AND DISCUSSION
Ten able-bodied participants were recruited (M/F=4/6; age=42±15years; height=1.69±0.09m; weight=73±11kg). Duration including set-up, practice and test was <12min. Table 1, summarizes DTP and Lap Length, Time, Velocity results.
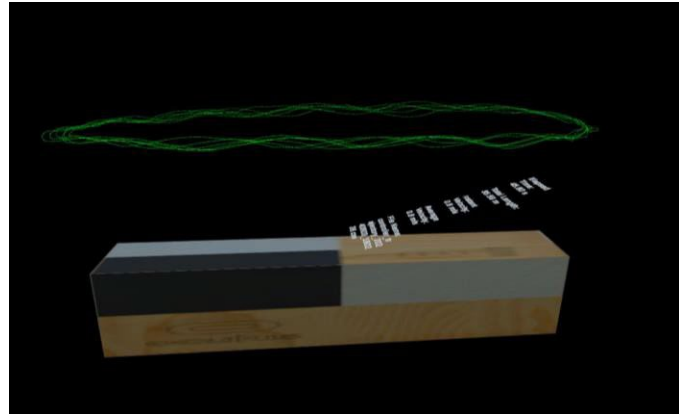
Figure 1: The virtual box is projected on the environment floor. A green line registers the controller's trajectory in the mixed reality 3D view. Immediate feedback of the trajectory length, time and instant and average velocity is displayed above the virtual box.

Table 1: DTP and Lap Length, Time and Velocity.

		Length (m)	Time (s)	Velocity {m/s}
DTP	Average	33.74	36.28	0.95
	SD	1.00	1.52	0.04
	CV	**3%**	**4%**	**4%**
Lap	Average	6.70	7.22	0.95
	SD	0.10	0.23	0.03
	CV	**1%**	**3%**	**3%**

Further investigation assessing the reliability and validity of this tool are required in both able-bodied and impaired populations prior to clinically applying the tool to assess improvements in both balance and walking tasks.

CONCLUSIONS
The DTP using a MR headset was successfully implemented in a convenient sample of able-bodied participants. Only requiring a small area, MR measurement tools have the capability of quickly and easily collecting practical quantitative data to objectively assess movement efficiencies in the clinic in addition to establishing environments to repetitively practice a variety of core movement patterns.

REFERENCES
1. Darras N, et al., *Gait Posture,* **38**:S115.
2. Wolf S, et al., *Phys. Ther.* **79**:1122-1133, 1999.

ABC 14 MELBOURNE

ANZSB
anzsb.asn.au

ASSESSING AN INTRA-SESSION TACKLE TECHNIQUE INTERVENTION IN RUGBY LEAGUE FOR ALTERING HEAD KINEMATICS: A PRELIMINARY ANALYSIS

Oscar Stelzer-Hiller[1], Andrew J. Gardner[1], Kenneth L. Quarrie[2-4], Grant L. Iverson[5] and Suzi Edwards[1]

[1]Faculty of Medicine and Health, The University of Sydney, Sydney, NSW, Australia

[2] New Zealand Rugby, New Zealand; [3] Sports Performance Research Institute New Zealand (SPRINZ), Auckland University of Technology, Auckland, New Zealand; [4] Auckland Bioengineering Institute (ABI), The University of Auckland, Auckland, New Zealand

[5]Department of Physical Medicine and Rehabilitation, Spaulding Rehabilitation Hospital and Harvard Medical School, Boston, MA, USA.

email: Oscar.Stelzer-Hiller@sydney.edu.au

INTRODUCTION

Rugby League is a physically demanding sport associated with a high injury incidence, including concussions, compared to other collision sports [1,2]. Concussions can result from rapid brain acceleration and deceleration, applied indirectly or directly to the head [3]. Approximately 90% of rugby league injuries occur during tackles [4], with direct head collisions the most frequent impact mechanism in concussed tacklers [5]. Injury risk can potentially be modified by an intervention to change player tackling behavior that addresses their capability, opportunity, and motivation [6], in conjunction with the current regulatory approach of coercive intervention (i.e., sanctions) through changes in the laws of the sport (i.e., tackle height) [7,8]. This study aims to determine if altering coaching instructions for traditional tackle techniques can mitigate inertial head kinematics when tacklers contact above or below the level at which the ball-carrier is holding the ball [9].

METHODS

Semi-professional male rugby league players (n=40) wore a full-body retroreflective marker set and performed 3 tackles each of self-selected "over-the-ball" and "under-the-ball" techniques, then received a coaching re-education intervention. Participants received feedback against predetermined tackle technique variables using a constraints-led approach and Aboriginal 8-ways pedagogy, then repeated the protocol [10]. Data was collected via a 16-camera Qualisys motion capture system, analysed in Visual 3D. Preliminary analysis of 17 out of 40 athletes was inputted into a series of generalized linear mixed models to determine if any significant changes (P < 0.05) occurred within the means of any head kinematic variables in the four tackling conditions [9].

RESULTS AND DISCUSSION

Head upward and forward/face up is known to have the lowest propensity for a head injury assessment in the rugby codes [11]. This study shows when participants adhered to the coaches' over or under the ball tackle instructions, there were statistically significant differences in head and neck flexion, in that they positioned their head with less neck flexion and had a more neutrally aligned head (i.e. less lateral neck flexion) compared to when they performed their own tackle techniques without coaching instruction. No significant change was observed in head rotation angles between coaching conditions.

Overall, this study did not alter the peak resultant inertial head kinematics in the preliminary analysis, except in the "over-the-ball" instructed tackle condition compared to the self-selected condition. Results from this preliminary study with semi-professional rugby league players do not support our previous findings from a different competition level, which indicated the instructed technique would reduce peak inertial head kinematics. [9].

CONCLUSIONS

Intra-session coaching effectively modified head position at contact during one-on-one tackles in semi-professional male rugby league players, but it did not alter their peak inertial head kinematics in the first 17 players completing this study. Results from the full study might reveal which specific 3D whole-body kinematics alter inertial head kinematics which could help inform future tackle technique interventions.

ACKNOWLEDGEMENTS

REFERENCES

[1] Glassbrook DJ, et al., *Sports Medicine – Open.* **5**:24, 2019.
[2] Seward H, et al., *Med J Aust.,* **159**(5):298-301, 1993.
[3] Giza CC, et al. *Neurosurg.*, **75**(Suppl 4):24-33, 2014
[4] King D, et al., *Res. Sports Med.*, **20**:86-104, 2012.
[5] Gardner AJ, et al., *Sports Med. Open*, **7**:84, 2021.
[6] Michie S, et al., *Implement Sci.,* **6**:42, 2011.
[7] Raftery M, et al., *BJSM*, **Vol 55**, No 10, May 2021.
[8] Stokes K, et al., *BJSM,* **55**: 220-225, 2021.
[9] Edwards S, et al., *MSSE*, **54**(9):1560-1571, 2022.
[10] Yunkaporta T, Aboriginal Pedagogies at the Cultural Interface: *James Cook University*:2009.
[11] Tierney G, et al., *MSSE*, **50**(3):603-608, 2018

Table 1. Tackler head kinematics (mean ± SD) at contact in one-on-one rugby tackling.

Tackle Instruction		Peak Angular Acceleration (rad/s²)	Peak Linear Acceleration (g)	Flexion (°)	Lateral Flexion (°)	Rotation (°)
Under	**Self-Selected**	320 ± 116	4.5 ± 1.5	-37.0 ± 19.6	-31.7 ±8.0	14.0 ±18.6
	Instructed	405 ± 149	5.2 ± 1.8	-15.5 ± 14.4* (*P*<0.001)	-18.0 ± 8.4* (*P*<0.001)	16.7 ± 14.6
Over	**Self-Selected**	339 ± 185	3.8 ± 1.7	-12.8 ± 15.6	-24.4 ± 9.4	17.5 ± 14.1
	Instructed	396 ± 199	5.0 ± 2.1* (*P*=0.011)	-3.8 ± 13.0* (*P*=0.003)	-14.8 ± 6.2* (*P*<0.001)	17.8 ± 14.5

Note: *Significantly different between self-selected and instructed conditions.

INFLUENCE OF OSSEOINTEGRATED IMPLANT LENGTH ON FEMORAL FRACTURE STRENGTH

Ryan Tiew, Hans Gray, Dale Robinson, David Ackland and Peter Lee

Department of Biomedical Engineering, University of Melbourne, Melbourne, VIC, Australia
email: etiew@student.unimelb.edu.au

INTRODUCTION

Bone-anchored prostheses (BAPs) are gaining wider acceptance as an alternative to socket-suspended prostheses to restore mobility for lower limb amputees [1]. This is because osseointegrated implants used in BAPs avoid some of the shortcomings of sockets such as poor fit and dermal irritation [1], especially in transfemoral amputees. However, up to 5.5% of these implanted femurs fail within the first year of surgery, which is concerning given that femoral fracture risk among socket users is only 2-3% within the first 5 years [2].

Implanted femoral strength is likely influenced by the design parameters of the implant used, which varies by type, length and diameter. Currently, implant selection is largely based on the surgeon's experience, but no study has investigated how these parameters affect femoral fracture strength.

The aim of this study was to investigate how femoral fracture strength varies with the length of an osseointegrated implant used in a transfemoral amputee.

METHODS

A finite element (FE) model of a cadaveric femur (68 M) was constructed from computed tomography (CT) scans. Using a bone mineral density phantom, heterogenous elastic moduli were assigned to the FE model using an established density to modulus power law [3]. Osseointegrated implants of three different lengths were then virtually implanted in three separate resected femur models following surgical guidelines. Unit loads of 1000N and 100Nm were applied at the knee [4] in the anterior, medial, and superior directions (total of 3 forces and 3 moments). The stresses generated from the six FE analyses were then linearly scaled up along the anterior-posterior, medial-lateral, and superior-inferior directions until femoral fracture occurred [4]. The magnitude of load just enough to fracture the implanted femur in all cases were compared.

RESULTS AND DISCUSSION

The strength of the femur-implant construct generally increased as the implant was lengthened for most of the loading conditions investigated (Figure 1). The most notable exceptions to this observation were for the superior and inferior forces, where the fracture load decreased when the implant length was increased from 120 mm to 140 mm, but then increased again when implant length was increased to 160mm. This discrepancy could be the result of the 160mm implant placement, which protrudes into soft trabecular region. The presence of a stiffer

implant could have increased the load bearing capacity in this region and shifted the predicted fracture location elsewhere with more cortical bone. Nevertheless, future work will explore a wider range of implant lengths to determine the cause of this discrepancy.
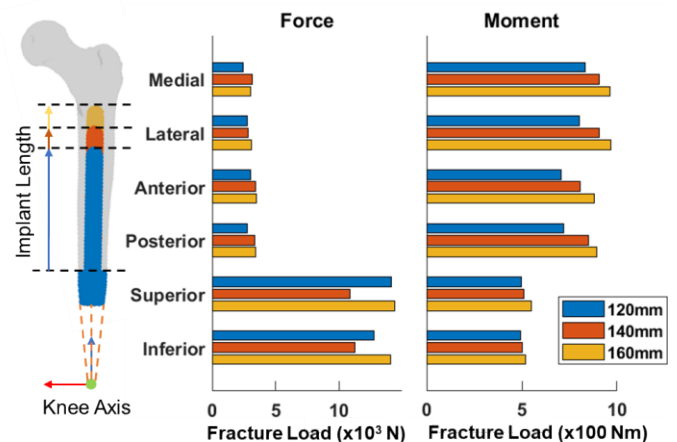
Figure 1: *Left*: Finite element model of a cadaveric femur fitted with osseointegrated implants of different lengths. Loading was applied to the knee axis and transferred to the implant abutment. Bar charts show the magnitude of load (*mid*: forces and *right*: moments) just sufficient to cause fracture.

CONCLUSIONS

In general, longer osseointegrated implants resulted in higher femoral fracture strength. Future work will investigate a wider range of implant lengths and how other design parameters such as implant diameter and type influence femoral fracture strength.

ACKNOWLEDGEMENTS

REFERENCES

1. Hoellwarth J.S., et al., *JBJS Rev,* **8**: 43, 2020.
2. Hoellwarth J.S., et al., *Bone Joint J,* **102-B**:162-169, 2020
3. Morgan E.F., et al., *J Biomech,* **36:** 897-904, 2003.
4. Bergmann G., et al., *PLOS One*, **11:** e0155612, 2016
5. Edwards W.B., et al., *Med Eng Phys,* **34:** 290-8, 2012

ABSTRACT SUBMISSION GUIDELINES FOR THE 2024 ABC-ANZORS MEETING

Effects of Arm-Cycling Exercise during Triceps *Surae* Neuromuscular Electrical Stimulation on Torque Output and Fatigue

[1]Sami K. Alahmari, [2]Lucas B.R. Orssatto, [3]Anthony J. Shield and [3]Gabriel S. Trajano

[1]Department of Physical Therapy, College of Applied Medical Sciences, Taif University (TU), Taif, Mecca, Kingdom of Saudi Arabia.
[2]Institute for Physical Activity and Nutrition (IPAN), School of Exercise and Nutrition Sciences, Faculty of Health, Deakin University, Geelong, VIC, Australia
[3]School of Exercise and Nutrition Sciences, Faculty of Health, Queensland University of Technology (QUT), Brisbane, QLD, Australia.
email: samikhaloufahm.alahmari@gmail.com

INTRODUCTION

These instructions contain information about the abstract Neuromuscular electrical stimulation (NMES) is commonly used in research and therapeutic settings to induce involuntary muscle contractions. This is an effective interventional and rehabilitative method to prevent muscle atrophy when voluntary contractions are unable due to illness or injury [2]. Additionally, wide-pulse (WP) NMES-combined methods such tendon vibration (VIB) have increased motor unit recruitment and torque production [1, 4]. Superimposing rhythmic arm-cycling during lower-body NMES may enhance WP-NMES+VIB-induced responses, especially for patients who cannot freely activate lower limb muscles. During the rhythmic localized motor activity, such as arm cycling, the entire motor system experiences an increased state of excitability [3]. It was hypothesised that ARM-CYC would increase time-torque integral (TTI) and delay neuromuscular fatigue after NMES compared to WP+VIB-NMES alone.

This investigation compared the responses of arm-cycling during triceps *surae* neuromuscular electrical stimulation (NMES) on torque-time integral (TTI) and neuromuscular fatigue in healthy young adults.

METHODS

Achilles tendon vibration (VIB) (110 Hz) coupled with wide-pulse (WP) (1 ms) NMES (WP+VIB) of triceps *surae* alone or in combination with arm-cycling exercise (ARM-CYC) were delivered in two separate sessions in a randomised order (n = 22; 20 men; 29.9 ± 4.4 years). NMES intensity was set to elicit 20% of maximal voluntary isometric contraction (MVC) force. The stimulus pattern was comprised of four sets of 20 repetitions (5 s On and 5 s Off) superimposed to ongoing VIB with a 1-min inter-set interval. TTI was measured for each NMES condition. MVC, voluntary activation level (VAL), peak twitch torque ($Peak_{twitch}$), and peak *soleus* (EMG_{SOL}), medial (EMG_{MG}) and lateral *gastrocnemius* (EMG_{LG}) electromyography were measured before and immediately after each condition.

RESULTS AND DISCUSSION

No significant differences were observed for TTI ($P = 0.371$) between ARM-CYC and WP+VIB protocols. MVC force and $Peak_{twitch}$ torque decreased ($P < 0.001$) immediately after both conditions. No changes were observed for VAL ($P = 0.333$) and EMG_{SOL}, EMG_{LG}, and EMG_{MG} amplitudes ($P = 0.146$).

Contrary to our expectations, ARM-CYC did not provided additional TTI than WP+VIB alone. Both conditions presented similar fatigue levels (i.e., reduced MVC), underpinned by peripheral (reduced $Peak_{twitch}$ torques) but not central mechanisms (i.e., unchanged VAL and EMG amplitudes). These findings suggest no benefit of superimposing ARM-CYC to WP+VIB in order to increase the amount of work produced during a session.
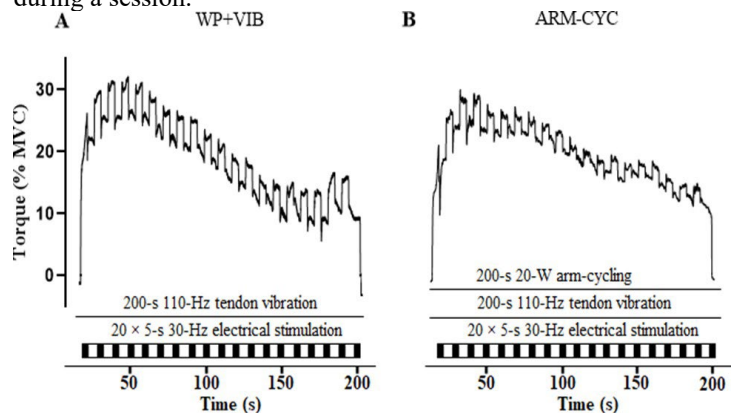
Figure 1: An illustration of the torque trace obtained during the first set for the following experimental conditions: (A) WP+VIB and (B) ARM-CYC. Panel (A) shows a plantar flexor torque trace of contractions elicited by wide-pulse NMES with the superimposition of VIB and panel (B) shows the same

stimulation protocol performed during arm cycling. Note that

VIB elicited sustained contractions during the off phase of the duty cycle that progressively got smaller with repetition.

CONCLUSIONS
Rhythmic arm- cycling in combination with triceps *surae* NMES did not increase TTI compared to WP+VIB. This was accompanied with similar levels of peripheral fatigue with no indicative of central fatigue across both protocols.

ACKNOWLEDGEMENTS

REFERENCES
1. Alahmari, S. K., Shield, A. J., & Trajano, G. S. (2022). Effects of three neuromuscular electrical stimulation methods on muscle force production and neuromuscular fatigue. *Scandinavian Journal of Medicine & Science in Sports*, *32*(10), 1456-1463.
2. Dirks, M. L., Wall, B. T., Snijders, T., Ottenbros, C. L., Verdijk, L. B., & Van Loon, L. J. (2014). Neuromuscular electrical stimulation prevents muscle disuse atrophy during leg immobilization in humans. *Acta physiologica*, *210*(3), 628-641.
3. Forman, D., Raj, A., Button, D. C., & Power, K. E. (2014). Corticospinal excitability of the biceps brachii is higher during arm cycling than an intensity-matched tonic contraction. *Journal of neurophysiology*, *112*(5), 1142-1151.
4. Maffiuletti, N. A. (2010). Physiological and methodological considerations for the use of neuromuscular electrical stimulation. *European journal of applied physiology*, *110*, 223-234.

TEST-RETEST RELIABILITY STUDY OF THREE DIMENTIONAL KINEMATIC GAIT MODELING PARAMENTERS AND ANTROPOMETRIC MEASURMENTS IN OVERWEIGHT OBESE ADULTS WITH KNEE OSTEOARTHRITIS

[1]Yareni Guerrero, [1]Suzi Edwars and [1]Maria Fiatarone Singh
[1]The University of Sydney, Faculty of Medicine and Health, Exercise and Sport Science Discipline Sydney, Australia
email: yareni.guerrero@sydney.edu.au

INTRODUCTION

Three-dimensional (3D) motion optoelectronic systems are identified as a gold standard of practice in research and clinical settings to allow objective and quantifiable 3D biomechanical gait analysis. Marker placement on the specific anatomical points in the human body has been identified as the largest source of variability in 3D biomechanical modelling [1] and may be exacerbated in cohorts where bony landmarks are more difficult to palpate due to overlying adipose tissue (e.g. overweight/ obese populations) or inflammation (e.g. joint effusions/oedema). Thus, the aim of this retrospective analyses was to evaluate whether a published 12-month randomised controlled trial The Train High Eat Low for Osteoarthritis Study (THE LO Study) [2] adhered to the new Australian and New Zealand Clinical Motion Analysis Group (ANZ-CMAG) clinical practice recommendations [1] by evaluating the test-retest reliability of marker placement in overweight/obese adults with medial knee osteoarthritis.

METHODS

Out of the 110 overweight or obese adults with medial knee osteoarthritis enrolled in THE LO Study, it was identified that there was a sub-sample of nine participants who had minimal or nil body weight changes across the three timepoints in this 12-month study and were selected to perform the test-retest reliability analysis (n=6 female, n=3 male participants, BMI at baseline:33.37 (7.23) kg/m²).

Clinical 3D gait analysis was conducted by capturing 3D kinematic and kinetic data (Eagle cameras, Cortex 5 software, Motion Analysis Corporation, Rohnert, CA, USA; three force platforms 9281, Kistler, Winterthur, Switzerland) that was analysed in Visual 3D software (v2022.08, C-Motion Germantown, MD, USA) four years after the last participant's final assessment (analysis conducted between January 2022 to March 2024). Reliability was assessed comparing segment distances (m; n=18); segment angles (º; n=5) and joint angles (º; n=4) within sagittal, frontal and coronal plane across the three timepoints (baseline to 6 months, baseline to 12 months and 6 months to 12 months) counting a total of 135 pairs of variables. Statical analysis included interclass correlation coefficient (ICC) with 95% confidence intervals, mean significant changes via paired sample t-test (P<0.05), Standard Error of Measurement (SEM = SD/$\sqrt{2}$), Minimal detectable difference (MDD = SEM ×1.96×$\sqrt{2}$)] [4], and coefficient of variation (CV = ($\sqrt{mean squared/mean}$) ×100].

RESULTS AND DISCUSSION

Paired sample t-test comparisons showed significant differences (P= <0.05) in 26 out of 135 (19.26%) pairs of variable comparisons: (15 segment distances, 5 segment angles and 6 joint segments). To contextualise the paired sample t-test results by itself would not be sufficient alone as we need to understand the nature and difficulty of the marker placement process, e.g. a 1-cm difference in the measurement from the greater trochanter to the femoral condyle will not reflect a similar magnitude of the error compared to 1-cm difference between the medial and lateral femoral condyles. For that reason, we need to calculate reliability measures such as the CV%. High percentages of variance (CV= <20%) was observed in 25% of pairs of variables.

The ICC also demonstrated low to moderate reliability (ICC= <0.70) in 82 pairs of variables out of the total 135 (61%) measured in this study (29 segment distances, 30 segment angles and 23 joint segments). Birmingham et. al, 2007 [5] reported an ICC of <0.86 in kinematic gait parameters in a similar cohort and this was considered good reliability.

Overall, across the analysis performed by pared sample t-test, ICC, CV and MDD, 67% of 135 pairs of variables were not reliable.

CONCLUSIONS

In identifying the effect of marker placement in a subgroup of nine overweight/obese participants with medial knee osteoarthritis, 67% out of 135 of kinematic gait modelling parameters were not reliable. This demonstrates that the often-forgotten part of a 3D movement data collection is the reliability of marker placement and the immense impact it can have on study outcomes. Although most errors in gait analysis are probably 'acceptable', they are not small enough to be ignored during data interpretation [3]. This reinforces reliability analysis of marker placement must be conducted prior to data collection and if not performed before a study commences should be retrospectively undertaken to ensure high quality 3D clinical gait data. It is recommended that 3D clinical gait researches report their marker placement reliability as a mandatory element in peer-reviewed manuscripts in this field.

REFERENCES

1. Phillips T, et al. *Gait & Posture*.**106**, 2023.
2. Guerrero, et al., Journal of Physiotherapy **61**(4), 2015.
3. McGinley JL, et al., *Gait & Posture*. **29(3)**, 2009.
4. Hopkins WG. Sports Med. **30(1)**:1-15, 2000.
5. Birmingham TB, et al., *Arthritis Rheum*. 7(6), 2007.

Effect of altering ligament-bone attachment bushing stiffness on multibody dynamics simulation of wrist motion.

[1]Zhengxu Cheng, [2]Carl Howard, [3]Michael Sandow and [2]Claire F. Jones

[1] Adelaide Medical School, The University of Adelaide, Adelaide, SA
[2]School of Electrical and Mechanical Engineering, The University of Adelaide, Adelaide, SA
[3]Wakefield Orthopaedics Clinic, Adelaide Calvary Hospital, Adelaide, SA
email: zhengxu.cheng@adelaide.edu.au

INTRODUCTION

The wrist remains a challenging structure for surgeons and researchers to understand, in part due to individual variation in anatomy and consequently mechanics [1]. Computational modelling approaches have the potential to offer individualized analysis and simulations for surgical interventions. Rigid multi-body dynamics simulations can model "parent-child relationships" between bone-to-bone interactions; however, it is challenging to define the mechanics of ligaments and their bony attachments in these modelling environments, such that bony motion is appropriately constrained. The aim of this study was to explore the effect of modelling ligaments using a combination of rigid beams and bushings, where bushings provide translational and rotational degrees of freedom at the ligament-bone interface. Here we report the preliminary modelling outcomes for a single study participant.

METHODS

The right wrist of one participant (male, 27 years) was scanned with high resolution Computed Tomography (CT) in sequential positions (10° increments: neutral to 20° radial deviation; neutral to 40° ulnar deviation), and in neutral by Magnetic Resonance Imaging (MRI), T2 gradient echo sequence [ethics approval H-2024-019]. CT and MRI images were segmented in Materialise Mimics to obtain carpal bone and cartilage geometries, respectively. Carpal bone poses, compared to neutral, for each position were determined by rigid registration of bone geometries, using an iterative closest point rigid registration function 'pcregistericp' in MATLAB (v2023b). MSC Adams (MSC software, Hexagon AB) was used for multibody dynamics modelling. Cartilage geometries were imported into Adams as rigid bodies (density: 1.3 g/cm^3, Poisson's ratio: 0.2). Surface contact was defined between all rigid bodies (penetration depth: 0.1mm, friction coefficient: 0.5 static, 0.2 dynamic). The distal row carpal bones and the triquetrum were 'driven' continuously with kinematic data (interpolated from static poses corresponding to: neutral → 20° radial deviation → neutral → 40° ulnar deviation → neutral), and the motion response of the scaphoid and lunate were simulated. The scaphoid and lunate were constrained by modelled ligaments constructed with solid cylindrical beams joined to the bone surfaces with bushings (MSC Adams native construction). Ligament-to-bone attachment positions corresponded to isometric measurements [2] located within anatomical ligament attachment regions [3]. The ligaments

modelled were: long radial-lunate (LRL), dorsal-scapholunate (DSL), scapho-trapezio-trapezoid (STT), dorsal intercarpal (DIC), and lunotriquetral (LT). Simulated lunate and scaphoid motion (translation, rotation) were measured and the root-mean-squared error (RMSE) between simulated and "real" interpolated kinematics were calculated. Bushing stiffness was varied from 10 to 1×10^6 N/mm, uniformly for all ligaments.

RESULTS AND DISCUSSION

Mean simulated motion (both rotation and translation) error was lowest at a bushing stiffness of 1×10^4 N/mm (Figure 1). Beyond the extremes of the presented stiffness range the simulation was unrealistic: either the scaphoid and lunate did not remain in radial fossa (low bushing stiffness), or relative bone motion could not occur (high bushing stiffness).
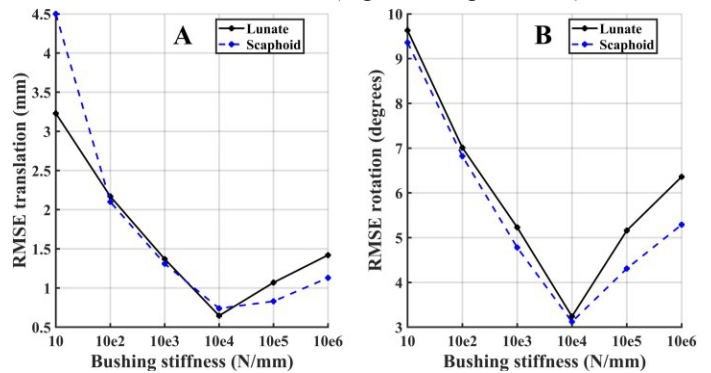
Figure 1: Simulated Lunate and Scaphoid RMSE error vs. bushing stiffness in: A) translation; and B) rotation.

CONCLUSIONS

Using bushings to connect rigid beam element "ligaments" to the carpal geometries provided some control of flexibility throughout the wrist complex in these multibody simulations. Adjusting bushing stiffness appeared to provide higher simulation accuracy than a previous similar multibody model [4]; however, this is preliminary data for a single participant. Ligament-specific tuning of bushing stiffness will be explored as this modelling approach is further refined.

REFERENCES

1. Moojen T, et al., *J Hand Surg Am* **28(1)**: 81-7, 2003
2. Sandow M, et al., *J Hand Surg Eur* **39(4)**: 353-63, 2014
3. Nagao S, et al., *J Hand Surg Am* **30(4)**: 685-92, 2005

4. Fischli S, et al., *J Biomechanics* **42(9)**: 1363-1366, 2009

# Wednesday, December 4

POSTERS DAY 2

COMPUTATIONAL TOOLBOX FOR BONE DEFORMATION MODELLING IN FINITE ELEMENT ANALYSIS OF THE FEMUR TO AID CLINICAL DIAGNOSES AND SURGICAL PLANNING

[1]Alireza Bavil, [1]Emmanuel Eghan-Acquah, [1]Laura Diamond, [1]Rod Barrett, [1]Christopher Carty, [1]David Saxby, [2]Stefanie Feih
[1]Griffith Center of Biomedical and Rehabilitation Engineering (GCORE), Griffith University, Australia; [2]School of Engineering and Build Environment, Griffith University, Australia
email: alireza.yahyaieebavil@griffithuni.edu.au

INTRODUCTION
Paediatric femoral deformities are common disorders requiring orthopedic correction. Finite element analysis (FEA) can be used to optimize these corrective procedures. However, comparative analysis of pre- and post-surgery femur mechanics is onerous. Recently, several open-source toolboxes have been released enabling deformation of typical femur models to approximate specific anteversion (AVA) or neck-shaft (NSA) angles [1,2] and yielding models suitable for rigid-body musculoskeletal modelling. We present a computational toolbox for FEA of the femur, which accepts finite element input (.inp) files and applies gradual torsion/rotation to targeted regions to achieve selected NSA or AVA.

METHODS
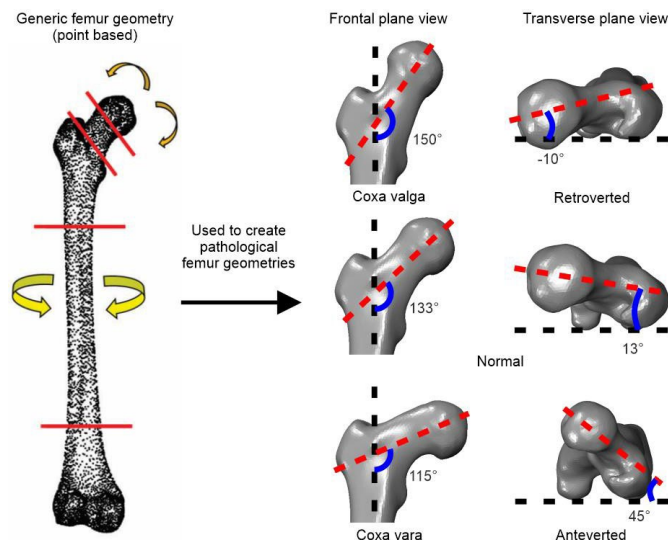
Fig 1. Femoral deformities produced by the deformation toolbox.

A model of the typical femur was obtained by segmenting computed tomography images in Mimics (v25, Materialise, Belgium) and then assigned material properties to the volumetric segmentation. A neuromusculoskeletal model was used to generate personalized loads for FEA of the femur [3] by computing muscle and joint contact forces using an EMG-informed neuromusculoskeletal model [4]. An ABAQUS .inp file was generated for the FE femur model. The deformation toolbox reads the .inp file and registers locations of the individual nodes. For AVA, datum planes are fitted to both ends of the femoral diaphyseal section and the user-specific torsion is gradually applied to interposed nodes. For NSA, neck-shaft axis is estimated and two parallel datum planes perpendicular to the neck-shaft axis are positioned at the femoral neck base and head-neck junction. Gradual transformation is applied to the interposed nodes (Figure 1). To evaluate toolbox accuracy, we specified a set of pathological AVA and NSA targets (Fig 1) and evaluated error between toolbox modified femur geometries and specified deformities. To evaluate suitability for mechanical analysis, toolbox created femurs were subject to personalized motion and loading and resulting bone mechanics scrutinized against normative patterns.

RESULTS AND DISCUSSION
Toolbox created femoral NSA and AVA were produced <30 seconds and had mean error ~2° relative to specified targets. The FEA of deformed femur models resulted in expected stress and strain distributions in femoral neck region (Fig 2).
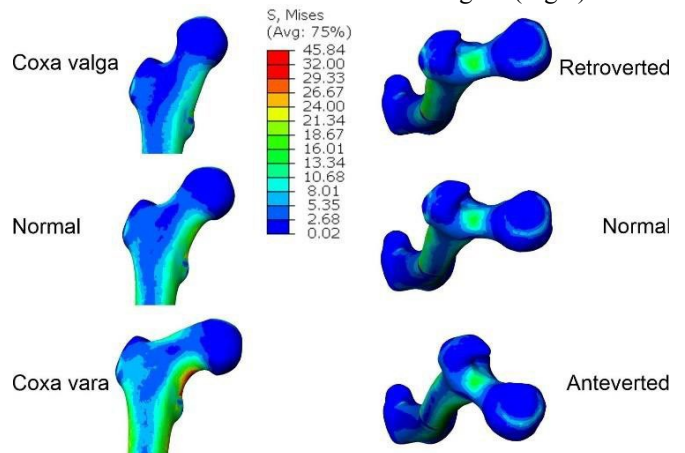
Fig 2: Von Mises stress distribution of a normal femur compared to toolbox created pathological femurs under physiological boundary conditions across walking stance.

CONCLUSIONS
This fast user-friendly toolbox can be used for predictive purposes in the surgical planning of osteotomies to investigate changes in stresses and strains due to changes in bone anatomy.

REFERENCES
1. Modenese L, et al. *Gait Posture,* **88**: 318-321, 2021.
2. Veerkamp, et al. *J Biomech,* **125**: 110589, 2021.
3. Bavil, et al., *Sci Rep*, 14 (**1**): 10808, 2024.
4. Pizzolato, C., et al, *J Biomech,* **48**: 3929-3936, 2015.

HOW KNEE KINEMATICS RELATE TO FUNCTION IN ADULTS WITH KNEE OSTEOARTHRITIS.

[1]Benjamin Carling, [1]Jennie Scarvell, [2]Joeseph Lynch, [3]Catherine Galvin, and [1]Andrew Woodward

[1]Faculty of Health, The University of Canberra, Canberra, ACT
[2]Trauma and Orthopaedic Research Unit, Canberra Health Services, Canberra, ACT
[3]School of Engineering, Australian National University, Canberra, ACT
email: benjamin.carling@outlook.com

INTRODUCTION

Knee osteoarthritis (KOA) is one of the most prevalent causes of functional disability. Osteoarthritis causes a joint to degenerate which impairs how the articulating bones move, thus changing joint kinematics [1]. The tibiofemoral joint experiences kinematic motion in six degrees of freedom [2]. Knees affected by KOA have reduced flexion-extension, internal-external rotation, and anterior-posterior translation range of motion compared to healthy knees [3]. Furthermore, KOA also impairs functional activities such as walking, stair climbing, and sit-to-stand.

While it is evident that KOA impairs joint kinematics and that people with KOA have reduced physical function, it is unclear the relationship between kinematic changes and functional limitations [4, 5]. This study will investigate the relationship between tibiofemoral kinematics in six degrees of freedom captured during a step-up and common physical function.

METHODS

This was a cross-sectional study of 37 participants with KOA. Function tests were the six-minute walk test (6MWT), ten-meter walk test (10mWT), timed up-and-go test (TUG), and five times sit-to-stand test (5STS). Kinematics of the step-up were captured by fluoroscopy, and then 3D multimodal image registration to CT using the software 'Othovis' [6]. This allowed tibiofemoral kinematics to be expressed in six degrees of freedom. Relationships between tibiofemoral kinematics and functional test scores were analysed using multivariable linear regression.

RESULTS AND DISCUSSION

Further 6MWT distance was associated with more femoral anterior translation range between 20° flexion and maximum extension (β=16.86 (7.70)). Femoral anterior translation allows the knee to extend during the last 20° of extension (Figure 1) [3]. Greater translation range may improve knee extension and improve walking endurance measured on the 6MWT.

A faster 10mWT time was associated with more femoral internal rotation range between 50° flexion and 30° flexion (β=-0.45 (0.17)). A faster TUG time was associated with more femoral internal rotation range between 50 flexion° and 30° flexion (β=-0.28 (0.14)). Femoral internal rotation occurs throughout knee extension (Figure 2) [3]. Greater rotation range may improve knee extension and improve walking speed measured on the 10mWT and TUG.

No kinematic variables were found to have a relationship with the 5STS test. Performance on the 5STS test may be more affected than knee extensor muscle strength than joint

kinematics
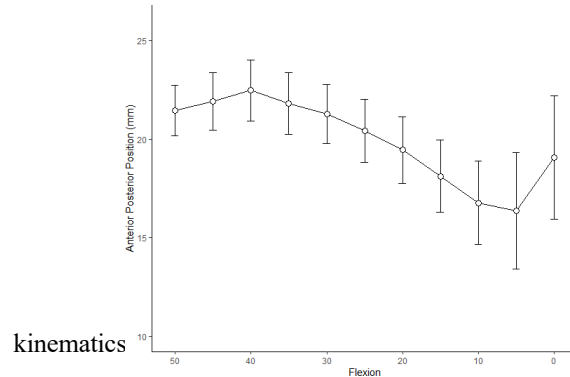
Figure 1: Anterior-posterior translation of the femur during a step-up from 50° into maximal extension

Figure 2: Internal-external rotation of the femur during a step- up from 50° into maximal extension

CONCLUSIONS

Femoral internal rotation and anterior translation range during knee extension have a relationship with functional tests that assess walking. Allied health professionals should consider tibiofemoral kinematics to be a source of walking limitation in people with KOA.

REFERENCES

1. Loeser R, et al., *Arthritis and Rheumatology*, **64**:1697- 1707, 2012.
2. Hirschmann M, et al., *Knee Surgery, Sports Traumatology, Arthroscopy*, **23**:2780-2788, 2015.
3. Scarvell J, et al., *Journal of Biomechanics*, **75**:108-122, 2018.
4. Galvin C, et al., *The knee*, **25**:514-130, 2018.
5. Hodge P, et al., *The Journal of Arthroplasty,* **39**:343-349, 2014.
6. Scarvell J, et al., *Journal of Orthopaedic Research*, **28**:334-340, 2010.
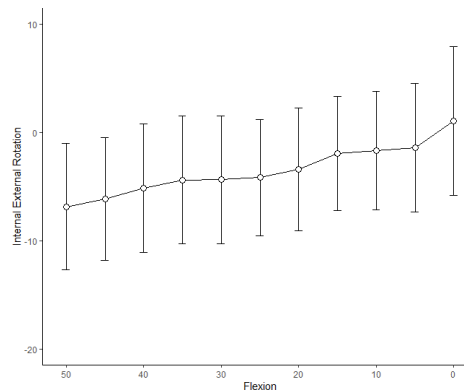
SYNCHRONISATION OF MULTIPLE UNCONNECTED INERTIAL MEASUREMENT UNITS

[1,2,3] Brook Galna, [1] Emily Wood, [3] Steve Griffiths, [4] Daniel Jackson, and [3] Iain Spears

[1] Centre for Health Ageing | School of Allied Health (Exercise Science), Murdoch University, Australia
[2] Centre for Molecular Medicine and Innovative Therapeutics, Murdoch University, Australia
[3] School of Biomedical, Nutritional and Sport Sciences, Newcastle University, United Kingdom
[4] Open Lab, Newcastle University, United Kingdom
email: brook.galna@murdoch.edu.au

INTRODUCTION

Subtle differences of inertial measurement unit (IMU) internal clock speeds can result in desynchronisation when testing for long periods, precluding multi-segment analysis such as interlimb coordination, or the interaction between people or objects. We conducted three experiments to establish the:

- Variation of clock speeds between multiple IMUs over 24 h under static conditions (experiment 1).

- Consistency of relative clock speeds between sessions under static (experiment 2) and dynamic (experiment 3) conditions, and accuracy of correcting for relative internal clock speeds (using corrections derived from experiment 1).

METHODS

Data were collected using 13 IMUs (AX6, Axivity, 100 Hz) taped on a rigid board (Figure 1). Calibration comprised tilting the board several times over 15 s (Figure 2), creating multiple epochs of shared signals between the devices. One IMU was chosen to be the reference ('parent') device which all other 'child' devices were synchronised to. We resampled the data from each device to a shared isochronous timestamp (1000 Hz) to account for sampling errors.
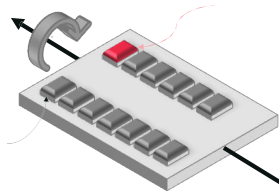
Figure 1: The rigid calibration board with 13 IMUs was tilted several times per calibration to create a shared signal.

Delays between parent and child devices were calculated using normalised cross correlation of angular velocity signals for each calibration. After correcting for initialisation delays (detected at the first calibration), we calculated relative clock speeds using the timing offset at the final calibration divided by the duration between calibrations. For experiment 1 and 2, the IMUs remained attached to the board and static between calibrations. We repeated the process for experiments 1 and 2 under static conditions. For experiment 3, we performed calibrations before

hours of dynamic exercises (IMUs were placed on the head, trunk, lower back, chest, and bilateral upper and fore-arm, and thigh, shank and foot. We then corrected the resampled data from each IMU for experiment 2 (static) and 3 (dynamic), adjusting for differences in relative clock speeds derived from experiment 1.
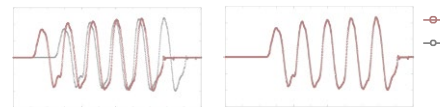
and after participants (n = 44 healthy adults) completed ~2

Figure 2 Example calibration after resampling, and correcting initialisation errors and different internal clock speeds).

RESULTS AND DISCUSSION

Experiment 1: After resampling and correcting for initialisation errors, the shared signals differed between devices by up to 2,829 ms after 24 hours (mean: 247 ms; SD: 1004). Agreement between corrected and predicted timings of five intermediate calibrations (performed between the first and last calibrations) was near perfect (LoA$_{95\%}$: 1.3 ms), suggesting a constant rate of desynchronisation between devices.

Experiment 2: Correcting for relative clock speeds (calculated from experiment 1) resulted in almost perfect synchronisation when applied to experiment 2 data (LoA$_{95\%}$: 3.0 ms at 24 h).

Experiment 3: Correcting for relative clock speeds calculated from experiment 1 resulted in excellent synchronisation after 2 hours of dynamic exercise (LoA$_{95\%}$: 5.8 ms at 2 h).

CONCLUSIONS

Desynchronised data from unconnected IMUs can be corrected by a simple process using two 15 s calibrations performed at the start and end of testing. If collecting data under similar conditions, relative clock speeds corrections can be applied between sessions. Further testing is required to assess the correction technique over longer periods of dynamic activity.

ACKNOWLEDGEMENTS

ESTIMATING BONE MODULUS OF SHEEP MANDIBLE USING INVERSE METHODOLOGY COMBINING FINITE ELEMENT UPDATING METHOD, EX VIVO MECHANICAL TESTING, AND DIGITAL IMAGE CORRELATION

Ben M. Ferguson[1], Ali Kiapour[2], Jonathan R. Clark[3,4,5], Qing Li[1]

1. School of Aerospace, Mechanical and Mechatronic Engineering, The University of Sydney, NSW 2006, Australia
2. Department of Neurosurgery Massachusetts General Hospital, Harvard Medical School, Boston, MA, USA
3. Department of Head and Neck Surgery, Chris O'Brien Lifehouse, Sydney, NSW 2050, Australia
4. Central Clinical School, Faculty of Medicine and Health, The University of Sydney, NSW 2006, Australia
5. Royal Prince Alfred Institute of Academic Surgery, Sydney Local Health District, Sydney, NSW 2050, Australia

Email: Ben.Ferguson@sydney.edu.au

INTRODUCTION

The mechanical properties of sheep mandible bone tissue are crucial inputs required for developing a finite element (FE) model of a reconstructed sheep mandible. This research addresses the lack of published data by estimating the cortical bone modulus of a sheep mandible specimen using an inverse methodology. This approach combines *in silico* computed tomographic (CT)-based modelling, the FE updating method, *ex vivo* whole bone mechanical testing, and digital image correlation (DIC) deformation profile measurements. The FE model assumes that the cortical bone is homogeneous, isotropic, and linear elastic, allowing the cortical bone Young's moduli to be represented by a single value for the whole mandible, referred to as the 'bone modulus'.

METHODS

First, a CT-based FE model of an intact sheep mandible under 150 N load with the condyles embedded in a block of casting resin is developed. Using the FE updating method, twelve simulations are run to compute the deformation profiles for the range of bone modulus values from 4 GPa to 15 GPa in increments of 1 GPa. A two-camera DIC setup is used to measure the 3D deformation profile of the *ex vivo* sheep mandible. The *ex vivo* experiment is simulated computationally by applying an equivalent virtual load in the FE model. Next, the image of the DIC-captured deformation is spatially aligned with each of the images captured within the *in silico* virtual environment. Each pair of images is compared by their pixel similarity percentage, determined by the number of identical grayscale values at each pixel coordinate.

Second, a pair of defects are created by surgical excision of bone from the intact *ex vivo* sheep mandible; one defect is located on one side of the mandible along the inferior border of the ramus, and the other located symmetrically on the other side of the mandible. Both defects are reconstructed with site-specific one-body scaffold-based bone implants. The same DIC experiment performed on the intact *ex vivo* mandible is repeated on its reconstructed version. The FE model of the reconstructed mandible, now having the estimated bone modulus input value, predicts the deformation profile. The DIC measurements are similarly compared with the deformation profile predicted by the FE model of the reconstructed sheep mandible.

RESULTS AND DISCUSSION

Figure 1 shows the process of comparing the DIC-measured deformation data of the intact sheep mandible with each of the FE model-predicted output images for the range of bone modulus values. A polynomial function is fitted to the data, and the peak of the curve, representing the maximum pixel similarity percentage, corresponds to a bone modulus of 9.5 ± 0.5 GPa.
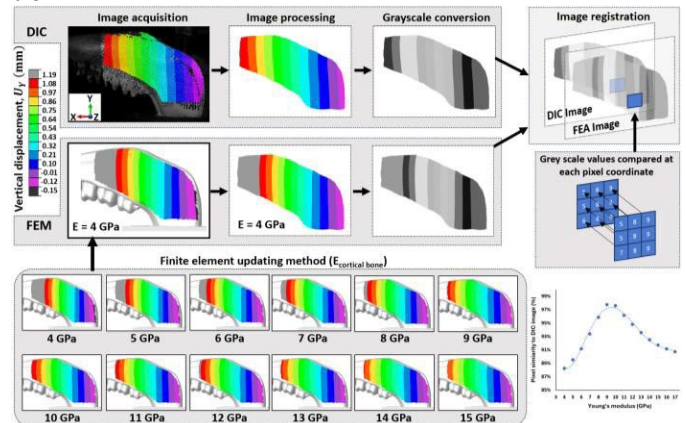
Figure 1: Images of the distributions of vertical displacements from DIC camera and FE-predicted outputs.

The deformation profile predicted by the FE model of the reconstructed sheep mandible and the *ex vivo* DIC-measured profile had a total pixel similarity of 98%, which confirms the validity of the FE model.

CONCLUSIONS

This study is anticipated to provide fundamental mechanical property data of sheep mandible host bone and a validated FE model for a scaffold implant design optimisation study [1] and surgical planning risk assessment for an *in vivo* sheep trial [2].

REFERENCES

1. Ferguson BM et al., *J. Mech. Behavior Biomed. Mater*; 2024, [preprint] https://ssrn.com/abstract=4843981
2. Xin, Ferguson, Wan, et al. *ACS Biomater. Sci. Eng.* 2024, **10**, 5, 2863–2879. https://doi.org/10.1021/acsbiomaterials.4c00262

225

NON-INVASIVE ESTIMATES OF NEUROMUSCULAR PROPERTIES USING ULTRA-WIDEBAND RADAR

[1,2]Christopher S. Bird, [3]Antonio P. L. Bo, [2]Wei Lu and [1]Taylor J. M. Dick

[1]School of Biomedical Sciences, The University of Queensland, St Lucia, QLD
[2]Australian e-Health Research Centre, Commonwealth Scientific and Industrial Research Organisation (CSIRO), Herston, QLD
[3]Department of Mechanical, Electrical and Chemical Engineering, Oslo Metropolitan University, Oslo, Norway
email: christopher.bird@uq.edu.au

INTRODUCTION

Although we can easily measure the external forces generated by multiple skeletal muscles during movement, obtaining direct *in vivo* measurements of muscle force is highly invasive and generally not feasible in humans [1]. Instead, estimates of muscle forces based on non-invasive measures are particularly attractive. Here, we test the capacity of ultra-wideband (UWB) radar as a potential non-invasive technology to indirectly estimate muscle forces, by measuring changes in the electromagnetic properties of the quadriceps muscles during isometric knee extensions across a range of activation levels.

METHODS

Sixteen participants (f=6, m=10, age 19-34) completed voluntary isometric knee extension contractions with their knee positioned at 110°. Joint torque was measured using a 3-axis load cell, and participants were provided biofeedback to follow a time-varying force curve with intermittent contractions of intensity up to 45% MVC (maximum voluntary contraction) for 20 minutes. UWB radar sensors were placed centred over vastus lateralis (VL) and vastus medialis (VM), with scans recorded synchronously with load cell sampling (10Hz). Surface electromyography (EMG) of VL and VM sampled at 2048Hz was used to monitor for changes in load sharing and muscle fatigue (via changes in EMG amplitude). Long short-term memory (LSTM) machine learning models were trained with a 70/15/15 train/validate/test split on individual participant's data to predict muscle force from the UWB radar scan data.

RESULTS AND DISCUSSION

LSTM machine learning models trained on individual participant data were successful in estimating muscle forces, although there was some variation in model accuracy among participants, with outliers of lower accuracy in P07 and P16 (Table 1). Figure 1 shows the predicted and actual forces for participants P01 and P04.

While the specific physiological mechanisms behind the changes in the UWB radar signal remain unknown, these results provide promising cause for further investigation into the use of this technology for non-invasive estimation of muscle forces.
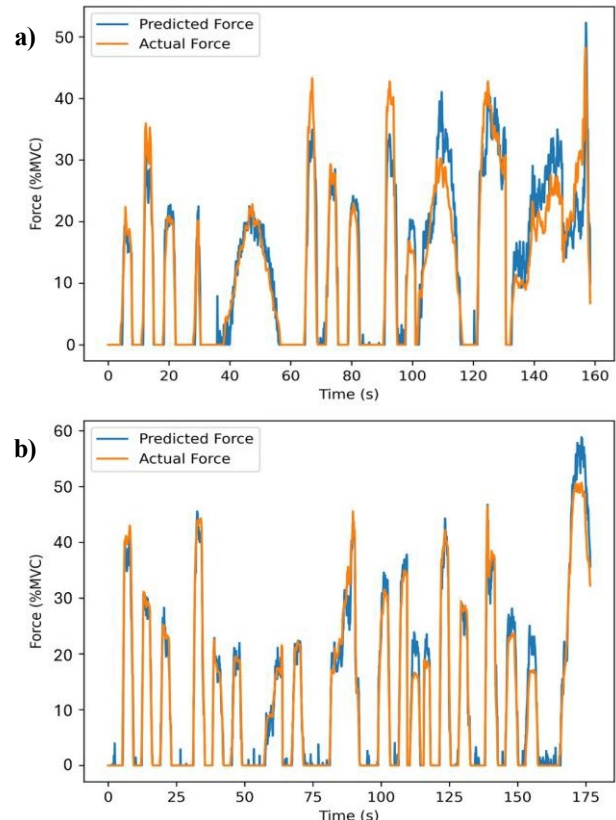
Figure 1: LSTM predicted normalised force test output (blue) compared to actual normalised force (orange) for participants: **a)** P01 (R^2=0.902), and **b)** P04 (R^2=0.973).

CONCLUSIONS

Ultra-wideband (UWB) radar has been demonstrated as a potentially viable novel technology to non-invasively estimate skeletal muscle forces. Future studies will investigate the physiological mechanisms responsible for the changes in the radar signal, as well as the use of this technology with other muscle groups and during dynamic muscle contractions.

REFERENCES

1. Komi P V, *J Biomech*. **21**(1):23-34, 1990.

Table 1: Coefficient of determination (R^2) for predicted and actual force across participants. Median 0.921, Mean 0.905, SD 0.063.

PID	P01	P02	P03	P04	P05	P06	P07	P08	P09	P10	P11	P12	P13	P14	P15	P16

| R^2 | 0.902 | 0.908 | 0.897 | 0.973 | 0.949 | 0.890 | 0.708 | 0.923 | 0.950 | 0.957 | 0.921 | 0.920 | 0.895 | 0.925 | 0.952 | 0.806 |

Optimal Control Simulations Tracking Wearable Sensor Signals Provide Comparable Running Gait Kinematics to Marker-Based Motion Capture

[1]Grace McConnochie, [3]Aaron Fox, [2]Clint Bellenger, [1]Dominic Thewlis

[1]Centre for Orthopaedic Trauma and Research, Adelaide Medical School, University of Adelaide
[2]Alliance for Research in Exercise, Nutrition and Activity (ARENA); University of South Australia
[3]Institute for Physical Activity and Nutrition Research, School of Exercise and Nutrition Sciences, Deakin University
Email: g.e.mcconnochie@gmail.com

INTRODUCTION

Inertial measurement units (IMUs) are an increasingly popular modality for collecting biomechanical data outside the constraints of the laboratory environment. However, IMU based joint kinematics are subject to errors from signal noise and drift, soft tissue artefacts, device calibration, and model scaling [1]. Hence, data collection has been predominantly limited to controlled laboratory environments or involved few isolated outcome measures. Optimal control simulations can combine a predictive and tracking approach to modelling gait - including physiologically based objectives of locomotion, and having less reliance on error-prone experimental data [2]. Integrating IMU data with optimal control simulations holds the potential to enhance the accuracy and applicability of gait analysis in real-world settings. The aim of this study was to compare two IMU-based modeling approaches (inverse kinematics and optimal control simulations) with optical marker-based motion capture in reconstructing running gait kinematics. It was hypothesized that an optimal control approach would produce greater fidelity in outcomes compared to inverse kinematics at the expense of greater computational costs and time.

METHODS

The study protocol was approved by our local HREC (REF here). All participants provided written informed consent. Gait data were collected on six participants running on a treadmill at three speeds between 8 and 14 km/hr. Eight Blue Trident IMUs (Vicon Motion Systems Ltd, Oxford, UK) were attached to the torso and lower limbs. Simultaneous optical marker-based motion capture data were collected with a 10-camera Vicon 4.2 Vantage V5 system at 100 Hz. Sensor orientations on the subject were calculated from two static poses. The 3D OpenSim model was scaled using statistical shape modeling (MAP Client), via anatomical landmarks on a skeletal mesh fitted to the LiDAR point cloud of the subject [3]. The objective of the optimal control simulations was to track the accelerations, angular velocities, and orientations (from offline signal fusion) of eight sensors with simulated signals from the model sensors. Additional constraints, reflecting physiological and biomechanical principles and targeting dynamic consistency were enforced, and ground contact was modelled using eleven Hill-Crossley foot contact spheres. A tracking simulation of generic running kinematics served as the initial guess, with a low weight placed on these kinematics in the simulations. The objective of IMU-based inverse kinematics was to minimize differences between input and simulated sensor orientations.

RESULTS

266 out of 277 optimal control simulations converged on a solution, with three outliers removed for not resembling running gait. Mean computational times for optimal control simulations were 46 ± 60 min and 0.32 ± 0.06 min for IMU-based inverse kinematics. Compared to motion-capture, optimal control simulations had lower absolute errors in joint angles (RMSE 7°±1, range: 4-12°) that were consistent across all speeds. IMU-based inverse kinematics exhibited greater differences with motion capture compared to optimal control simulations (RMSE 10°±1, range: 4-26°), with errors more significant at faster speeds. Both methods showed the largest inaccuracies in sagittal angles. IMU-based inverse kinematics had greater errors than optimal control simulations in 10 out of 11 joint angles, with errors up to 26° in knee flexion. Considering joint range of motion, normalized errors were smallest in knee flexion for optimal control simulations.

CONCLUSIONS

An optimal control approach employing a scaled musculoskeletal model with a hybrid objective function combining IMU tracking and effort terms provided a more comparative representation of optical motion capture joint kinematics than IMU-based inverse kinematics. This highlights the potential of optimal control methods to provide a comprehensive understanding of gait across diverse applications. Incorporating constraints that reflect physiological and biomechanical principles and target dynamic consistency enhances the realism and reliability of simulations. Moreover, this approach can estimate outputs such as joint and ground reaction forces, and muscle forces, enhancing its utility. IMU-based inverse kinematics remains a viable option for faster computation times, and when model fidelity (e.g. dynamic consistency) is less of a concern.

REFERENCES

1. Weygers I et al. Sensors 20(3): 673, 2020
2. Dembia C et al. Comput. Biol.16(12): 2020
3. McConnochie, G et al. SSRN.
   https://doi.org/10.2139/ssrn.4860098

PRE-OPERATIVE EQ-5D-5L IS A STRONG PREDICTOR OF MEANINGFUL IMPROVEMENT IN QUALITY OF LIFE FOLLOWING PRIMARY TOTAL KNEE ARTHROPLASTY

[1]FJ McCabe, [1]J Davies, [1]C Doran and [1]JP Cashman

[1]Department of Orthopaedic Surgery, National Orthopaedic Hospital Cappagh, Dublin, Ireland
Email: jamesgdavies6@gmail.com

INTRODUCTION
Despite rapid growth in total knee arthroplasties performed worldwide, a significant proportion of patients are not satisfied with the outcome of their surgery [1]. Patient reported outcome measures (PROMS), such as the EQ-5D-5L, can be used to assess quality of life and knee function in these patients. Our hypothesis was that pre-operative EQ-5D-5L could predict the likelihood of a patient achieving post-operative improvement in PROMS to a level of minimum clinically-important difference (MCID).

METHODS
This was a retrospective analysis of a prospective cohort of total knee arthroplasty patients. EQ-5D-5L and Oxford Knee Scores were recorded pre-operatively, 6 months and 2 years post-operatively. The primary outcome measure was achievement of MCID in EQ-5D-5L at 2 years. Multivariable analysis through multiple logistic regression was performed to assess for independent predictors of MCID in EQ-5D-5L, OKS and re-operation at 2 years.

RESULTS AND DISCUSSION
400 patients were included in this study, with 57% female, mean age of 66 years and a mean BMI of 32. Pre-operative EQ-5D-5L was the only strong predictor of post-operative EQ-5D-5L MCID (OR: 0.016), when controlling for age, gender, BMI, ASA, smoking status and surgeon grade. The receiver operator curve had AUC of 0.76. The optimal pre-operative EQ-5D-5L threshold was found to be 0.53, with a sensitivity of 70% and specificity of 73%.
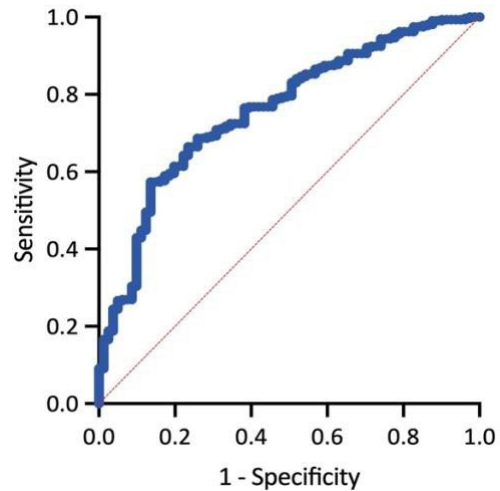
Figure 1: Receiver operator curve for ability of pre-operative EQ-5D-5L to predict MCID improvement EQ-5D-5L at 2 years

CONCLUSIONS
Pre-operative quality of life as measured by EQ-5D-5L is a strong independent predictor of reaching MCID in EQ-5D-5L following total knee arthroplasty. Those with worse EQ-5D-5L are more likely to gain meaningful benefit from knee replacement, with an optimal threshold of 0.53.

REFERENCES
1. DeFrance MJ, Scuderi GR. Are 20% of Patients Actually Dissatisfied Following Total Knee Arthroplasty? *J Arthroplasty* 2023; **38**, 594-9.

Table 1. Multivariable analysis for independent predictors of MCID in EQ-5D-5L at 2 years post-operatively

Variable	Odds Ratio	95% CI	P value
Pre-operative EQ-5D-5L	**0.016**	**0.004 to 0.06**	**<0.0001**
Age*	**0.97**	**0.94 to 0.9986**	**0.0456**
Female gender	0.93	0.54 to 1.62	0.81
Smoking status	0.87	0.32 to 2.85	0.81
ASA	1.4	0.86 to 2.3	0.18
BMI	0.98	0.93 to 1.03	0.40
Surgeon grade	1.20	0.70 to 2.10	0.51

* Not clinically significant

IDENTIFICATION OF NOVEL SMALL-MOLECULE MODULATOR OF SORTING NEXIN 10 TO INHIBIT OSTEOCLASTIC BONE RESORPTION

[1,2]Yihe Li, [3]Haiming Jin, [2]Ariela Samantha, [4]Ruth Seeber, [4]Kevin Pfleger, [1]Kai Chen, [2]Alice Vrielink, [1]Jiake Xu

[1]School of Biomedical Sciences, The University of Western Australia, Australia, Perth, WA
[2]School of Molecular Sciences, The University of Western Australia, Australia, Perth, WA
[3]Department of Orthopaedic Surgery, The Second Affiliated Hospital and Yuying Children's Hospital of Wenzhou Medical, Wenzhou, China
[4]Molecular Endocrinology and Pharmacology, Harry Perkins Institute of Medical Research, QEII Medical Centre, Perth, WA
email: yihe.li@research.uwa.edu.au

INTRODUCTION

Current antiresorptive agents reduce bone loss by inhibiting the formation and functions of osteoclasts, which has potential side effects due to their decoupling activity on osteoblasts through inhibiting osteoclast formation, necessitating the development of novel treatment. Sorting nexin 10 (SNX10) plays a crucial role in osteoclast function and bone homeostasis, mutations in *SNX10* are associated with autosomal recessive osteopetrosis [1]. This study aimed to discover novel small molecules targeting SNX10 as a potential drug candidate for osteoporosis treatment.

METHODS

We screened lead compounds from a library of several million compounds using a multi-step approach combining artificial intelligence (AI)-driven virtual screening with high-throughput screening methods, and identified novel binding partners of SNX10. Subsequent in vitro functional assays were carried out to examine the effects of lead compounds on osteoclast differentiation and function, and the results were further validated in vivo using an ovariectomised mouse model. We also conducted quantitative PCR, Western blot analysis, and immunofluorescence assays to explore the underlying molecular mechanisms. Additionally, in silico docking analysis was performed to elucidate the binding model between SNX10 and the compound.

RESULTS AND DISCUSSION

Our results demonstrated that AW-006 effectively inhibited bone resorption *in vitro* and prevented bone loss *in vivo*, without disrupting osteoclast formation. Mechanistically, AW-006 targeted SNX10 through its PI3P binding site, modulating its interaction and colocalisation with RAB7 *in vitro* and enhancing the expression of osteoclast marker genes (Figure 1).
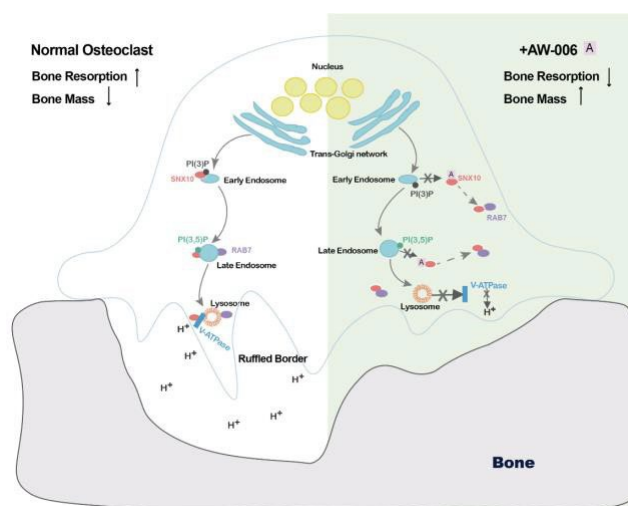
Figure 1: Proposed mechanism for AW-006-mediated inhibition of bone resorption via the endo-lysosomal pathway. This schematic illustrates how the SNX10 PPI inhibitor AW-006 potentially interferes with the endo-lysosomal pathway in osteoclasts, leading to reduced bone resorption.

CONCLUSIONS

In conclusion, our study identified a novel small molecule AW-006 as a promising anti-resorptive candidate without suppression of osteoclast formation and decoupling of osteoblast activity. These findings also provided new insights into SNX10's molecular interactions and indicated that SNX10 could serve as a promising therapeutic target for osteoporosis treatment.

ACKNOWLEDGEMENTS

REFERENCES

1. Pangrazio A, et al., *J Bone Miner Res*. **28(5)**:1041-9, 2013.

RELEVENCE OF BILATERAL ASYMMETRY FOR MIRROR RECONSTRUCTION TECHNIQUES IN THE MANAGEMENT OF DISTAL TIBIAL FRACTURES

[1,2]Laura A. B. Wilson, [3]Gerard Bourke, [3,4]Joseph Lynch and [3,4]Paul N. Smith

[1] School of Archaeology and Anthropology, The Australian National University, Canberra, ACT, Australia
[2] School of Biological, Earth and Environmental Sciences, UNSW Sydney, Sydney, NSW, Australia
[3] School of Medicine, The Australian National University, Canberra, Australia
[4] Trauma and Orthopaedic Research Unit, The Canberra Hospital, Canberra, Australia
[5] School of Engineering, The Australian National University, Canberra, ACT, Australia
email: laura.wilson@anu.edu.au

INTRODUCTION

Tibial plafond fractures often involve the articular surface, which makes them challenging to treat and increases the risk of post-operative complications [1, 2]. Mirror reconstruction techniques use the uninjured side as a model for pre-operative planning and plate shaping, to improve the fit of the plate by individualizing the design workflow. This approach assumes bilateral asymmetry is negligible, with limited evidence. To test this assumption, we quantified bilateral asymmetry and patterning of variation across the distal tibia, and assessed the relationship between bilateral asymmetry, age, and sex.

METHODS

A total of 93 (46 female, 47 male) bilateral CT scans of healthy individuals who had undergone lower limb CT imaging were collected from The Canberra Hospital Radiology database.
Segmentation of the CT images was performed by semi-automated segmentation using 3D Slicer version 5.2.2 and 3D models were extracted, and then aligned using iterative closest point alignment (5000 iterations) with cloud compare version 2.1.3. Nine landmarks were chosen to provide an accurate representation of the distal tibia structure (Figure 1). The inferior surface of the tibia was divided into three regions, an anterior, medial, and lateral region in alignment with the four-column classification of tibial plafond fractures (Figure 1A). Left-right distances between landmarks were extracted from each 3D model. Linear regression was used to assess the relationship between asymmetry and age, morphological disparity was used to quantify variance at each landmark, and group differences in left-right distances were tested using t-tests, and ordinated with Principal Component Analysis.

RESULTS AND DISCUSSION

Our results demonstrate a low magnitude and similar patterning of bilateral asymmetry in the distal tibia for both males and females. Contra to expectations, we find that age is not related to changes in the magnitudes of bilateral asymmetry. Left-right difference was on average less than 1 mm. The patterning of asymmetry appeared to mostly cluster around the lateral aspect of the distal tibia and the inferior articular surface (IAS). The IAS receives compressive bone contact forces from between

four to 13.5 times body weight during locomotion [3, 4]. Given the established gait asymmetry during locomotion in healthy human subjects, a high degree of tibial asymmetry around the IAS may be expected. The larger magnitude of asymmetry may reduce the efficacy of pre-operative planning and plate shaping for antero-lateral and posterior-lateral tibial plafond fractures, when asymmetry is clinically significant.
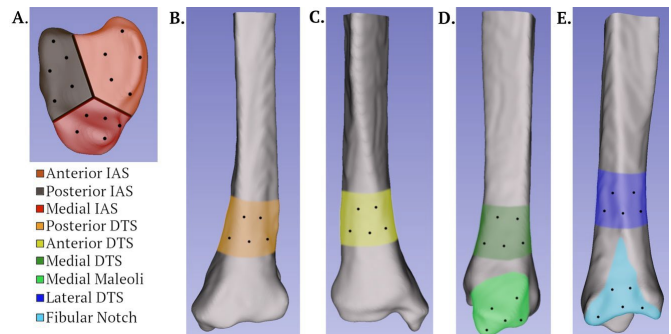
Figure 1: Anatomical landmarks (black points) and regions (coloured) for evaluation of bilateral asymmetry. Labels are, Inferior articular surface (IAS) and Distal Tibial Shaft (DTS).

CONCLUSIONS

Our findings of low magnitudes of bilateral asymmetry indicate that the use of the contralateral distal tibia in the implementation of mirror reconstructive surgery is likely to be an effective method in healthy individuals in middle and late adulthood,

ACKNOWLEDGEMENTS

REFERENCES

1. Millar S, et al., *Injury.* **49**:473-490, 2018.
2. Yao P, et al., *International Orthopaedics.* **46**:2153-2163, 2022.
3. Sasimontonkul S, et al., *J. Biomech.* **40**:3503-3509, 2007.
4. Walker E, et al., *J. Biomech.* **133**:110969, 2022

THE DESIGN AND VALIDATION OF AN APPARATUS FOR BIOMECHANICAL TESTING OF PATELOFEMORAL AND KNEE JOINTS USING A ROBOTIC TESTING PLATFORM

[1]A. Mounir Boudali, [1]Jobe Shatrov, [1,2]Koki Abe, [1]Marcus Zavala, [1]David Parker, [1,2]William L. Walter, and [1,3]Elizabeth Clarke

[1] Sydney Muskuloskeletal Health, Kolling Institute, Faculty of Medicine and Health, University of Sydney, Sydney, NSW
[2] Department of Orthopaedics and Traumatic Surgery, Royal North Shore Hospital, St. Leonards, NSW
[3] Murray Maxwell Biomechanics Laboratory, Kolling Institute, Northern Sydney Local Health District, St. Leonards, NSW
email: Elizabeth.clarke@sydney.edu.au

INTRODUCTION

After Total Knee Arthroplasty (TKA), between 33-54% of patients report ongoing symptoms or functional problems [1]. These patients often experience reduced range of motion (ROM) and significant kinematic discrepancies in gait analysis studies [2], indicating that despite surgical intervention, many continue to face challenges in regaining optimal knee function and normal gait patterns. Soft tissue structures in the knee joint play a crucial role in maintaining joint stability, flexibility, and overall function. Some of these structures run from the hip joint to the tibia making biomechanical studies of the knee joint challenging. Here we describe a testing apparatus for the study of knee joint biomechanics on cadaveric specimens, designed to preserve the hip joint and the foot, and allow the tracking of the patellar bone. This system was tested and validated on the simVITRO platform (Cleveland Clinic, Ohio, USA).

METHODS

The simVITRO platform uses a software to control an industrial robot to perform custom and pre-defined motion trajectories in both force and position control. It also collects and processes data from a motion capture system to provide tracking data in the testing joint coordinate system. Furthermore, to perform arthroplasty using CORI navigation system (Smith+Nephew, London, UK), it is necessary to preserve the hip joint to allow the registration of the patient's anatomy. A testing apparatus was designed to allow for the preservation of the pelvis as well as the foot to satisfy the requirements of both systems. The testing jig [3] is made of three elements: (1) the femoral clamp is made of a base that forms 30 degrees with transverse plane, allowing for deep nee bend (120deg) without the tibia colliding with the mounting pedestal (Figure 1). It also comprises a minimum of three rings that can be positioned along the mounting plate. The rings are made of two halves secured with two bolts. Each half rings incorporates a series of M8 holes allowing for the insertion of securing bolts that form contact with the femur bone. (2) The tibia clamp is made of base, and a cylinder split in half which allows the clamping of the tibia without the need to remove the foot. Each section has similar features to the femur rings. (3) The patella tracker is made of a plat that mounts on the patella with two small screws and an L shaped plat holding four reflective markers that attaches to the plate using two sets of magnets. This feature allows for the removal of the marker set when performing surgery.

We acquired a fresh-frozen pelvis-to-toe human cadaver specimen to test and validate the testing apparatus. Ethics approvals were obtained to conduct this study.

RESULTS AND DISCUSSION

We tested and validated the testing apparatus on a pelvis-toe fresh-frozen cadaver specimen. We performed passive flexion, stand-to-sit, stairs descent, and deep knee flexion trajectories adapted from the Orthoload database [4]. The femur and tibia clamps showed minimal translation between the specimen and the clamp under load (600N). Using a calibrated motion capture system, we evaluated the repeatability of the patella tracker removal/placement. We recorded the 6 DOF data of the tracker from 20 cycles of removal and placement of the tracker on the magnetic plate. Results showed variation less than 0.21mm in X Y and Z, and less than 0.14 degree in Roll and Pitch, and less than 1.37 degree in Yaw.
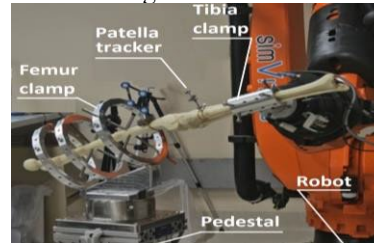
Figure 1: A femur-tibia bone model mounted on the simVITRO platform using the designed testing jig.

CONCLUSIONS

The testing jig was tested and validated using a pelvis-to-toe cadaver specimen. The setup was capable of withstanding more than 600N knee compression and allowed for the achievement of deep knee bend.

REFERENCES

1. Nam D., R.M. Nunley, and R.L. Barrack, Patient dissatisfaction following total knee replacement: a growing concern? *Bone Joint J*, 2014. **96-B**: p. 96-100.
2. McClelland JA, Webster KE, Feller JA. Gait analysis of patients following total knee replacement: a systematic review. *Knee*. (2007) **14**:253–63.
3. https://github.com/Mboudali/simVITRO-Jigs.
4. Orthoload: Standard Loads Knee Joint « OrthoLoad

Cyclic Loading of Achilles Tendon Using Physiologically Representative Loads

[1]Nisal Jayaneththi, [1]Hans Gray, [1]Dale Robinson, [1]David Ackland, [1]Ranjith Unnithan and [1]Peter Lee

[1]Faculty of Engineering and Information Technology, The University of Melbourne, Melbourne, VIC
email: njayaneththi@student.unimelb.edu.au

INTRODUCTION

Between 6% and 18% of athletes suffer some form of Achilles tendon injury every year. These injuries are becoming more common with increasing participation in recreational sports, particularly high-intensity sports. There is a limited understanding of the Achilles tendon's failure mechanism during walking, running and jumping. Therefore, this study aims to perform a cyclic loading experiment on Achilles tendon specimens to understand the effect of various physiologically representative loads on tendon failure and damage.

METHODS

A pilot study has been conducted on a single ovine specimen Achilles tendon due to their relative abundance and similar geometric profile to the human Achilles tendon.

The sample had approximately 70mm of the distal end of the gastrocnemius and soleus muscles, the entire Achilles tendon, and the entire calcaneus. A portion of the tibia was also preserved to help alignment during loading.

The distal end of the Achilles tendon (calcaneus and tibia) was placed into a potting block (Acrylic One, ACS Pty Ltd, NSW Australia). A pair of purpose-built aluminium clamps cooled by liquid nitrogen froze and gripped the gastrocnemius and soleus to prevent slip and internal shear [1].

The specimen was subjected to a series of sinusoidal cyclic loading scenarios between 100N and a peak load (Instron 8874, Instron, MA USA). The peak loads and frequencies tested were 1600N at 1Hz, 1600N at 2Hz, 2100N at 1Hz and 2100N at 2Hz. In each case, the specimen was subjected to 200 cycles except the final test with a peak load of 2100N at 2Hz when the specimen was tested to failure.

RESULTS AND DISCUSSION

The data presented is from the linear region of each curve from the 140th cycle to the 200th cycle (Figure 1 and Table 1). As expected, length increased more rapidly with higher loads, indicating a greater rate of damage [2]. However, the increase in frequency decreased the rate at which lengthening occurred. The decreased rate may be due to the reduced time spent in the loaded position per cycle, resulting in less damage caused over a cycle.

Failure occurred at the tendon insertion at the calcaneus, as opposed to the mid-substance of the tendon, like humans [3].

Tendon insertion failure can be attributed to the young age of the ovine specimen tested, where growth plates are present, therefore becoming a point of weakness.
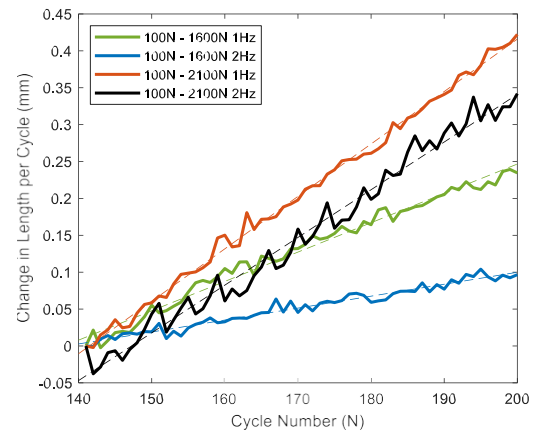
Figure 1: Change in length plotted against cycle number for each of the four different cyclic loading scenarios. The length at each cycle was measured at the instance the load reached its minimum value – 100N. The change in length was calculated relative to the length of the specimen at the 140th cycle.

Table 1: Line of best-fit equations alongside an R^2 value.

Loading Scenario	Equation	R^2
100N to 1600N at 1Hz	$0.0040\,N - 0.549$	0.981
100N to 1600N at 1Hz	$0.0016\,N - 0.224$	0.960
100N to 2100N at 1Hz	$0.0071\,N - 1.005$	0.996
100N to 2100N at 2Hz	$0.0065\,N - 0.952$	0.980

CONCLUSIONS

The pilot study has shown there is a change in the rate of tendon damage with different loadings, however a conclusion cannot be made on the effect of the tendons failure mechanism. The next stage of the study is to integrate the use of Digital Image Correlation to measure local strains on the surface of the tendon and finally test cadaveric Achilles tendons to overcome issues present in ovine tendons and obtain data that is directly applicable to humans.

REFERENCES

1. Riemersa D, *Journal of Biomechanics,* **15**:619-620, 1982
2. Fung D, et al., *Journal of Orthopaedic Research.* **27**:264-273, 2009.

3. Hess W, *Foot & Ankle Specialist*, **3**:29-32, 2010

EVALUATING THE INTELLEVENT ALGORTIHM ON AN EXTERNAL NORMAL DATASET

[1]Patrick Gu, [2]Nikos Darras, [1]Qiuhong Ke, [2]Anna Murphy, and [2]Corey Joseph
[1]Faculty of Engineering and Information Technology, Monash University, Melbourne, VIC
[2]Clinical Gait Analysis Service, Monash Health, Melbourne, VIC
email: patgu@proton.me

INTRODUCTION

Recent advancements in machine learning have led to the development of algorithms capable of detecting gait cycle events using 3-dimensional motion capture data. One such algorithm, IntellEvent [1], has demonstrated state-of-the-art detection accuracies. However, these results were achieved on data generated from the same laboratory as its training data, and little is known about its application and accuracy on other datasets.

To further investigate this, we present an exploratory characterization of the IntellEvent algorithm's performance on a normal motion capture dataset, collected at the Clinical Gait Analysis Service (CGAS; Monash Health). By focusing only on foot events during normal gait, we aimed to isolate the algorithm's inherent detection error. That is, by excluding the confounding factor of pathological gait variability. This approach allows us to better assess IntellEvent's baseline performance and generalizability across different laboratory settings.

The aim of this study was to comprehensively evaluate IntellEvent's ability to generalise and perform consistently on data from a laboratory different to the one that generated its training data.

METHODS

154 trials containing 564 forceplate-identified events and 840 clinician-identified events from subjects 18 to 78 years old were used in the evaluation. All data was collected at the CGAS in Melbourne, Australia. Custom Python code was developed to automate the analysis, which imported motion capture data from individual .c3d files, applied the IntellEvent model to generate event predictions, and calculated detection rate and accuracy metrics by comparing these predictions to both forceplate-identified ground-truth events and clinician-identified events.

RESULTS AND DISCUSSION

Our analysis revealed detection rates and accuracies for both foot contact (FC) and foot-off (FO) events (shown in Table 1) lower than those reported in the original IntellEvent paper. For instance, ground-truth FC and FO event detection rates on our dataset were 83.12% and 92.10% respectively, compared to ≥99% and ≥95% as originally reported. Similarly, FC and FO

events in our dataset were detected within 30.24ms and

15.96ms, respectively, compared to 5.4ms and 11.3ms as originally reported.

These findings underscore the challenges in translating gait event detection machine learning models across different laboratory settings, a phenomenon also noted by the IntellEvent authors and others [1, 2, 3]. The reduced detection accuracy and rate observed when applying IntellEvent to our dataset likely stem from methodological differences between laboratories, particularly in the placement of heel, toe, and ankle markers.

Table 1: Detection rate and accuracy of forceplate-identified ground-truth events and clinician-identified events by IntellEvent.

Event	Type	Detection Rate, % (95% CI)	Avg. Prediction Err., ms (95% CI)
FC	Forceplate	83.12 (77.93 - 88.30)	30.24 (23.20 - 37.29)
FC	Clinician	76.32 (71.12 - 81.52)	34.70 (27.65 - 41.75)
FO	Forceplate	92.10 (87.88 - 96.32)	15.96 (13.35 - 18.57)
FO	Clinician	90.26 (85.60 - 94.92)	22.39 (16.93 - 27.84)

CONCLUSIONS

IntellEvent was able to detect foot events to a reasonable degree on our dataset, albeit with lower detection rates and accuracy than originally reported, possibly due to methodological differences in marker placement between laboratories. While IntellEvent shows potential for streamlining data processing, close oversight of predicted events is crucial due to the variability in prediction accuracy and detection rate, as most events were identified slightly after actual occurrence. As is common in machine learning research, expanding the dataset through multi-institutional collaborations could lead to more robust and universally applicable models, enhancing the reliability of automated gait analysis tools across diverse settings.

ACKNOWLEDGEMENTS

REFERENCES
1. Dumphart B, et al., *PLOS ONE.* **18**(8):e0288555, 2023.
2. Kidzinski L, et al., *PLOS ONE.* **14**(1): e0211466 , 2019.
3. Lempereur M, et al., *J Biomech.* **98**: 109490, 2020.

Patient Related Factors Affect Bone Mineral Density in the Proximal Tibia Six Months Following Total Knee Replacement Surgery

[1]Salindi P. Herath, [1]David Hobbs, [2]Dominic Thewlis, [3]Christopher Wilson, [1]Mark Taylor

[1]Medical Device Research Institute, College of Science and Engineering, Flinders University, Adelaide, SA, Australia
[2]Faculty of Health and Medical Sciences, University of Adelaide, Adelaide, SA, Australia
[3]College of Medicine and Public Health, Flinders University, Adelaide, SA, Australia
email: salindi.herath@flinders.edu.au

INTRODUCTION

Bone mineral density (BMD) in the proximal tibia changes following a primary total knee replacement surgery [1]. Changes to bone are in part due to loading where increased loading may lead to increased bone. Patient specific factors that may affect these changes include lower limb alignment, body mass, and component size. People with osteoarthritis tend to have lower limb malalignments that are modified during surgery and has been shown to affect medial to lateral bone volume fraction in cadaveric proximal tibias [2]. Body mass can affect the amount of load that passes through the knee joint. Finally, component size may affect how the bone models as a reflection of body mass or due to changes in stress shielding. This The study aimed to investigate if alignment, mass and component size are related to postoperative changes in BMD in the proximal tibia up to 6 months following a primary total knee replacement surgery.

METHODS

This study included 20 total knee replacement patients (9 male). All participants received weightbearing X-rays and supine CT scans preoperatively and postoperatively. Dual energy X-ray absorptiometry scans of the proximal tibia were taken preoperatively, and then 3 and 6 months postoperatively.

Lower limb alignment was measured as the medial angle connecting the hip, knee, and ankle (HKA) joint centres. HKA angle was measured preoperatively via full lower limb weightbearing X-rays and postoperatively from virtual X-rays of 3D segmented bone geometries mapped onto weightbearing X-rays of the affected knee joint.

BMD was measured using Hologic software in 2 regions of interest (ROI) each in the medial, lateral, and diaphyseal bone close to and further away from the implant Each area was determined based on the size of the implant stem.

Relationships between patient factors and changes in the BMD were tested using linear regression ($p < 0.05$).

RESULTS AND DISCUSSION

Preoperative HKA angle was significantly negatively correlated with changes in the distal medial ROI from 3 to 6 months post-operation (Figure 1, left). Similarly, postoperative HKA angle was significantly positively correlated with proximal lateral BMD changes from 3 – 6 months (Figure 1, right). People with larger body masses also tended to have a greater increase in both diaphyseal ROI at 6 months compared

had a greater increase in people who had a larger component size ($R^2 = 0.36$, $p = 0.0025$).
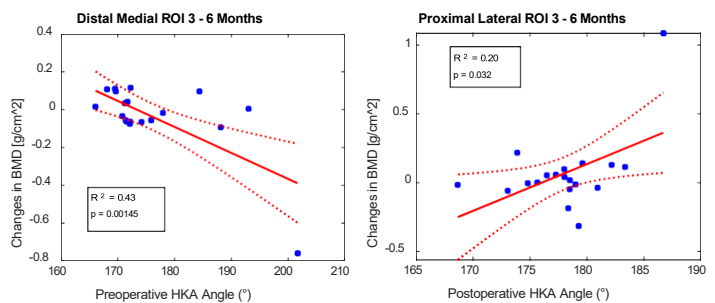
to pre-operation ($R^2 = 0.21$, $p = 0.025$). Diaphyseal BMD also

Figure 1: Changes in the BMD from 3 – 6 months in the medial (left) and lateral BMD (right) correlated with preoperative and postoperative HKA angle, respectfully.

Preoperatively varus participants tended to have less decrease of BMD in the medial ROI from 3 to 6 months post-operation. People whose alignment was unchanged from a varus knee, similarly, had a decrease in their lateral BMD from 3 to 6 months post-operation. Alignment affects where the loading axis is in the proximal tibia and this correlates with the amount of load that passes through the medial and lateral condyles. Increasing mass and component size was associated with an increase in the BMD under the implant stem suggesting an increase in the amount of load that passes through the stem into the region below.

CONCLUSIONS
Patient specific factors can affect bone modelling in the proximal tibia following a total knee replacement surgery. The results in this study suggest that lower limb alignment, body mass, and component size affect bone remodeling in the proximal tibia. With further research, these results can be used for personalization of surgeries to counteract implant loosening.

ACKNOWLEDGEMENTS

REFERENCES
1. Jaroma A, et al., *Acta* Orthopaedica. 87 (**3**): 268 – 273, 2016
2. Roberts BC, et al., *Osteoarthritis and Cartilage*. 26: 547 – 556, 2018

A framework for the design of patient-specific porous femoral stems
[1]Sarah Safavi, [1]Hans Gray and [1]Peter Lee

[1]Department of Biomedical Engineering, University of Melbourne / ARC CMIT, Melbourne, Australia
email: ssafavi@student.unimelb.edu.au

INTRODUCTION

Aseptic loosening of femoral stems caused by stress shielding and subsequent bone resorption remains a concern for patients undergoing total hip replacement surgery. To reduce stress shielding, implant stiffness needs to be decreased to better match the stiffness of the surrounding bone. 3D printed titanium diamond lattice structures may be considered for such implants due to their biomimetic mechanical properties [1]. We aimed to develop a methodology for designing patient-specific diamond lattice structure based porous femoral stems.

METHODS

A design framework was developed to optimise the porous structure of the femoral stem to reduce stress shielding while maintaining sufficient strength to withstand typical in vivo loads in the hip joint (Figure 1).

A CAD model of a commercially available implant geometry was virtually implanted into a segmented human femur bone model for finite element analysis. Femoral head load and simplified muscle forces representative of activities of daily living (walking, stair climbing) were applied on the model [2, 3] to quantify stress shielding during each iteration of the optimisation process. Additionally, a finite element simulation of the standardised endurance test for the femoral stem (ISO 7206-4) was performed to ensure structural strength [4].

Four implant design variants were investigated by varying the portion of the implant that was solid and the portion of the implant that was porous. The neck of the implant was kept solid in all design variants, while the remaining portion was either fully or partially porous. The partially porous designs were proximal porous, proximal porous with a shell around the distal end, and fully porous with a solid shell excluding a proximal porous opening.

The porous parts were created using diamond lattice structures with selected strut and pore sizes, considering manufacturability and facilitation of bone ingrowth. To determine the relationship between lattice structure parameters (unit cell size and strut radius) and mechanical properties (elastic modulus and yield strength), 13 additively manufactured cubic samples were experimentally tested as specified in ISO 13314 for compression testing of porous metals [5]. The samples were designed with unit cell sizes between 1.0 – 1.3 mm and varied in porosity, within the FDA-approved range [1]. These relationships were incorporated into the above-mentioned finite element analyses for the optimisation process.

RESULTS AND DISCUSSION

Mechanical testing of the manufactured diamond lattice cubic samples revealed quadratic relationships between elastic modulus and strut radius. Yield strength increased linearly with larger stiffness. The relationship between elastic modulus and strut radius was used to translate the optimised stiffness into CAD files of the patient-specific porous femoral stem (Figure 1).
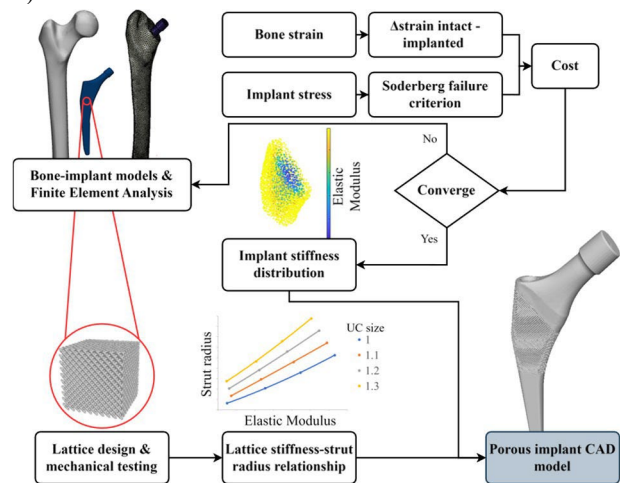
Figure 1: Custom porous implant design workflow for a proximally porous stem.

CONCLUSIONS

Diamond lattice structures can be used to design custom porous femoral stems for stress shielding reduction under the consideration of mechanical strength. Future studies aim to explore the performance (e.g. stress shielding reduction, micromotion) of the porous implant designs based on this workflow for a larger sample size.

ACKNOWLEDGEMENTS

REFERENCES

1. D Martinez-Marquez et al., *Materials (Basel).* **13**, 2020.
2. G Bergmann et al., *PLoS One.* **11**, e0155612, 2016.
3. MO Heller et al., *J Biomech.* **38**, 1155-1163, 2005.

4. ISO 7206-4:2010, 2010

PREDICTING ACHILLES TENDON FORCE USING 2D VIDEO DATA

[1]Zhengliang Xia, [1]Bradley M. Cornish, [2]Daniel Devaprakash, [1]Rod S. Barrett, [1]David G. Lloyd,
[1]Andrea H. Hams and [1]Claudio Pizzolato

[1]Griffith Centre of Biomedical & Rehabilitation Engineering (GCORE), Griffith University, Gold Coast, QLD
[2]VALD Performance, Newstead, QLD,
email: zhengliang.xia@griffithuni.edu.au

INTRODUCTION

The therapeutic outcomes of Achilles tendon (AT) rehabilitation may be improved by controlling its mechanical loading [1]. At present, however, no practical and cost-effective tools exist to provide real-time feedback on AT loading in the clinical or training environment. Integrating computer vision and neural networks to bypass traditional neuromusculoskeletal modelling approaches that are typically used in research laboratories could enable rapid biofeedback of AT function in clinical settings. We developed a combined computer vision and neural networks approach to predict AT forces from 2-dimensional (2D) video data. We evaluated the accuracy of the proposed method by simulating different camera angles and comparing its AT forces predictions to the gold-standard estimates from a personalized electromyography (EMG)-informed neuromusculoskeletal model [2].

METHODS

The dataset comprised of 16 participants performing five motor tasks: walking, running, countermovement jump, single leg landing and single-leg heel rise [2]. Three-dimensional marker trajectories, ground reaction forces, and EMG of lower limbs were collected and employed to estimate AT forces using personalized EMG-informed neuromusculoskeletal modelling [2]. To prepare the dataset, ten 3-dimensional (3D) keypoints, typically generated from the OpenPose BODY_25 model, were first synthesized from marker trajectories with triaxial noise added [3]. The synthesized keypoints were then projected onto multiple, randomly generated 2D planes equidistant from the participant's right side, from the participant's back (-90°) to the front (90°), using OpenCV. Occluded data for the left side's lower limb 2D keypoints were created based on a distance threshold, with their corresponding values set as *NaN*.

The process created 6200 trials to train a long short-term memory neural network (LSTM) model. Each trial consisted of a sliding time window of 10 × 22 matrices, i.e., 10 keypoints with 10 time-frames for each keypoint's x and y positions concatenated with discrete values of each participant's height and mass. The target output for each time window was the AT force value of the last time frame. The task-specific LSTM models were trained for each task, which incorporated two bi-directional LSTM layers connected with batch normalization and dropout layers. The hyperband algorithm was used to select the optimal hyperparameter combinations for each task-specific

LSTM model, using a 7:1 split of training to validation data. Leave-one-subject-out cross-validation (LOSOCV) was used for model validation. Each task-specific model was tested with unseen 2D pose datasets from 19 distinct camera angles ranging from -90° to 90° with 10° intervals. Differences between predicted and gold-standard AT forces were quantified via root mean squared error normalized to peak values (nRMSE) and the coefficient of determination (R^2) for each trial.

RESULTS AND DISCUSSION

The LOSOCV task-specific models estimated AT force with nRMSE ranging from 11 to 20% and an R^2 value between 0.79 and 0.92. Although worse predictions were found at extreme angles, no clear and consistent best camera angle was identified across participants over the five tasks (Figure 1).
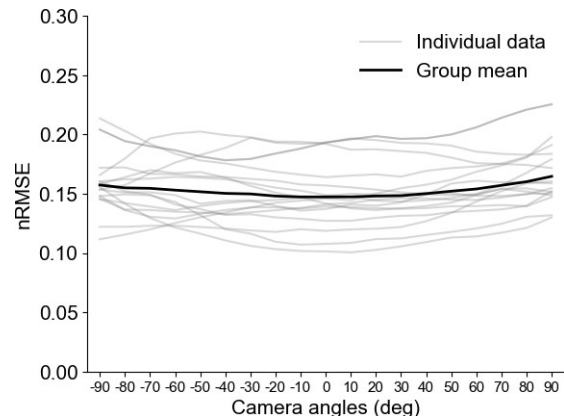
Figure 1: The variations of nRMSE relative to the camera angles in individual and group level for testing dataset.

CONCLUSIONS

Using synthesized single video views, computer vision and LSTM neural networks yielded reasonable AT force predictions across a range of motor tasks. However, no optimal single camera angle was identified for prediction accuracy of task-specific models. Further refinement is needed to improve the clinical utility in exercise-based AT training.

REFERENCES

1. Pizzolato C, et al., *Br J Sports Med*. **53**: 11-12, 2019
2. Devaprakash D, et al., *J Appl Physiol*, **132**: 956-965, 2022
3. Needham L, et al., *Sci Rep*, **11**: 20673, 2022

Impacts of Anterior Cruciate Ligament Rupture on the Nuclei of Ligament Cells: A Histology and Single-Cell Gene Expression-based Study

[1]Ziming Chen, [1]Natjira Tassaneesuwan, [1]Peilin Chen, [3]Zhantao Deng, [1]Euphemie Bassonga, [3]Qiujian Zheng, [1]Ming Hao Zheng, [2]Toby Leys

[1]Centre for Orthopaedic Translational Research, Medical School, University of Western Australia, Nedlands, WA, 6009, Australia
[2]Department of Orthopaedic Surgery, Sir Charles Gairdner Hospital, Nedlands, WA, 6009, Australia
[3]Department of Orthopedics, Guangdong Provincial People's Hospital, Guangdong Academy of Medical Sciences, Guangzhou, 510000, Guangdong, China
email: ziming.chen@uwa.edu.au

INTRODUCTION

Ligament cells of the anterior cruciate ligament (ACL) are typically situated between the collagen fibers and have elongated nuclei. This highly organized structure is crucial for providing stability to the knee joint. ACL rupture is a common injury that frequently occurs in athletes involved in vigorous activities and leads to adverse effects on the career. The present study aims to investigate the effects of ACL rupture to nuclear phenotype.

METHODS

ACL tissues from patients were processed for hematoxylin and eosin (H&E) staining. Histological scoring of H&E-stained ACL tissues was performed using a semi-quantitative histology scoring system. Pathological grades were categorized as slightly, moderately, and severely abnormal. Furthermore, healthy and ruptured ACL tissues were collected from human donors for single-cell RNA-sequencing.

RESULTS AND DISCUSSION

A total of 41 ruptured ACL tissues were collected for histological observation. 254 H&E-stained images were obtained from different fields of these samples. Generally, 26 fields were identified as slightly abnormal, 134 fields as moderately abnormal, and 94 as severely abnormal (Fig. 1A). The number of cells in severely abnormal fields was significantly higher than in slightly and moderately abnormal fields. Additionally, nuclear eccentricity was significantly decreased, and fibers were more disarranged in severely abnormal fields compared to the others. Correlation analysis of the medical records and histological scoring showed a positive linear correlation between the duration of injury and histological scores (Fig.1B). Moreover, nuclear eccentricity was negatively related to fiber arrangement scores (Fig.1C). Single-cell RNA-sequencing analysis, including 10048 cells from healthy ACL and 8407 cells from ruptured ACL, indicated the presence of six types of cells in ACL tissues (Fig.1 D). Notably, we identified a subtype of ligament cells (COL1A1- ligament cell) with less ligamentogenic function (Fig.1E), mainly from ruptured ACL tissue. By comparison to the subtype of ligament cells with high functioning (COL1A1+ ligament cell), we found that the COL1A1- ligament cells had

high expression of the Linker of Nucleoskeleton and Cytoskeleton (LINC) complex (Fig.1F), an essential intracellular structure responsive to and conveying mechanical stress from extracellular environments into the nucleus [1].
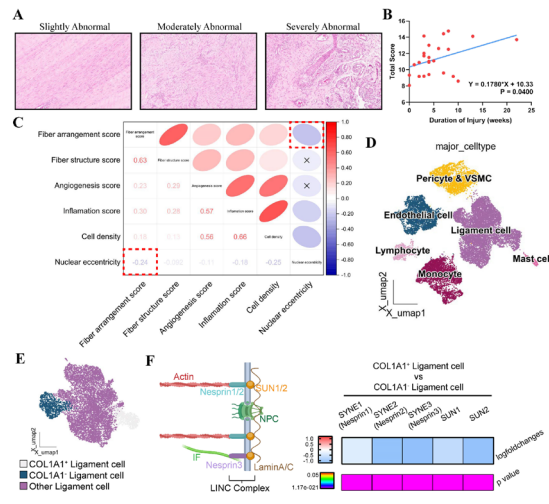
Figure 1: ACL rupture changes the nuclear phenotype. (A) Histological assessment and **(B,C)** correlation analysis of the medical record and histological scores. Single cell RNA-sequencing analysis to ACL tissues **(D)** identified 6 types of cells and **(E,F)** characterized subtypes of ligament cells with different levels of ligamentogenesis.

CONCLUSIONS

ACL rupture leads to collagen fiber disarrangement, decreases nuclear eccentricity, and increases the expression of the LINC complex in tendon cells, which correlates to decreased ligamentogenesis.

ACKNOWLEDGEMENTS

REFERENCES

1. McGillivary RM, et al., *Curr Opin Cell Biol.* **85**:102260, 2023.

List of Registered Delegates

(at the time of printing, surname ordered alphabetically)

First Name	Last name	Institution	Email
Alan	Abraham	Deakin University	alan.abraham0209@gmail.com
David	Ackland	University of Melbourne	dackland@unimelb.edu.au
Sami Khaloufah	Alahmari	Taif University	Samikhaloufahm.alahmari@gmail.com
Rami	Al-Dirini	Flinders University	rami.aldirini@flinders.edu.au
Enzo	Allevard	University of Auckland	eall036@aucklanduni.ac.nz
Reza	Arjmandi	University of Auckland	r.arjmandi@auckland.ac.nz
Heather	Badger	University of Adelaide	heather.badger@adelaide.edu.au
Martina	Barzan	Griffith University	m.barzan@griffith.edu.au
Jack	Beard	Epworth Healthcare / University of Melbourne	jack.beard@epworth.org.au
Patrick	Beaumont	University of Queensland	patrick.beaumont1999@gmail.com
Kieran	Bennett	Flinders University	kieran.bennett@flinders.edu.au
Thor	Besier	University of Auckland	t.besier@auckland.ac.nz
Nils	Betzler	Qualisys	nils.betzler@qualisys.com
Christopher	Bird	University of Queensland	christopher.bird@uq.edu.au
Carina	Blaker	University of Sydney	carina.blaker@sydney.edu.au
Pavel	Bogachko	Qualisys	pavel.bogachko@qualisys.com
Bart	Bolsterlee	NeuRA / UNSW	b.bolsterlee@neura.edu.au
Mounir	Boudali	University of Sydney	mounir.boudali@sydney.edu.au
Elizabeth	Bradshaw	Deakin University	liz.bradshaw@deakin.edu.au
Maya	Braun	University of Sydney	mbra4709@uni.sydney.edu.au
Alexis	Brierty	University of Sydney	alexis.brierty@sydney.edu.au
Francois	Bruyer-Monteleone	Queensland University of Technology	f2.bruyermonteleone@hdr.qut.edu.au
Richard	Burt	Tracklab	richard@tracklab.com.au
Anna	Butcher	University of Waikato	annajbutcher@gmail.com
Stuart	Callary	University of Adelaide	stuart.callary@adelaide.edu.au
Benjamin	Carling	University of Canberra	benjamin.carling@outlook.com
Christopher	Carty	Griffith University	c.carty@griffith.edu.au
Miyuki	Chamberlain	University of Queensland	miyuki.chamberlain@student.uq.edu.au
Michael	Chang	Charles Sturt University	mchang@csu.edu.au
Xiaojun	Chen	University of Western Australia	xander.chen@research.uwa.edu.au
Ziming	Chen	University of Western Australia	ziming.chen@research.uwa.edu.au
Kai	Chen	University of Western Australia	kai.chen@uwa.edu.au
Zhengxu	Cheng	University of Adelaide	zhengxu.cheng@adelaide.edu.au
Chan Hee	Cho	University of Adelaide	a1749658@adelaide.edu.au
Julie	Choisne	Auckland Bioengineering Institute	j.choisne@auckland.ac.nz
Christopher	Chong	La Trobe University	19376794@students.latrobe.edu.au

Elizabeth	Clarke	University of Sydney	elizabeth.clarke@sydney.edu.au
Eduardo	Cofre	Swinburne University	eduardocofre@swin.edu.au
Celeste	Coltman	University of Canberra	celeste.coltman@canberra.edu.au
Bradley	Cornish	Griffith University	bradley.cornish@griffith.edu.au
Jacqui	Couldrick	University of Canberra	jacqui.couldrick@canberra.edu.au
Kay	Crossley	La Trobe University	k.crossley@latrobe.edu.au
Taisha	D'Apollonio	University of Adelaide	taisha.dapollonio@adelaide.edu.au
Nicolaos	Darras	Monash Health	Nikolaos.darras@monashhealth.org
James	Davies	Royal Melbourne Hospital	jamesgdavies6@gmail.com
Divya	Dayal	Materialise	divya.dayal@materialise.com.au
Laura	Diamond	Griffith University	l.diamond@griffith.edu.au
Taylor	Dick	University of Queensland	t.dick@uq.edu.au
Tim	Doyle	Macquarie University	tim.doyle@mq.edu.au
Harry	Driscoll	University of Melbourne	hdriscoll@student.unimelb.edu.au
william	du Moulin	Griffith University	william.dumoulin@griffithuni.edu.au
Nicholas	Ducey	Delsys	nducey@delsys.com
Kayne	Duncanson	University of Adelaide	kayne.duncanson@adelaide.edu.au
Leanne	Dwan	Sydney Children's Hospitals Network	leanne.dwan@sydney.edu.au
Ben	Dziekan	Davies Collison Cave	Bdziekan@ddc.com
Emmanuel	Eghan-Acquah	Griffith University	emmanuel.eghan-acquah@griffithuni.edu.au
Zhou	Fang	University of Melbourne	zhouf1@student.unimelb.edu.au
Haydee	Ferguson	Deakin University	hrferguson@deakin.edu.au
Ben	Ferguson	University of Sydney	ben.ferguson@sydney.edu.au
David	Findlay	University of Adelaide	david.findlay@adelaide.edu.au
Aaron	Fox	Deakin University	aaron.f@deakin.edu.au
Brook	Galna	Murdoch University	brook.galna@murdoch.edu.au
Denni	Goodchild	Queensland Children's Motion Analysis Service	denni.goodchild@outlook.com
Sienna	Gosney	Griffith University	sienna.gosney@griffithuni.edu.au
Tamara	Grant	Griffith University	tamara.grant@griffith.edu.au
Hans	Gray	University Of Melbourne	hans.gray@unimelb.edu.au
Shanyuanye	Guan	University of Melbourne	shanyuanye.guan@unimelb.edu.au
Yareni	Guerrero	University of Sydney	yareni.guerrero@sydney.edu.au
Stephen	Hale-Worrall	Charles Sturt University	stephen@nativus.com.au
Michelle	Hall	University of Sydney	michelle.hall@sydney.edu.au
Matthew	Hambly	Griffith University	matthew.hambly@griffithuni.edu.au
Aaron	Hammat	University of Adelaide	aaron.hammat@adelaide.edu.au
Alice	Hatt	Neuroscience Research Australia	a.hatt@neura.edu.au
Simon	Heinrich	Friedrich Alexander Universität	simon96.heinrich@fau.de
Salindi	Herath	Flinders University	salindi.herath@flinders.edu.au
Ben	Hoffman	University of Southern Queensland	Ben.Hoffman@unisq.edu.au
Brooke	Hoolihan	University of Newcastle	brooke.hoolihan@uon.edu.au
Daniel	Hopkins	University of Melbourne	dchopkins@student.unimelb.edu.au
Maggie-May	Hornigold	Queensland University of Technology	Maggiemay.hornigold@gmail.com
Zara	Jackson	Tracklab	zara.j@tracklab.com.au
Nisal	Jayaneththi	University of Melbourne	njayaneththi@student.unimelb.edu.au
Harrison	Johansen	University of Sydney	hjoh2985@uni.sydney.edu.au
Nicole	Jones	University of Southern Queensland	Nicole.Jones@unisq.edu.au
Benjamin	Jones	La Trobe University	benjamindavidmichael.jones@latrobe.edu.au
Corey	Joseph	Noraxon / Monash	corey.joseph@monash.edu
Ayda	Karimi Dastgerdi	Griffith University	ayda.karimidastgerdi@griffithuni.edu.au

Meghan	Keast	Queensland Academy of Sport	mf.keast@gmail.com
Nikki	Kelp	AIMedical / Noraxon	nikki@aimedical.com.au
John	Kerr	University of New South Wales	john.kerr@unsw.edu.au
Britney	Kerr	Royal Children's Hospital Melbourne	britneykerrr@gmail.com
Hyeyeon	Kim	University of Auckland	hkim375@aucklanduni.ac.nz
Hui Jean	Kok	Indiana University	jeankok@iu.edu
Ryan	Konno	University of Queensland	r.konno@uq.edu.au
Praveen	Krishna	University of Melbourne	pkkris@student.unimelb.edu.au
Matilda	Krywanio	University of Adelaide	matilda.krywanio@adelaide.edu.au
Melody	Labrune	Macquarie University	melody.labrune@hdr.mq.edu.au
Tyra	Lange	Flinders University	tyra.lange@flinders.edu.au
Maxence	Lavaill	Queensland University of Technology	maxence.lavaill@qut.edu.au
Robert	Lees	University of Queensland	brisbanerobert22@gmail.com
Claire	LI	University of Western Australia	yihe.li@research.uwa.edu.au
Rachel	Li	Australian National University	rachel.li@anu.edu.au
Glen	Lichtwark	Queensland University of Technology	glen.lichtwark@qut.edu.au
Yi-Chung	Lin	Australian Catholic University	yilin@acu.edu.au
India	Lindemann	University of Queensland	i.lindemann@uq.edu.au
Fuyuan	Liu	University of Melbourne	fuyuanl@student.unimelb.edu.au
Jess	Loone	Deakin University	jess.loone@deakin.edu.au
Jinella	Lopez	Royal Children's Hospital Melbourne	jinella.lopez@rch.org.au
Melissa	Louey		melissalouey@yahoo.com.au
Fatemeh	Malekipour	University of Melbourne	fmal@unimelb.edu.au
Kerry	Mann	Charles Sturt University	kmann@csu.edu.au
Saulo	Martelli	Queensland University of Technology	saulo.martelli@qut.edu.au
Dean	Mayfield	University of California	dean.mayfield@uqconnect.edu.au
Brody	McCarthy	La Trobe University	brodyjm147@gmail.com
Ayden	McCarthy	Macquarie University	ayden.mccarthy@hdr.mq.edu.au
Jodie	McClelland	La Trobe University	j.mcclelland@latrobe.edu.au
Grace	McConnochie	University of Adelaide	grace.mcconnochie@adelaide.edu.au
Alec	Mckenzie	Queensland academy of sport	alec.mckenzie2@griffithuni.edu.au
Benjamin	Mentiplay	La Trobe University	b.mentiplay@latrobe.edu.au
Karen	Mickle	The University of Newcastle	karen.mickle@newcastle.edu.au
Kane	Middleton	La Trobe University	k.middleton@latrobe.edu.au
Stuart	Millar	Lockheed Martin Australia	stuart.c.millar@global.lmco.com
Patrick	Moase	Marine Biomedical	patrick.moase@marinebiomedical.com.au
Luca	Modenese	University of New South Wales	l.modenese@unsw.edu.au
Corinna	Modiz	Queensland University of Technology	corinna.modiz@hdr.qut.edu.au
Hossein	Mokhtarzadeh	Motek Medical	hossein.mokhtarzadeh@dih.com
Anita	Mudge	Sydney Children's Hospitals Network	mudgey1105@gmail.com
Natalia	Mühl Castoldi	Queensland University of Technology	n.muhlcastoldi@qut.edu.au
Anna	Murphy	Monash Health	anna.murphy2@monashhealth.org
Linh	Nguyen	University of Melbourne	linhng304@gmail.com
Andy	Nie	University Of Melbourne	andy.nie3@gmail.com
Kubra	Onerge	Murdoch Children's Research Institute	kubra.onerge@gmail.com
Ioana	Oprescu	UNiversity of Queensland	i.oprescu@student.uq.edu.au
Richard	Page	Deakin University	richard.page@deakin.edu.au
Olga	Panagiotopoulou	Davies Collison Cave	OPanagiotopoulou@dcc.com

Elyse	Passmore	Murdoch Children's Research Institute	elyse.passmore@rch.org.au
Ben	Patritti	Flinders Medical Centre	ben.patritti@sa.gov.au
Nathan	Pavlos	The University of Western Australia	nathan.pavlos@uwa.edu.au
Andrew	Pearce	AIMedical	andrew@aimedical.com.au
Meeghage Randika	Perera	University of Auckland	randikaperera.m@gmail.com
Egon	Perilli	Flinders University	EGON.PERILLI@FLINDERS.EDU.AU
Luke	Perraton	Monash University	luke.perraton@monash.edu
Daniel	Petrovski	Swinburne University of Technology	dpetrovski@swin.edu.au
Matheus	Pinto	Edith Cowan University	m.pinto@ecu.edu.au
Peter	Pivonka	Queensland University of Technology	peter.pivonka@qut.edu.au
Per	Prisell	University of Tasmania	perprisell@gmail.com
Ryan	Quarrington	University of Adelaide	ryan.quarrington@adelaide.edu.au
Ceridwen	Radcliffe	University of Canberra	ceridwen.radcliffe@canberra.edu.au
Roshni	Raghvani	University of Auckland	rrag962@aucklanduni.ac.nz
Rahm	Ranjan	University of New South Wales	rahm.ranjan@unsw.edu.au
Cristian	Riveros-Matthey	University of Queensland	c.riverosmatthey@uq.edu.au
Dale	Robinson	University of Melbourne	drobinson@unimelb.edu.au
Tess	Rolley	Deakin University	tlrolley@deakin.edu.au
Rui	Ruan	University of Western Australia	chris.ruan@uwa.edu.au
Monica	Russell	Materialise	monica.russell@materialise.com.au
Sarah	Safavi	University of Melbourne	ssafavi@student.unimelb.edu.au
Matthew	Savage	La Trobe University	mc1savage@gmail.com
David	Saxby	Griffith University	d.saxby@griffith.edu.au
Andrea	Sgarzi	University of New South Wales	a.sgarzi@unsw.edu.au
Deepti	Sharma	Royal Adelaide Hospital	deepti.sharma@sa.gov.au
Beichen	Shi	Griffith University	beichen.shi@griffithuni.edu.au
Behzad	Shiroud Heidari	University of Western Australia / Marine Biomedical	behzad.shiroudheidari@uwa.edu.au
Anne	Silverman	Colorado School of Mines	asilverm@mines.edu
Peter	Smitham	University of Adelaide	peter.smitham@adelaide.edu.au
Jess	Snedeker	University of Zurich / ETH Zurich	snedeker@ethz.ch
Scott	Starkey	University of Melbourne	scott.starkey@unimelb.edu.au
Samuel	Staude	University of Adelaide	samuel.staude@adelaide.edu.au
Oscar	Stelzer-Hiller	University of Sydney	oscar.stelzer-hiller@sydney.edu.au
Jack	Stern	Maccabi Health Fund	dr.stern.jack@gmail.com
Daniel	Tait	University of Canberra	daniel.tait@canberra.edu.au
Javad	Tavakoli	RMIT University	javad.tavakoli@rmit.edu.au
Mark	Taylor	Flinders University	mark.taylor@flinders.edu.au
Dominic	Thewlis	University of Adelaide	dominic.thewlis@adelaide.edu.au
Simon	Thwaites	University of Adelaide	simon.thwaites@adelaide.edu.au
Ryan	Tiew	University of Melbourne	etiew@student.unimelb.edu.au
Oren	Tirosh	Swinburne University of Technology	oren.tirosh@rmit.edu.au
Phil	Townsend	University of Canberra	phil.townsend@canberra.edu.au
KM	Tse	Swinburne University of Technology	ktse@swin.edu.au
Kylie	Tucker	University of Queensland	k.tucker1@uq.edu.au
Natali	Uribe Acosta	Queensland University of Technology	natali.uribeacosta@hdr.qut.edu.au
Wolbert	van den Hoorn	Queensland University of Technology	w.vandenhoorn@qut.edu.au
Kate	Van Der Hoeve	University of Sydney	khoa0785@uni.sydney.edu.au
Mat	Van Heerden	AIMedical	mat@aimedical.com.au
Danielle	Vickery-Howe	La Trobe University	D.Vickery-Howe@latrobe.edu.au

Sansalone	Vittorio	Université Paris-Est Créteil	vittorio.sansalone@u-pec.fr
John	Waters	Swinburne University of Technology	103774971@student.swin.edu.au
Gavin	Williams	University of Melbourne / Epworth Healthcare	gavin.williams@epworth.org.au
James	Williamson	University of Queensland	j.williamson@uq.edu.au
Jodie	Wills	Macquarie University	jodie.wills@mq.edu.au
Laura	Wilson	Australian National University	laura.wilson@anu.edu.au
Lachlan	Winter	Deakin University	winterlachlan99@gmail.com
Elizabeth	Wojciechowski	Children's Hospital at Westmead	elizabeth.wojciechowski@sydney.edu.au
Zhengliang	Xia	Griffith University	zhengliang.xia@griffithuni.edu.au
Alireza	Yahyaiee Bavil	Griffith University	alireza.yahyaieebavil@griffithuni.edu.au
Mohammad	Yavari	University of Melbourne	myavari@student.unimelb.edu.au
Longbin	Zhang	Nanyang Technological University	longbin.zhang@ntu.edu.sg
Minghao	Zheng	University of Western Australia	minghao.zheng@uwa.edu.au
Yixiao	Zhou	University of Western Australia	yixiao.zhou@research.uwa.edu.au
Manuela	Zimmer	University of Stuttgart	manuela.zimmer@isd.uni-stuttgart.de